

Fall 2019

# CDSE Quantum Dot Surface Chemistry Thermodynamics via Isothermal Titration Calorimetry: An Emphasis on the Fundamentals

Megan Y. Gee

Follow this and additional works at: <https://scholarcommons.sc.edu/etd>

 Part of the [Chemistry Commons](#)

---

## Recommended Citation

Gee, M. Y.(2019). *CDSE Quantum Dot Surface Chemistry Thermodynamics via Isothermal Titration Calorimetry: An Emphasis on the Fundamentals*. (Doctoral dissertation). Retrieved from <https://scholarcommons.sc.edu/etd/5507>

This Open Access Dissertation is brought to you by Scholar Commons. It has been accepted for inclusion in Theses and Dissertations by an authorized administrator of Scholar Commons. For more information, please contact [digres@mailbox.sc.edu](mailto:digres@mailbox.sc.edu).

CDSE QUANTUM DOT SURFACE CHEMISTRY THERMODYNAMICS VIA  
ISOTHERMAL TITRATION CALORIMETRY: AN EMPHASIS ON THE  
FUNDAMENTALS

by

Megan Y. Gee

Bachelor of Science  
University of South Carolina, 2011

---

Submitted in Partial Fulfillment of the Requirements

For the Degree of Doctor of Philosophy in

Chemistry

College of Arts and Sciences

University of South Carolina

2019

Accepted by:

Andrew B. Greytak, Major Professor

Mark A. Berg, Committee Member

Sheryl L. Wiskur, Committee Member

Yanwen Wu, Committee Member

Cheryl L. Addy, Vice Provost and Dean of the Graduate School

© Copyright by Megan Y. Gee, 2019  
All Rights Reserved.

## DEDICATION

*This dissertation is dedicated to:*

**My parents Phil & Julia Gee**, whose unwavering support has always motivated me through every endeavor, whim, phase and quest; **my younger sister Frannie**, whose very existence inspires and compels me to be the best version of myself; **my older sister Dana Young**, whose unconditional love has repeatedly outweighed my lowest and darkest moments; and her husband **Cornell** for always striving to provide a safe, creative space. To **my best friends Celina Grace and Victoria Noel Violante** who encourage me beyond reason and have sat with me at countless coffee shops just so I can feel their support, even looking out for new coffee and tea shops that I might like when I'm not around; and to **Anna Kori** – it's like looking into a mirror through time.

## ACKNOWLEDGEMENTS

Dr. Greytak and the entire Greytak lab group. Through all iterations of this group, I am very grateful for each of you!

Committee members: Dr. Mark Berg, Dr. Yanwen Wu, Dr. Maksymilian Chruszcz, Dr. Sheryl Wiskur. Faculty and staff of particular influence: Dr. Perry Pellechia, Dr. Nina Moreno, Dr. Amy Taylor-Perry, Dr. Sophya Garashchuk, Dr. Vitaly Rassolov, Dr. Leslie Lovelace; Dr. Neil Demarse; Dr. Silke Henrich; Sam Burgess, Jennifer Merkel.

Starbucks Baristas! All of you are heroes for dealing with people who haven't yet had their caffeine fix, day-in and day-out. I want to specifically acknowledge any barista who has worked in the Greater Columbia, SC area over the course of this saga, with a special thanks to my friends in the Vista. You have provided a safe & friendly atmosphere, encouraging words, genuine interest & concern, and so many free treats whether I was meeting you as the store opened or frantically packing up as you were trying to close. It is no stretch to say that this degree was not possible without you!

Briana Jackson, Kelly Vicario, Shaney Milling, Tawina McNeely, Tamarah Fant, Dani McClain, Sam Doscher, Nikki Keeve, Kam Jacob, Eric Thomas, Tia Bollinger, Shanaria Johnson, Sara Young, Danielle Scott, Marcum Core, Janoah Sallie, Rachel Acosta, Cathy Peavy, Gwen & Syriac, Tom and Becky and Lauren Smith, Linda Shain; Mark and Fiona Sanders; Jacqueline Clemmons; Ms. Jean; Dr. Clorissa Washington-Hughes, Shelby Dickerson, Otega Ejegbavwo. I'm so blessed to have so much incredible support!

## ABSTRACT

For several decades, the study and development of colloidal semiconductor nanocrystals, or quantum dots (QD), has become a rich field heralding improved integration into applications ranging from photovoltaics and photocatalysis to biomedical imaging and drug delivery.  $\text{Cd}_x\text{Se}_y$  is the most extensively studied QD system, however numerous compositional details still confound the nanocrystal field. Although CdSe QDs with native ligand coatings can show high fluorescence quantum yield and may be suitable for some applications, often times these original ligand layers are comprised of long aliphatic chains that preclude incorporation into biological matrices or severely impede charge transfer – depending on the end goal functionality.

While the innermost core can be highly crystalline, due to the QD size regime a large fraction of the constituent atoms is found at the surface; the nature of which strongly influences optoelectronic properties. Indeed, the necessary ligand surfactant layer is anything but innocuous; dictating synthetic morphology, determining solubility, quenching or enhancing photoluminescence, or even modulating the nanocrystal's band gap. A detailed, consistent and unambiguous profile for QD surface composition and thermodynamics would be extremely advantageous toward controlling and improving photophysical properties. This dissertation highlights several caveats for appropriately compiling a thermodynamic profile *in situ* for the dynamic nature of QD surfaces, and to describe approaches to address them.

I have focused on developing commonly employed metrics for investigating CdSe QD surface chemistries. I begin by thoroughly considering how various purification techniques alter the most significant aspects of QD investigations and performance. Among these, I illustrate the gel permeation chromatography (GPC) approach that I helped to establish as a highly effective technique for nanoparticle purification. Finally, I delineate in several fundamental CdSe-based QD systems the capacity of isothermal titration calorimetry as a sensitive and precisely quantitative technique to directly probe reaction thermodynamics in organic phase. Even in cases where common spectroscopic techniques have been of limited use, ITC is employed to elucidate complex binding phenomena. Beginning with the highly reproducible GPC purification technique for a consistent QD starting material, this dissertation depicts my efforts to provide consistent equilibrium thermodynamic data for relevant QD surface chemistry interactions.

## PREFACE

Statement about body of works referred to first for which I am first author, followed by that addressing works for which I am not the [sole] first author:

The manuscript entitled “Purification Technologies for Colloidal Nanocrystals” is a review article published (*Chem. Commun.* **2017**, 53, 827-841) originally as a Feature Article in the themed collection: *Frontiers in Nanocrystal Surface Chemistry*, and appears as the bulk of Chapter 2 in this dissertation. Dr. Yi Shen and I contributed equally to this publication in every aspect as equally contributing primary authors. He and I worked very closely together from the moment I joined the Gretyak lab and on to publishing this article during his postdoctoral fellowship, specifically to establish gel permeation chromatography as a preparative purification method for nanocrystals; in many ways more suitable for numerous applications and systems in the colloidal semiconductor nanocrystal field.

The manuscript entitled “Non-spectroscopically Dependent Study of Neutral Amine Ligand Binding Interactions with CdSe Quantum Dots” with author list in order: M.Y. Gee, P.J. Pellechia and A.B. Gretyak; is to be submitted in an ACS journal, and comprises the latter half of Chapter 3 of this dissertation. I would like to acknowledge Dr. Rui Tan, relevantly in his work to further elucidate the best practices for applying selective ionic layer adhesion & reaction to QD core/shell synthesis (*Chem. Mater.*, **2015**, 27 (21), 7468–7480), out of which this manuscript content was borne. As we investigated the impacts of differently branched amines comprising the growth solvents for CdSe quantum dots, an ITC



study to determine the thermodynamic parameters associated with the trends we observed was initially intended as an ancillary measurement to that very elegant publication on isotropically engineered inorganic CdS shells. However, as additional analytical techniques seemed to adequately substantiate the hypothesis about amines and Cd-carboxylates competing for QD core surface sites – thereby influencing the precursor conversion of the shell material – Dr. Rui Tan strongly urged me to construct a separate manuscript that could uniquely rely on methods outside the exhausted spectroscopic studies pervasive throughout nanocrystal literature and to utilize ITC as the primary technique to resolve decades of ambiguity and inconsistency in the area of neutral ligand thermodynamic parameter values. He was instrumental in establishing a consistent synthetic procedure for very high quality phosphonate-capped CdSe core materials, and provided initial samples used to determine optimal ITC experimental parameters.

The manuscript entitled “Isothermal Titration Calorimetry Resolves Sequential Ligand Exchange and Association Reactions in Treatment of Oleate-capped CdSe QDs with Alkylphosphonic Acid” with author list in order: M.Y. Gee, Y. Shen, and A.B. Greytak; is to be submitted to a Wiley InterScience journal, and appears as the extensively reformatted bulk of Chapter 4 of this dissertation. A significant portion of the data for this project was acquired very early in my PhD program, but until now has lacked adequate data interpretation. I would like to acknowledge Dr. Yi Shen’s support and considerable contribution to sample preparation and experimental design toward the success of this research endeavor. Before year end, per the much-appreciated request of my Dissertation Committee Chair Dr. Mark Berg the latter two titles are to be submitted.

The manuscript entitled “Quantum Yield Regeneration: Influence of Neutral Ligand Binding on Photophysical Properties in Colloidal Core/Shell Quantum Dots” with author list in order: Y. Shen, R. Tan, M.Y. Gee and A.B. Greytak; was published (*ACS Nano*, **2015**, *9*, 3345-3359), and of which substantial references comprise the introduction in Chapter 3 of this dissertation. While I am solely responsible for the ITC portion of this manuscript, I would like to acknowledge the work of the first two authors in their roles to conceptualize and conduct the bulk of the quantum yield measurements and analyses; the synthetic work of Dr. Rui Tan who provided all of the core/shell quantum dots, and is primarily responsible for the photoluminescent lifetime measurements and analyses. Inasmuch, I have not included any direct reproduction or figure specifically pertaining to the lifetime analysis in this dissertation. I have discriminately included only that work and discussion from this manuscript to which I significantly contributed. A memo from my advisor and Major Professor Dr. Andrew Greytak was submitted to the Graduate School confirming as much.

Copyright Permissions are provided in the Appendix for all manuscripts mentioned in this section that have been published previously. There are two figures in this dissertation that have been modified from their original version in the manuscript entitled “Purification of Quantum Dots by Gel Permeation Chromatography and the Effect of Excess Ligands on Shell Growth and Ligand Exchange” with author list in order: Y. Shen, M.Y. Gee, R. Tan, P.J. Pellechia and A.B. Greytak; was published (*Chem. Mater.*, **2013**, *25*, 2838-2848). Again, I contributed equally with the first author in the design and experiments conducted to provide the data represented in those figures. I contributed to the writing of this manuscript as well, though not in equal capacity to the first author. Inception and conception of this research project is originally attributed to the first author Dr. Yi Shen.

## TABLE OF CONTENTS

Dedication.....	iii
Acknowledgements.....	iv
Abstract .....	v
Preface .....	vii
List of Tables .....	xii
List of Figures.....	xiii
Chapter 1: Introduction to Direct Investigations of Quantum Dot Surface Chemistry and Isothermal Titration Calorimetry .....	1
1.1 Introduction to colloidal semiconductor nanocrystal quantum dots.....	1
1.2 Impact of quantum dot surface chemistry .....	2
1.3 Typical spectroscopic techniques employed to characterize quantum dots.....	5
1.4 Introduction to isothermal titration calorimetry .....	11
1.5 Dissertation Overview .....	14
Chapter 2: A Review of Purification Technologies and Their Impact on Colloidal Semiconductor Nanocrystals.....	17
2.1 Introduction .....	17
2.2 Polarity-based purification techniques.....	19
2.3 Electrophoresis-based techniques .....	23
2.4 Size-based separation techniques .....	25
2.5 Purification and nanocrystal surface chemistry.....	36
2.6 Conclusion .....	43

Chapter 3: <i>Langmuir</i> Association of Neutral Ligands to CdSe Quantum Dots and Subsequent Effect on Photophysical Properties .....	45
3.1 Introduction .....	45
3.2 Spectroscopic investigation of reversible quantum yield regeneration in Cd-based core/shell quantum dots .....	48
3.3 Observing kinetic and thermodynamic contributions to resolve influence of neutral ligand relative binding strengths on quantum yield.....	55
3.4 Investigation of neutral amine ligand binding interactions with CdSe quantum dots via isothermal titration calorimetry .....	62
3.5 Conclusion .....	79
3.6 Materials & Methods .....	81
Chapter 4: Isothermal Titration Calorimetry Resolves Sequential Ligand Exchange and Association Reactions in CdSe Quantum Dots.....	90
4.1 Introduction.....	90
4.2 Experimental design for ITC applied to CdSe quantitative ligand exchange .....	93
4.3 Timetrace analysis toward separated heats isotherm .....	106
4.4 Variation in synthetic preparation for further investigation .....	120
4.5 Conclusion .....	129
4.6 Materials & Methods .....	131
References .....	135
Appendix A: Copyright Permissions.....	176

## LIST OF TABLES

Table 1.1 Common CdSe quantum dot synthetic descriptions.....	3
Table 3.1 Thermodynamic equilibrium parameters for amine association to CdSe TDPA ..	71
Table 3.2 Thermodynamic equilibrium parameters for amine association to aged CdSe TDPA .....	77
Table 3.3 Thermodynamic equilibrium parameters for amine association to CdSe TDPA approximated from aged $\Delta H$ .....	78
Table 4.1 Thermodynamic equilibrium parameters for oleate exchange with ODPa .....	115
Table 4.2 Q test for ‘Gross Outliers,’ on Site1 for ~2x initial CdSe OA <sup>-</sup> .....	115
Table 4.3 Characteristic thermodynamic equilibrium parameters for OA exchange with ODPa on Rapid Quench quantum dots comparing Toluene GPC vs THF GPC purification solvent .....	127
Table 4.4 Brandt’s c parameter for each titration’s thermodynamic profile; c < 10 signifying $N_2$ and $\Delta H_2$ are not independently constrained.....	128

## LIST OF FIGURES

Figure 1.1 Representative carboxylate-CdSe UV-Visible absorption spectrum depicting quantum confinement .....	6
Figure 1.2 Powder X-ray diffraction for two major morphologies of CdSe quantum dots.....	8
Figure 1.3 Thermogram and integrated isotherm for standard ITC titration of $\text{Ca}^{2+}$ into EDTA as standard titration experiment example .....	12
Figure 1.4 Thermograms for CdSe ligand exchange with photo of GPC purification on ligand-exchanged CdSe QDs.....	16
Figure 2.1 Schematic of unpurified and subsequently purified colloidal QDs .....	18
Figure 2.2 Comparison of CdSe QDs purified by either Precipitation/Redissolution or toluene gel permeation chromatography .....	34
Figure 3.1 Absolute quantum yield of alloy-shell CdSe/CdZnS after 1×PR.....	49
Figure 3.2 Representative $^{31}\text{P}$ NMR, $^1\text{H}$ NMR, absorption and emission profiles of core/shell CdSe/CdZnS before after GPC purification.....	50
Figure 3.3 Relative quantum yield of thin alloy-shell CdSe/CdZnS as putative ligands reintroduced compared to GPC purified stock .....	52
Figure 3.4 Time evolution of quantum yield regeneration for thin alloy-shell CdSe/CdZnS upon reintroduction of TOP or TOPO ligands.....	56
Figure 3.5 Normalized absorption and emission of thin alloy-shell CdSe/CdZnS upon excess reintroduction of TOP or TOPO.....	57
Figure 3.6 ITC thermograms and isotherms of thin alloy-shell CdSe/CdZnS titrated with TOPO, Oleylamine and TOP .....	60
Figure 3.7 Schematic of amines titrated to core CdSe TDPA.....	66
Figure 3.8 Quantitative $^{31}\text{P}$ NMR of core CdSe TDPA for ligand population with triphenyl phosphate internal standard .....	67
Figure 3.9 ITC isotherm traces comparing Oleylamine, Decylamine and Trihexylamine association to CdSe TDPA.....	69

Figure 3.10 Thermograms for control titrations amine–THF solvent and THF–THF .....	70
Figure 3.11 Normalized absorption and photoluminescence of CdSe TDPA after THF GPC and after ITC experiment .....	73
Figure 3.12 ITC traces of repeated Oleylamine and Decylamine titrations compared to after desorption of initial Cd-phosphonate by adventitious solvent .....	77
Figure 4.1 Vertically offset UV-Vis absorption spectra normalized at 1 <sup>st</sup> excitonic peak and through course of titration reaction .....	94
Figure 4.2 Quantitative <sup>1</sup> H NMR spectra of GPC-purified CdSe OA <sup>-</sup> in both Toluene-d <sub>8</sub> and Tetrahydrofuran-d <sub>8</sub> .....	96
Figure 4.3 Reference/Control raw heat titration thermograms that did not contribute significant heat .....	97
Figure 4.4 Reference/Control raw heat titration thermogram for ODPA–THF that did contribute significant to subtract for exchange reaction titration .....	99
Figure 4.5 Representative raw heat titration thermogram of ODPA titrated into CdSe OA <sup>-</sup> with sequential exchange then association processes highlighted .....	100
Figure 4.6 Repeated raw heat titration thermograms for ODPA–CdSe OA <sup>-</sup> : raw without baseline correction and baseline corrected thermogram with model waves indicated .....	101
Figure 4.7 Schematic for proposed sequential exchange and association reaction .....	102
Figure 4.8 Olefin region for quantitative <sup>1</sup> H NMR ODPA–CdSe OA <sup>-</sup> titration .....	103
Figure 4.9 Quantitative <sup>31</sup> P { <sup>1</sup> H} NMR parallel titration for ODPA–CdSe OA <sup>-</sup> after THF GPC purification in THF-d <sub>8</sub> .....	104
Figure 4.10 Comparison of ODPA–THF control titration with ODPA–CdSe OA <sup>-</sup> exchange reaction titration to demonstrate ITC instrument response function (IRF) consideration ..	107
Figure 4.11 Representative timetrace analysis fundamental waveform components .....	109
Figure 4.12 Representative isotherms depicting separated heats and effectively sequential two independent types of sites model fits .....	111
Figure 4.13 Powder XRD for CdSe QDs before and after ODPA ligand exchange .....	118
Figure 4.14 Quenching trajectories for Standard (Std) and Rapid Quench (RQ) CdSe OA <sup>-</sup> sample synthetic comparison .....	121
Figure 4.15 Optical characterization of Std and RQ CdSe QDs purified via either Toluene or THF GPC including UV-Vis absorption, emission, and TEM .....	122

Figure 4.16 Comparison of Standard (Std) vs Rapid Quench (RQ) raw heat thermograms of Toluene GPC-purified CdSe OA <sup>-</sup> QDs .....	124
Figure 4.17 Comparison of Standard (Std) vs Rapid Quench (RQ) raw heat thermograms of Toluene vs THF GPC-purified CdSe OA <sup>-</sup> QDs for purification comparison.....	125
Figure 4.18 Overlays of Rapid Quench QD raw heat thermograms purified by either Toluene GPC or THF GPC.....	126
Figure 4.19 Bar chart for Rapid Quench QD exchange parameter statistics.....	129



## CHAPTER 1

# INTRODUCTION TO DIRECT INVESTIGATIONS OF QUANTUM DOT SURFACE CHEMISTRY AND ISOTHERMAL TITRATION CALORIMETRY

### 1.1 Introduction to colloidal semiconductor nanocrystal quantum dots

Colloidal semiconductor quantum dots (QDs) are roughly spherical, direct bandgap, nanometer sized portions of bulk semiconductor crystals suspended in solution. As-synthesized QDs are most commonly comprised of an inorganic crystalline core capped by an organic ligand surfactant layer that dictates the photophysical properties of the QD.<sup>1-3</sup> Characterized by broad absorption cross sections and narrow size-tunable emission spectra, QDs also exhibit high molar extinction coefficients and extraordinary photo-stability when compared to organic fluorophores.<sup>4-6</sup> The size of these particles approaches the length scale of their exciton Bohr radius in the nanocrystals with diameters ranging from  $\sim 1$ -10 nm, and so quantum confinement effects are apparent, following the “Particle-in-a-Box” model wherein the delocalized electron (exciton) represents the “particle” and the QD is the “box.” This phenomenon is most clearly depicted as larger QDs emit at longer wavelengths.<sup>7-9</sup> Due to these unique optoelectronic properties, QDs are intensely investigated and developed toward applications that would benefit from the energy and charge transfer that can be engineered with these nanomaterials. II-VI semiconductor QDs, such as Cd-based colloidal nanoparticles and nanocrystals (NCs) alike persist as the benchmark system by which new emerging materials are investigated.<sup>10,11</sup>

## 1.2 Impact of quantum dot surface chemistry

Most notably, QDs have a high surface-to-volume ratio with rather labile electronic structures situated between the confined bulk-like, inorganic core and the surface-adsorbing ligands.<sup>1,5,12</sup> The composition and passivation afforded by surface ligand interactions strongly influence exciton radiative and nonradiative pathways, which dictate QD application in either charge transport or biosensing. At the surface of the inorganic core termination of the semiconductor lattice is frequently incompletely passivated, leaving dangling bonds as surface defects. This interface between the inorganic core and incomplete ligand surfactant layer consequently contains localized states that can act as traps.<sup>12</sup> Trap state emission generally originates from smaller spacing between energy levels below the QD conduction band, is significantly red-shifted, and in some instances more intense than band edge emission.<sup>13</sup> As QD size is reduced, the energy gap is increased as well as influence of (undercoordinated) surface atom properties.<sup>14</sup>

A major objective is that excitonic decay pathways be tuned to achieve optimal dissociation of charge carriers or radiative recombination, depending on the desired optoelectronic application. Therefore, understanding QD surface chemistry is paramount. An ensemble of QDs is inherently heterogeneous in particle radii, quantity of surface ions/undercoordinated atoms, ratio of surface cation-to-anion enrichment, and amount and of bound ligands.<sup>1,15</sup> Synthetic techniques for high quality, nearly monodisperse Cd-chalcogenide – especially CdSe – QDs employ a combination of fatty acids, amines, phosphines, and phosphonic acids with long aliphatic chains as their ligand surfactant layer.<sup>16–18</sup> Table 1.1 displays a few common synthetic conditions, especially those of which I have personally researched.

**Table 1.1** Common CdSe quantum dot synthetic descriptions

CRYSTAL STRUCTURE	ZINC BLENDE (CUBIC)		WURTZITE (HEXAGONAL)	
STANDARD PROCEDURE	Hot Injection	Non injection	Hot Injection	Rapid Injection
CADMIUM PRECURSOR	$\text{Cd}(\text{COO})_2$	$\text{Cd}(\text{COO})_2$	$\text{Cd}(\text{TDPA})_2$	$\text{Cd}(\text{COO})_2$
SELENIUM PRECURSOR	TOPSe/Se- suspension (ODE)	$\text{SeO}_2$ /Se- suspension (ODE)	TOPSe	Se-Amine/Se- suspension (ODE)/ Se-Phosphine
NUCLEATION TEMP	270°C	230-240°C	350°C	Room temp-300°C
REACTION SOLVENT	ODE	ODE	TOP:TOPO (1:1)	ODE/Phosphine/ Alkylamine
FURTHER OLEIC ACID DOSE	No	Yes	Yes	No
POSSIBLE SURFACTANT	Carboxylate	Oleate/ Carboxylate	mono-Phosphonate/ Phosphonate anhydride/ Carboxylate	Unclear
SIZE VARIATION FEASIBILITY	Aliphatic Chain Length, Time; DIFFICULT	Aliphatic Chain Length, Time; RELATIVE	Aliphatic Chain Length, Time; RELATIVE	Aliphatic Chain Length, Temperature; MODERATE

The synthetic organic ligands are critical for providing surface passivation and steric stability; however, after synthesis these insulating ligands hinder conduction or are not soluble in aqueous media. Size and shape variation can render uniquely tunable optoelectronic QD properties, but ligand exchange (or some other route for surface modification) is almost universally required in order to utilize and better control their photophysical properties for any rational application. Areas of concern for QD photophysical properties are band-edge emission quenching/oxidation, PL lifetimes, non/radiative emission pathways. Photovoltaic applications require long radiative lifetimes achieved by enhancing exciton dissociation relative to recombination or multiple exciton generation, and strong coupling to conductive substrates; light emitting diode devices require shorter radiative lifetimes optimized by increased passivation, decreased interparticle distance and weak chemical coupling to their external environment; and bio-labelling applications

require distances between donor and acceptor molecules to be optimized depending on specific effects of local environment on excited state relaxation pathways.<sup>10,19</sup>

A number of surface studies as well as theoretical computations verify that ligands tend to bind preferentially to Cd surface atoms, leaving the Se unpassivated and more subject to oxidation.<sup>20–22</sup> Knowles et al. reported on certain factors that heavily influence photoinduced charge separation interpreted through Marcus Theory, while considering complexities in electronic coupling, reorganization energy and driving force parameters.<sup>23</sup> A number of trapping events, elucidate the complications these trapping events can pose to carrier transfer dynamics, as well as how trapping of either the electron or hole within an orbital uncoupled from its delocalized carrier quenches band edge photoluminescence (PL). Photoinduced electron or hole transfer rates can be separated, but ligands may also be engineered to selectively sequester holes from the valence band of the QD to their HOMO, (for example in phenyldithiocarbamate).<sup>24</sup> Buckley et al. published a study on various photophysical properties influenced by hole transfer to thiol, selenol and tellurol ligands.<sup>25</sup> It has been well established that thiols extract holes from CdSe surface by creating midgap hole trap states, reducing wavefunction overlap with the complementary electrons, and so induce substantial PL quenching. Aromatic chalcogenol ligands are able to both extract and stabilize holes and provide greater stability against oxidative processes than the typical thiol ligands. While analogous to strongly binding thiol ligands, the selenol and tellurol ligands were found to have more substantial influence on the driving force for hole transfer.

Contrary to the hole sequestering and PL quenching nature of the thiol and aromatic ligands, ligands functionalized with an amine group have been shown in numerous cases to enhance PL.<sup>10</sup> In the case of primary amines, generally the QD valence band lies above the

amine HOMO, thus preventing hole transfer.<sup>1</sup> A very common, neutral, datively binding ligand that has frequently been employed to treat CdSe QDs is pyridine. Typically pyridine has been applied as a weakly binding ligand to replace native ligands, and then been exchanged for subsequent ligands with a particularly desired functionality.<sup>26</sup> Although often employed as this intermediate ligand cap for further ligand exchange, pyridine is not able to quantitatively displace native CdSe QD ligands, and does not provide adequate stability toward aggregation upon multiple treatments.<sup>15</sup> Thiocyanate, inorganic ions (i.e. chloride and sulfide), and some metal ions (i.e.  $\text{Ca}^{2+}$  and  $\text{Mn}^{2+}$ ) as links between anionic inorganic ligands bound covalently to surface  $\text{Cd}^{2+}$  ions have been studied in ligand exchanges; which enable conductivity and carrier mobility enhancement through short interparticle separations, which are optimal for field effect transistor, photodetector, magnetization, and electrocatalytic applications.<sup>27,28</sup> Bernt et al. reported photocatalytic cleavage of both 1,1-dithiooxalate and its ester to the production of carbon disulfide (which has some therapeutic benefits) and carbon dioxide as mediated by CdSe QDs.<sup>29</sup> Polymers, proteins, and some small molecules (i.e. zwitterionic thiols and functionalized polyethylene glycols) have been utilized in direct ligand exchange or encapsulation with the QD surface in order to provide biocompatibility while maintaining passivation.<sup>30–32</sup>

### **1.3 Typical spectroscopic techniques employed to characterize quantum dots**

The most facile and globally employed methods to monitor effects on QD optical properties are band edge absorption and emission; narrow, well-resolved, consistent features indicate the quality of sample size and monodispersity; time-resolved PL decay as exponential components indicate probability of radiative and nonradiative pathways; and PL quantum yield (QY) to determine sample brightness and the efficiency of exciton recombination.

Because the electronic transitions of QDs are size dependent, the absorption (HWHM) and PL emission (FWHM) spectra line widths are routinely employed to indicate size distribution in QD samples.<sup>9,33</sup>

While this hopefully provides a thorough picture of the desire to optimize optoelectronic properties of colloidal semiconductor QDs, this is not an exhaustive description of the surface functionalities employed to render these materials effective charge

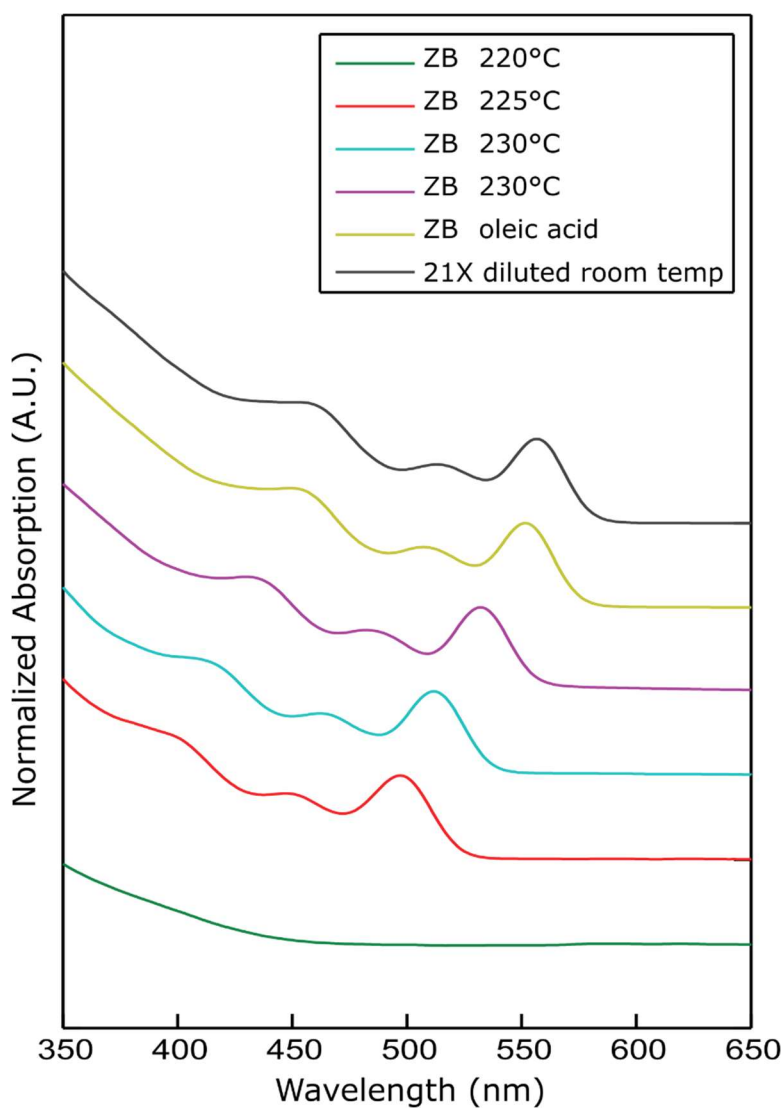


**Figure 1.1** Waterfall UV-visible absorption of carboxylate-ligated CdSe, demonstrating QD size evolution over time.

carriers or labelling/targeting devices. The aforementioned examples of ligands interacting with the QD surface have some similarities for which a few generalizations can be stated. Except in the case of ions ligated to and between the QD surfaces, the polar headgroups that bind or coordinate to the QD surface, particularly during NC synthesis contain oxygen, nitrogen, phosphorus and/or sulfur. QD surface coordination (in organic environments) occurs by three proposed motifs following the Covalent Bond Classification: anionic ligands that yield net neutral surfaces by covalently binding to the metal cations; dative binding Lewis bases; or neutral Lewis acids – referred to as X-type, L-type and Z-type ligands respectively.<sup>34–36</sup>

Although current CdSe QD synthetic techniques yield high quality and nearly monodisperse samples, QDs may have highly crystalline cores with lattice terminated surface defects. QDs inherently have different facets, which are most accurately described as having different types of binding sites with various binding affinities. The <10nm diameter regime might prove difficult to probe beyond computational methods;<sup>22,37</sup> however, investigating differences in thermodynamics in Wurtzite versus Zinc Blende QD structures could provide fundamental insight to ligand interactions with possibly preferred facets (e.g. it has been established that CdSe nanorods may be synthesized as extensions of Wurtzite nanocrystals extended from the  $c$  axis.<sup>38–40</sup> X-ray Diffraction (XRD) is commonly used to verify QD crystal structure because the features are easily distinguished, as demonstrated below in Figure 1.2.

Nuclear Magnetic Resonance (NMR) spectroscopy is another technique extensively applied to probe NC surface chemistry.<sup>41–43</sup> Most nuclei possess both a magnetic moment  $\mu$  and intrinsic angular momentum  $P$  which are vector quantities proportional to one another for isotopes of each element by the magnetogyric ratio  $\gamma$ . Owing to this fact, an isotope's

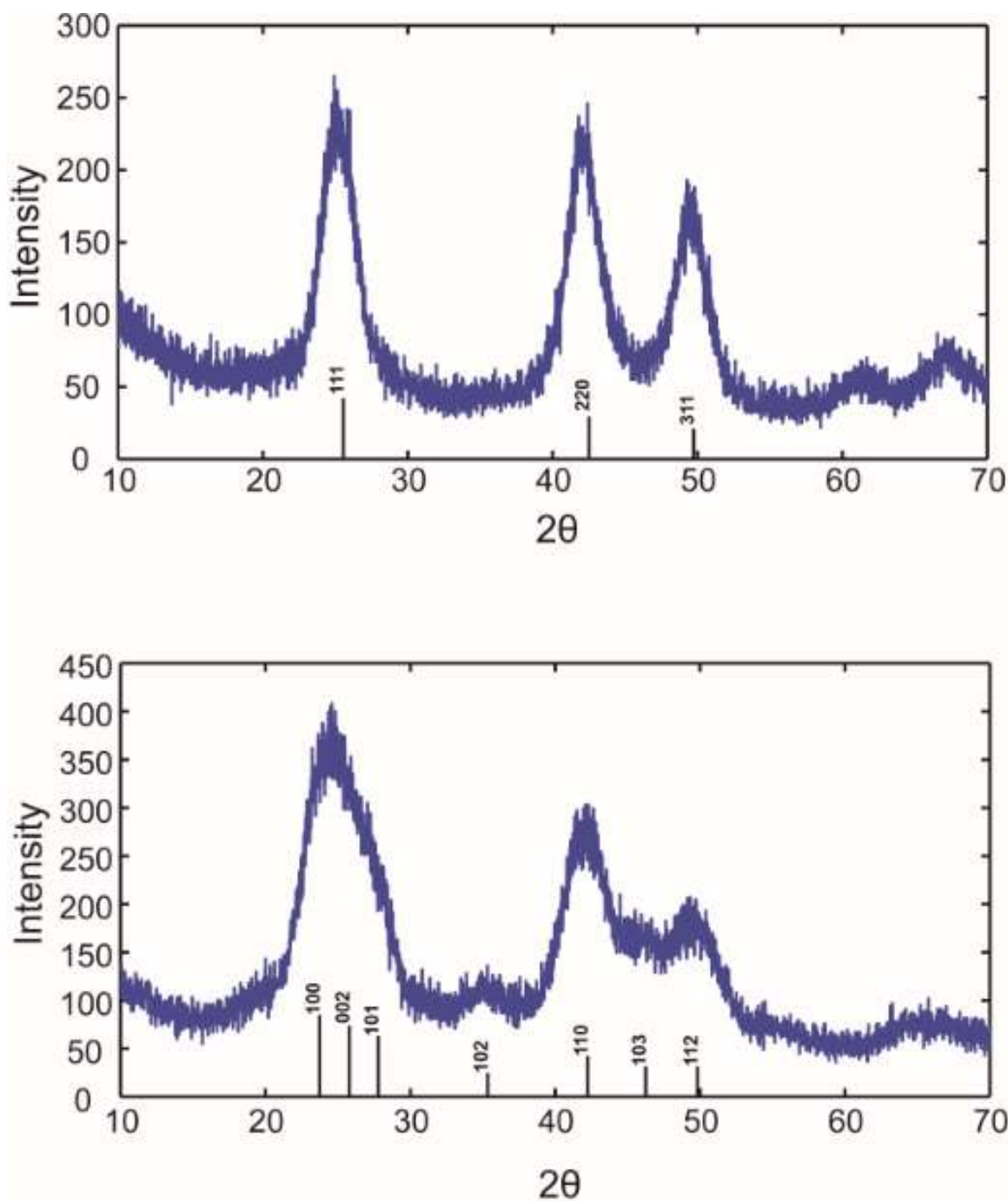


**Figure 1.2** Powder X-Ray Diffraction patterns of Zinc Blende (top) and Wurtzite (bottom) CdSe QDs, each with labeled vertical lines to indicate standard Bragg reflection peaks in the respective bulk material.



behavior can be manipulated under a magnetic field. Within an NMR experiment, nuclei are present at a macroscopic level and their population distribution among different energy states is described by Boltzmann statistics at thermal equilibrium. Transitions between energy levels are induced when the nuclei are irradiated with a magnetic field of an appropriate quantum energy. NMR spectra are shown as chemical shifts of relevant nuclei calibrated to peak positions of residual solvent. The chemical shift reflects how a particular nucleus is affected by its environment, and the resonance condition necessary to produce an NMR transition signal is:<sup>44</sup>

$$\nu_1 = \gamma/2\pi (1 - \sigma) B_0 \quad (1)$$

The aforementioned quantum energy is effectively an electromagnetic wave at a certain frequency  $\nu$ . The resonance frequency  $\nu_1$  and the magnetic flux density  $B_0$  are proportional and a shielding factor  $(1 - \sigma)$  that takes into account the electrons/other surrounding atoms, which cause chemically non-equivalent nuclei to yield different NMR resonance signals. The result of chemical bonds within molecules in the context of NMR is that nuclear spins display interactions between nuclei and local electrons in indirect spin-spin coupling. This is referred to as scalar or J-coupling and provides information on bond distances and angles. Interactions of chemical bonds within molecules determine multiplicity, magnitude and the sign of the coupling constant for adjacent nuclei that are magnetically nonequivalent in the NMR spectra.

In two-dimensional NMR spectroscopy intensities on two frequency axes are plotted to represent the chemical shifts associated with one of two-time variables. These time variables arise from a sequence of applied radio frequency (RF) pulses with specified delay

periods that occur as a four-step acquisition process: i) preparation period; ii) evolution period; iii) mixing period; and iv) detection period, wherein the free induction delay (FID) signal is observed as a function of time and subsequently Fourier transformed.<sup>44</sup> Whereas 1D NMR involves a preparation and detection sequence; the evolution and mixing periods allow nuclear spins to freely precess (or rotate), followed by additional RF pulses that induce the transfer of magnetization coherence from the first nuclei to the second. 2D NMR techniques (i.e. Correlated Spectroscopy, COSY) that display the results of a magnetization transfer between nuclei of the same type, which are correlated through J-coupling, can offer detailed descriptions of frequencies for single isotopes. Chemically bonded correlations can also be monitored for heteronuclear couplings wherein magnetization is transferred from an easily detectable nucleus (usually  $^1\text{H}$ ) to an insensitive nucleus with a small  $\gamma$  value. 2D NMR experiments can also be performed when the magnetization is transferred between nuclei that do not exhibit scalar coupling.

Spin-lattice relaxation as pertaining to NC surface chemistry is requisite in order to accurately probe ligand dynamics on the QD surfaces via NMR. Aside from expected differences in ligand population, the different solvents have different polarities and for example, comparison of olefin protons versus terminal methyl protons in different solvents for CdSe QDs ligated with oleates should require statistically different  $T_1$  relaxation times, which determines the rate at which the magnetized component establishes thermodynamic equilibrium.<sup>41</sup>  $T_1$  data appears as an exponentially increasing trajectory that plateaus as nuclei recover equilibrium, and resolvable exponential plots delineate structural features of adsorbed ligands in addition to providing distinctive relaxation times necessary for accurate ligand population analysis.<sup>45</sup>  $T_2$  relaxation (spin-spin) dynamics have recently been

investigated for QD systems, as the impact of solvent has been realized as a substantial driver for photophysical performance.<sup>43</sup>

Ultimately mechanistic studies of the binding thermodynamics between the incoming ligands and natively-capped QD are a crucial part of better understanding surface chemistry toward QD applications. The scarcity of reported quantitative descriptions of ligand binding strength dramatically hinders our ability to optimize the relationships between QD surface passivation, PL quantum yield and other desired photophysical properties.

#### **1.4 Introduction to isothermal titration calorimetry**

ITC is most often used in biochemistry and designed for well-defined aqueous systems.<sup>46,47</sup> Some investigations of synthetic nanoparticle interactions,<sup>48</sup> a very few CdSe core/shell QD interactions with representative proteins,<sup>49</sup> and even fewer reports on CdSe QDs interacting with a coordinating ligand used in synthesis<sup>50,51</sup> have utilized ITC to acquire binding equilibria. A well-respected professor in the field once cogitated that essentially this could not be done with ITC. This technique is a quantitative method of extracting thermodynamic data from various chemical reactions; usually as a smaller molecule binding to a larger (macro)molecule in solution. The fundamental thermodynamic relationship expressed as  $\Delta G^\circ = \Delta H^\circ - T\Delta S^\circ$  allows ITC to directly quantify temperature dependent changes in binding enthalpy ( $\Delta H^\circ$ ) and binding stoichiometry ( $n$ ) of the interactions between different species in the solution.<sup>47</sup> From these measurements a binding isotherm is generated, which allows simultaneous determination of the system's binding constant ( $K$ ); Gibbs free energy ( $\Delta G^\circ$ ); entropy ( $\Delta S^\circ$ ) of binding; and heat capacity ( $\Delta C_p^\circ$ ) as binding occurs in temperature dependent  $\Delta H$  studies.<sup>46</sup> The height of the isotherm determines  $\Delta H$ , and the width of the change in slope of the integrated heat determines the binding constant ( $K$ ). An example of a

standard instrument calibration titration reaction thermogram and isotherm is shown in Figure 1.3. Once a raw heat flow and an integrated isotherm are generated from the titration, the direction of the peaks and shape of the curve allow qualitative analysis of whether the reaction process was enthalpy or entropy driven. Interactive forces contributing to the

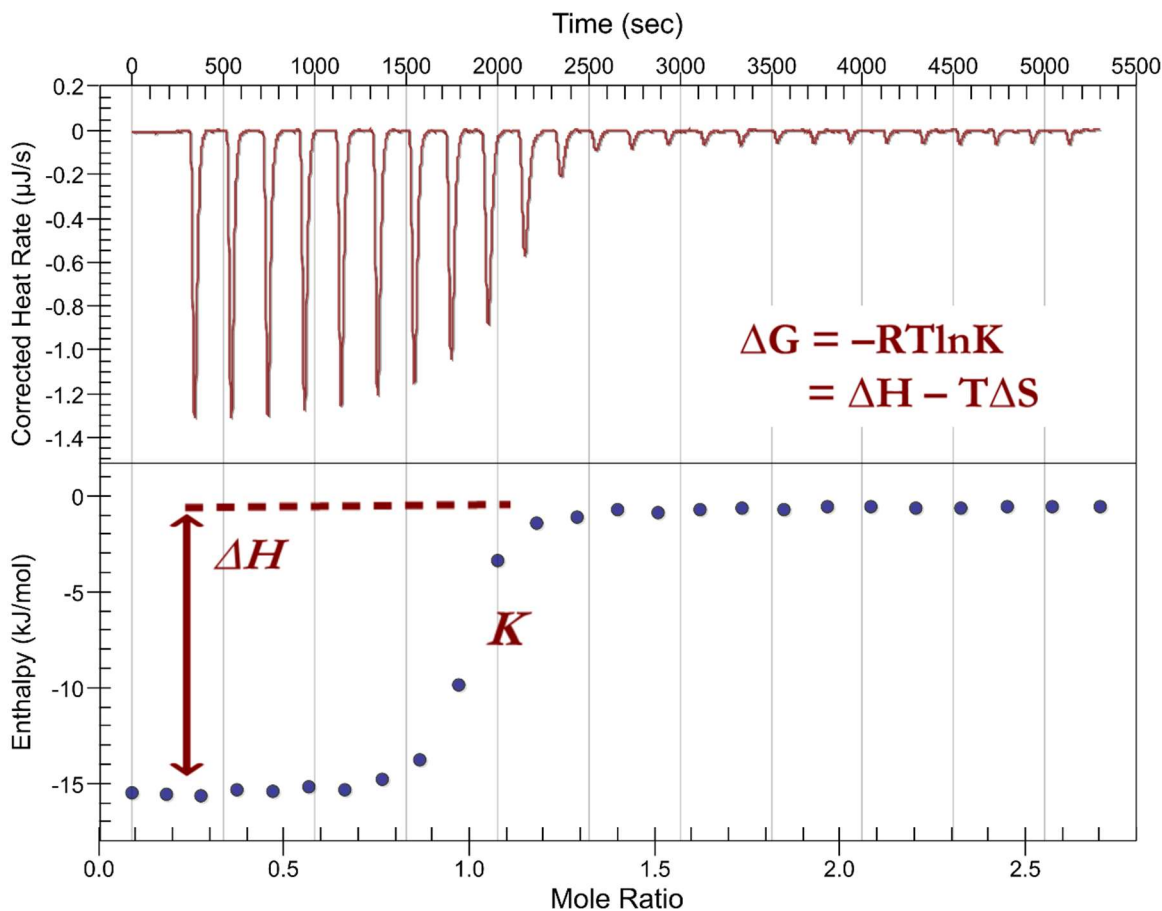


**Figure 1.3** Raw heat thermogram (top) and integrated isotherm (bottom). Thermodynamic parameter relationships are indicated for this standard  $\text{Ca}^{2+}$  into EDTA titration.

reaction can then be resolved upon characterization of reactants and product species. Exotherms are distinguished by negative trends in heat evolution, indicate enthalpy-driven reactions, and usually involve hydrogen-bonding, ionic and/or electrostatic interactions.<sup>52</sup> Conversely, endotherms indicate entropy-driven reactions involving possible hydrophobic

and/or ionic interactions.<sup>53</sup> Perhaps the greatest advantage of ITC is its ability to directly determine thermodynamic parameters of reactions. Inasmuch we can extract the apparent equilibrium constants  $K$ , changes in enthalpy  $\Delta H$ , numbers of sites  $N$  simultaneously.

There are several challenges specifically associated with ITC and QD-ligand interactions. By design titration calorimeters measure the heat associated with every process during the reaction,<sup>46</sup> especially competing equilibria intrinsic to QD ligand interactions:

$$\Delta q_{\text{corrected}} = q_{\text{rxn}} - q_{\text{dil,QD}} - q_{\text{dil,ligand}} + q_{\text{solvent blank}} \quad (2)$$

Therefore, a common [non-aqueous] solvent for both QDs and new ligands is preferable. Some ITC instrumentation is extremely sensitive to external environmental (temperature) changes, as well as moisture and air within the reactants. Very “clean” QDs that maintain colloidal stability so as not to aggregate during the titration are requisite. Characterization of the ligand exchange after the titration can be challenging. A reasonable concentration of the QDs loaded in the sample cell is relative to the magnitude of the binding constant, described by the so-called Brandt’s or Wiseman “ $c$ ” parameter.<sup>46</sup>

Although implemented to describe previous Cd-chalcogenide core QD-ligand ITC experiments,<sup>50,51,53</sup> it is highly unlikely that a 1:1 independent site model is sufficient to adequately describe all components of the QD-ligand system. QD surfaces present at least two distinct binding sites that interact with X-type and L-type ligands.<sup>54</sup> The independent site model also assumes the same intrinsic affinity for ligands associated with non-interacting sites.<sup>50</sup> This assumption is also unlikely considering the steric interactions of the native ligands, which prevent the QD from being completely passivated upon synthesis. A more appropriate analysis of ITC data requires consideration of cooperativity for heterotropic interaction between ligands, multiple binding sites, and a model that can accommodate

entropic ligand-ligand dynamics to further elucidate possible binding site overlap and interactions between neighboring ligands.<sup>55</sup> However there is a nontrivial complexity in deconvoluting heterogeneous ligands interacting with two binding sites, and an example of three types of binding sites on a macromolecule of repeating units.<sup>56,57</sup> In fact, there exist numerous models that could conceivably describe the thermodynamics for nanocrystal surface reaction isotherms, especially polynomial fitting; however without establishing a physical/chemical relevance to model parameters, the more advanced fitting has not precluded ambiguity.

## **1.5 Dissertation overview**

In order to effectively influence trapping states and PL quantum yield, ligand exchange or any other conceivable nanocrystal surface modifications that are employed researchers must take into account the original environment of the QD surface and how that environment will be perturbed. Chapter 2 presents a thorough review of typical purification technologies applied to colloidal nanocrystal as well as begin to address the effects purification (i.e. sample preparation) can have on resulting nanomaterial properties. Thoroughly understanding the initial ligand binding environment on the QD surface allows manipulating the initial state into rationally designed final QD states with appropriate metrics. The necessary reactions and “best” photophysical properties to accomplish desired functionalities in the final QD surface chemistry must be considered before subjecting the QDs to any surface treatments. Such consideration includes the curvature of the QD surface, which will increase as size decreases; solvent interactions; surface atom enrichment; and binding affinities of the native ligands versus new, incoming ligands. Effects of steric hindrance in the native bulky aliphatic chain and overall surface area at which sites are available to bind drive Cd surface enrichment as

well as ligand disorder are factors that will dictate surface reaction chemistry.<sup>1,58,59</sup> The first half of Chapter 3 will closely examine the impact of purification on NC quantum yield.<sup>60</sup> A number of studies have additionally demonstrated that ligands coordinated to the QD surface interact in a dynamic association-dissociation, which is heavily influenced by the solvent polarity and apparent equilibrium with ligands free in solution.<sup>1,42,61</sup> Products of QD surface modification must be either kinetically stable or able to reach equilibrium with their solvent/environment in order to fully probe the effects of applied surface treatments. The latter half of Chapter 3 will examine a fundamental surface chemistry interaction, utilizing ITC to render thermodynamic parameters that have historically been probed with various spectroscopic techniques though remain ambiguous. The final chapter of this dissertation will utilize both the gel permeation chromatography (GPC) purification method,<sup>62</sup> which I helped to establish as a robust purification technique for colloidal semiconductor nanocrystals, and ITC to investigate an irreversible reaction that has garnered considerable focus in the NC field<sup>63,64</sup> with attentions refocusing on elucidating nanoparticle surface chemistry. Figure 1.4 demonstrates thermograms extracted via ITC for this reaction and the post-quantitative exchange GPC purification that allowed me to unambiguously identify the sequential ligand exchange and association reactions for which equilibrium thermodynamic parameters were provided.

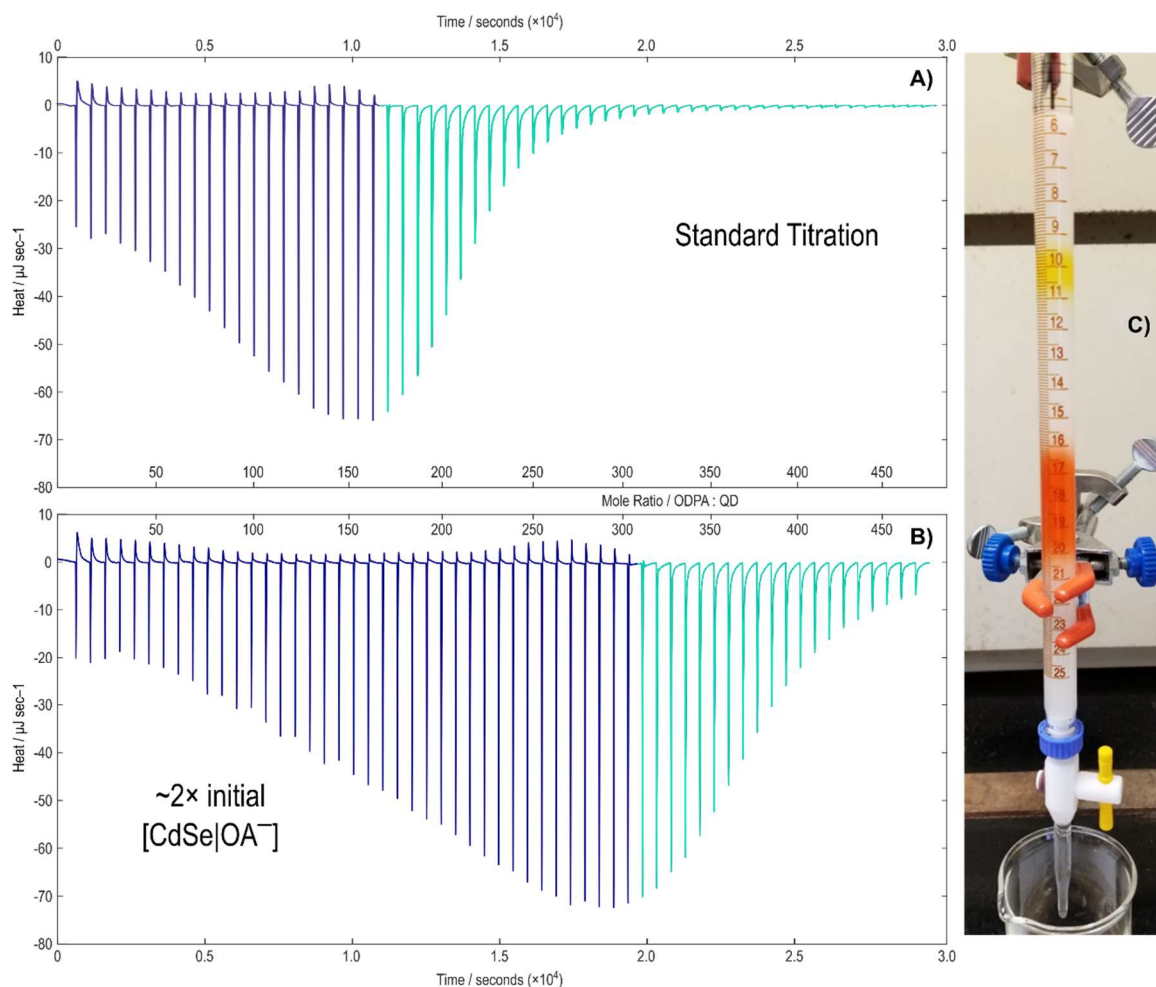


**Figure 1.4** Thermograms for a sequential ligand exchange and association reaction between an incoming phosphonic acid ligand that displaced the native carboxylate ligand on CdSe quantum dots (A-B). The navy and teal shading on the ITC thermograms indicate the exchange and association processes respectively. The ITC titrations and subsequent modeling discussed in Chapter 4 attest to the capacity of ITC to accommodate different solution concentrations that render typical spectroscopic investigations difficult or ambiguous. The photo in panel (C) demonstrates the capacity of GPC purification to maintain colloidal stability in surface-modified quantum dots in organic solvent. The yellow band is a ferrocene  $^1\text{H}$  NMR internal standard being separated from the orange band of ligand-exchanged CdSe quantum dots.



## CHAPTER 2

### A REVIEW OF PURIFICATION TECHNOLOGIES AND THEIR IMPACT ON COLLOIDAL SEMICONDUCTOR NANOCRYSTALS

#### 2.1 Introduction

Nanocrystals (NCs) in many forms and compositions including metals, semiconductors, and metal oxides have been extensively studied in the past several decades. Numerous studies have shown that these emerging materials can be used in a wide range of applications from imaging and display to catalysis and solar cells.<sup>3,65–68</sup> In order to better understand the properties of NC samples and to speed the commercial development of these materials with confidence, recent studies have focused on precise control of the material structure including particle morphology, polydispersity and ligand population.<sup>69–71</sup> Synthetic procedures for the highest quality NCs frequently use an excess of surface-passivating ligands or surfactants to maintain the colloidal stability of the particles during growth and influence the NC morphology that is achieved. However, these excess ligands, as well as the byproducts generated by decomposition of reagent compounds remain in the crude product solution. Additionally, the solvent that is selected for synthesis is rarely the same as the medium into which the NCs will be placed for physical property measurements or applications. Accordingly, effective means for isolating nanomaterials from solution-phase mixtures are required. The most common purification procedure for nanoparticles, especially quantum dots (QDs) entails precipitation and redissolution (the PR method). In this procedure,

addition of a miscible solvent in which the nanoparticles are poorly soluble (an anti-solvent) causes flocculation. The resulting flocculated nanoparticles precipitate rapidly (frequently accelerated by centrifugation) and can then be redissolved in a fresh solvent.

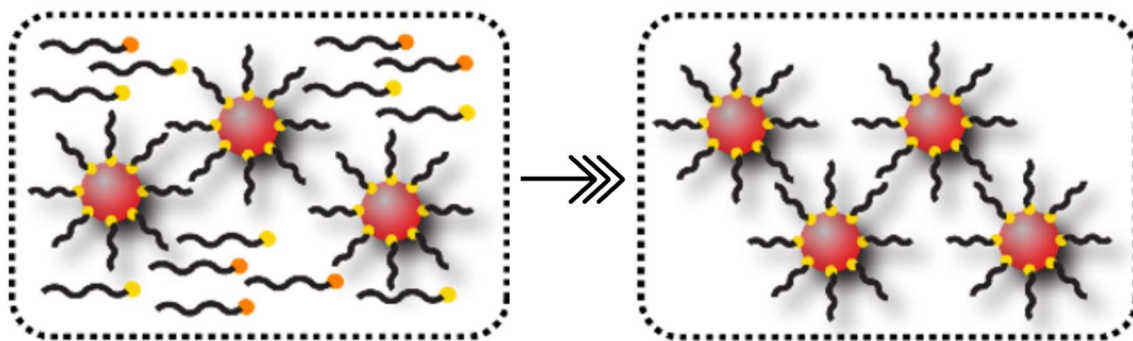


**Figure 2.1** Schematic of colloidal nanoparticles in solution initially with various impurities (e.g. solvent, unreacted precursors, weakly interacting and excess ligands; left), then undergoing purification whereupon they are left with only strongly adsorbed ligands adhered to their surfaces (right).

A challenge for any colloidal NC purification approach is that surface ligands can be subject to dynamic exchange between NC-bound and free-solution forms on experimental timescales; as a result, the actual surface may be a function of both the amounts and types of potential ligands that are present, and the solvent.<sup>3</sup> At the same time, residual impurities can affect shell growth and ligand exchange steps that are often required for NC end uses.<sup>62,72</sup> An effective means of isolating NC samples with well-defined properties is thus an important requirement for controlled NC synthesis and surface chemistry. While convenient, purification by PR entails several limitations that have been noted in studies of QDs.<sup>73,74</sup> As a result, there is increasing interest in alternative purification techniques, and some established techniques have shown performance that is comparable to or better than the PR method.

This chapter presents a review of the current status of NC purification. Previous reviews have examined some of the methods described, especially for separating or refining samples composed of several types of nanoparticles.<sup>75</sup> In a few cases, a unique physical response of the material can be used for purification, such as purification of iron oxide nanoparticles by differential magnetic catch and release.<sup>76</sup> More generally, common purification methods can be grouped based on the fundamental physical property by which separation is achieved: namely polarity-based techniques, electrophoresis-based techniques, and size-based techniques. These techniques are generally applicable to a wide variety of nanoparticles including inorganic semiconductors, metals, metal oxides, and carbon dots. Recently, increasing attention has been brought to the role of the surface in controlling photoluminescence (PL),<sup>42,60,77,78</sup> redox potentials,<sup>79</sup> and carrier trapping<sup>80</sup> in QDs. Additionally, current priorities in the field are to establish a quantitative description of ligand binding and exchange,<sup>81,82</sup> which requires well-defined initial and final states; and to extend the success with “classic” materials such as binary chalcogenides to new compositions, including those that are immune to the health and environmental sensitivity of Pb and Cd.<sup>83–</sup>  
<sup>85</sup> It will be important to consider the surface chemistry of these new compositions as well.

## **2.2 Polarity-based purification techniques**

### **2.2.1 Precipitation and redissolution**

Since the development of QD syntheses in either aqueous solution<sup>86</sup> or high-boiling anhydrous solvents,<sup>87</sup> a precipitation and redissolution (PR) method has been described together with the preparation procedure, and therefore it is the first reported purification method for QDs. For the frequent case of QDs prepared in non-polar solvents, flocculation of QDs is achieved by introducing anti-solvents that increase the polarity of the solvent

mixture. The supernatant, which retains impurities and excess ligands, can be decanted away and the QD precipitates can be redissolved in clean solvents. This process can be repeated several times until a desired purity of the NCs has been achieved. In addition to purification from synthetic solvents and byproducts, the PR method has also been used to refine the size distribution of the samples.<sup>85,88,89</sup> The particles are not fully precipitated (crashed out), but rather the anti-solvents are titrated only until the particles just start to flocculate. It is frequently observed that the larger particles precipitate more readily than the smaller ones as the solvent polarity is increased, and on this basis they can be separated. The PR method is convenient and scalable, and moreover has been utilized as the main purification technique in the majority of QD investigations. However, a number of studies have shown that there are some drawbacks to the PR method.

One of the main limitations is that the impurities and excess ligands sometimes have solubility properties similar to the nanoparticles, which makes them difficult to separate by this PR method. Many studies focusing on ligand chemistry describe multiple cycles of PR to remove free (unbound) and weakly adsorbed material. In some cases, even with a series of washing steps, the excess ligands cannot be removed by the PR method. For example, Nozik's group showed that excess indium precursor cannot be removed from InAs QDs after using toluene/methanol to dissolve/precipitate QDs.<sup>90</sup> Chaudret and coworkers were able to eliminate a synthetic byproduct from InP QDs after identifying an appropriate PR system, but even after multiple washes could not isolate the NC product from residual octadecene solvent isomers interacting with surface coordinated carboxylate ligands.<sup>91,92</sup> Weiss' group has shown that impurities such as cadmium phosphonate and amides formed as precursor byproducts cannot be separated from CdSe QDs with chloroform/methanol as

the solvent/anti-solvent for the purification.<sup>93,94</sup> Another severe issue is that the PR method may cause irreversible damage to the QD surface. One common observation is that the precipitated particles have a propensity to irreversibly aggregate after a number of necessary PR cycles, and so cannot be redispersed in solution.<sup>95,96</sup> Recently, a series of studies have shown that even for samples that maintain their colloidal stability, an improper choice of anti-solvent may remove ligands from the NC surface that were strongly bound in the original solvent. Owen's, Hens', Weiss' and Meulenberg's groups have shown that methanol can react with the QD surface and displace bound metal carboxylate ligands.<sup>34,73,74,97</sup> This displacement results in adverse changes to the brightness of the samples (which will be discussed in greater detail below). Up to the present, the PR method remains the most popular nanoparticle purification technique. However, the strong dependence of NC properties on the surface ligand population has also motivated researchers to study alternative purification techniques.

### 2.2.2 Extraction

An alternative method to separate NCs from the impurities, while still operating on the basis of differences in impurity and NC polarity, is extraction. The most common extraction system applied to QDs is liquid–liquid extraction. In general, the as-synthesized QD solution is stirred with an extracting solvent that is immiscible with the original solvent. By imposing a difference in the relative solubilities (partition coefficient) between the two liquids, the impurities and the QDs can be distributed into the different phases. In contrast with the popular PR method, the extraction method is intended to be a much gentler process, especially because the NCs tend to remain in their original phase during the purification, reducing the likelihood of irreversible aggregation or coalescence. However, numerous

extraction cycles are commonly required in order to effectively remove a majority of the impurities because of the finite partition coefficients that can be achieved.

The most commonly used extraction system for typical colloidal QD systems is comprised of methanol/alkane, as the QDs are prepared in alkanes, and methanol (as the immiscible polar antisolvent) is used to remove the impurities. Both Peng's group and Nie's group have applied this technique in purifying CdS, CdSe and CdTe based materials.<sup>98-100</sup> A limitation with this and similar systems, as shown in a recent study by Peng's group, is that when the metal precursor for the Cd-based synthesis is cadmium stearate, batchwise single stage extraction cannot effectively remove the impurities due to similar polarities between the particles and impurities.<sup>101</sup> To circumvent this issue, higher temperature and/or addition of co-extractants such as amines and phosphines were shown to significantly improve the extraction efficiency.<sup>101-103</sup> Such nucleophiles are known to coordinate both metal carboxylate precursors and NC surfaces, and are commonly used in QD synthesis. However, addition of such ligands during the extraction introduces an extra constituent to the purification process that could alter the final surface chemistry of the nanoparticles. The choice of both original and extracting solvents is important to the final extraction efficiency. Peng's group has shown that when the NC stock solution was extracted with a chloroform/methanol mixture, the impurities could be more effectively removed compared to the sample extracted with methanol only, each with hexane as the NC solvent.<sup>100,101</sup> Moreover, PR steps sometimes were used together with a sequence of several extraction cycles in order to completely segregate the nanoparticles from the impurities.

The extracting solvent is normally chosen to have a higher solubility for the impurities, and negligible solubility for the QDs. Conversely, Jiang's group described using

Triton X-114, a nonionic surfactant, to perform cloud point extraction (CPE), which effectively concentrated and separated NCs from their original solution.<sup>104</sup> In that work, Triton X-114 formed a micelle to encapsulate the NCs and subsequently extract them when the temperature was above the cloud point temperature (CPT). The NCs could then be redispersed into an aqueous solution once the temperature was lowered beyond that CPT. This method provides an alternative way to concentrate the NCs, but it may prove difficult for NCs to be ultimately isolated from the added micelle-forming surfactants. Another interesting study was done by Pal's group, where they used copper stearate as a solid extracting agent to selectively remove amine ligands from gold organosol.<sup>105</sup> Similar to what Peng has proposed in the co-extractants study, the coordination effect between the amine ligands and metal carboxylate is the likely driving force for this separation.

### **2.3 Electrophoresis-based techniques**

As the mobilities of nanoparticles and associated impurities under an electric field are generally different, electrophoresis has been applied as another purification technique. In an early example, Claridge et al. used gel electrophoresis to separate Au nanoparticles with varying numbers of thiolated DNA strands adsorbed to the surface.<sup>106</sup> Later, Parak's group demonstrated that this technique could be used to separate polymer-coated CdSe/ZnS or Au nanoparticles with different functional groups;<sup>107</sup> the resolution was sufficient to distinguish particles specifically bearing zero to three desired conjugates. Electrophoresis has also been used to separate QDs bearing a single copy of poly-histidine tagged protein from unfunctionalized or multifunctionalized QDs. Sonnichsen's group and Girault's group further showed that gel electrophoresis could be used to separate different shapes and sizes of Au and Ag nanoparticles functionalized with charged polymers.<sup>108,109</sup> However, as

described in the work done by Kotov's group on CdTe nanoparticles, the gel-based process is extremely time-consuming, which is not ideal for applying this technique in continuous and large-scale separations.<sup>110</sup> Consequently, they described using free-flow electrophoresis (FFE), specifically to narrow the size distribution of CdTe nanoparticles. Separation via FFE was achieved by applying a high voltage electric field perpendicular to the direction of laminar flow and differentiating based on the deflection of the charged particles. Employing this method, Kotov and co-authors were able to separate CdTe nanoparticles into more monodispersed populations on a preparative scale.

Electrophoresis generally requires aqueous systems, which would be a limitation for NPs synthesized by the typical organometallic route. Recently, however, Dubertret's group has succeeded in implementing electrophoretic deposition (EPD) in nonpolar or slightly polar solvents as a means to sort Cd chalcogenide nanomaterials,<sup>111</sup> enabled by non-zero zeta potentials. In addition to employing electrophoresis as a size- or shape-selective technique, it has also been established for purifying nanocrystals of synthetic byproduct and excess surfactant impurities. Bass and co-workers described implementing EPD to purify metal chalcogenide nanomaterials containing a common surfactant layer of greasy organic ligands directly from their post-synthetic solution.<sup>112</sup> By using reversible EPD processes, the nanoparticles can be effectively separated from the surfactant impurities in the suspension. After washing with polar non-solvents, the nanoparticles could be redispersed into clean nonpolar solvents. This method exhibited effective purification with no damage to nanoparticles, as confirmed by UV-Vis and NMR. The authors further demonstrated that this technique was versatile toward materials with different morphologies and capping ligands. Similar to the previously described PR method, however, the nanoparticles were



removed from the solution phase during the purification and the particles had to be washed by the anti-solvents. Nevertheless, this electropurification technique is more solvent-efficient and scalable as compared to the PR method, which is an advantage from the perspective of industrial purification.

Jeong's group has attempted to develop the FFE method to purify CdSe QDs continuously on a microfluidic chip.<sup>113</sup> In this arrangement, the purified QDs could be separated from the unreacted precursors and excess surfactants by exploiting the electrophoretic movement of the particles. As one of the first forays into the continuous purification of nanocrystals, the yield and purification efficiency are not yet as good as what has been achieved in batch processes. Even so, this study exemplifies the progress that may be achievable through additional work on purification of nanoparticles in flow, in order to achieve continuous production of nanoparticles on a fully automated system.

## **2.4 Size-based separation techniques**

### **2.4.1 Ultracentrifugation**

The significant size difference between the QDs and the impurities makes size-based separation an attractive alternative for NC purification. Ultracentrifugation, including density gradient centrifugation, is one of the most important size-based separation and characterization techniques in biological/colloidal studies. In contrast to the previously described PR method, in which the introduction of anti-solvents causes nanoparticles to lose their solubility and flocculate into aggregates that can be sedimented with modest centrifugal force, separation via ultracentrifugation is achieved by the difference in sedimentation velocities among dispersed solutes. If the solute–solute interaction and diffusive effects are

neglected, there are three main forces acting on a solute particle; namely centrifugal force, buoyant force and frictional force. The condition at steady state, when the above three forces are balanced, sets the Svedberg coefficient, defined as the sedimentation velocity normalized by the applied angular acceleration, equal to

$$S = \frac{v_s}{\omega^2 r} = \frac{V(\rho_p - \rho_l)}{f}$$

where  $v_s$  is the particle sedimentation velocity,  $\omega$  is the angular velocity,  $r$  is the distance between particle and rotation axis,  $V$  is the particle volume,  $\rho_p$  and  $\rho_l$  are the density of the particle and solvent respectively, and  $f$  is the friction coefficient.<sup>114</sup> When the Svedberg coefficients of the solutes are different, separation can be achieved with centrifugal techniques.

Since the Svedberg coefficient depends linearly on volume, in principle size separation should be effectively achieved with ultracentrifugation. As reported in various articles, this technique has been used to characterize and reduce the size distribution of nanomaterials including single-walled carbon nanotubes (SWNTs),<sup>115</sup> metallic nanoparticles (MNPs),<sup>116</sup> semiconductor nanoparticles,<sup>117</sup> and oxide nanoparticles.<sup>118</sup> Moreover, when the size of nanoparticle is smaller than 20 nm in diameter, the ligands on the surface contribute substantially to the overall particle density, which further allows ultracentrifugation to separate nanoparticles with different coatings. Ultracentrifugation can also be used to effectively sort nanoparticles with different shapes. Recently, a mathematical model has been established by Sun's group for parameter optimization using ultracentrifugation for separation of polydisperse colloidal nanoparticles.<sup>119</sup>

As alluded to above, not only is ultracentrifugation convenient for preparing monodispersed nanoparticle samples, but it can also be used to isolate nanoparticles from

excess functional ligands due to the significant size, density and friction coefficient differences between the particles and ligands. This method has frequently been used for the purification of QDs *after surface modification* for water stabilization. For example, Nie's group has used ultracentrifugation to separate excess polymer after NC encapsulation;<sup>120</sup> and Dubertret's group and Scholler' group have used ultracentrifugation to isolate NCs from phospholipids in a similar manner.<sup>121,122</sup> While most applications of ultracentrifugation have employed aqueous density gradients, which presents a general challenge of aggregation and instability for NCs synthesized via organo-metallic routes, investigations successfully employing this technique were recently reviewed by Medintz's group.<sup>123</sup> Furthermore, Bai et al. showed that ultracentrifugation can be used to purify as-synthesized nanomaterials in organic solvent from excess ligands such as oleylamine.<sup>124</sup> They obtained clear TEM images of metallic/semiconductor nanoparticles without any additional purification after size/shape separation was achieved. However, to the best of our knowledge, detailed surface characterization of the nanomaterials in organic solvents purified by ultracentrifugation has not been performed, nor has its efficiency as a purification technique been compared with other methods.

#### 2.4.2 Membrane-based separation

Separation using a membrane prepared by porous materials is another attractive method to narrow the size distribution of the as-synthesized nanomaterials, as well as isolate the nanomaterials from the excess ligands. Typically, dialysis and filtration are the two general techniques with size-based membrane separation involved. In the process of dialysis, a membrane should be selected with an effective molecular weight cut-off (MWCO) that permits the excess ligands and other small molecule impurities to diffuse from the high

concentration area (sample solution) to the low concentration solution (dialysate solution) until equilibrium is reached, but the pores must of course be small enough to prevent nanoparticles from transiting. After repeating the dialysis process several times, the concentration of the excess ligands in the sample solution will significantly decrease while the concentration of the nanoparticles can be maintained. This method has frequently been used for the purification of nanoparticles in aqueous solution and is generally done using commercially available membranes (dialysis tubing). For example, Stone's group and Ren's group have used dialysis to purify as-synthesized Au and CdTe nanoparticles in water;<sup>125,126</sup> Snee's group has recently used dialysis as a gentle technique to purify the water soluble QDs after silane coating;<sup>127</sup> and dialysis has also been used to isolate bio-labeled nanoparticles from excess bio-linkers after undergoing functionalization reactions.<sup>128</sup> One drawback of dialysis is that this process is time consuming as it normally takes several hours or more to allow the equilibrium between concentrations of small molecules at the two sides of the membrane to be reached.

Distinct from dialysis, where the separation is achieved by diffusion of the small molecules, filtration is more efficient in time, exploiting an extra driving force in the form of a difference in fluid pressure to accelerate the separation. The challenges lie in selecting a filter membrane with an appropriate size cutoff and solvent tolerance, and in avoiding aggregation of the nanoparticles as they accumulate at the membrane. A wide variety of filtration systems has been developed to purify and retain biomolecules such as proteins in aqueous solvents, typically using centrifugal force or vacuum to generate sufficient pressure difference. Accordingly, centrifugal filtration has in many cases replaced dialysis for purification, buffer exchange, and concentration of water-soluble biomolecules and

nanoparticles, especially those that will not aggregate during the filtration process. QDs stabilized in aqueous solution by ligand exchange or surfactant encapsulation are often purified by this method.<sup>129</sup> Snee et al. used centrifugal filtration to purify pH sensitive dye-conjugated CdSe/ZnS QDs to develop a ratiometric pH sensor.<sup>130</sup> Though commercial membranes were primarily designed to retain proteins and synthetic colloidal particles while passing only small molecules, researchers have developed membranes with larger size cutoffs that can be used to separate small particles from larger ones to refine the size distribution of the sample – a nanoscale form of sieving. Mesoporous silica hybrid membranes have been used to perform size separation of metal nanoparticles prepared in either aqueous or organic solvents.<sup>131,132</sup> Rybitchinski's group has also described using polymer-based membranes to perform size separation on metal nanoparticles and QDs in aqueous solution, as the organic solvent may lead to disassembly of the supramolecular structure.<sup>133</sup>

Ultrafiltration and diafiltration are two additional membrane-based separation technologies for nanoparticle purification. Ultrafiltration is also known as tangential flow filtration (TFF) and operates such that the feed solution flows parallel to the membrane surface, instead of perpendicular to it as in conventional “dead-end” filtration. A concentrated nanoparticle solution is retained. Many commercial centrifugal filtration units actually accomplish TFF, but ultrafiltration can also be scaled up for industrial process sizes. The set-up and operating principle of diafiltration is very similar to ultrafiltration; the only difference being that extra solvent is injected into the sample solution to maintain a constant total volume of the feed during the purification process. One major advantage of both ultrafiltration and diafiltration is that these two processes can be operated semi-continuously for in-line nanoparticle purification. Ulbricht's group has applied ultrafiltration and

diafiltration to purify gold and silica nanoparticles from excess small ligands or biomolecules.<sup>134</sup> Hutchison's group has performed a systematic study to compare the purification efficiency of diafiltration with other techniques on thiol-PEG coated Au nanoparticle samples.<sup>135</sup> Employing  $^1\text{H}$  NMR, it was demonstrated that diafiltration effectively separated the thiol-PEG coated Au nanoparticles, whereas these free ligand features remained in the samples purified by other methods. Their results demonstrated that diafiltration is an efficient purification technique for nanoparticles in aqueous solution. Similar to ultracentrifugation, most of the studies utilizing membrane-based separation still focus on the nanoparticle samples in aqueous solution. In order to purify nanoparticles prepared in organic solvents using membrane separation, advances in membrane technology will be necessary.

#### 2.4.3 Chromatography

Chromatography is another general strategy by which nanoparticles can be effectively purified, and one that my group has pursued for colloidal QDs. Whether preparative or analytical in scale, the premise of chromatography involves the elution of mixtures dissolved in a mobile phase (MP) through a structured stationary phase (SP), between which the sample components are partitioned. In affinity chromatographies, some specific and/or enthalpic interaction between the sample components and the stationary phase determines this equilibrium. Affinity chromatography has been developed to effectively isolate bio-conjugated nanoparticles from excess unbound peptides and unfunctionalized peptide-bearing nanoparticles. Alternatively, purely physical (entropic) interactions can be used to separate components on the basis of size. Because of the large variation in size among components in colloidal nanoparticle samples, the latter approach holds considerable appeal.

High resolution in separations and resulting chromatographs (often times coupled with additional detection equipment, e.g. absorption, photoluminescence, and mass spectrometers) provides in situ characterization of analytes in terms of size, surfactant interaction, states of thermodynamic stability and equilibrium, and purification.

Among inorganic materials, Au NPs have the most extensive chromatographic application history,<sup>136–138</sup> and as such have offered an important framework to develop such methods applied to characterize and purify QD systems. Tiede et al. developed hydrodynamic chromatography (HDC) coupled with ICP-MS for Au NPs as well as a number of oxide NPs,<sup>139</sup> and Pergantis et al. improved HDC detection limits for the study of Au NPs in environmental matrices.<sup>140</sup> HDC utilizes a nonporous SP, and the mechanism for separation is based on the parabolic flow profile of a Newtonian fluid in an open tube or within the interstitial volume of the column, such that smaller particles can migrate towards the outer areas while larger particles are deflected towards the center where the MP flow rate is fastest. The most popular and versatile chromatographic technique applied to NP suspensions, however, is size exclusion chromatography (SEC).

The general principle by which SEC operates is that analytes fractionate between the mobile phase (MP) and a porous stationary phase (SP) to an extent that depends monotonically on their hydrodynamic size, with larger particles eluting more rapidly than smaller constituents that can traverse the pores of the SP. The stationary phase is typically made up of cross-linked polymer gel beads characterized by an effective molecular weight cutoff (MWCO) above which analytes are largely excluded from the pores and transit only the “void volume” between gel beads. SEC can be accomplished with polar mobile phases (including water) using hydrophilic polysaccharide or polyacrylamide gels; this represents one

form of gel filtration chromatography (GFC), a term that also encompasses affinity chromatography methods using functionalized hydrophilic gels. SEC with anhydrous mobile phases is termed gel permeation chromatography (GPC) and is routinely used to characterize polymer molecular weight distributions.

Innovation in high-performance liquid chromatography (HPLC) technology has led to sophisticated instrumentation for both GFC and GPC. In its more conventional use, application of SEC to nanotechnology has sought to improve NP sample polydispersity through higher resolution sensitivity for both size and shape.<sup>65,66,141–146</sup> Differences in structure (hard spheres versus folded proteins or randomly coiled polymers) require that columns be properly calibrated against nanocluster standards<sup>143</sup> or polystyrene;<sup>147</sup> nevertheless, most investigations have successfully determined size-exclusion fractionation mechanisms.<sup>148,149</sup> One of the major challenges in this technique, which distorts elution profiles in QDs and other NPs alike, is the possibility of enthalpic interactions that result in increased retention or irreversible sorption of the sample onto the stationary phase. This makes it imperative to identify appropriate SP media. The most common strategy employed to circumvent this critical issue is to include MP additives that may include surfactants,<sup>75,141,144,150,151</sup> but a number of recent reports<sup>62,96,136,137,152,153</sup> have also demonstrated that suitable SP properties have been achieved with both polar and nonpolar MP solvents. An early success in resolution capacity when a properly chosen SP was combined with multiple on-line detectors for SEC (utilized as a high pressure liquid chromatograph for nanoparticle separation) was comprised of a cross-linked polystyrene SP, with a relatively larger pore size than was used when only eluting Au clusters in the same investigation and was lastly combined with tetrahydrofuran as the MP.<sup>148</sup>



Early application of HPLC/SEC to QDs proved successful in resolving elution fractions that contained narrower size distributions than the starting material. However, recent studies indicated that this technique could also be used to purify nanocrystals. The potential for SEC to achieve size separation as well as QD purification was apparent even in that earlier investigation as 2.0 nm Au nanoclusters and 1.8 nm CdSe NCs were well-resolved from linear alkanes that could conceivably represent excess ligands or surfactant impurities. Early examples to affect a type of purification with HPLC/SEC applied to QDs were mainly applied post-surface modification to separate QDs from excess polymers.<sup>149,151,154</sup> Shortly thereafter, Biesta et al. utilized GPC in a similar manner to separate excess dye molecules from nanocrystalline silica in an organic MP.<sup>155</sup> In a series of investigations toward biocompatible surface modification, water-soluble core/shell QDs functionalized with hydrophilic ligands were successfully analyzed with aqueous gel filtration chromatography (GFC) on the basis of their resultant sizes; this was used to demonstrate the strength of ligand binding and to assess the presence or absence of nonspecific adsorption of highly prevalent, endogenous serum proteins in QDs intended for bioimaging applications. In a preparative example, McLaurin et al. used GFC to isolate QD-based ratiometric oxygen sensors.<sup>156</sup> QDs functionalized with oxygen-sensitive, osmium-based FRET acceptor phosphors were separated from QD aggregates and unbound phosphors, as a step toward QD FRET-based oxygen sensors applicable in biological systems. A very recent investigation of Cd-based QD bioprobes purified by HPSEC post-ligand exchange confirmed significantly improved agglomerate removal, and consequently negligible nonspecific binding, with enhanced performance of the QD bioprobes in immunofluorescence imaging and stability for at least one year.<sup>157</sup>

Our group has recently established and continues to develop gel permeation chromatography (GPC) – an effort that has been a primary focal point of my own research – as a preparative, reproducible and robust purification technique for colloidal NCs; especially when directly pitted against the common PR purification procedure (Figure 2.2).<sup>62,137</sup> This novel approach for NC purification utilizes GPC to exert a continuous driving force in situ

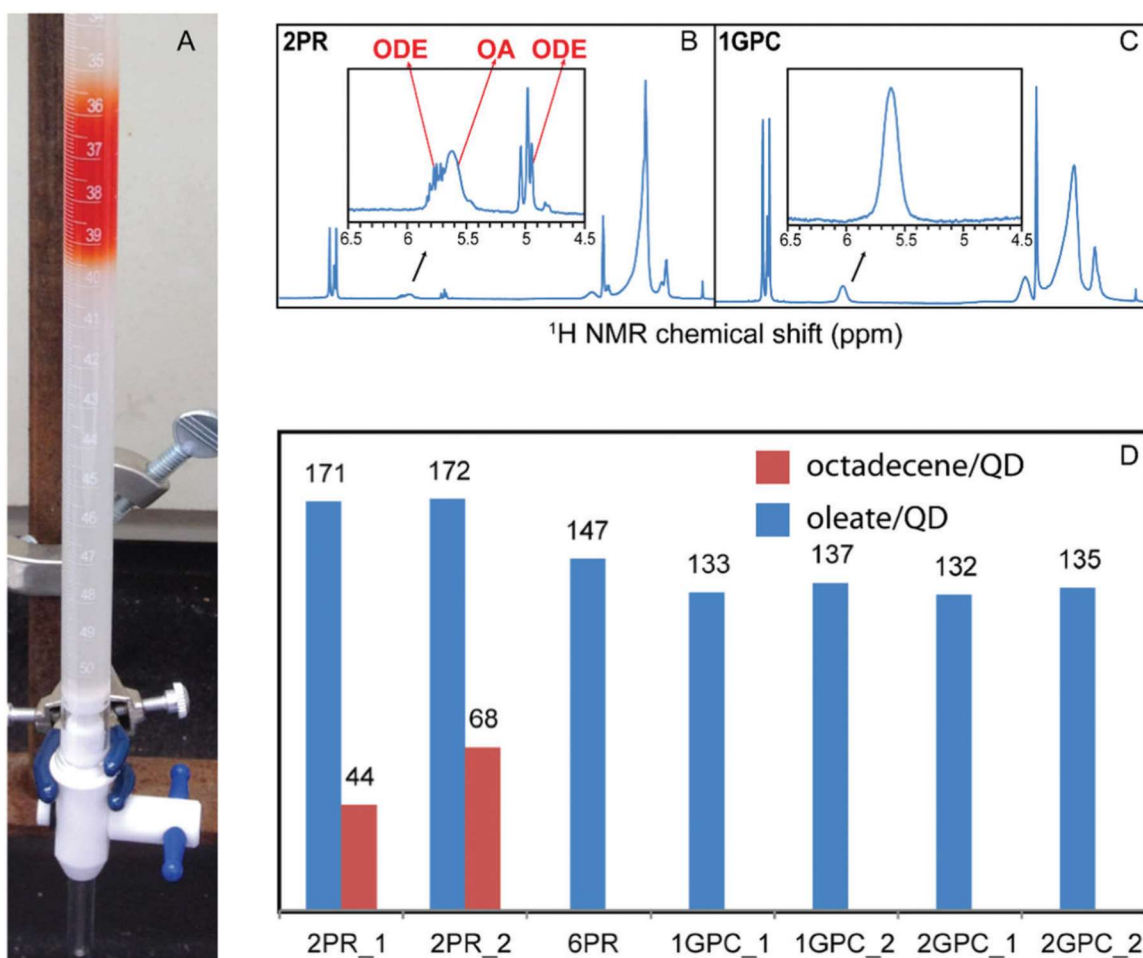


**Figure 2.2** GPC purification of oleate-capped CdSe QDs with toluene MP and polystyrene SP (A) photograph of QDs (red band) transiting column under gravity pressure. (B and C) <sup>1</sup>H NMR spectra of 2 cycle precipitation/redissolution purified (A) and GPC purified (B) CdSe QDs. The insets are the expanded views of the spectra in the range 4.5–6.5 ppm, capturing the olefin proton resonances of oleate species (OA) and residual octadecene synthesis solvent (ODE). (D) Ligand/impurities-to-QDs ratio (mole/mole) for CdSe QDs purified by different methods. Adapted with permission from ref. 62. Copyright 2013 American Chemical Society.

to separate unbound or weakly-bound small molecules. Only those ligands with very large association equilibrium constants and/or very slow desorption kinetics can remain adsorbed to the NC surface upon their elution from the column. A MP solvent can be selected that is the same as, or of similar polarity to, the initial solvent for the NCs and so maintains the solvent conditions under which the initial surface coordination environment was assembled.<sup>62</sup> The nature of the native solvent interactions is often overlooked as if it were a trivial matter. The SP consists of cross-linked polystyrene (Bio-Rad's Bio-Beads SX-1 in initial studies). This SP has proven to be compatible with Cd-based core and core/shell QDs capped with typical anionic and L-type ligands, polymer-functionalized Cd-based QDs with polar organic MP,<sup>151,158</sup> carboxylate-capped InP QDs,<sup>159</sup> thiol-capped Au NCs,<sup>137</sup> Cd-based nanorods of varying aspect ratios,<sup>158</sup> perovskite NCs,<sup>160</sup> and iron oxide NCs.<sup>153</sup> Moreover, it is also possible to use the GPC column as a multi-functional flow reactor that can accomplish in sequence the steps of initial purification, ligand exchange, and subsequent cleanup without requiring a change of phase.<sup>137</sup>

The dearth of SP media for preparative SEC that swell in organic solvents remains a limitation for the use of SEC for NP purification, given the relatively low MWCO and operating pressures of polystyrene Bio-Beads.<sup>74,151,158</sup> Technological emphasis in resolution and operating power has instead focused on small sizes.<sup>146</sup> Aside from typical column packing material used in GFC or other aqueous phase HPLC/SEC, a few additional SP media with organic MP have been identified as suitable for NCs. Namely, a cross-linked styrene/divinyl benzene SP, which is both similar to and compatible with polystyrene, was effective in eluting Cd-based core/shell QDs.<sup>147</sup> It is anticipated that SP media can be identified, or specifically engineered, to meet the need of a higher MWCO for larger

synthesized NPs and overall scalability. Though it will remain essential to carefully consider and test the compatibility of SP media with the NCs and the impurities being removed, to prevent or minimize enthalpic interactions or aggregation on the column and achieve high resolution separations.

## 2.5 Purification and nanocrystal surface chemistry

### 2.5.1 General implications of the impact of purification on colloidal quantum dot properties

Purification steps can alter free ligand concentrations and the solvent, so the need to understand how NC surfaces are affected by purification has become more apparent as it is typically the first processing step towards applications.<sup>1-3</sup> As previously mentioned, the putative ligands within the synthetic mixture provide colloidal stability, synthetic control over final crystal morphology, ultimate surface composition, and consequently orbitals of ligands bound to/interacting with the NC surface couple such that they contribute to the energy profile of the system's electronic states.<sup>1,19,60,94,161</sup> Because QDs are quantum confined chunks of bulk materials, much can be understood or inferred about the inorganic core's electronic structure; however, the higher density of states and disrupted crystal lattice periodicity at their surface is significantly impacted by the surfactant layer both *initially present* and *imposed upon* during surface modification which includes purification. Thus, the electronic structure occurring at the NC-ligand interface, which ultimately imposes photophysical properties salient primarily through photo- and electro- luminescence, is much less understood.

In order to preserve and/or improve NC luminescence this interface must be thoroughly investigated, at the very least where preventable or reversible processing can

cause defects contributing to mid-gap states that introduce thermodynamically accessible exciton traps. Oxidation in Cd-chalcogenide samples introduces defect trap states, which prompts faster decay dynamics with increased carrier recombination.<sup>10</sup> Molecular oxygen interacts reversibly with QD surface through so-called physisorption; while more detrimental chemisorption encompasses an oxide-formation reaction that etches surface atoms. Photooxidation can occur as Cd-chalcogenide QDs inject electrons into metal oxide receiving substrates, as intended with QD-based solar cells. Though this degradation process receives more attention as it adversely affects device performance; it can also occur in QDs stored under ambient atmosphere and light, in typical storage solvents such as toluene, and after multiple purification processes removing excess or weakly coordinated ligands. Therefore, both the ligands and solvent environment have a major impact on NC optoelectronic properties, especially when imparting or resolving surface defects. Some of the inherent consequences of purification on NC surface chemistry that have been documented as ultimately affecting electronic properties in NC suspensions are discussed below.

### 2.5.2 Surface coordination of compound semiconductor quantum dots

Firstly, the curvature and final composition of the QDs presents various facets either differing in the types of sites available for surfactant adsorption or possibly undercoordinated dangling bonds.<sup>12</sup> Due to the critical role of passivating ligands which determine the final morphology of the NC system as well as exchanging electron density with surface-terminating NC ions, it is crucial to identify and conceptualize ligand binding modes. In fact, these ligand binding modes are necessary to understand the substantial role

purification can have on modulating QD electronic properties and chemical reactivity in subsequent processing steps.

Primitive notions about post-synthetic capping ligands have been adamantly challenged by evidence that nominal solvents and non-labile reagent impurities, rather than the assumed reagents themselves, can dominate precursor reactivity and consequently become the most tightly bound and most prevalent surface species retained even after multiple purification cycles.<sup>62,93,162</sup> Motivated by the need to clarify how interactions between native ligands and QD surfaces influence further surface modifications, particularly in ligand exchange reactions, Owen's group and Hens' group have employed the covalent bond classification (CBC) to characterize the exchangeable groups, initially based on Cd chalcogenide QDs.<sup>2,36,163</sup> In this scheme, ligands are recognized as either L-type (2-electron donors, dissociating to yield neutral Lewis bases); X-type (formal 1-electron donors, dissociating to yield ions); or Z-type neutral Lewis acids (2-electron acceptors, dissociating to yield neutral Lewis acids). The original coordinating solvents and neutral carboxylic acids can thus be described as L-type, while carboxylates or halides are X-type.

The binding between L-type ligands and QDs can be labile especially when compared to strong-binding X-type ligands. L-type ligands can be subject to dynamic exchange between bound and free forms on experimental timescales. As a result, following le Chatelier's principle, this should lead to a predictable loss of such ligands in any of the aforementioned purification techniques applied to NCs, whether our GPC technique or otherwise. Ligand desorption, even that caused merely by dilution, leaves undercoordinated surface atoms when the system equilibrium favors increased free ligand fractions in solution and is generally accompanied by diminished NC PL properties.<sup>19,42,61,77,78</sup> Dissociation of

X-type ligands in non-polar solvents will not occur easily as it requires charge separation, radical formation, or reductive elimination. Drift velocity measurements have revealed that QDs with X-type ligands in a non-polar solvent carry no more than a few elementary charges.<sup>164</sup> However, numerous studies have revealed that purification by multiple PR cycles, especially with protic anti-solvents such as methanol, caused displacement of lattice-terminating core cations together with charge-balancing anionic ligands (Z-type ligands).<sup>34,74,101,165,166</sup> Therefore, in common purification practices, the ligands that have been removed are either L-type or Z-type, and the PL changes upon purification are predominately a result of changes in L-type or Z-type ligand population.<sup>13,167,168</sup> The relative strength of L-type ligand binding appears to vary widely: amines are labile at room temperature at CdSe and CdS NC surfaces, while primary amines exhibit very strong binding to CuInS<sub>2</sub> QD surfaces and were found to be labile only on heating.<sup>169</sup>

While the conventional CBC as described above has served as a useful model for describing binary chalcogenide QDs coated with carboxylates, phosphonates, and amines, it is likely an incomplete picture of ligand binding modes in different NC systems. For example, thiols are well known as strong ligands for many metal and metal chalcogenide NCs. Within the CBC above, thiols could bind as L-type ligands via their lone pairs, or as X-type thiolates following deprotonation. However, the MacDonald group has reported purification and ligand exchange results indicating a further distinction between “surface-bound” thiolates that are subject to exchange, and thiol-derived “crystal-bound” sulfur that retains a covalent bond to an organic tail group, but exists in a highly coordinated environment resembling the anion site of the crystal lattice.<sup>170</sup> Crystal-bound thiol ligands on Cu<sub>2</sub>S, CuInS<sub>2</sub>, and CdSe/ZnS QDs are resistant to loss or displacement in purifications

steps. Cd-based QDs represent the vast majority of NC surface chemistry investigations and are the primary focus of this dissertation, and so the conventional CBC will be referred to when ligand types are mentioned. Nonetheless, recent reports from De Roo et al. presenting perhaps a more universal binding classification relevant to various NC compositions including metal oxides are noted.<sup>36,171</sup>

### 2.5.3 Photoluminescence responses associated with purification

It is well known that ligand exchange can affect PL quantum yield (QY); for example, introduction of thiols has frequently been seen to quench QY in CdSe QDs and this has been attributed to the formation of hole traps at the QD surface. However, changes in QY have been observed upon mere purification or dilution as well. In 2006 Bullen and Mulvaney published a quantitative investigation on the relative strength of binding for ligands as a function of solvent polarity, purity or temperature;<sup>61</sup> it was one of several reports around the same time that demonstrated how merely diluting QD suspensions displaced strongly adsorbed ligands. Much like our group's study of regenerated PLQY in Cd-chalcogenide QDs,<sup>60</sup> Akdas et al. conducted an investigation to elucidate effects of purification on optical properties in CuInS<sub>2</sub> and CuInS<sub>2</sub>/ZnS. This investigation revealed PL lifetime amplitude trends that were enhanced for both the core and core/shell systems, though more so for the core/shell architecture, once an optimal purification system was identified.<sup>84</sup> Despite the concomitant roles of the thiol as both a NC precursor material and final passivating ligand for that system, the QDs better maintained QY and PL lifetime components associated with radiative decay depending on electronic isolation provided by the shell and even more so with a proper PR anti-solvent/solvent combination for their purification. Another recent study developing an aqueous-based gradient ultracentrifugation purification for fluorescent



carbon NPs, also reported that maintaining exciton radiative recombination was influenced primarily by retained hydrophilic surface groups.<sup>172</sup> While it would be inappropriate to consider all QD surfaces as completely analogous to Cd-chalcogenide systems, these observations suggest that at least some observations can be transferred to more complex semiconductor-ligand interfaces.

#### 2.5.4 Improving structural interpretation and material scope

Over the last few years a number of groups have published reports on less toxic alternatives to the very familiar Cd and Pb chalcogenide NCs, and the emerging systems are usually more complex quantum-confined fluorophores.<sup>36,65,84,172</sup> Findings from Cossairt's group after a closer investigation of shell precursor material added to InP QDs to improve QY, revealed another example of NC surface engineering. When adding what they term "exogenous Lewis acids" in the form of specific Cd- and Zn-carboxylates, the QD surface was altered such that significant PL enhancement could be achieved,<sup>83</sup> as well as a tuning of the InP absorption and emission lowest energy electronic transitions. QY enhancement upon the post-synthetic treatment with the metal carboxylates might be described as passivation through introduction of a Z-type ligand. If so, the ligand association is very strong, as a portion of the added metal was retained even after excess metal carboxylates and indium-oxide impurities were removed by a combined PR and filtration purification process. Final indium-to-metal ratios along with the PL responses suggested that the metal carboxylates strongly adhered to undercoordinated surface phosphorus sites, and to some degree were also integrated in the crystal lattice to displace native indium atoms. Again, while Cd-based NC investigations dominate the field and offer an important foundation for other complex semiconductor–ligand interfacial studies, the responses to purification in this metal-doped

InP system cannot be directly interpreted on the basis of the Cd chalcogenide system; especially since the drastic changes in lowest energy electronic transition wavelengths were not accompanied by a change in the NC size. The ability to identify reversible or non-perturbing purification techniques tailored to specific QD materials in specific processing environments is imperative. This is especially true if analysis of the final product is difficult; for example, if ligand exchange leads to a quenched product, it may be difficult to distinguish successful ligand exchange from repercussions of purification.<sup>64</sup>

Many descriptions of NC ligand binding modes are purely schematic and do not account for the specific structural characteristics of the NC surface. Yet, this is beginning to change with more examples of single-crystal X-ray diffraction-based structures for inorganic clusters and small NCs,<sup>173,174</sup> and with more closely integrated theoretic and experimental analysis. The crystal phase, size, and stoichiometric excess of NCs influence the number and character of the ligand binding sites that are available at their surfaces. For example, the eight symmetrically equivalent {111} faces of the rocksalt crystal structure adopted by PbS NCs are formed by alternating layers of cations and anions; terminating them with a complete monolayer results in a charged surface requiring a high density of X-type ligands for charge balance, while the {100} and {110} facets are charge-neutral. This effect of this requirement was demonstrated in a combined theoretical and experimental study by Zherebetskyy et al.<sup>175</sup> of oleic acid-passivated PbS NCs, which showed that water generated as a synthetic byproduct results in hydroxide serving as an X-type ligand at the {111} facets. Hydroxide was necessary to completely passivate the {111} facets, in addition to oleate, due to steric constraints. In contrast, the {100} facets could be passivated by readily exchangeable oleic acid. An investigation on ligand interactions at certain CdS facets further supported the

increasing need to probe QD surface structure to control processes such as interparticle charge transfer or extended crystal growth.<sup>82</sup>

Precise purification methods, supported by surface metrics that can gauge their effects, should enable the handling of NCs with sub-monolayer surface termination and accurate measurement of ligand stoichiometries. Consequently, purification technologies will be a useful tool in developing structurally grounded models of surface chemistry and ligand exchange at NC surfaces. Purification technologies must also be shown to work for emerging classes of nanocrystalline materials, including Cd- and Pb-free compound semiconductors such as InP and LiZnP.<sup>65,176</sup> These compounds can have more complex ligand binding modes and increased sensitivity to oxidation compared to chalcogenides, which will increase the need for precision in describing their surface chemistry and spectroscopy.

## 2.6 Conclusion

As the value contributed by colloidal NCs becomes increasingly clear, the need for a detailed understanding of their surface chemistry and of appropriate means to describe and isolate the structures that give rise to their remarkable and useful properties becomes increasingly urgent. The works described in this chapter clearly illustrate that the surfaces of colloidal NCs are subject to dynamic equilibrium with the surrounding medium and may change upon purification or dilution, leading to changes in properties critical to their performance. Purification methods are now available that allow a high degree of process control and repeatability, and many of them do not require a change in solvent that could disrupt ligand binding free energies. Additionally, analytical techniques such as NMR, TGA, Mass Spectroscopy and calorimetry can help to profile samples to allow the results of

different purification techniques to be compared, and in principle to permit a standard description of nanoparticle samples across the field.<sup>169</sup> Such standardization will greatly benefit interpretation of physical property measurements and accelerate the development of more sophisticated, multistep preparative routes to highly efficient absorbers, emitters, and multifunctional materials. Increased rigor in reporting of purification methods and analytical metrics will be helpful in achieving these goals. Ultimately, matters of scalability and cost will be important in selecting the most appropriate purification method for a particular task. Engineering studies examining purification of nanocrystals at larger scale and in integrated and/or continuous processes could help optimize current technologies and achieve useful cost figures.

## CHAPTER 3

### ***LANGMUIRESQUE ASSOCIATION OF NEUTRAL LIGANDS TO CdSe*** **QUANTUM DOTS AND SUBSEQUENT EFFECT ON PHOTOPHYSICAL** **PROPERTIES**

#### **3.1 Introduction**

3.1.1 Photoluminescent properties of colloidal quantum dot surfaces and general implications of purification

Quantum dots (QDs) are simultaneously extremely promising and perplexing hybrid materials, in particular due to the numerous intrinsic and extrinsic influences of their surface chemistry on relevant photophysical properties and only perpetuated by their high surface area-to-volume ratio. Efficient and size-tunable photoluminescence (PL) is one of the most distinctive characteristics of colloidal QDs and has led to their initial commercial applications.<sup>67,177–185</sup> Indeed, the most facile and globally employed methods to monitor changes in QD electronic structure are band edge optical absorption and emission. Narrow, well-resolved, and consistent features in continuous-wave absorption spectra can be sensitive to changes in QD radius and polydispersity but reveal limited or no information about localized states.<sup>8,186,187</sup> The PL quantum yield (QY) and lifetime are sensitive to trapping and non-radiative decay,<sup>188</sup> in some cases, radiative decay from trapped excitons can be observed. Time-resolved absorption and PL spectroscopy can additionally reveal reversible trapping,

and information about the distribution of non-radiative decay rates that is present among QDs in the sample.<sup>80</sup>

QD purification results in removal of impurities and ligands alike, which inevitably affects exciton binding energies via radiative and nonradiative emissive pathways. Consequently, purification methods can modify the QD surface through dissociation or exchange of various ligand types with a number of possible binding modes. Therefore, it is important to understand how ligand binding affects PL, and whether PL changes observed on purification, dilution, or a change of solvent are a direct result of ligand ad/desorption, or are associated with aggregation, surface oxidation, or surface reconstruction that may be irreversible.<sup>14,73,78,85,97,189</sup> The ligands and solvent also directly modulate energy levels through classical dielectric confinement effects, though this has been shown to be a small contribution in most cases.<sup>190,191</sup> Purification methods that do not require a change in solvent offer the opportunity to *directly* characterize ligand dissociation kinetics and thermodynamics. For example, by continuously exposing QDs to a low or zero concentration of free ligands, only those surface-bound equivalents with off-rate lifetimes greater than the experimental timescale will remain.<sup>137</sup> As such purification at different speeds could potentially detect off-rate kinetics for molecules with very small dissociation equilibrium constants. This data could help to distinguish associative and dissociative ligand exchange mechanisms. Ligand exchange rates could in turn be investigated as a function of solvent polarity or the presence of solvent impurities such as moisture, which has already been shown to play a role in NC growth kinetics but to our knowledge has not been thoroughly examined in the context of ligand exchange. Quantitative kinetic and thermodynamic measurements using purification

may emerge in the near future, though a concern is the propensity of NCs to aggregate if steric and/or electrostatic stability imparted by labile surface groups is lost.

As the major impact purification tends to have in modulating QD electronic properties and dictating chemical reactivity in subsequent processing steps becomes more apparent, the need for further discourse on ligand binding modes and dynamics in order to understand fundamental effects on exciton behavior is simultaneously established.<sup>13,39,168,192–196</sup> Much of what has been discovered about as-synthesized QD–ligand binding dynamics has emerged in the course of surface modification procedures designed to replace native ligands.<sup>54,197</sup> Early understanding of QD growth hinged on the concept of a coordinating solvent: the use of compounds, typically Lewis bases, in high concentration to saturate the surfaces of particles and serve as a steric barrier to aggregation even at high growth temperatures.<sup>87</sup> Unexpected roles of the coordinating solvent and identities of post-synthetic capping ligands, such as amines in CdSe core syntheses as well as shell incorporation or strongly bound phosphorus-containing impurities populating QD surfaces,<sup>40,72,163,198</sup> have paved the way for critically needed fundamental revisiting of basic surface chemistry reactions and analysis.<sup>14,199,200</sup>

### 3.1.2 Associating PL changes with effects of purification

Whereas purification of some degree is inherently required either directly after nanocrystal synthesis or prior to incorporation into material applications, PL quenching upon purification is pervasive in many cases.<sup>163,166,191,201,202</sup> Fortunately, it has now been established that such luminescence responses are frequently reversible, as demonstrated in both absorption and emission spectra.<sup>19,162,171,201</sup> Two separate investigations conducted 10 years apart, but attaining remarkably similar profiles, have illustrated this phenomenon.

Kalyuzhny and Murray observed a slight bathochromic shift of band-edge absorption and PL maxima of diluted CdSe QDs at the conclusion of a number of purification steps. Additionally, QD sub-bandgap emission attributed to surface defects increased while band edge emission decreased by almost 90% of its original intensity with repeated purification steps.<sup>78</sup> The reverse of this process was depicted in a later study conducted by Krause et al., with the addition of an L-type ligand (butylamine) capable of passivating surface cadmium sites, suppressing surface electron trap emission and increasing overall PL efficiency.<sup>14</sup> A fundamental investigation by Bullen and Mulvaney on the effects of solvent on PL dynamics given ligand interactions primarily considered to bind datively to Cd-chalcogenide QDs revealed that mere dilution could displace native ligands, thereby perturbing QD electronic properties.<sup>61</sup> The PL response they observed suggested an effective binding constant governs fractional occupation especially of L-type ligands at the QD surface.

### **3.2 Spectroscopic investigation of reversible quantum yield regeneration in Cd-based core/shell quantum dots**

#### **3.2.1 Purification effects on photoluminescence in core/shell quantum dots**

It is apparent with such literature precedent that purification techniques can be an important tool in both studying and manipulating NC surface chemistry. Changes in optical properties of QDs associated with purification are ubiquitous, and our in-depth investigation of PLQY regeneration on core/shell QDs serves as an example of how purification influences NC surface chemistry from their electronic properties. A wider bulk band gap shell material is typically added to encapsulate core QDs; thereby providing both chemical and electronic passivation, specifically toward some level of isolating the exciton wavefunction within the core. This is perhaps the most robust and widely employed



procedure to engineer QDs with lower nonradiative decay rates, higher ensemble QY and more on-time fractions even among single QDs.<sup>203–205</sup> As shown in Figure 3.1, even in samples with shells only a few monolayers thick in which the excited states are not entirely isolated from the surface and therefore surface states, very high QY can be achieved.<sup>206</sup> This demonstrates that molecular surface termination can indeed be achieved in which almost no intergap states or resonant excitations are present, though recently reports of core-only Cd-based QDs have achieved similar results.<sup>39,201</sup>

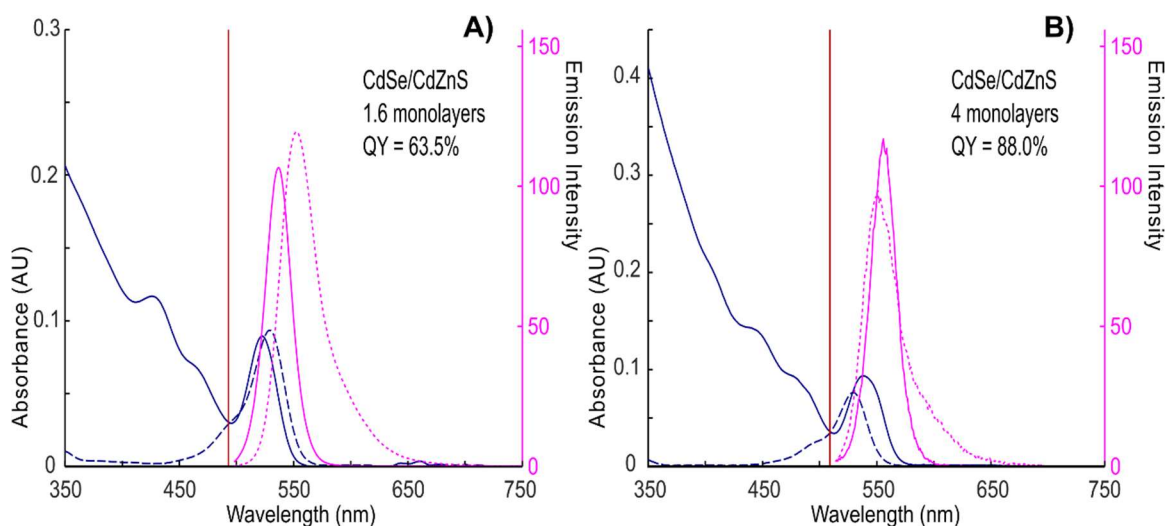


**Figure 3.1** Quantum yield of thin 1.6 monolayer (A) and 4 monolayer (B) CdZnS alloy shell QDs after 1 cycle of precipitation/redissolution (considered “before purification”). The red line marks the excitation wavelength. The absorption spectra (navy) and emission spectra (fuchsia) of QDs are shown as solid lines, while dashed lines indicate rhodamine 590 in ethanol as the reference dye. Adapted with permission from ref. 60. Copyright 2015 American Chemical Society.

As-synthesized colloidal QD samples typically or inherently contain large concentrations of molecules that could coordinate the surface as well as allow larger fractions of molecules to interact with surface states.<sup>5</sup> It is essential to understand whether [adverse] changes in QY ensuing mere purification are reversible, how ensemble QY and

decay profiles depend on ligand occupation, and the conditions under which surface structures that support high QY can be maintained or restored.<sup>2</sup> Until this investigation, the direct impact of putative ligands present in as-synthesized Cd-based core/shell QDs initially displaying high QY had not been exhaustively studied.

Our previously established gel permeation chromatography (GPC) purification was demonstrated to effectively remove impurities and weakly associated ligands in the QD native organic solvent.<sup>62</sup> Owing to the robust yet gentle capacity of the GPC to yield purified QDs with low and consistent populations of Cd-carboxylate equivalents, we were able to take advantage of this highly reproducible technique to prepare oleate-capped core/shell samples for this study. Nuclear magnetic resonance (NMR) was used to evaluate the extent of ligand interaction and coverage on the QDs; as adsorbed ligands display broadened line

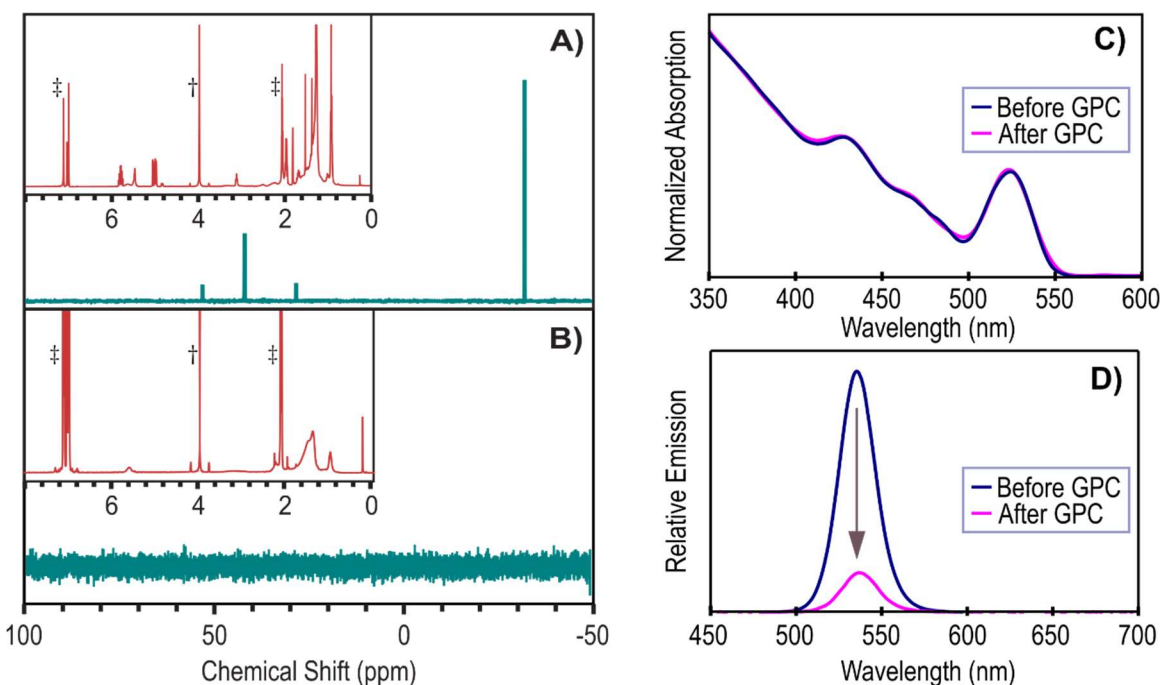


**Figure 3.2**  $^{31}\text{P}$  NMR of CdSe/CdZnS before (A) and after (B) GPC purification. A ferrocene internal standard is marked with † and the toluene-d8 solvent is marked with ‡ in the  $^1\text{H}$  NMR insets. Absorption profile (C) normalized to the first excitonic peak and band edge emission showing decrease in PL after GPC purification (D). Adapted with permission from ref. 60. Copyright 2015 American Chemical Society.

shapes, whereas free ligand species will show typical fine splitting with narrow linewidths.<sup>41</sup> Figure 3.2 demonstrates the efficacy of the GPC purification technique on relevant CdSe/CdZnS QDs, as the most drastic differences appeared in the NMR spectra and the significant decrease in PL emission, concurrent with removal of neutral L-type (and likely Z-type) ligands. There was no shift in the first excitonic peak in the absorption profile, which strongly suggested that the QDs suffered no degradation resulting from the GPC purification. The <sup>31</sup>P NMR in Figure 3.2A contains four sharp peaks pertaining to free trioctylphosphine oxide (TOPO,  $\delta=53.5$  ppm), tetradecylphosphonic acid (TDPA,  $\delta=42.3$  ppm), dialkylpyrophosphonic acid (PPA,  $\delta=28.7$  ppm), and trioctylphosphine (TOP,  $\delta=-32.3$  ppm).<sup>56</sup> These free molecules, largely displaced from the core CdSe QDs upon shell addition, are completely removed after GPC, Figure 3.2B. Pertinent <sup>1</sup>H NMR in the insets have the toluene-d8 NMR solvent (†) and ferrocene internal standard (‡) indicated. Also in Figure 3.2B the vinyl protons of OA bound to the QDs appear as broadened peaks in the chemical shift range  $\delta=4.8\text{--}5.8$  ppm, from which all impurities and excess unbound oleic acid had been removed; the remaining narrow peaks belong only to the NMR solvent and internal standard used to quantify the surface ligands.

### 3.2.2 Reintroduction of putative ligands to restore quantum yield

Molecular species present in the shell synthetic mixture and subsequently confirmed by NMR to have been removed upon purification included oleate (OA), oleylamine (OlAm), octadecene (ODE), TOP, TOPO and TDPA. It is presumable that Cd(OA)<sub>2</sub> and Cd(TDPA)<sub>2</sub> were also removed,<sup>34</sup> although such molecules would not be resolved from OA and TDPA, respectively. Especially avoiding ligand exchange of the OA for TDPA,<sup>63,64</sup> each of the neutral ligands were systematically reintroduced to the QDs at two ratios

representative of an equivalence to surface sites (300:1) and an excess (3000:1),<sup>50,77</sup> in order to determine whether the QY could be restored. A possible slow evolution of QY restoration was allowed as the putative ligand additions were monitored over a 7-day period. It may be noted that the relative QY among QDs with similar absorption and emission spectra as well as solvent can be measured with high precision, and therefore this value was reported. The bar graph in Figure 3.3 shows 1.6 monolayer CdSe/CdZnS QYs when mixed with reintroduced putative ligands and displayed relative to a GPC-purified core/shell control sample. Generally decreasing PL trends for the QDs only GPC-purified upon prolonged storage in dilute solution were likely due to a slow re-equilibration of surface-bound and/or free [metal] oleates further desorbing/dissociating from the QD surfaces into solution, given that no additional ligand was introduced to these control samples.<sup>61</sup>

In total four core/shell QD samples were prepared for this investigation: CdSe/CdZnS of 1.6 and 4 monolayer equivalents shell thickness and CdSe/CdS also of 1.6

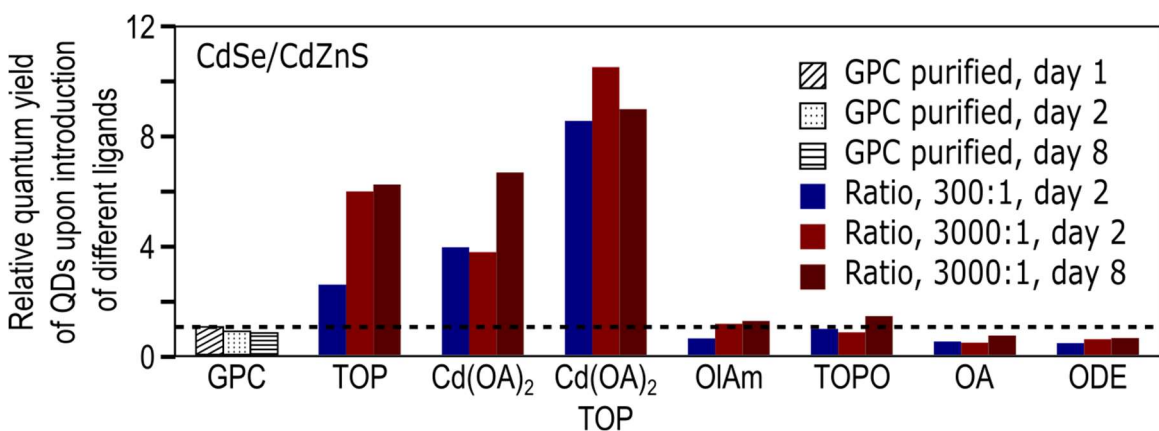


**Figure 3.3** Relative QY of GPC-purified CdSe/CdZnS 1.6 monolayer (thin shell) core/shell QDs after reintroduction of given neutral ligands and binary ligand system, normalized to the immediate QY of GPC-purified samples shown by the dashed line. Adapted with permission from ref. 60. Copyright 2015 American Chemical Society.

and 4 monolayer equivalents shell thickness.<sup>60</sup> The absolute QY (Figure 3.1) for the thinner alloy shell QDs began at 63.5% and decreased 84% relative to that initial value after GPC, and the 4 monolayer QDs decreased 23% relative to its initial 88.0% QY. The decrease in QY was ultimately attributed to an increase in nonradiative decay consequent to the removal of weakly associated ligands. Whereas ODE, OA and TOPO reintroductions did not significantly improve QY relative to the GPC-purified QDs; the remaining neutral ligand systems did restore QY at least to some degree for certain samples. Those QDs with 4 monolayer equivalents thick shells had relatively less QY regeneration overall, which was expected since the excitons in these samples should have been better isolated from surface trap states.

Not surprisingly, Cd(OA)<sub>2</sub> substantially regenerated QY in all core/shell samples as numerous studies have associated Cd-enriched surfaces comprised of such Lewis acidic ligands to be nearly solely responsible for mitigating localized surface states.<sup>13,34,39,94,167</sup> While Cd(OA)<sub>2</sub> is typically considered an electrostatically neutral Z-type ligand, the consistent and significant restoration in QY ensuing its reintroduction was irreversible – likely due to its role as an electrophilic shell precursor material<sup>62,72,207</sup> – and this ligand was deemed inappropriate for further investigation within the objectives of this study. TOP proved in all QDs investigated, the ligand that demonstrated reversible and substantial QY regeneration both alone and when combined with Cd(OA)<sub>2</sub>. Interestingly, OlAm demonstrated the least consistent trends of restoring QY among all of the core/shell QDs investigated: OlAm significantly restored QY in the thinner CdS shell QDs, comparable to the level of Cd(OA)<sub>2</sub> and TOP; moderately in the thicker CdS shell; moderately, though not maintained within the thicker CdZnS alloy shell; while having little to no effect on the thinner CdZnS alloy shell

QDs. Although the capacities of TOPO and OlAm to restore QY appear comparable for the 1.4 monolayer equivalent CdZnS material shown in Figure 3.3, this was not the case for the remaining core/shell QDs investigated. Despite some earlier theoretical calculations suggesting that OlAm and TOPO interact similarly,<sup>21,208</sup> or that TOPO has a stronger binding energy associated with Cd-based QDs,<sup>20</sup> generally amines are accepted as stronger coordinating ligands than TOPO.<sup>61,209,210</sup> An interpretation of the mechanism by which L-type ligands maintain QY is that ligand orbitals mix with QD interfacial localized states so as to move them outside the band gap.<sup>3,211,212</sup> CdZnS has a larger bulk band gap than pure CdS and therefore band edge quantum- sigma donor) and probable surface trap states would not be strong enough to move those states outside the larger shell band gap.<sup>1,12,194</sup> TOP, contrarily, can contribute  $\pi$ -bonding as L-type and/or Z-type ligands.

### 3.2.3 Effect of *reversible* reintroduction of putative ligands on photoluminescence

Time-resolved fluorescence spectroscopy was then employed to gain further insight on possible mechanisms for PL quenching and QY restoration as functions of reintroduced L-type ligand concentrations on the thinner shell QDs. Ultimately the PL decays and QY trends were congruent in that the samples that yielded higher QYs also demonstrated longer average lifetimes. Our approach comprised an interpretation of rate dispersion being either primarily or entirely inhomogeneous in QD samples apparently consequent of subpopulations having varying decay rates, which has been supported in both ensemble and single QD studies.<sup>80,213</sup> Accordingly subpopulations with lower QYs are generally expected to display shorter lifetimes due to elevated nonradiative decay rates. With this consideration, it ultimately proved possible to constrain models of nonradiative decay by decomposing the observed decays into multiple lifetime components.<sup>60</sup> In analyzing the rates and amplitudes

of said lifetime components, we sought to distinguish whether quenching in GPC-purified samples versus samples with reintroduced ligands were associated chiefly with changes in lifetime among all lifetime components or with changes in relative population fractions of QDs with distinct decay rates. Such was assessed from the amplitudes of the short and long lifetime components considered in the fits: we reported amplitude average lifetimes as they are nominally proportionally to steady-state fluorescence intensity.<sup>214</sup>

Our analysis revealed that the change in QY between samples prior to and after GPC purification, as well as between GPC purification and QY regenerated samples, were accompanied by a change in the amplitudes of the lifetime components; though with little change in the lifetime value. For example: where TOP and OlAm restored QY a reduction, but not complete elimination, of the accelerated decay at early times occurred. Whereas values of component lifetimes changed no more than 30%, ratios between the shortest and longest amplitude-averaged lifetime components increased up to nearly 7-fold. Therefore, the reduction we observed in QY upon removal of putative L-type ligands by purification appeared to be driven primarily by a large increase in decay rate among a subset of the QDs.

### **3.3 Observing kinetic and thermodynamic contributions to resolve influence of neutral ligand relative binding strengths on quantum yield**

#### **3.3.1 Steady state absorption and PL emission to indicate putative ligand binding strength**

Two immediate and reasonable assumptions pertaining to the QD surfaces are that each QD contained a number of binding sites for L-type ligands and those sites were left predominately vacant after GPC purification. Initial reintroductions of the putative ligands unambiguously distinguished which of those surfactants could restore QY, for which core/shell systems, and to what degree restored QY could be maintained over the week-long

period over which samples were measured. The lifetime component analysis was moreover applied to excess (3000:1 ligand-to-QD) TOP additions to the thinner shell samples, again over a week-long observation period, seeing as though the thinner shell QDs displayed relatively higher QY responses to ligand reintroduction and TOP significantly regenerated

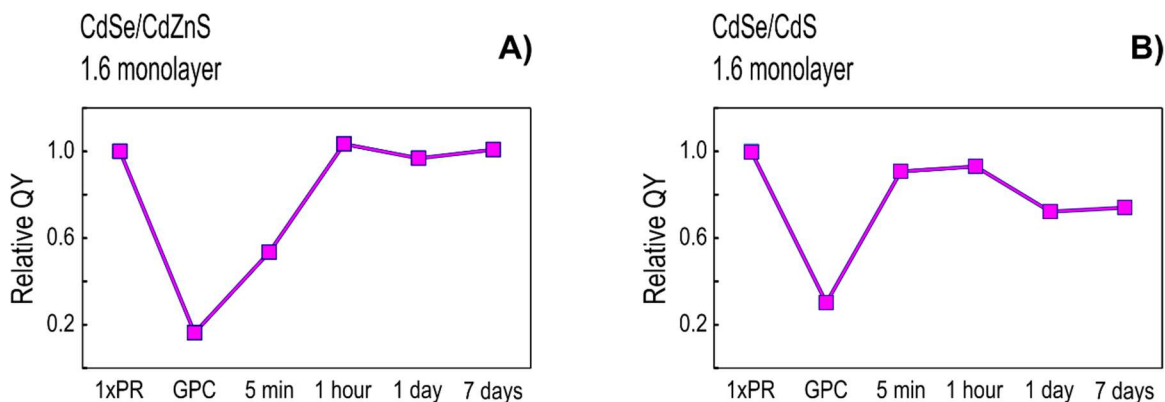


**Figure 3.4** Time evolution of QY regeneration upon reintroduction of trioctylphosphine (TOP) to thin alloy CdZnS (A) and pure CdS (B) QDs. Adapted with permission from ref. 60. Copyright 2015 American Chemical Society.

QY in all samples. As for the time evolution in the restored QY, the CdZnS alloy shell samples tended to require longer equilibration times compared to the pure CdS shell samples but subsequently maintained higher QY. Figure 3.4 conveys this phenomenon as QY was not fully regenerated until an hour after reintroduction to the CdZnS system; however, QY was nearly entirely restored within 5 minutes for the CdS shell followed by a slight decrease that was then maintained after 1 day. The distinct PLQY equilibration times presents a noteworthy and somewhat unexpected observation. Not allowing systems to fully equilibrate, especially when the result of that equilibration would yield an optimal system, is a bit daft and has led to decades of contradictory reports even in similar NC systems.<sup>14</sup>



Yet another intriguing observation was between the capacity of TOP to effectively restore QYs while TOPO consistently had no appreciable effect. If both ligands behaved similarly as merely L-type ligands, then the drastic differences in QY regeneration capacity seem counterintuitive. The sterics of these ligands would clearly be synonymous, and therefore the primary difference is in the interaction between the O- and P- adsorption to [presumably] Cd surface sites. Theoretical investigations have found those bonds to be comparable in both strength and effect on non/radiative carrier dynamics.<sup>20,37,215</sup> Historically TOPO has been a commonly asserted passivating ligand for Cd-based QDs; even a Google Image search for “ trioctylphosphine oxide ” will render cartoon depictions of ligands adsorbed to CdSe QD surfaces. However more recent findings claim this surfactant does not adsorb to the QD surface even when 99% TOPO is used as the coordinating synthetic solvent.<sup>94,163,198</sup> Our own steady state absorption and PL emission results clearly demonstrated that TOP substantially increased PLQY and TOP did not (Figure 3.5) for each

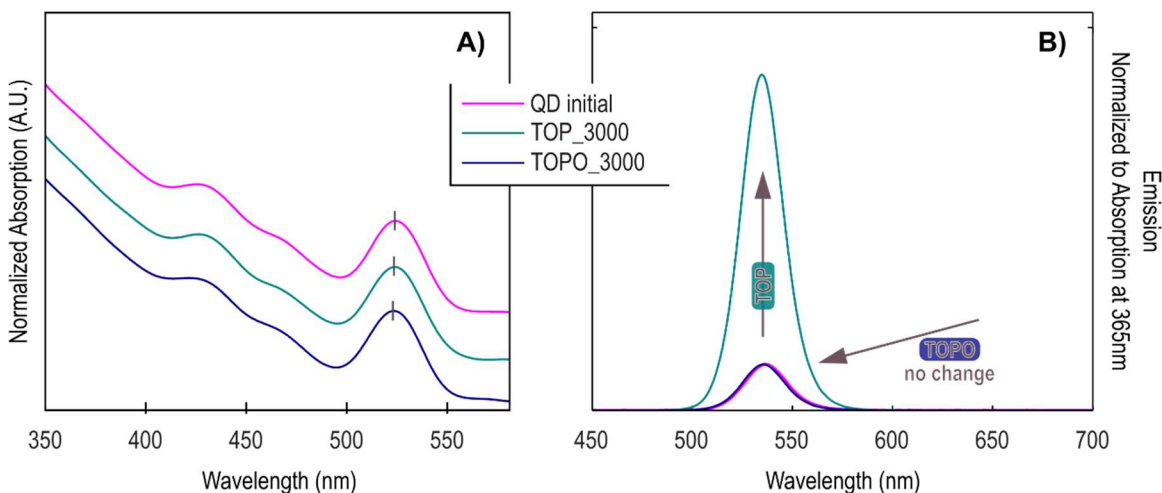


**Figure 3.5** Steady state absorption normalized to 365 nm (A) and PL emission normalized to the absorption at the 365 nm excitation wavelength (B) for initial 1.4 monolayer CdSe/CdZnS alloy shells immediately after GPC purification (fuschia), after 3000 equiv. TOP addition (teal) and after 3000 equiv. TOPO addition (navy). Optical spectra here are analogous to relative QY monitored in Figure 3.3 displayed as a bar chart. Adapted with permission from ref. 60. Copyright 2015 American Chemical Society.

of the CdS and CdZnS core/shell QD samples monitored.<sup>60</sup>

### 3.3.2 NMR spectroscopy to indicate putative ligand binding strength

On the basis of our results above as well as previous literature reports, L-type ligands (including TOP, TOPO, and OlAm) can reversibly attach to and detach from the QD surface.<sup>5,50,61</sup> However, as shown in the spectroscopic regeneration and lifetime studies, not all of these surfactants contributed directly to the photophysical property changes in QDs. Ligand–QD interactions are known to influence the energy levels and occupation of interfacial states, affecting electron and hole trapping rates and intraband decay rates.<sup>1,3,205</sup> The effect of a certain total ligand concentration will thus depend on the adsorption isotherm and on the effect of such binding on the interfacial states. Inasmuch it is desirable to have an independent measurement of the extent of binding so that those factors can be distinguished. NMR has been proven to be a powerful technique for the determination of the interactions between ligands and the nanocrystal surface. In some cases of rapidly exchanging species, however, changes in the general one dimensional NMR line shape distinguishing bound versus free ligands are not resolvable.<sup>73</sup> Diffusion-ordered NMR analysis has been employed specifically to characterize the bound and free ligand population on QDs in previous work.<sup>41,62,91,216</sup> However, in this study, we could not observe any significant difference in diffusion constant measured by DOSY.<sup>60</sup> Differences in the effective diffusion constant probed by diffusion-ordered spectroscopy can prove difficult to detect for low bound-ligand-fractions. Likewise, neither  $T_1$  measurements on  $^{31}\text{P}$  nor NOE response on  $^1\text{H}$  spectra with selective saturation on the  $^{31}\text{P}$  resonance upon introduction of TOP or TOPO to GPC-purified QDs solutions were able to conclusively resolve apparent differences in these surfactant interactions with the QD surface. Both phosphine surfactants

behaved similarly to free ligand controls in each of these NMR experiments. These results strongly suggested a fast (relative to the NMR timescale) dynamic adsorption/desorption equilibrium, where the bound ligands are exchanging rapidly with the excess of unbound ligands in the solution.<sup>73</sup>

### 3.3.3 Isothermal titration calorimetry to determine putative ligand binding strength

As NMR techniques were incapable of resolving binding environments of TOP versus TOPO, despite the unequivocal differences in their optical spectra, I therefore employed isothermal titration calorimetry (ITC) to detect and characterize the binding between the neutral ligands and QDs. Although widely used in biochemistry, ITC has only recently begun to be applied to nanoparticles to assign parameters for multiple binding problems.<sup>50,51,53,217,218</sup> In this study, we titrated the same amount of TOPO, OlAm, and TOP to the GPC-purified 1.6 monolayer equivalent CdSe/CdZnS sample to measure the heat response. Any response of the system as equilibrium is re-established that has nonzero enthalpy change, such as bond formation upon ligand binding, will generate a heat response. The shape of the heat response over the course of the titration can be used to characterize the equilibrium constant and stoichiometry of reactions, while the sign and magnitude of the signal characterize the associated enthalpy change. Due to the intolerance of the machine toward toluene, anhydrous tetrahydrofuran (THF) was used as the solvent for this study.

As shown in Figure 3.6, when TOPO is titrated, the overall heat response is small and no trend can be observed in the integrated curve, which indicates that there is no significant interaction between TOPO and the QDs, at least at these concentrations. A somewhat recent Perspective article by Krause and Kambhampati noted that gaining a “proper understanding of what ligand actually binds to the NC surface” and the mechanism

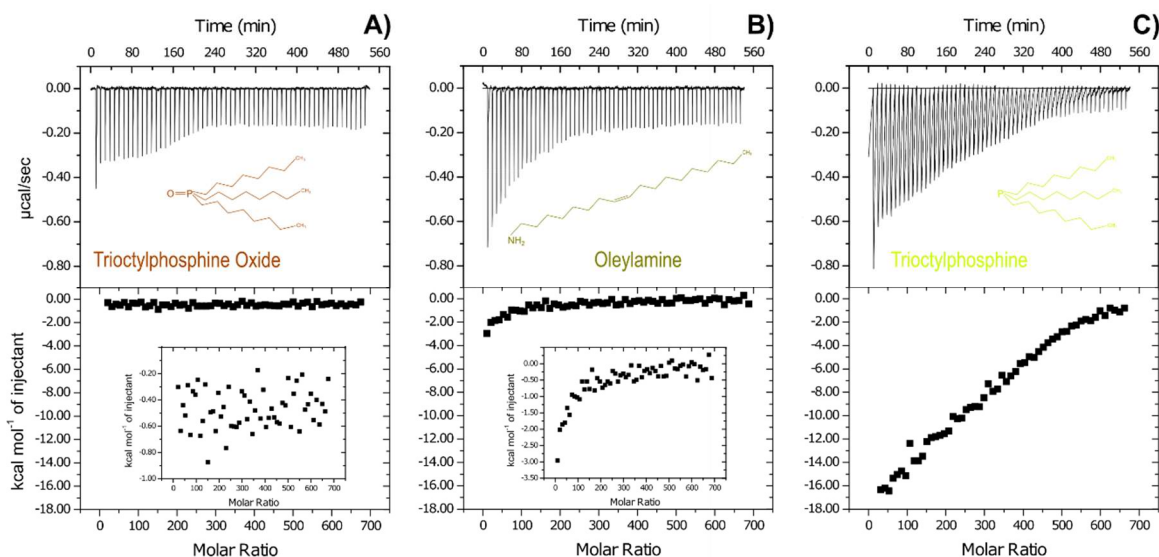


**Figure 3.6** ITC traces for 1.6 monolayer equivalent CdSe/CdZnS QDs titrated with TOPO (A), OLAm (B), and TOP (C) at equal QD and ligand concentrations. Top panels display raw heat per injection thermograms, while the bottom panels show the integrated isotherm curves scaled to the TOP titration axis. Insets in the bottom panels (A) and (B) reveal zoomed-in integrated curves for TOPO and OLAm titrations, respectively. Ligand-to-solvent reference titrations have been subtracted from the traces shown; as solvent-to-solvent and solvent-to-QD runs yielded negligible responses. Adapted with permission from ref. 60. Copyright 2015 American Chemical Society.

by which surface modification could occur is critical for the rational tuning of NCs toward applications.<sup>194</sup> In the context of TOPO interacting with Cd-based QD surfaces, ITC has shown rather unambiguously that TOPO indeed does not bind to this surface. Though it is imperative to choose adequate concentrations, reaction/association parameters and basis for comparison (e.g. OLAm or other control titrations) in order to confidently assert as much. Otherwise a slight trend in the raw thermogram, even as our data depicts until ~200 molar ratio, might lead one to analyze such data as though this ligand binds and plays a critical role in emissive pathways.<sup>50</sup> The ITC trace for introduction of OLAm shows a small exothermic response at low ligand concentration that rapidly saturates. This rapid saturation indicates a high association equilibrium constant. The thermogram was fit with the simple independent identical sites model by varying the number of sites per QD  $N$ , equilibrium constant  $K$ , and

molar enthalpy change  $\Delta H$ . The best fit was obtained when the number of sites is close to  $N = 10$ , with  $K = 2.3 \times 10^4 \text{ M}^{-1}$  and  $\Delta H = -27 \text{ kcal/mol}$ . However, since the magnitude of the equilibrium constant  $K$  is small and the QD concentration is low, the molar enthalpy change  $\Delta H$  and the number of sites  $N$  are correlated in the fit. In particular, the shape of heat response curves within this model are parametrized by Brandt's  $c$  parameter ( $c = [\text{QD}]KN$ , where  $[\text{QD}]$  is the concentration of the QDs).<sup>46</sup> For data that are characterized by  $c$  values smaller than 1 (indicating a small mole fraction of bound ligands out of the total added), the enthalpy change and the number of sites are correlated, but the equilibrium constant  $K$  is well-constrained. When TOP was introduced, a much greater exothermic response than for the reaction with OlAm was observed (an overall exothermic heat approximately 14 times more than that of OlAm). The greater heat indicated that TOP has a more negative molar enthalpy of binding and/or binds to a greater number of sites per QD than does OlAm. As seen in the PL response during QY regeneration (Figure 3.4), slower kinetics were also observed in the raw heat thermogram signal, which did not rapidly return to baseline between injections when TOP was introduced to the thinner shell CdSe/CdZnS QDs. The thermogram for TOP could not be well-fit by a simple independent identical sites model. In order to compare the results for TOP and for OlAm, one approach was to consider the difference in  $\Delta H$  and  $K$  that would be required if the number of binding sites per QD is constrained to the same value. In this case, a fit with  $N$  fixed to 10 revealed a ratio of  $\Delta H_{\text{TOP\_QD}}/\Delta H_{\text{OlAm\_QD}} = 37$  and  $K = 4.3 \times 10^3 \text{ M}^{-1}$  for TOP. Despite an apparently larger equilibrium constant for OlAm than for TOP, introduction of OlAm led to much less change in QY than TOP, particularly in the alloy shell QDs. This could indicate that the ITC signal for OlAm corresponds to binding to only a subset of active trapping/quenching sites or that binding of OlAm does not sufficiently perturb the energy levels associated with

trapping and recombination, as was postulated earlier. However, due to the steric and electronic differences between these molecules, it is highly possible that OlAm and TOP bind to different sites on the QD and the number of sites is therefore not the same. While the possibility of TOP binding to more sites than OlAm is contrary to recent experimental results by Anderson et al.,<sup>200</sup> the trends we observed in ligand binding strength from ITC are consistent with those predicted in Rempel's work for ligands binding to the Se-terminated (0001) surface of wurtzite CdSe<sup>215</sup> and in our case were very reproducible. The theoretical value of the binding energy between TOP to wurtzite CdS S-terminated (0001) surface is 3.13 eV.<sup>219</sup> If we assume the binding behavior of TOP to the CdZnS alloy shell surface is similar to that for pure CdS, then the total heat response that we observed of approximately -200 eV/QD (obtained by integrating the response shown in Figure 3.6C) corresponded to about 60 available sites for TOP per QD. Clearly a more adequate model accounting for interactions among similar and dissimilar ligands is needed to describe such ligand association, dissociation, and exchange reactions more thoroughly, and that could be an important target for future studies. Nevertheless, it seemed reasonable for the study at hand,<sup>3</sup> particularly for ligands behaving as  $\sigma$  donors, to argue that a strongly exothermic bond-forming step leading to a large energy separation between bonding and antibonding orbitals, could assist in displacing electron traps from within the band gap.<sup>202</sup> The trend of enthalpy change and QY regeneration that we observed supports this argument.

### **3.4 Investigation of neutral amine ligand binding interactions with CdSe quantum dots via isothermal titration calorimetry**

#### **3.4.1 A confounded history of amines and Cd-based QDs, especially alkylamines**

Amines present a particular ligand system that has garnered much attention for Cd-based QDs, as well as produced extremely contradictory results. One particular conundrum is that while alkylamines have been well-established to decompose  $\text{Cd}(\text{OA})_2$  polymers into smaller complexes,<sup>220</sup> the common initial QD ligand oleate will neither prevent amines from coordinating to  $\text{Cd}^{2+}$  nor will OA be displaced in the framework of an L-type for X-type ligand exchange.<sup>34,54</sup> This behavior has resulted in perplexing results<sup>221</sup> originally intended to elucidate the impact of amines on NC growth, especially since alkylamines significantly affect QDs of groups II-VI and IV-VI.<sup>72,102,222–224</sup> In the case of core-only CdSe QDs, the presence of amines in the synthetic mixture at varying concentrations can determine expected size regime, morphology and concentration of surface defects.<sup>40,192,224</sup> Teunis et al. recently utilized the apparent temperature and aliphatic chain length dependence on QD precursor activation<sup>225,226</sup> to provide further insight on their proposed fourth stage concluding the widely accepted LaMer and Dinegar model<sup>227</sup> of monomer production toward NC nucleation and growth.<sup>228</sup> Conversely, upon addition of wider band gap shell material, our own investigations have explored the role of amines competing with complete conversion of shell precursor material toward isotropic particles,<sup>72</sup> as would be reasonably explained by the capacity for alkylamines to coordinate  $\text{Cd}(\text{OA})_2$  complexes..

Additionally, amines have had a nontrivial effect on QD optical properties, to some degree explored in the previous QY regeneration investigation. At one point amines were thought to induce crystal structure reorganization by mere ligand exchange,<sup>221</sup> conversely however, the narrowing energy gap between the first and second excitonic absorption bands upon amine association was unambiguously attributed to ligand-induced modification of transition energy and extinction coefficient in the QD's excitonic band.<sup>196</sup> As alkylamines are

particularly potent Z-type displacing ligands in Cd-chalcogenide QDs, this displacement can be monitored by a typical decrease in PLQY as well as a significant decrease in intensity of the  $1S_e-2S_{3/2h}$  absorption.<sup>34,196</sup> For years amines were reported to both diminish<sup>229,230</sup> and enhance<sup>78,201,231–233</sup> PL in NCs. It is now accepted that when amines associate as L-type ligands they will likely enhance PL, but beyond a large excess amine addition will quench PL as this addition promotes Z-type ligand displacement.<sup>14,34,77,168,234</sup> To reiterate a point made earlier in this chapter, the vast majority of what has been discovered about QD surface chemistry has ensued surface modification rather than directly probing the as-synthesized system. Since Anderson et al. confirmed Z-type displacement in 2013, a number of recent investigations have relied on this reactive displacement regime to elucidate QD surface chemistry and thermodynamic parameters, especially where incorporating a shell is not advantageous to projected applications (e.g. photovoltaics).<sup>13,167,168,197</sup>

Prompted by longstanding contradictory investigations, the established propensity of  $Cd(OA)_2$  or Cd-phosphonate Z-type ligands to associate to QD surface sites having analogous impacts on QD photophysical properties as those of amine ligands<sup>167</sup> and an overall scarcity of consistent equilibrium thermodynamic parameters,<sup>61,235,236</sup> I sought to conduct a systematic investigation of amine association to CdSe QDs via isothermal titration calorimetry. Elegant NMR investigations of amine–QD surface dynamics have been published to establish relatively strong binding, however the rapid ad/desorption dynamics become difficult to resolve toward equilibrium constant values. ITC allows extremely sensitive characterization of such dynamics within the QD–ligand system without relying on a spectroscopic signature which could be indistinguishable or suppressed *in situ*. Furthermore, given the complexity of the colloidal QD system and the convolution of



reaction components contributing to overall heat signals in the ITC, a simplified reaction coordinate describing amine association to well-defined vacant QD surface sites could be conceived that could ultimately mimic the hallmark 1:1/single type of independent site model. Results from our QY regeneration and competitive shell growth solvent studies could also be used to determine reaction parameters.<sup>60,72</sup>

### 3.4.2 Determining amine association reactions to investigate via ITC

Whereas the previous investigation sought to resolve the more significant impact of electronic behavior or steric hindrance on QD–ligand interactions comprising putative neutral ligands that had already been shown to alter QD photophysical properties, this study employed an amine L-type association reaction that are directly advantageous toward further defining the complex landscape of the NC surface. ITC entails the considerable advantage of providing a full thermodynamic profile for an interaction within one experimental trial once proper reaction parameters are discovered,<sup>46,237</sup> yet reasonable targets for such a deliberately “simple” investigation constitute ligand systems that are most relevant to the CdSe QD system. Oleylamine (OlAm) possesses a central double bond which creates a kink in the 18-carbon aliphatic chain and is constantly employed in QD synthetic procedures, especially pertaining to shell growth.<sup>60,72,207,224</sup> Decylamine (DecAm) is a straight 10-carbon chain alkylamine that has been reported to have a temperature-dependent equilibrium constant, ranging  $1.56 \times 10^4 \text{ M}^{-1} - 2.68 \times 10^4 \text{ M}^{-1}$  with moderately decreasing temperature, in one of the most heavily cited reports on QD–ligand interactions.<sup>61</sup> Trihexylamine (TriHexAm) is a tertiary amine with roughly similar molar mass to commonly employed Cd-based NC synthetic and surface modification reaction additives.<sup>72</sup> Although some studies have claimed that amine chain length does not have as significant an impact as steric impact, ligands will

undoubtedly contribute entropic effects as fractional occupation on the QD surface increases.<sup>59,238</sup> Accordingly, QD samples used in this study were kept within a narrow size range as determined by their lowest energy extinction peak.<sup>33,82</sup>

So as to closely resemble a single independent type of site model system, phosphonate (TDPA)-capped CdSe cores were chosen as the starting material. Phosphonate X-type ligands have long been established as one of the strongest binding ligand constituents for Cd-based QDs in native organic solvents.<sup>1,2,37,239</sup>

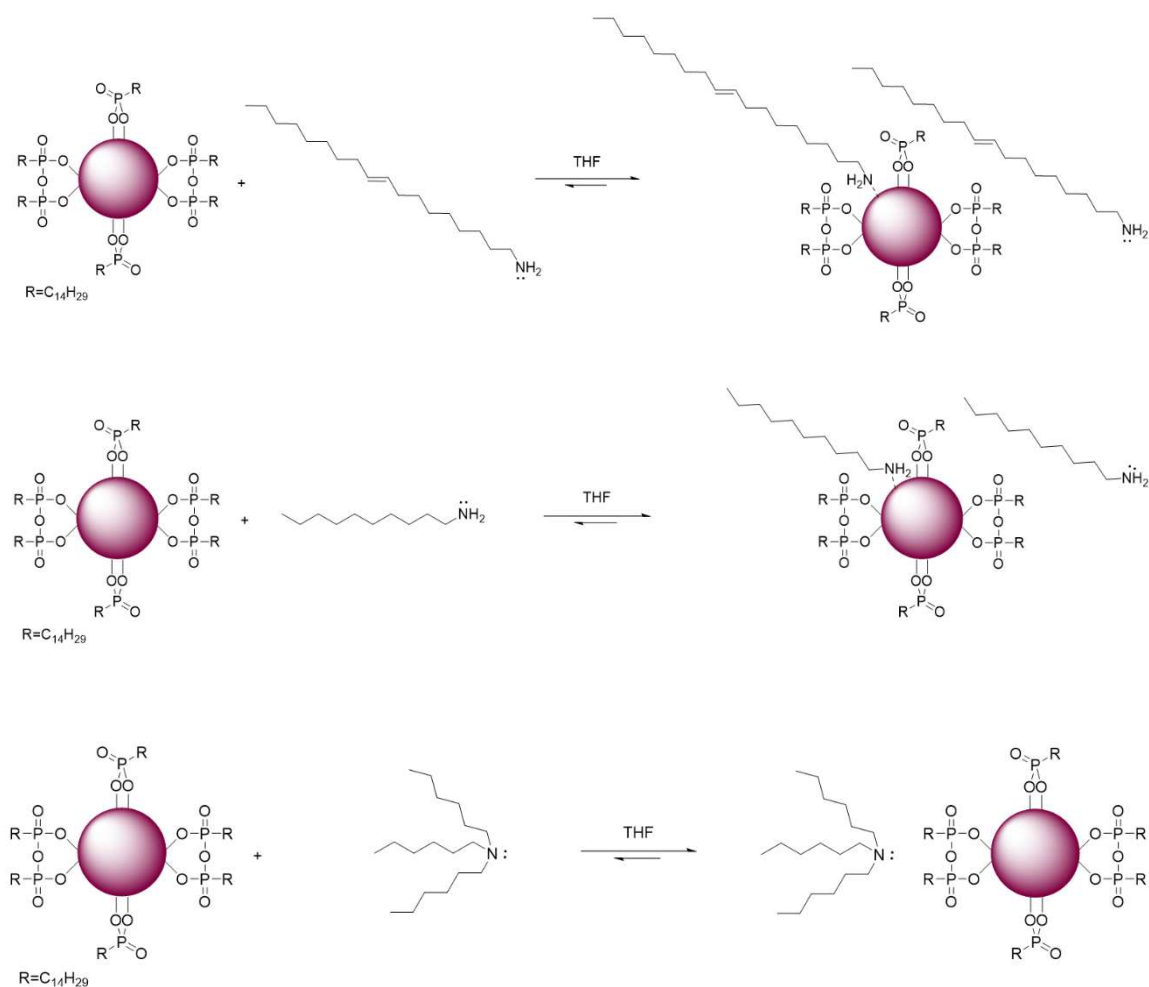


**Figure 3.7** Reaction scheme for neutral L-type ligands association to TDPA-ligated CdSe QDs: oleylamine (OAm), decylamine (DecAm), trihexylamine (TriHexAm) from top.

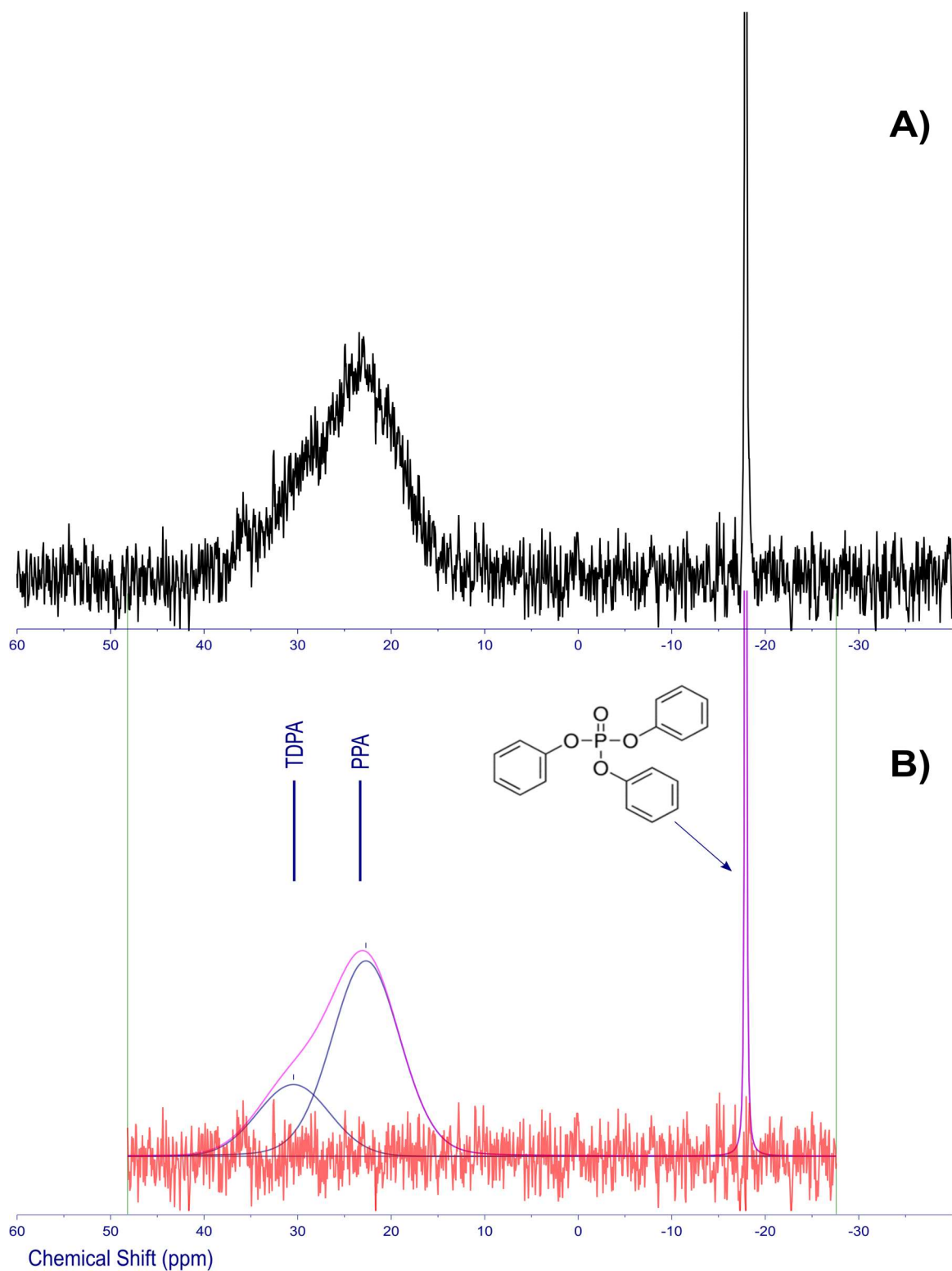


**Figure 3.8** Quantitative  $^{31}\text{P}$   $\{^1\text{H}\}$  NMR of GPC-purified CdSe/TDPA with triphenyl phosphate internal standard (A) showing peak fits (navy and fuschia) and fit residual (red) using MNOVA software package to analyze NMR spectrum (B). THF GPC purified QDs were brought into THF-d<sub>8</sub>.

GPC purification was employed to produce consistent starting material, though in this case the mobile phase solvent was anhydrous THF (this solvent is suitable for both the QDs and titrant ligands, as well as proven compatible with the SX-1 Bio-Beads and ITC). Figure 3.8 depicts quantitative  $^{31}\text{P}\{^1\text{H}\}$  NMR of the purified  $\text{CdSe}/\text{TDPA}^-$  QD starting material in THF- $d_8$ . At least two peaks are resolved in the broad bimodal resonance representing P-containing ligands adsorbed to the QD surface. Dialkylpyrophosphonate (PPA,  $\delta=22.7$  ppm) has been confirmed as a ligand alongside TDPA ( $\delta=30.4$  ppm) both ionically bound to the CdSe QDs.<sup>137,163,198</sup> The sharp peak belongs to the internal standard triphenyl phosphate (TPP,  $= -17.9$  ppm). To a carefully monitored ligand equivalence, incoming amines should only associate with vacant QD surface sites but will not be potent enough to replace phosphonate X-type ligand species. Furthermore, given the relatively small fraction of amine ligands expected to adsorb/interact with the QD surface ( $\leq 10\%$  of the entire ligand population of approximately 300 ligands per QD, which coincides with previous reports of P-containing ligands adhered to CdSe QD surfaces of comparable diameters)<sup>63,93</sup> each amine ligand might reasonably be supposed to interact with the QD surface independently of one another,<sup>81</sup> thus validating this interpretation via the simplest isotherm model. The initial sections of this chapter outline our previous assertions about the delicate interplay between electronic and steric interactions dictating the relative strength of ligand adsorption. Moreover, a meticulous investigation of sterically different amine solutions implemented in shell growth solvents implicated the substantial impact of either homotropic or heterotropic steric interactions dictating the relative strengths of QD–ligand interactions. The results of the current investigation concur with those previous results, in that among binding headgroups with similar electronic properties, sterically encumbered ligands (e.g. TriHexAm)

will not fit onto surface sites at discernable densities (Figure 3.9C). The present results furthermore directly and quantitatively confirm that relative amine strength of binding interactions vary with amine structure.

Immediately following THF GPC purification, the amine solutions were diluted to the titration concentrations as determined by their lowest energy extinction peak<sup>33</sup> and loaded into the standard volume NanoITC. Amine solutions were prepared in a N<sub>2</sub> atmosphere glovebox, and the titrant syringe was immediately loaded into the organic solvent titrant burette handle. All titrations occurred at equal amine and QD solution concentrations and were repeated at least in triplicate. While it is customary to subtract control titrations that produce significant heat compared to the “mechanical baseline” established by a THF–THF titration, an analysis protocol allowed a constant to be subtracted from the entire titration (as outlined in the NanoAnalyze software manual ©TA Instruments). This protocol was appropriate in these dilute titrations due to the extensive

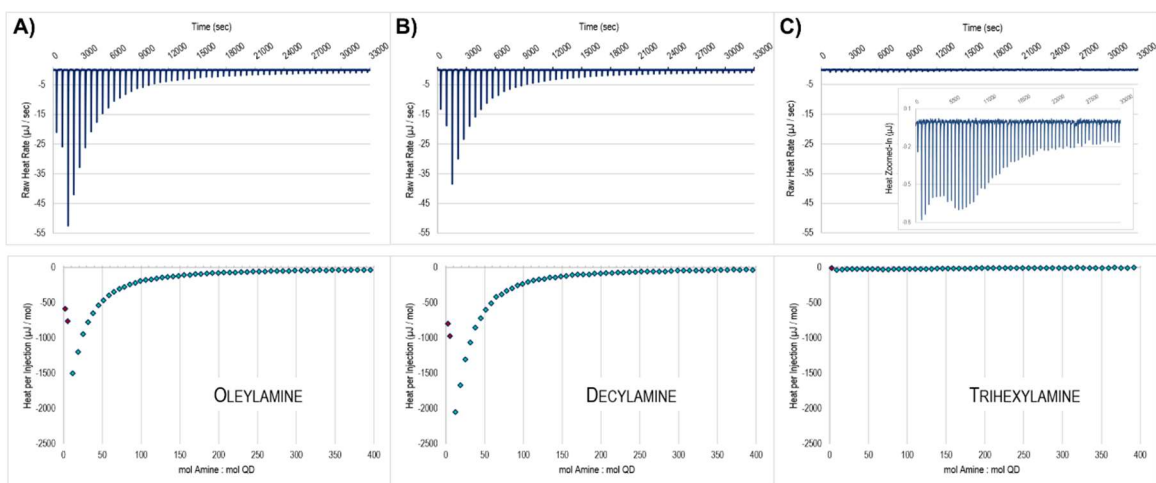


**Figure 3.9** ITC traces for OlAm (A), DecAm (B) and TriHexAm (C) titrated into CdSe|TDPA solutions in anhydrous THF. The inset in panel (C) depicts a “zoomed-in” thermogram for the TriHexAm titration, confirming impact of sterics to prevent binding.

and consistent thermogram saturation tails, and consequently determined for each individual titration by examining the peak height of the final 5-10 injections. Still, thermograms for the reference titrations are shown in Figure 3.10 to confirm that indeed there were no significant amine–solvent interactions, especially as compared to the magnitude of the peak heights alluding the endpoint saturations for each titration experiment.

At room temperature the two primary amines (of different aliphatic length and saturation) titrated into GPC-purified CdSe|TDPA showed prominent exothermic heat responses (Figure 3.9A & B). The two primary amines demonstrated relatively rapid equilibration, both between injections and becoming saturated on the QD surfaces titrated at 400:1 ligand-to-QD mole ratios, consistent with the thermogram shapes we observed in the QY regeneration amine titration. This rapid saturation indicates a relatively high association equilibrium constant. The thermogram was effectively fit with the simple independent model by allowing the number of sites per QD  $N$ , equilibrium constant  $K$  and molar enthalpy change  $\Delta H$  to vary. In particular, alkylamine–QD titrations were evaluated over a number of

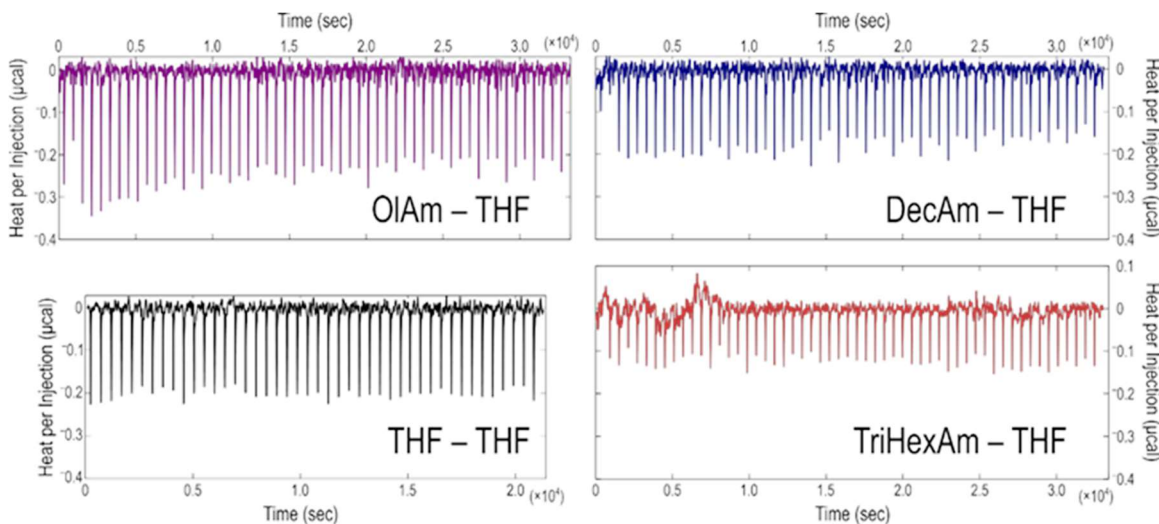


**Figure 3.10** Raw heat thermograms for each amine into anhydrous THF as well as the solvent–solvent titration (bottom left).

concentrations and resulting  $K$  values were consistent, further affirming the adequate choice of the identical independent sites model.<sup>56</sup> However, since the overall magnitude of the equilibrium constant  $K$  is small and the QD concentration is low, the molar enthalpy change  $\Delta H$  and the number of sites  $N$  are correlated in the fit. The shapes of heat response thermogram curves within this model are parametrized by Brandt's  $c$  parameter ( $c = [\text{QD}]KN$ , where  $[\text{QD}]$  is the concentration of the QDs)<sup>46</sup> even while titrant solution concentrations are well above 20 $\times$  that of the titrand solution.<sup>240</sup> The product of  $N \times \Delta H$ , on the contrary, is well constrained and therefore both reported and employed to analyze the robustness of repeated titration parameters within this investigation. Table 3.1 lists the equilibrium thermodynamic parameters for the titrations contributing to the traces depicted in Figure 3.9. While  $Ka$  was the only well-constrained parameter that can therefore be appropriately evaluated against previous reports at this stage, it was in good agreement with published values.<sup>61,167,228</sup>

**Table 3.1** Thermodynamic equilibrium parameters for amine association to CdSe|TDPA

ASSOCIATION	$Ka$ $\times 10^3 \text{ M}^{-1}$	$N \times \Delta H$ $\times 10^3 \text{ kJ}$	$N$ per QD	$\Delta H$ $\text{kJ mol}^{-1}$	$\Delta G$ $\text{kJ mol}^{-1}$	$\Delta S$ $\text{J mol}^{-1} \text{ K}^{-1}$
<i>Oleylamine</i>	$5.18 \pm 0.39$	$-2.15 \pm 0.22$	$8.80 \pm 0.62$	$-248 \pm 22$	$-21.0 \pm 0.15$	$-511 \pm 0.082$
<i>Decylamine</i>	$6.56 \pm 0.68$	$-2.02 \pm 0.076$	$11.7 \pm 0.17$	$-172 \pm 7.2$	$-21.5 \pm 0.17$	$-769 \pm 0.19$

Standard errors of the means on ITC model parameters:  $K$ ,  $N$ ,  $\Delta H$ ; Propagation of errors on calculated parameters:  $\Delta G$ ,  $N \times \Delta H$ ,  $\Delta S$ . \*Reported as product due to low  $c$  parameter value,<sup>46</sup> signifying  $N$  and  $\Delta H$  are not independently constrained.

### 3.4.3 Verification of L-type association reaction, rather than Z-type reactive displacement

Firstly, QD stability and consistent initial surface concentrations were firmly established despite employing anhydrous THF solvent – in which TDPA and  $\text{Cd}(\text{TDPA})_2$  can be presumed quite labile compared to less polar organic solvents (e.g. toluene and hexanes)<sup>241</sup> –

throughout the entire purification and titration processes via optical spectroscopy as well as  $^{31}\text{P}$   $\{^1\text{H}\}$  NMR characterization. The 1×PR preparation involves deliberately diluting the QDs to allow unreacted precursor material to further separate from the QD solution in an overnight refrigeration step, followed by additional centrifugation prior to GPC purification. To prevent detrimental oxidation or other form of QD surface decomposition; QDs were immediately concentrated under  $\text{N}_2$  flow, loaded onto the GPC column, and immediately either loaded into the ITC for titration experiments or worked up into deuterated solvent for NMR experiments. The reproducibility of relevant spectra and isotherms confirmed that this procedure was effective toward exceptionally consistent sample preparation.

Upon air-free titrations of neat DecAm or OlAm into CdSe|TDPA in THF- $d_8$ , quantitative additions at and beyond the mole ratio used in repeated ITC trials did not reveal liberation of native TDPA (or PPA) in  $^{31}\text{P}$   $\{^1\text{H}\}$  NMR<sup>200</sup> (data not shown). Rather,  $^{31}\text{P}$   $\{^1\text{H}\}$  NMR spectra demonstrated no change in the broad bimodal peaks of bound phosphonate species at ~400:1 molar equivalents (analogous to the ITC endpoint mole ratios), nor were sharp peaks indicative of liberated P-containing ligands apparent in the spectra until roughly 4× that amine equivalent was introduced. We remain confident that even slightly beyond that ~1600:1 amine-to-QD mole ratio Z-type reactive displacement was not incurred, as our own investigations of Cd-based QDs subjected to amine environments both in the present and previous studies revealed substantial differences between dilute amine solution versus amine solvent additions.<sup>60,72</sup> At exceedingly high mole fractions of titrated DecAm, up to 40,000-fold excess,<sup>14</sup> whereupon  $^{31}\text{P}$   $\{^1\text{H}\}$  NMR spectra no longer showed the broad peak for P-containing ligands adsorbed to the QD surface we do not rule out the possibility of ammonium ions having been formed. Distinguishing the possible formation of an



ammonium ion ligated between the QD surface and persistently interacting P-containing ligands from a more straightforward reactive displacement of Cd-phosphonate complexed with amines in solution could not be achieved unambiguously in the scope of our 1D  $^{31}\text{P}$   $\{^1\text{H}\}$  NMR titrations.<sup>196,199</sup> Monitoring reactive displacement reactions via ITC could present a critical component to better understanding QD surface interactions, but was outside the scope of the aims of this investigation.

Amine ligand additions at the 400:1 mole ratio were further characterized by standard optical measurements during the course of the titration experiments. Steady state absorption and emission profiles should be sufficient to indicate structural maintenance of the QDs. As mentioned previously, loss in intensity of the  $1\text{S}_e-2\text{S}_{3/2\text{h}}$  absorption feature can indicate that reactive displacement of Cd-phosphonate ligands has occurred. We did not note any significant difference that could be attributed to such ligand interactions. Presented

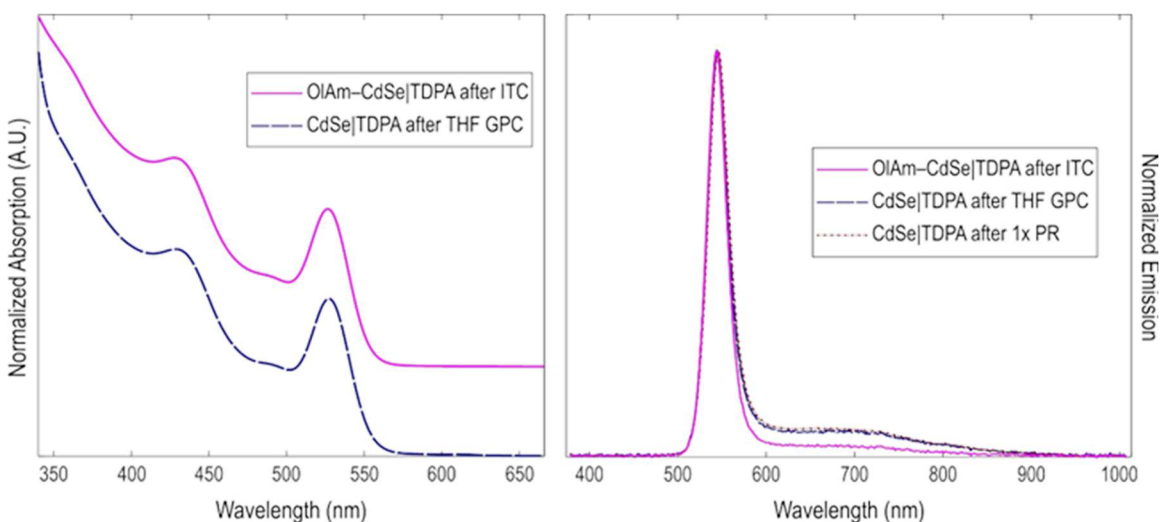


**Figure 3.11** Absorption (left) and PL emission (right) of CdSe|TDPA in anhydrous THF normalized to the lowest energy extinction peak: after THF GPC purification (dashed navy lines), then after OIAm ITC traces (fuchsia lines). Aliquots of QD solutions at each stage of amine association reactions were routinely monitored to verify QD structure viability throughout the course of purification and titration experiments.

in Figure 3.11, the absorption profiles appeared nearly superimposable. Additionally, PL emission profiles of the samples would exhibit a hypsochromic shift in the band edge core excitonic peak along with an increase in intensity of broad low energy PL, if in fact reactive displacement were affected<sup>242</sup> in the ligand addition regime of amine association as outlined below. Rather than a degradation of the normalized PL, the band edge core peak became slightly narrower with a notable reduction of the broad emission band attributed to a mitigation of surface defects by amine passivation.<sup>243</sup> At the chosen titration equivalencies, the steady state photoluminescence suggests amines were only added to an extent that provided surface trap remediation.<sup>234</sup>

#### 3.4.4 Sigmoidal ITC thermogram by way of adventitious purification solvent

Having unequivocally confirmed that my original aim of monitoring a neutral association of L-type amine ligands to intrinsically vacant QD surface sites after GPC purification had been achieved, I returned to ITC reactions in an attempt to discover reaction conditions that would allow for more robust thermodynamic parameters to be extracted from this system. As the curvature of the thermograms is a function of titrand concentration and equilibrium constant, we hypothesized that the QD concentration could prove a useful knob to extract more accurate equilibrium thermodynamic data while obtaining an adequate  $c$  parameter value,  $1 < c < 1000$ . Essentially, the CdSe|TDPA concentration was systematically increased in a manner of *chasing* a sigmoidal ITC thermogram. Titrations were executed in an Affinity low volume ITC (TA Instruments) in order to conserve QD sample, while ascertaining appropriate experimental parameters. It should be noted that despite advertising and marketing pitches, transferring calorimeters (even manufactured from the same parent company) within the span of one investigation is no trivial feat.<sup>244</sup> The first objective should

be to establish reproducible titration parameters that reflect results obtained with the initial calorimeter. In the present study due to differences in cell active volume and injection volume, that translated to half the ligand concentration and double the QD concentration. Once repeated titrations were accomplished for the DecAm–CdSe|TDPA, the work of optimizing conditions toward an *S*-shaped sigmoidal thermogram could be realized. This particular curvature signifies that at early injections significant heat is produced with decreasing heat signal through an inflection point also defined over multiple injections and finally through saturation characterized by insignificant heats of dilution, as all binding sites have been saturated at this point. DecAm concentration was maintained constant while the QD concentration was increased in increments of roughly 75%. Surprisingly, rather than ever obtaining data that presented in the sigmoidal curvature, the thermograms appeared to become more linear until the heat signal itself saturated at a constant  $\Delta H$  of interaction. A similar isotherm was produced in the QY regeneration titrations with TOP (Figure 3.6, far right panel). Lindman et al. depicted a similar thermogram trend in their investigation of polymeric nanoparticle size and consequent surface curvature on the capacity for protein binding.<sup>245</sup> Their study alluded to a size-dependent limit on protein binding properties, at which limit binding dynamics would begin to resemble those expected on a flat surface and therefore independent of curvature. Whereas the present study maintained QDs of the same synthetic batch (and therefore same size) for this aim, it could be suspected that while the surface saturation of labile ligands produced some heat a concentration gradient impaired ligand interactions with the QDs. Inasmuch, there could be some optimal range of QD concentration to which the neutral alkylamines could be titrated to a “complete” surface saturation.

Despite not achieving a sigmoidal thermogram through direct and immediate experimental variation, we were able to generate a system in which significantly more vacant sites could be made available to the neutral ligands. The initial 1×PR that is directly followed by a dilution and refrigeration ultimately provided an environment for the QDs such that ligands were displaced from the surface to expose more electron deficient sites to accept amine association. In effect, QDs were diluted in anhydrous THF after an initial PR cycle and subsequently left in the refrigerator for several weeks. Presumably the THF solvating labile surface ligands over this timeframe while a concomitant process of the excess unreacted phosphorus precursors served as a ligand reservoir thus maintaining lipophilic stabilization for the QDs. THF had previously been identified as a Lewis base of moderate potency to displace Cd-containing Z-type ligands from Cd-chalcogenide surfaces. Figure 3.12 compares titrations of the two primary amines, OlAm and DecAm, to the “aged” CdSe|TDPA. Aside from the purification aging procedure, all experimental parameters were kept the same as for the “fresh” CdSe|TDPA QDs. With these remarkable results, a Langmuir association model could be fit to the isotherms to obtain thermodynamic parameters on which the initial fresh titration trial fits could be approximated. NanoAnalyze (TA Instruments) models for a combined “Constant Blank” and “Independent” model fit was applied to the isotherms as shown in Figure 3.12 C,F. The equilibrium thermodynamic parameters for the aged CdSe|TDPA QD titrations are presented in Table 3.2.

Error analysis was also applied from the NanoAnalyze software from the Statistics function. Thermodynamic equilibrium parameter uncertainties at a 95% confidence interval were calculated by adding perturbations to the optimized fits, and subsequently refitting the model over a chosen 100 trials. Each of the perturbations is engineered to follow a Gaussian

**Table 3.2** Thermodynamic equilibrium parameters for amine association to aged CdSe|TDPA

ASSOCIATION	$K_d$ $\times 10^{-5}$ M	$N$ per QD	$\Delta H$ kJ mol <sup>-1</sup>	$*K_a$ $\times 10^3$ M <sup>-1</sup>	$*\Delta G$ kJ mol <sup>-1</sup>	$*\Delta S$ J mol <sup>-1</sup> K <sup>-1</sup>
<i>Oleylamine</i>	$6.97 \pm 0.66$	$175 \pm 2.0$	$-92.4 \pm 1.9$	14.4	-23.5	-234
<i>Decylamine</i>	$10.4 \pm 0.51$	$198 \pm 1.6$	$-91.6 \pm 0.92$	9.62	-22.5	-234

NanoAnalyze (TA Instruments) isotherm fit parameters for combined Blank (constant) and Independent models with reported errors based on perturbations as 100 trials over a Gaussian distribution for a 95% confidence limit applied to the *Blank*,  $K_d$ ,  $N$  and  $\Delta H$  parameters. \*No error analysis was provided from software modeling for these thermodynamic parameters.

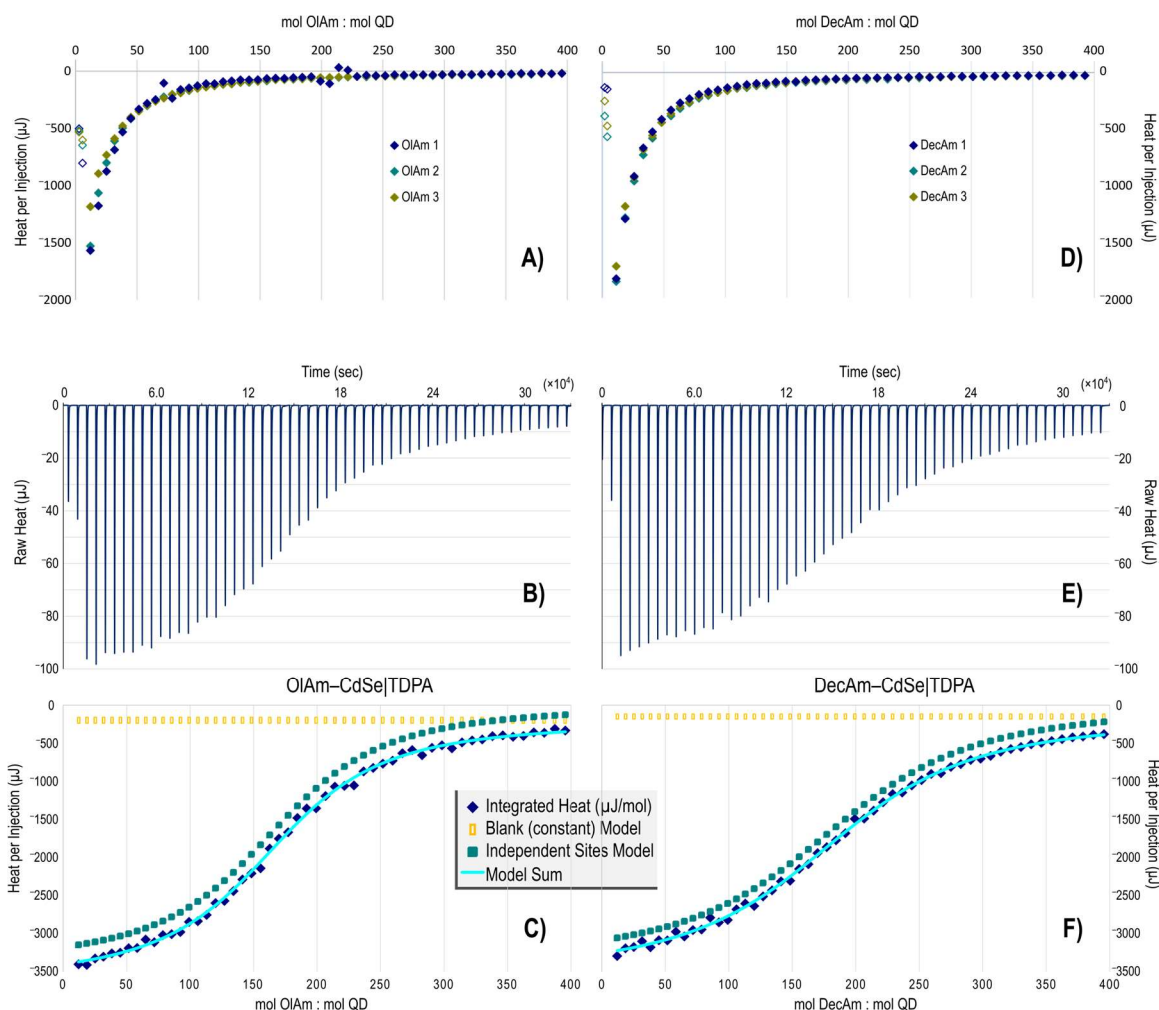


**Figure 3.12** ITC traces of OIAM-CdSe|TDPA (A-C) and DecAm-CdSe|TDPA (D-F) in anhydrous THF solvent. Repeated isotherms of QDs immediately introduced to the ITC and alkylamines after GPC purification are shown at the top (A,D). The remaining panels depict titrations carried out under the same experimental procedures, but for aged CdSe|TDPA QDs.

distribution toward the established confidence limit. In the case of the aged OlAm–CdSe|TDPA titrations the Blank value was  $-224 \pm 34 \mu\text{J}$  (Figure 3.12 C, open marigold squares). In the case of the aged DecAm–Cdse|TDPA titrations the Blank value was  $-169 \pm 44 \mu\text{J}$  (Figure 3.12 F, open marigold squares). The  $c$  parameters were of adequate magnitude to deem  $N$ ,  $\Delta H$  and  $K$  independently constrained. Finally, the aged  $\Delta H$  was used to determine thermodynamic equilibrium parameters for the relevant values not precisely determined in the titrations over which heat signals quickly saturated. The results of the *age*-corrected parameters are presented in Table 3.3.

**Table 3.3** Thermodynamic equilibrium parameters for amine association to CdSe|TDPA approximated from aged  $\Delta H$

ASSOCIATION	$K_a$ $\times 10^3 \text{ M}^{-1}$	$\Delta G$ $\text{kJ mol}^{-1}$	<sup>a</sup> aged $c$ parameter	<sup>a</sup> aged $\Delta H$ $\text{kJ mol}^{-1}$	<sup>b</sup> $N$ per QD	<sup>b</sup> $\Delta S$ $\text{J mol}^{-1} \text{ K}^{-1}$
<i>Oleylamine</i>	$5.18 \pm 0.39$	$-21.0 \pm 0.15$	15.1	$-92.4 \pm 1.9$	$23.3 \pm 0.12$	$-242 \pm 1.2$
<i>Decylamine</i>	$6.56 \pm 0.68$	$-21.5 \pm 0.17$	11.4	$-91.6 \pm 0.92$	$22.0 \pm 0.053$	$-237 \pm 1.4$

With the applied  $\Delta H$  approximation from the aged-sample titrations  $K$  and  $\Delta G$  were not affected and reported as previously determined. <sup>a</sup>Values were directly used from aged-sample model fits. <sup>b</sup>Values were calculated from aged-sample model fit parameter  $\Delta H$ .

Utilizing the sigmoidal isotherm model fit results in conjunction with those parameters that were well-constrained from the initial Langmuir model fits enabled us to ultimately observe that initial vacant sites appear analogous with intrinsic vacant sites, even if they are exposed as a result of adventitious solvent interactions. The values printed in Table 3.2 suggest that there is no significant difference in equilibrium thermodynamic parameters between OlAm and DecAm. A recent investigation comparing the relative adsorption strength and ligand densities of linear versus branched aliphatic carboxylate ligands by De Nolf et al. observed that linear carboxylate ligands introduced to an oleate-capped CdSe QD solutions yielded binary ligand populations at approximately equivalent ligand populations.<sup>246</sup> As OlAm is analogous to an oleate ligand, these results are in good agreement. While a

number of reports have observed that at room temperature alkylamine chain length does not significantly affect binding strength,<sup>61</sup> intuitively one might hypothesize that smaller (shorter) ligands would better traverse a mono- and bidentate phosphonate ligand-populated QD surface, so it is possible that a smaller primary amine ligand than DecAm would yield statistically significant differences in binding equilibrium thermodynamic parameters. Lastly, although we did not expect the equilibrium constants  $K$  and certainly the number of sites  $N$  to be the same for the aged and fresh CdSe|TDPA titrations, a notable parameter value the negative  $\Delta S$ . In the freshly purified QDs  $\Delta S$  is negative, though this value should be considered approximation at best, since it was calculated from on a parameter that was not initially independently constrained, signifying unfavorable entropic interactions. Likewise, the aged QD titrations yielded a negative  $\Delta S$ . One interpretation of this result is that the large density of vacant sites on either the aged or fresh CdSe|TDPA merely became accessible to the incoming neutral amine ligands, as the result of a relatively smaller fraction of Z-type Cd-phosphonate ligands having been extruded from the QD. Such a QD surface landscape would have retained a significant fraction of the initial ligands as well as the subsequent binding of new ligands; both the large amount of amine ligands for the aged sample and tens of ligands for the fresh sample, resulting in a substantial grafting density of intrinsic phosphonate ligands alongside introduced amine ligands. The association interactions were driven by ligand affinity, as the relatively small molar equivalencies also attest.

### 3.5 Conclusion

We have investigated PL dynamics in core/shell Cd-chalcogenide QDs, which displayed a characteristic decrease in PLQY, decrease in average lifetime, and increase in rate dispersion when purified by GPC in toluene. After each surfactant component from the

shell growth reaction was systematically reintroduced to the purified core/shell QDs, it was observed that L-type ligands trioctylphosphine (TOP) could most effectively and oleylamine (OlAm) could moderately and both reversibly recover PLQY. A binary L- and X-type ligand system could universally regenerate QY for the purified QDs, however this was attributed to irreversible surface reconstruction as evinced by bathochromic shifts in related optical spectra.<sup>28,152,153</sup> The change in PL upon GPC purification could thus be attributed to a complete loss of L-type ligands, while some population of strongly-bound Z-type ligands was retained on the experimental timescale. The QY regeneration was accompanied by restoration of the PL lifetime; the lifetime changes were associated with a change in the amplitude of the longest lifetime components. Ensemble QY, average decay rate and rate dispersion of the QDs was shown unequivocally to change in response to [L-type] ligand concentration. Therefore, I employed isothermal titration calorimetry to differentiate the extent of L-type ligand binding, specifically for the thinner alloy shell sample. Although more qualitatively, ITC revealed an exotherm associated with introduction of TOP to purified QDs, confirming an interaction of the ligand with the QD surface; whereas trioctylphosphine oxide (TOPO), which failed to restore the QY, did not generate a heat response, consistent with a lack of binding over the same range of concentrations.

Applying ITC to specifically and directly probe neutral L-type amine interactions with QD cores allowed extraction of well-constrained equilibrium association constants, binding energies and ligand populations. Although I have chosen to model the amine ligands as binding to distinct independent sites relative to those occupied by the native phosphonate ligands, we recognize that the process by which ligands interact with vacant sites may indeed be more complex. However, the consistency with which we were able to obtain equilibrium



values; as well as the reasonable model of non-interacting, randomly distributed sites available specifically for amines (neutral L-type ligands) attests to this model being perfectly adequate for this system.

An immediate experimental advantage of employing ITC to elucidate QD–ligand interactions is apparent for unanticipated slower kinetic responses, as may be relevant to the TOP–CdSe/CdZnS ITC traces,<sup>60,202</sup> or as has evidently misconstrued alkylamine–QD dynamics.<sup>14</sup> It should be further noted that spectroscopic and thermodynamic profile analyses must be performed on samples with well-specified ligand populations and concentrations, consistently reproducible given the applied method of purification/preparation, if results of such studies are to be compared or eventually applied to the general understanding of NC surface chemistry even in new NC systems. The ability to identify reversible or non-perturbing purification techniques tailored to specific QD materials in specific processing environments is imperative. This is especially true if analysis of the final surface-modified product is difficult, as is typically the case for QDs post-surface modification.

### 3.6 Materials & Methods

**Materials.** The following chemicals were used as received. Cadmium oxide (CdO; 99.999%), Zinc oxide (ZnO; 99.999%), Trioctylphosphine (TOP; 97%) and Trioctylphosphine oxide (TOPO; 99%) were purchased from STREM Chemicals. Oleic Acid (OA; 99%), 1-Octadecene (ODE; 90% technical grade), and Selenium (Se; 99.999%) were purchased from Alfa Aesar. 1-Tetradecylphosphonic Acid (TDPA; >99%) was purchased from PCI synthesis. Bio-Beads S-X1 GPC medium was obtained from Bio-Rad Laboratories. Toluene-d8 (D, 99.5%) was obtained from Cambridge Isotope Laboratories.

Decylamine (95%) and Triphenyl Phosphate (>99%) was purchased from Sigma Aldrich. Oleylamine (80-90%) and Bis(trimethylsilyl)sulfide ((TMS)<sub>2</sub>S; 95%) were purchased from Acros Organics. Rhodamine 590 chloride (R590, MW 464.98) was obtained from Exciton. Toluene (99.5%) and Tetrahydrofuran (THF, 99%) were purchased from Mallinckrodt Chemicals. 200 Proof Ethyl Alcohol (Ethanol) was obtained from Decon Laboratories. Acetone (99.9%) was purchased from VWR. Methanol (99.9%) was purchased from Fisher Scientific. Toluene was dried with activated 4A molecular sieves. THF was dried using the Puresolv system from Innovative Technologies. Synthetic or analytical procedures under inert conditions were carried out using Schlenk line techniques, or in a glovebox under N<sub>2</sub> atmosphere.

**Synthesis of CdSe QDs.** The CdSe cores were prepared by hot-injection method using cadmium tetradecylphosphonate as the Cd precursor, trioctylphosphine selenide as the Se precursor and a mixture of TOP and TOPO as the reaction solvent. The two precursors were mixed by rapid injection at high temperature (350 to 365°C) and cooled down with an air blower immediately after the injection. The lowest energy extinction peak for the CdSe core in CdSe/CdZnS samples was at 509nm, while that of the CdSe cores used for the CdSe/CdS sample was at 522 nm. Multiple CdSe cores batches were used for the amine titration investigations had lowest energy extinction peaks ranging within 521-530 nm.

**CdZnS overcoating.** A previously published selective ionic layer adhesion reaction (SILAR) method<sup>207</sup> was employed for the core/shell QDs investigated in the QY regeneration work. Briefly, a portion of as-synthesized CdSe core was flocculated by methanol and acetone. After decanting the supernatant, the QDs were redissolved into hexane and stored in the freezer (4°C) for more than 12 hours. All the undissolved materials

were removed by centrifugation and the sample was precipitated again by an addition of methanol and acetone. Afterward, the QDs were brought into a measured volume of hexane. The UV-Vis absorption spectrum was recorded at a known dilution of the sample to determine the size and quantity of QDs. The solution of QDs in hexane was transferred to a solvent of 1:2 oleylamine:ODE (v/v, 9mL total) and degassed at 100°C to remove hexane. Before the addition of the reagent via syringe pump, the system was heated to 200°C under nitrogen. For the CdZnS alloy shell growth, the metal precursor is prepared by diluting a 0.2M mixture of Cd(oleate)<sub>2</sub> and Zn(oleate)<sub>2</sub> (Cd:Zn is 3:7) in ODE with 2 equivalents of decylamine and a volume of TOP to yield a metal concentration of 0.1M. The S precursor was always a 0.1M solution of (TMS)<sub>2</sub>S in TOP. The volume increase associated with 1 monolayer coverage of CdZnS is calculated based on the radius increase of 3.37 Å, which is the half of the wurtzite *c*-axis unit cell dimensions for CdS (3.37 Å). Alternating injections of metal precursor and sulfur precursor were performed, adding the metal precursor solution first, with injections starting every 15 minutes for CdS shell and 20 minutes for CdZnS shell. The flow rate was adjusted to complete each injection over the course of 3 minutes. The volume of each injection was calculated to apply 0.8 monolayers coverage each cycle (a cycle is defined as one metal precursor injection and one sulfur precursor injection). For the thin shell CdSe/CdZnS sample, two cycles were performed. The growth processes were monitored by both UV-Vis absorption and fluorescence spectrometers. After the reaction, the mixture was cooled down to the room temperature and the molar extinction coefficient was estimated based on the amount of core introduced at the beginning and the total volume of the solution after the synthesis.

**Optical spectroscopy.** The optical absorption spectrum was recorded using a Thermo Scientific Evolution Array UV-Visible Spectrophotometer with toluene as the solvent as well as the blank in a 1cm path quartz cuvette. Emission spectra were recorded by an Ocean Optics USB 4000 spectrometer under ~365 nm excitation.

**Absolute quantum yield measurement.** The quantum yield (QY) of QD samples was measured relative to rhodamine 590 (R590, QY=99% in ethanol). The excitation wavelength was chosen based on the optical isosbestic point of the QDs-toluene solution and R590 in ethanol. Fluorescence spectra of QD and R590 dye were taken under identical spectrometer conditions on Varian fluorescence spectrometer in triplicate and averaged. The optical density was kept below 0.1 from excitation wavelength to 800nm to avoid internal filtering effects. The QY was calculated based on the integrated intensities of the emission spectra, the absorption at the excitation wavelength and the refraction index of the solvent using the following equation:

$$QY_{QDs} = QY_{dye} * \frac{Absorbance_{dye}}{Absorbance_{QDs}} * \frac{Emission\ integral_{QDs}}{Emission\ integral_{dye}} * \frac{Refraction\ index_{toluene}^2}{Refraction\ index_{ethanol}^2}$$

The precision of this measurement in our case is limited by the precision of the absorbance measurement (~1%) while the accuracy among samples in different solvents will be limited by the accuracy of the refractive index correction term.

**1×precipitation/redissolution (1×PR) for CdSe|TDPA core QDs.** Prior to titration experiments a portion of the as-synthesized QD batch was centrifuged to remove any undissolved material. Acetone and methanol were used as the antisolvent to flocculate the QDs. After centrifuging for 5 min, the QDs could be adequately separated from the mixture and the supernatant discarded. The QDs were redispersed in excess 7.5–10mL anhydrous THF and put in the fridge at overnight (~12 hours). Afterward the QDs were

immediately centrifuged to remove any excess P-containing impurities, then concentrated under a stream of  $N_{2(g)}$  before being loaded onto the THF GPC column.

**GPC purification of the QDs.** In order to remove most of the synthetic solvent and concentrate the QD sample in either toluene or THF, a single PR cycle was carried out before the GPC purifications. 1×PR QDs (concentration ranges from 5–150  $\mu$ M with 0.5–1 mL injection volumes) were then added to the GPC column.

**QY regeneration core/shell GPC.** The GPC column was packed by the previously described method with toluene as the eluent.<sup>62</sup> The as-synthesized core/shell QDs were purified by 1× precipitation with acetone only and redispersed in toluene. Then the QD solution was added to the column and the sample was collected when the elution volume equaled  $\sim 1/3$  of the total volume of the column (the expected void volume for irregularly spaced spherical beads); this volume corresponds to the fraction at which the purified QDs eluted. The GPC column was rinsed thoroughly (3x the total volume of the column) before using it for subsequent purifications. After each purification, all QD samples were immediately transferred into a  $N_2$ -filled glove box to avoid oxidation on the surface.

**Amine association core-only THF GPC.** The GPC column was packed similarly to a previously described method<sup>62</sup> with anhydrous THF as the eluent. A constant flow of  $N_{2(g)}$  was maintained over and through the THF GPC to prevent hygroscopic degradation of the column. The Bio-Rad SX-1 Bio-Beads were best swollen if introduced to the anhydrous solvent, applied to the Schlenk line for near complete removal of the solvent, and reswelling the Bio-Beads without allowing contact to air. Again, the purified QD sample was collected when the elution volume reached  $\sim 1/3$  of the total volume of the column. The GPC column was rinsed thoroughly (4x the total volume of the column) before subsequent

purifications. After each purification, all QD samples were immediately diluted to the titration reaction concentration and injected into the ITC.

**Preparation of pure cadmium oleate ( $\text{Cd}(\text{OA})_2$ ).** The  $\text{Cd}(\text{OA})_2$  used as a ligand in the regeneration study was prepared as follows.  $\text{CdO}$  and oleic acid (99%) were introduced to a three-neck flask (the ratio of  $\text{CdO}$ : OA is 1:5), where OA was used as both acid and solvent. The mixture was degased and then slowly heated up to  $270^\circ\text{C}$  under  $\text{N}_2$  to form a colorless and clear solution. Then the sample was cooled down to room temperature and transferred into the fridge ( $4^\circ\text{C}$ ). The extra oleic acid was separated by filtration and the insoluble  $\text{Cd}(\text{OA})_2$  has been washed by ethanol for more than 5 times to remove the remaining oleic acid. FTIR and  $^1\text{H}$  NMR were used to confirm the removal of uncoordinated oleic acid.

**Quantum yield regeneration and relative quantum yield measurement.** After GPC purification, the QDs samples are transferred into sealed  $\text{N}_2$  environment and pumped into glove box immediately to avoid any possible oxidation. The ligand solutions are also prepared in the glove box. For the regeneration process, the concentration of the QD samples are fixed to be  $0.5\mu\text{M}$  and the ligand concentration is controlled to be  $1.5\text{mM}$  or  $0.15\text{mM}$  to provide two different ligand-to-QD ratios (1:3000 and 1:300). The total volume of the mixing solutions is  $1\text{mL}$  and the solutions have been kept stirring for 7 days. The relative QY is characterized by diluting a portion of the above solutions into toluene and measure the absorption and emission spectra. The optical densities of the sample solutions were kept below 0.1 after  $365\text{nm}$  to avoid internal filtering effects. The relative QY is calculated by comparing the integration the emission spectrum divided by the absorption at  $365\text{nm}$  (the excitation wavelength of the fluorescence spectrometer).

**NMR analysis of QDs.** Routine NMR samples of the QDs were prepared in toluene-d<sub>8</sub>. The QDs' concentration is set at approximately 20  $\mu\text{M}$ ; the exact value in each case was measured by UV-Vis using the calculated molar extinction coefficient. Spectra were recorded on Bruker Avance III 400 MHz. The quantitative  $^1\text{H}$  NMR spectra were measured with ferrocene as the internal standard and 30s relaxation delay, allowing the system to reach a reliable equilibrium. The  $^{31}\text{P}$   $\{^1\text{H}\}$  NMR spectra of QD samples were measured with 512 scans to improve signal-to-noise on the Bruker Avance III 400 MHz.

**Advanced NMR techniques.**  $T_1$  is measured by the vendor-supplied inversion recovery pulse sequence experiment. Diffusion ordered spectroscopy (DOSY) measurements and NOE difference measurements on  $^1\text{H}$  spectra with selective saturation on the  $^{31}\text{P}$  resonance were performed Bruker Avance III HD 400 and analyzed by Topspin version 3.2 software. DOSY spectra were collected on  $^{31}\text{P}$  of free TOP ( $\delta = -32.3$  ppm) vs TOPO ( $\delta = 53.5$  ppm), and TOP vs TOPO as combined with 1.6 monolayer CdSe/CdZnS sample at a 300 ligand-to-QD ratio. Neither TOP nor TOPO could be distinguished from free ligands after mixing with QDs: the diffusion constant of TOP was  $9.3 \times 10^{-10} \text{ m}^2/\text{sec}$  and that of TOPO was  $8.6 \times 10^{-10} \text{ m}^2/\text{sec}$ . The diffusion constant of QD was  $1.9 \times 10^{-10} \text{ m}^2/\text{sec}$  based on the  $^1\text{H}$  DOSY measurement of the olefin protons. The diffusion constant of the toluene-d<sub>8</sub> solvent was  $2.4 \times 10^{-9} \text{ m}^2/\text{sec}$ .

**Quantitative  $^{31}\text{P}$   $\{^1\text{H}\}$  NMR for amine association:** Spectra were recorded either on a Bruker Avance III HD 400 MHz equipped with a nitrogen-based cryogenic probe (Prodigy) or a Bruker Avance III HD 500 MHz with NOE suppression routines applied.

**Isothermal titration calorimetry (ITC).** To account for and deconvolve heats of dilution contributing to the exchange heat of interest, several reference titrations were

conducted with each analyte at the specified concentration of its respective QD–ligand interaction solution. In addition to serving as the common solvent for both QDs and ligands, anhydrous THF was also always in the reference cell. A mechanical heat baseline was established by a THF into THF titration. Whether remaining reference titrations were deemed substantive depended on the magnitude of their raw thermograms compared to the raw THF–THF thermogram. The titrations are expressed *titrant* (to be injected) into – *titrand* (in the sample cell).

**QY Regeneration Study.** ITC titrations were performed on a VP-ITC calorimeter (Microcal Inc., Northampton, MA). Ligand solutions were titrated from the 300 $\mu$ L syringe to the sample cell overfilled to its 1.8mL capacity, and the heat response to maintain a constant temperature between the sample cell and reference was monitored. Each experiment was conducted at 22°C and midrange reference power; allowed to equilibrate prior to an initial 600 sec delay; and in order to allow adequate equilibration between each injection, 8-9 min intervals were set between each injection for a total 60 injections in 5 $\mu$ L increments. Anhydrous THF was chosen as the solvent for both the ligands and QDs, as well as the blank solvent in the reference cell. Reference titrations were conducted to determine any significant heat of dilution between the solvent, ligand solution and QD solutions that may have accounted for signal in the final ligand-QD titrations. Only ligand-solvent titrations were subtracted from ligand-QD titrations, as other reference titrations were determined negligible. The QD solutions were 0.5 $\mu$ M (equal to the regeneration concentration) loaded in the sample cell and ligand solutions were 1.5mM loaded in the syringe (final ligand-to-QD molar ratio was  $\sim$ 500:1 ligand-to-QD).



**Amine Association Study.** ITC titrations were performed primarily on a NanoITC standard volume calorimeter (TA Instruments). Ligand solutions were titrated from the 250 $\mu$ L syringe to the sample cell overfilled to its 1.3mL capacity, and the heat response to maintain a constant temperature between the sample cell and reference was monitored. Each experiment was conducted at 22°C and midrange reference power; allowed to autoequilibrate prior to an initial 600-3600 sec delay; and in order to allow adequate equilibration between each injection, 8-9 min intervals were set between each injection for a total 55–60 injections in 4.5 $\mu$ L increments; the first 1-2 injections were only 2 $\mu$ L. Anhydrous THF was used as the solvent for both the ligands and QDs, as well as the blank solvent in the reference cell. Reference titrations were conducted with the same parameters relevant to the titration reaction to determine any significant heat of dilution between the solvent, ligand solution and QD solutions that may have accounted for signal in the final ligand-QD titrations. An AffinityITC low volume calorimeter was used to ascertain parameters for the elusive sigmoidal shape thermograms. Ligand solutions were titrated from the 250 $\mu$ L syringe, freshly filled to slightly more than 50 $\mu$ L for each titration, to the sample cell overfilled to its 350 $\mu$ L capacity (active volume 185 $\mu$ L), and the heat response to maintain a constant temperature between the sample cell and reference was monitored. Each experiment was conducted at 22°C at midrange reference power; allowed to autoequilibrate prior to an initial 600-3600 sec delay; and in order to allow adequate equilibration between each injection, 8-9 min intervals were set between each injection for a total 55–60 injections in 1 $\mu$ L increments

## CHAPTER 4

### ISOTHERMAL TITRATION CALORIMETRY RESOLVES SEQUENTIAL LIGAND EXCHANGE AND ASSOCIATION REACTIONS IN CdSe QUANTUM DOTS

#### 4.1 Introduction

##### 4.1.1 Complexity of colloidal semiconductor nanocrystal (NC) surface chemistry

Colloidal semiconductor nanocrystals (NC), also referred to as quantum dots (QDs), persist as a unique and attractive class of hybrid organic/inorganic nanoparticle (NP) materials of a size regime that allows tunable photophysical properties. QDs can also serve as the building blocks for higher dimensional NPs. Although their [inorganic] core is often highly crystalline, a significant fraction of their constituent atoms resides at their surfaces. These high surface-to-volume semiconductors are coordinated by ligands that affect their overall colloidal stability, confinement potential and exciton behavior.<sup>1,34,40,63,64,168,171,196,197,228,247,248</sup> As such QD surface chemistry is a critically important theme in NP research and development, primarily in terms of rational surface engineering toward biomedical applications as well as optoelectronic device architecture.<sup>1,247</sup> The best coordinating ligands for synthetic control over QD nucleation kinetics, morphology, stability and relative monodispersity appear to be chemisorbed surfactant molecules with long aliphatic chains.<sup>17,40,196,228</sup> Though subsequent to producing high quality nanomaterials, those ligands preclude QD incorporation into many desired applications. To conceive the QD–ligand system as molecules in a dynamic self-

assembled monolayer of either adatoms or chemisorbed ligands, only begins to address the complexity of this interface. Over the past decade, generally *desorption* studies directed by the Covalent Bond Classification have been employed to guide post-synthetic surface modification<sup>34,168,171,197,228</sup>. The fundamental science of further elucidating mechanistic insights on NC surface chemistry concepts is not trivial. In fact, providing comprehensive descriptions of the thermodynamics that govern QD ligand binding and overall surface chemistry persists as a primary objective in the field.<sup>1,17,34,40,50,51,60,63,64,168,171,196,197,228,247,248</sup>

Notably, the outermost coordination layer of QDs encompasses surfaces having multiple facets with numerous edges and vertices, and so allows for various possible ligand binding motifs that are also relevant to other NP systems. QD facet heterogeneity and the capacity for ligands to dictate solubility, functionalization and optoelectronic properties even from a significantly small number of binding events w.r.t the total initial ligand populations;<sup>81</sup> render mass action-driven descriptions primitive, while prompting investigations of site-specific ligand affinity where feasible.<sup>34,50,51,60,63,64,168,171,197,228,248</sup> Theoretical simulations have offered valuable insights for QD surfaces but accounting for realistic QD and ligand sizes along with relevant solvent/matrix interactions on such dynamic interfaces with attention to unique facets is computationally expensive.<sup>1,22,37,168,197,247</sup> Experimental techniques applied to QD surface chemistry must sensitively probe concomitant ligand adsorption/desorption, which may entail simultaneous equilibria among other caveats whether qualitatively or quantitatively.

#### 4.1.2 Various techniques employed to probe nanocrystal surface chemistry in situ

Since nearly all QD–ligand interactions significantly influence photophysical properties absorption, photoluminescence (PL), FRET and IR are routinely employed to characterize

NP systems and ligand populations,<sup>40,196,249</sup> and have resolved site-specific thermodynamics of ligand binding.<sup>1,81,168,197,228,247</sup> Solution NMR spectroscopy has emerged as a standard and versatile technique for probing the QD–ligand interface, affording both structural and chemical information with bound ligand species as broadened, shifted resonances relative to the narrow linewidth resonances of their free analogues.<sup>1,17,34,62–64,168,171,197,228,247,248</sup> Absorption/PL measurements require low sample concentration for appropriate optical density versus the high concentrations necessary for adequate NMR signals. Moreover, each of these techniques requires spectroscopically distinct signatures that can be unambiguously assigned to details of the QD surface. Herein we demonstrate the sensitivity, precision and accuracy of isothermal titration calorimetry (ITC) for probing QD–ligand interactions.<sup>46,47,50,51,60</sup> ITC quantifies physicochemical processes that generate heat, and has allowed us to probe and resolve ligand exchange thermodynamics that have remained infeasible with typical spectroscopic methods.

#### 4.1.3 Introduction of isothermal titration calorimetry to probe NC surface equilibria

While standard in aqueous-based biochemical research, ITC has recently been employed to investigate QD–ligand interactions in more native organic solvents.<sup>50,51,60</sup> ITC can accommodate low concentrations appropriate for optical measurements as well as higher loading levels more analogous to NMR investigations.<sup>42,60</sup> Although a constraint with which thermodynamic parameters obtained by ITC at very low (high) concentrations coupled with too low (high) magnitudes of generated heat can suffer, even when the isotherm has the appropriate curvature,<sup>46,47,50,250</sup> the technique itself is not limited in the ways that spectroscopic measurements are to diagnostic signatures. ITC is sensitive to identify multiple binding events visible in the apparent binding stoichiometries and relevant to QD surface

investigations, especially those with distinct  $\Delta H$ .<sup>55,57,237</sup> Perhaps the greatest advantage of ITC compared to other techniques is its ability to directly determine thermodynamic parameters: equilibrium constants  $K$ , changes in enthalpy  $\Delta H$ , binding site stoichiometries  $N$  of reactions simultaneously. Previously ITC has also been reported to supply kinetic information in addition to thermodynamic profiles;<sup>23,29</sup> and although kinetic information evinced in raw heat thermograms has been probed,<sup>60,252</sup> to our knowledge this is the first investigation to apply a timetrace analysis to raw ITC data in order to extract physically relevant microscopic multisite thermodynamic parameters. Despite the appreciable sensitivity and comprehensive quantitative thermodynamics acquired by ITC, the limitation of this technique is its inability to identify specific interactions that contribute to each heat signal. A systematic titration investigation is presented alongside several ancillary experiments conducted to elucidate the ITC-resolved processes<sup>55–57</sup> that occur during our titration reactions.

## 4.2 Experimental design for ITC applied to CdSe quantitative ligand exchange

### 4.2.1 Choice of CdSe QDs and ligands for investigation

CdSe QDs are the most extensively investigated nanocrystal system and the benchmark for probing NP–ligand surface chemistry. We present an incremental ITC titration of carboxylate-capped zincblende CdSe QDs with an alkylphosphonic acid. Driven by proton transfer,<sup>36,198</sup> this ligand exchange is well understood and documented as a spontaneous, irreversible, quantitative replacement reaction extended beyond traditional II-VI QD systems.<sup>1,63,64,247,248</sup> Since 2004 theoretical results have indicated that ligands phosphorus-containing headgroups bind stronger to CdSe surfaces than those containing carboxyl groups.<sup>20,37,215</sup> The specific ligands chosen for this investigation were oleic acid (OA) which possesses diagnostic vinyl protons to monitor by NMR; and octadecylphosphonic acid

(ODPA) which has a similar aliphatic chain length, eliminating possible entropic contributions from ligand size-dependent adsorption rates.<sup>228</sup> Lastly, this exact exchange reaction was investigated because its in situ thermochemical equilibrium parameters have remained infeasible and an apparent reaction quotient for it a forlorn ambition.<sup>1,63,64,247,248</sup>

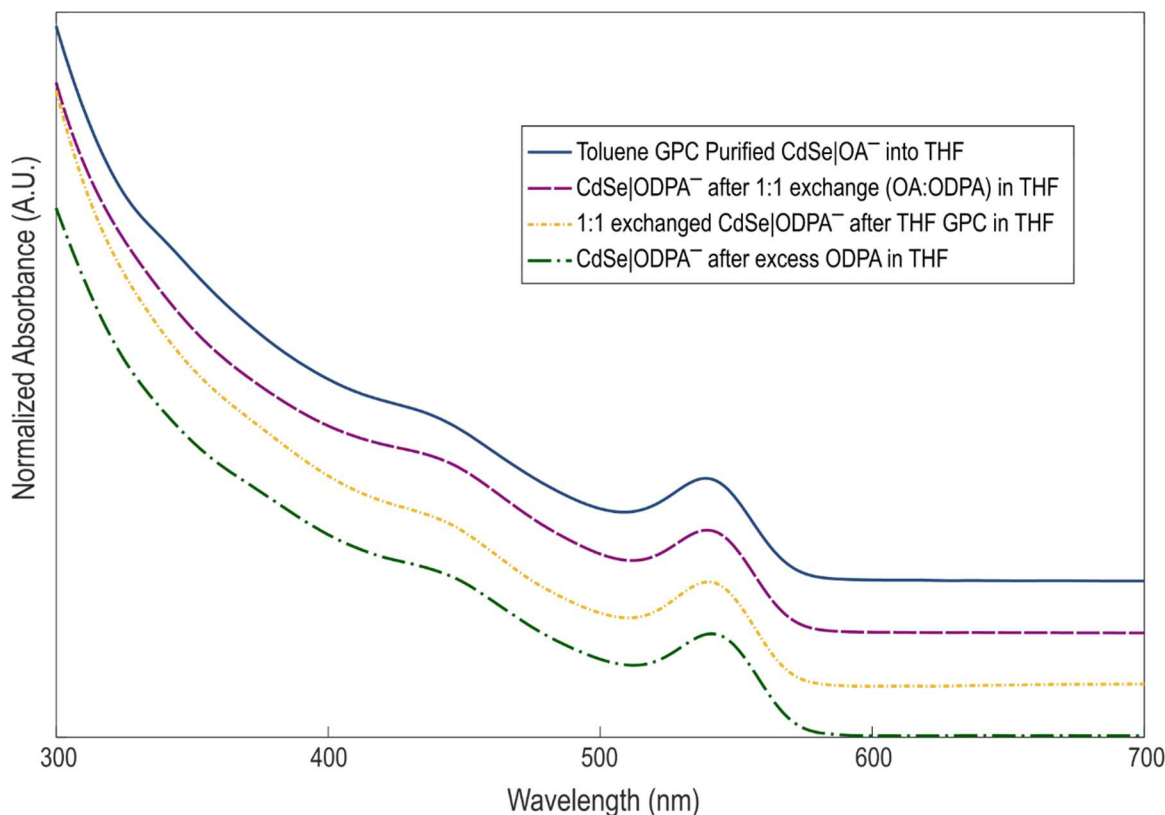


**Figure 4.1** Vertically offset absorption spectra, normalized to the lowest energy excitonic peak & through course of titration experiment.

The CdSe QDs were synthesized according to a previously reported hot injection procedure: CdO decomposed with OA to form Cd(oleate)<sub>2</sub>, and at the nucleation temperature rapidly injected with trioctylphosphine-Se in octadecene non-coordinating solvent.<sup>62</sup> This rapid precursor hot injection synthesis was chosen to ensure the QDs were ligated exclusively with oleate (OA<sup>-</sup>), and such that no other carboxylate ligands were present

and neither octadecene nor OA became reducing agent reactants in the synthetic mixture.<sup>17</sup> It was particularly imperative to obtain a single ligand on the QD surface to limit as much ambiguity as possible in our isotherm interpretation. Despite a more recent assertion about saturated and unsaturated carboxylate ligands behaving “identically” w.r.t. ligand exchange<sup>246</sup> this assumption seems suspicious given that previous synthetic results have suggested otherwise,<sup>18</sup> and this likely confounding variable was ultimately avoided.

Previously we have emphasized our well-established gel permeation chromatography (GPC) as a gentle yet robust method of purifying nanocrystals.<sup>60,62,137</sup> The precision of GPC purification provided consistent starting material for every aspect of the investigation. Prior to each titration, QDs were purified via toluene mobile phase GPC and then brought into tetrahydrofuran (THF) solvent. Absorption spectra, like that shown in Figure 4.1, were used to determine QD concentration by their lowest energy excitonic peak,<sup>62</sup> and consistently confirmed that no degradation of the QDs occurred during reaction preparation and even subsequent to post-ligand exchange GPC purification. Integrating pertinent <sup>1</sup>H NMR resonances 1) confirmed the QDs were coordinated exclusively with oleate ligands by the 2:3 ratio obtained when comparing the peaks for vinyl vs terminal methyl protons; and 2) via ferrocene internal standard, quantified the initial ligand population so that precise ODPA equivalents could be titrated (Figure 4.2). Appropriate relaxation delay and acquisition times were determined with known amounts of added ferrocene internal standard. T<sub>1</sub> experiments were conducted to ensure adequate relaxation times for accurate quantitative analysis and applied such that relaxation delays and acquisition times totaled at least 5×T<sub>1</sub>.<sup>41,62</sup>

Within the ITC system, all titration components indiscriminately contribute to the evolved heat, and therefore control of the reaction system is necessary to limit and identify

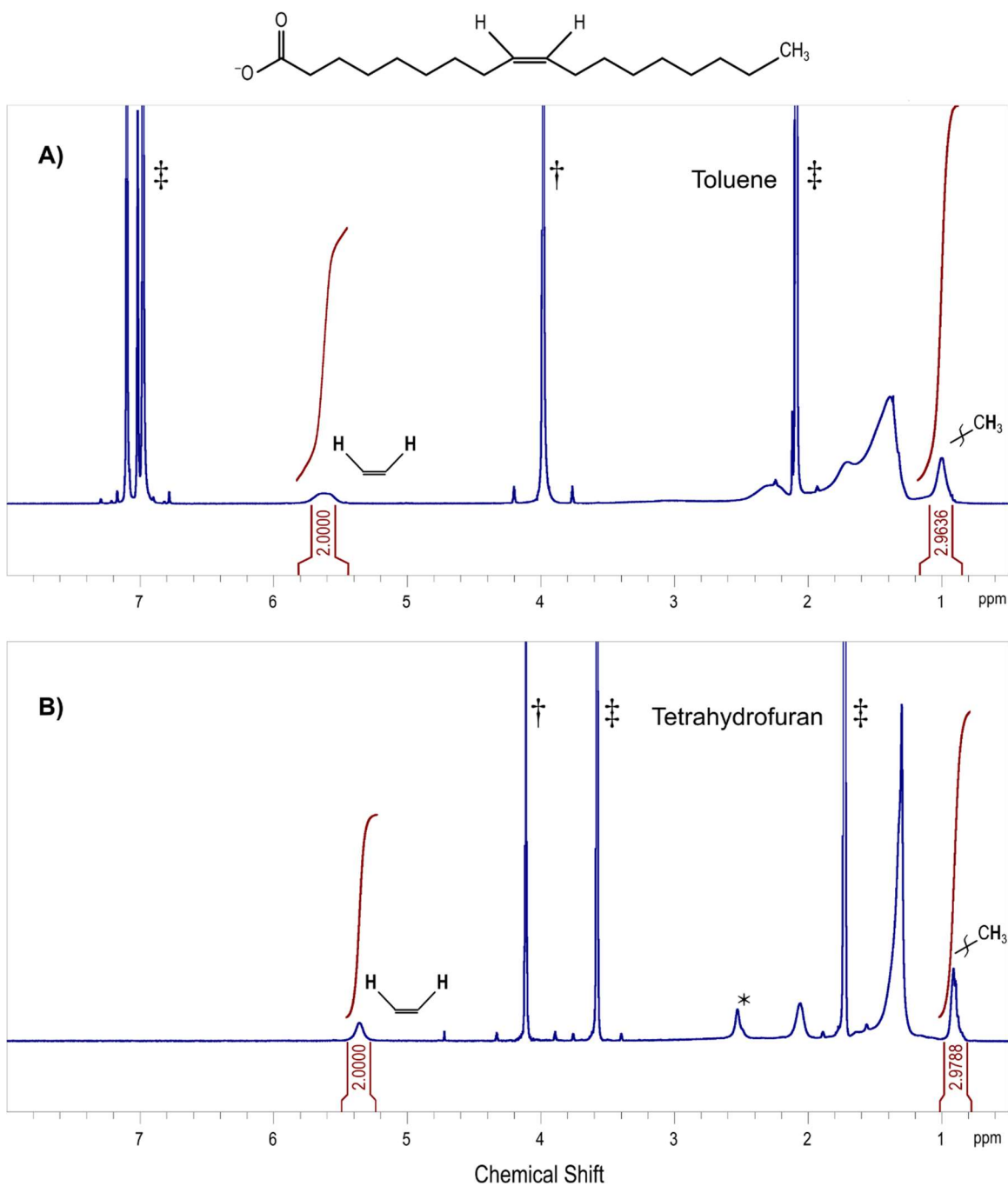


**Figure 4.2** Quantitative  $^1\text{H}$  NMR spectra of CdSe|OA – purified either by toluene GPC (A) or anhydrous THF GPC (B) and in those respective deuterated solvents. The integrals demonstrate that the QDs are only ligated by oleate ligands with vinylic:methyl integral ratios of 2:3. Deuterated solvents are marked with ‡ while the ferrocene internal standard is marked by †.



unintentional side reactions and heats of dilution. Firstly, incremental titrations of ODPA solution were injected into GPC-purified OA-capped CdSe QDs at an excess mole ratio of 400:1 ODPA-to-QD, with anhydrous THF as the common solvent for both the ligand and

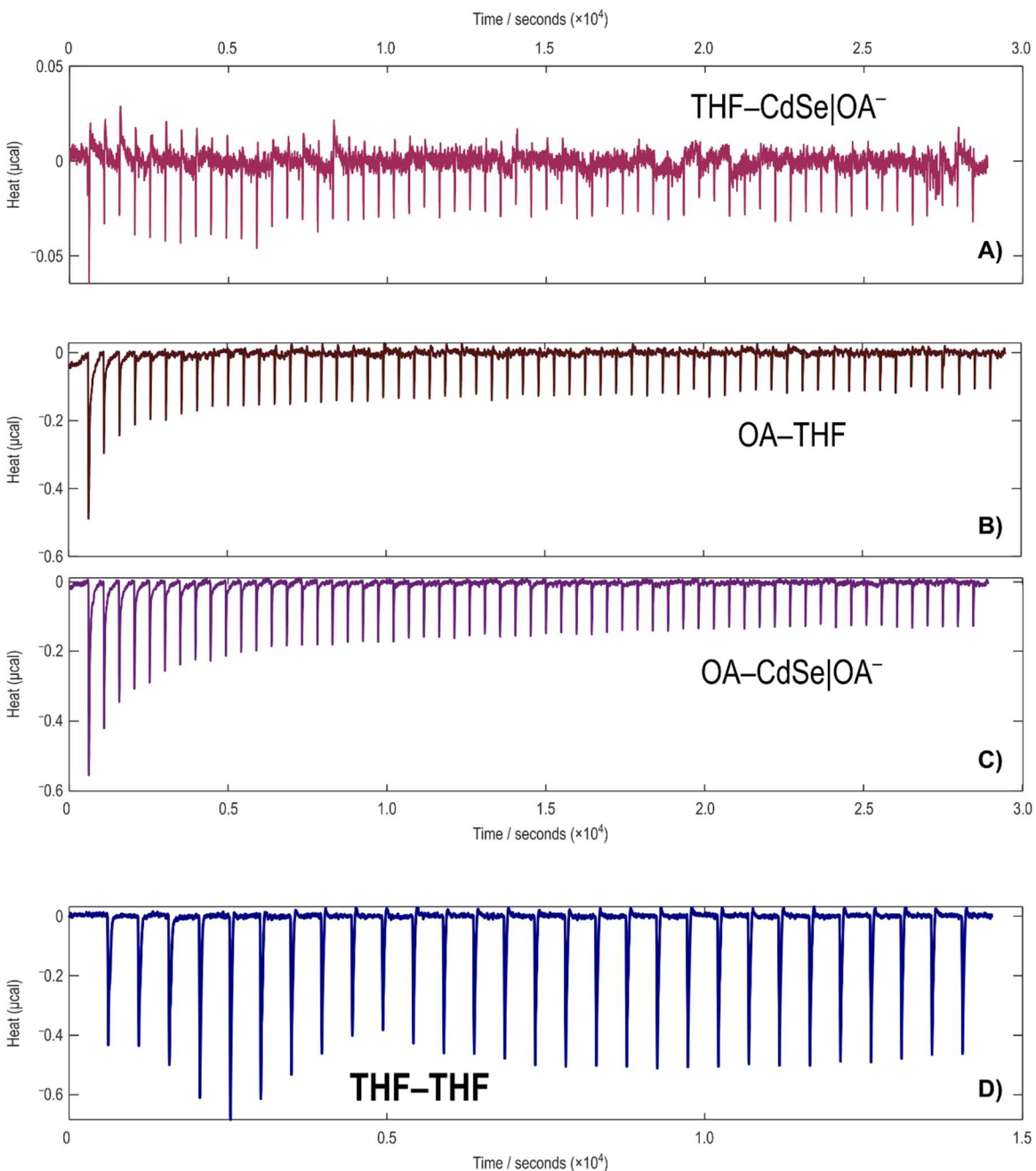


**Figure 4.3** Thermograms for control titrations that did not produce significant heat to the thermogram raw heat signal for ODPA-CdSe|OA<sup>-</sup>. Note different vertical axis for THF solvent titrated to purified QDs as significantly less heat was generated.

QD solutions.

To account for and deconvolve heats of dilution contributing to the exchange heat of interest, several reference titrations were conducted with each analyte at the specified concentration of its respective exchange reaction solution. In addition to serving as the common QD/ligand solvent, anhydrous THF was also always in the reference cell. Additionally, a mechanical heat baseline was established by a THF into THF titration. Whether the other reference titrations were deemed substantive depended on the magnitude of their raw thermograms compared to the raw THF–THF thermogram. The control titrations included ODPA–THF and THF–CdSe|OA<sup>−</sup>, expressed as *titrant* (to be injected) into – *titrand* (in the sample cell). Figures 4.3 and 4.4 illustrates each of the reference titrations with an additional OA–CdSe|OA<sup>−</sup> reference titration thermogram. Ultimately only ODPA–THF had a nontrivial heat of dilution and was subtracted<sup>46,47</sup> from the ODPA–CdSe|OA<sup>−</sup> exchange titration. Although the exchange liberates OA from the QD surface at ca 1:1 equiv., which would be directly represented as an OA–THF reference titration, the endpoint is reasonably matched by the titration of free ODPA into THF. In fact with ODPA titrated to excess into QD solutions, final injection signals were found to coincide exactly with this ODPA–THF reference titration, as illustrated later in our analysis of the thermogram. As discussed below, ITC revealed two equilibria processes that effectively occur in sequence.

#### 4.2.2 Discussion of raw heat ODPA–CdSe|OA<sup>−</sup> thermogram of interest

Figure 4.5 shows the representative ITC thermogram for the ODPA–CdSe|OA<sup>−</sup> ligand exchange titration; from which the reference ligand–solvent titration (which includes baseline mechanical heat) has been subtracted. Sufficient time is given between each ligand

return to baseline before subsequent injections. Rather than produce a typical sigmoidal thermogram often seen in ITC data analyzed with a 1:1 independent sites (Langmuir)

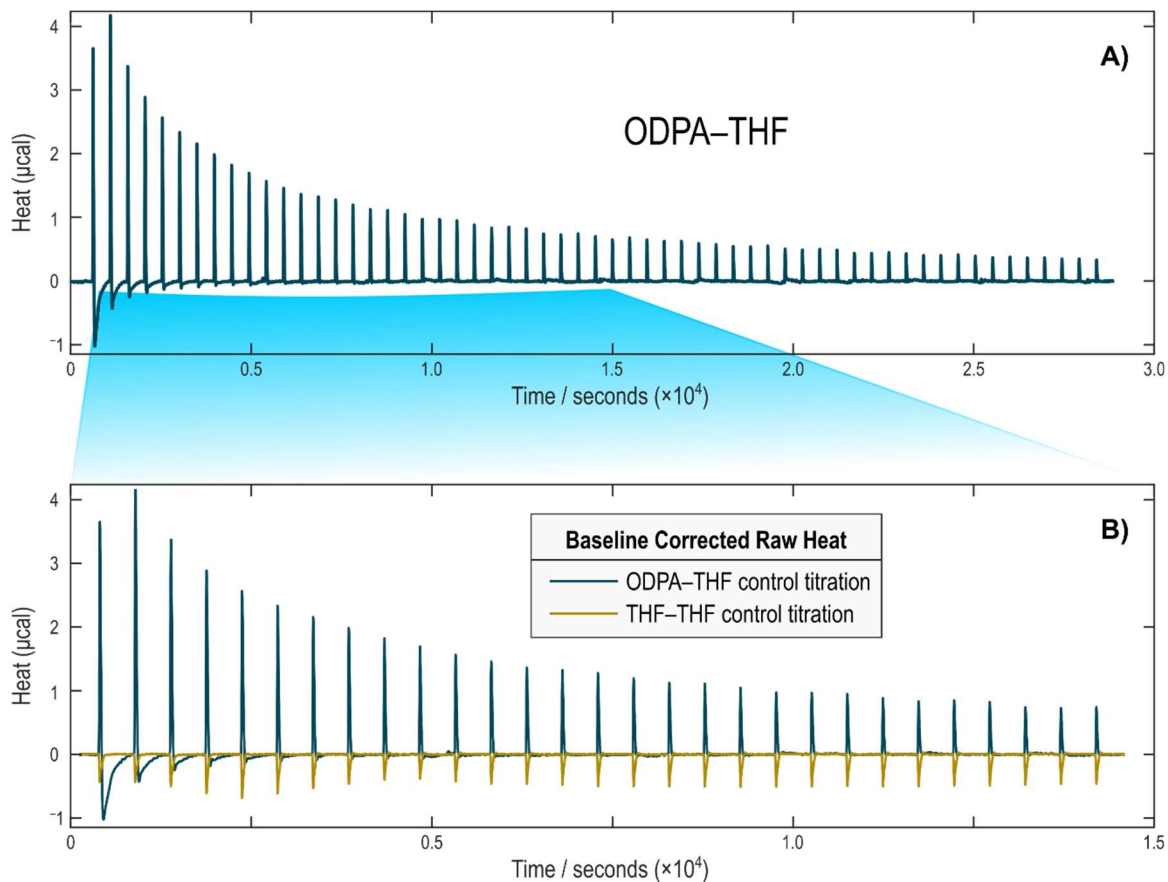


**Figure 4.4** Control titration OA–THF (A) and plotted against THF–THF (marigold) in the highlighted region. This titration did significantly contribute to the thermogram raw heat signal for ODPa–CdSe|OA<sup>−</sup> and was subtracted as its reference control titration.

model,<sup>50,51,60</sup> the raw thermogram suggests at least two independent sequential sites, the first of which having a stronger binding affinity with a less exothermic injection to allow the system to reach both thermal and chemical equilibrium, as heat signals enthalpy than the subsequent lower binding affinity site.<sup>46,57</sup> Repeated titrations are nearly superimposable, particularly at the point of QD site saturation (Figure 4.6). The heat evolution over the course of the titration, simply put is comprised of a rapid initial exotherm followed by a slow

endotherm, and finally a relatively slow exotherm through the latter half of the titration. It appeared that the complexity of this reaction system could be deconvolved into at least 2 or 3 distinct thermodynamic processes. During the titration experiment the raw thermogram is the power supplied in response to heat produced by the system, required to maintain an isothermal calorimeter cell over time. Endothermic heats appearing at the beginning of each titration were initially assumed to be an overcompensation within the feedback power supply, but upon repeated titration reactions and closer investigation a consistent pattern

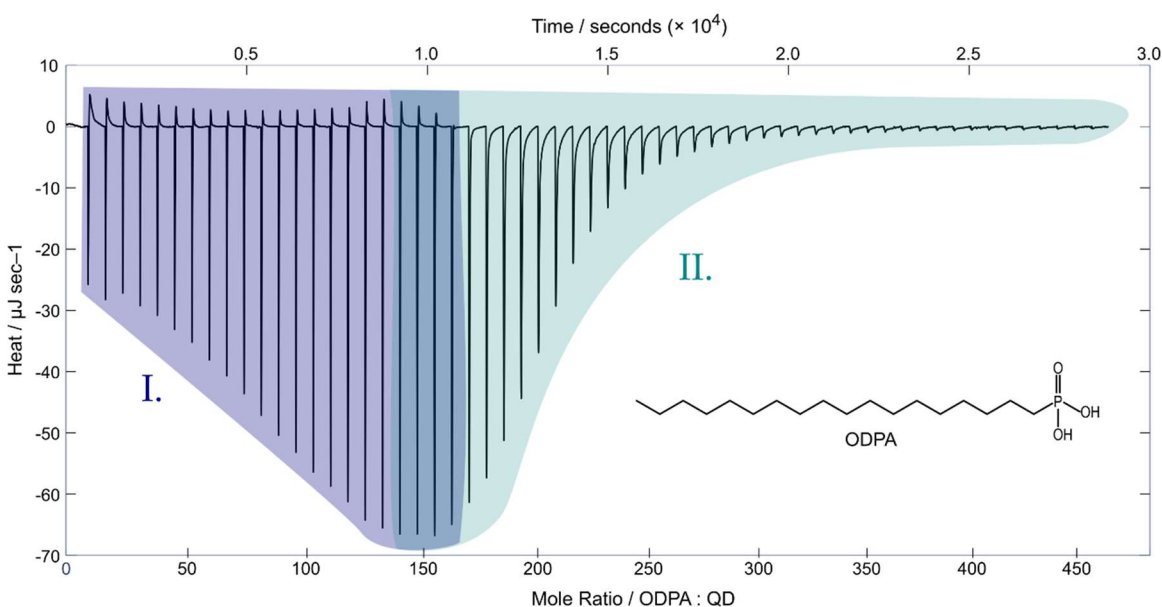


**Figure 4.5** Raw heat signal thermogram for titration of ODPA – CdSe | OA<sup>-</sup> with exchange vs association in navy & teal respectively.

was realized. The magnitude of heat in the endothermic signals was significant compared to aforementioned control titrations and can be clearly distinguished from overcompensation signals relative to the mechanical heats. A complete attenuation of isotherm heat signals is expected as binding sites become saturated, but the endothermic heat diminished completely

in each titration exactly at the expected molar ratio of a quantitative X-type ligand exchange. Hence, the endothermic heats following the rapid initial exothermic heats (navy shading) had to be considered as a physically relevant thermodynamic process that ITC resolved during the quantitative exchange of ODPA<sup>-</sup> for OA<sup>-</sup> ligands. The latter portion of the thermogram,

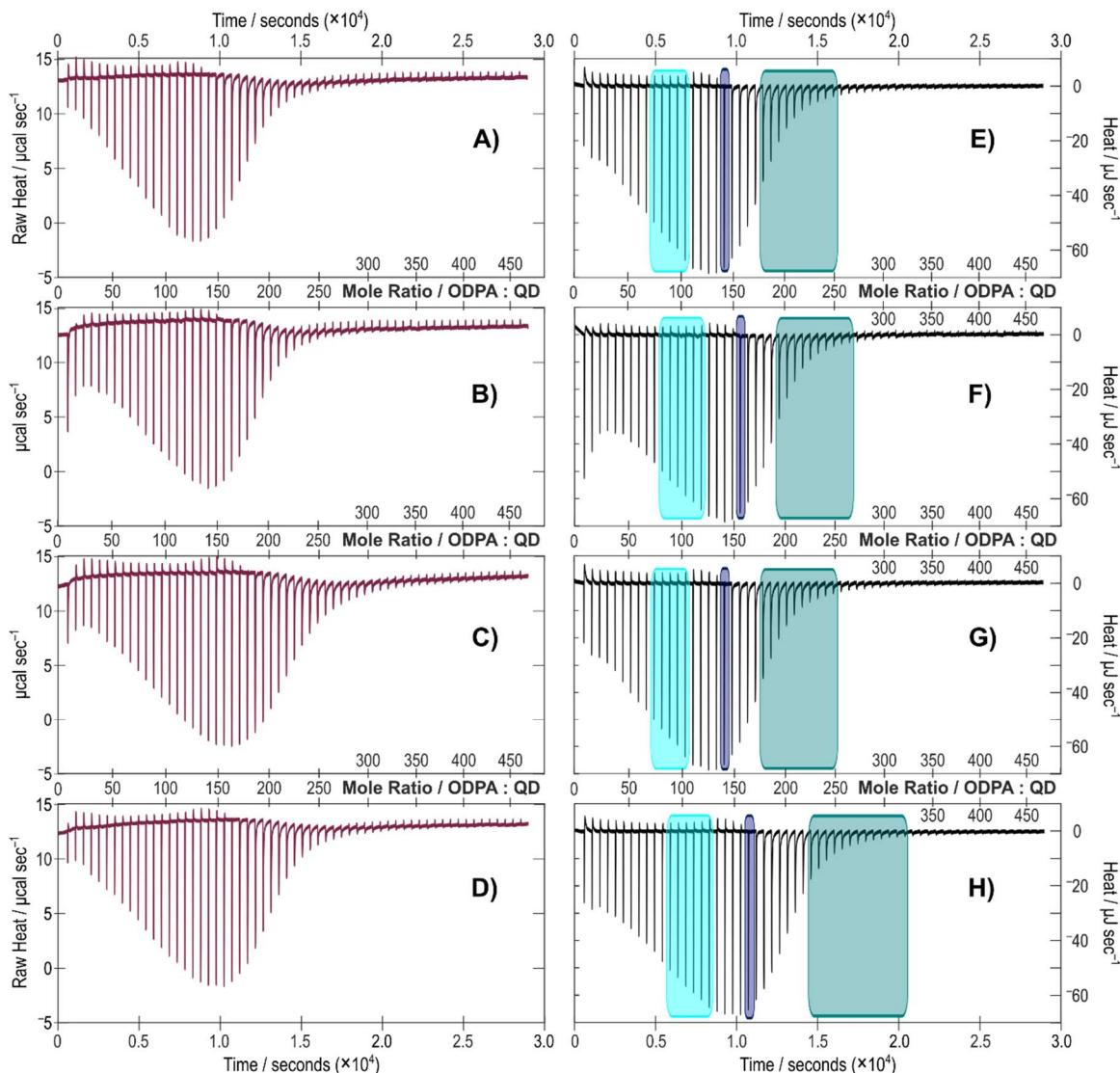


**Figure 4.6** Repeated raw heat thermograms for ODPA–CdSe|OA<sup>-</sup> titration without baseline correction or reference titration subtraction (A-D) and with baseline correction, reference titration subtraction as well as injections highlighted in aqua, navy and teal (left to right) that were used to construct waveform components for the applied two independent types of sites model – the colors of the highlighted regions (E-F) correspond directly to the waveform component models and eventual isotherm displays.

shaded in teal, resembles a rather straight-forward ligand association that could correspond to neutral ODPA adsorbing to the QD and perhaps exhibiting self-exchange with bound ODPA<sup>-</sup>. Figure 4.7 shows the proposed X-type ligand exchange preceding a neutral L-type association, as has been found in previous studies for QD surface reactions with these ligands.<sup>63,64</sup> Support for this sequential reaction assignment, quantitative analysis, and the

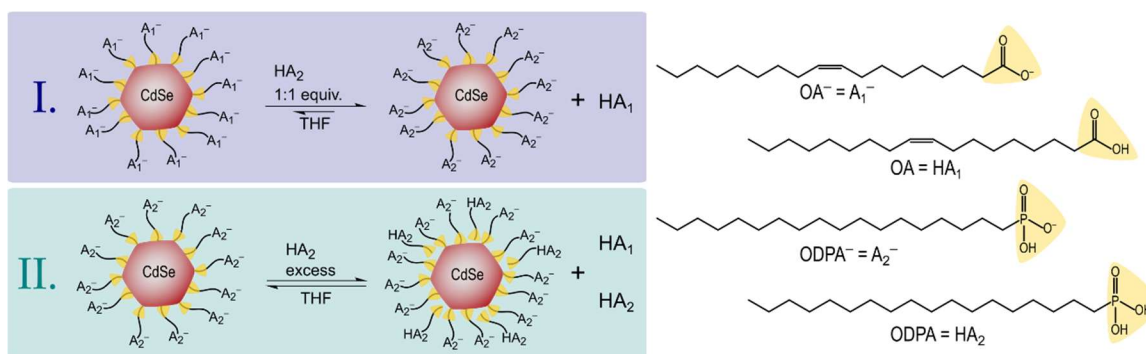


**Figure 4.7** Proposed reaction coordinates for ODPA–CdSe|OA<sup>-</sup> exchange titration (left) and ligands involved in exchange reaction (right).

influence of preparative conditions on the titration profile are discussed below.

#### 4.2.3 Ancillary parallel NMR titrations to verify exchange reaction coordinates

In addition to preparative characterization, especially to confirm that all ligands were oleate and bound to a highly reproducible extent from GPC purification, several quantitative parallel <sup>1</sup>H and <sup>31</sup>P NMR experiments were conducted in THF-d<sub>8</sub> to monitor and verify an anionic ligand exchange followed by the neutral ligand association.<sup>54</sup> A broad and shifted NMR resonance relative to the fine structure of freely rotating molecules distinguishes the slower tumbling of ligands tethered to a NP surface.<sup>41,43</sup> We first monitored the ligand exchange reaction of interest via <sup>1</sup>H NMR as bound OA<sup>-</sup> becomes wholly dissociated OA

over the course of a parallel ODPA titration, most apparent from the vinylic H's chemical shift 5.1–5.6 ppm shown in Figure 4.8. This has become a prevalent method of asserting initial ligands have been effectively displaced from NP surfaces.<sup>34,41,63,64,137,168,171,197,248,253</sup> As expected, the extrusion of OA at ca. 1:1 titrated ODPA by X-type ligand exchange is demonstrated in this titration; however, the <sup>1</sup>H NMR was insufficient to clarify the proposed L-type phosphonic acid association.

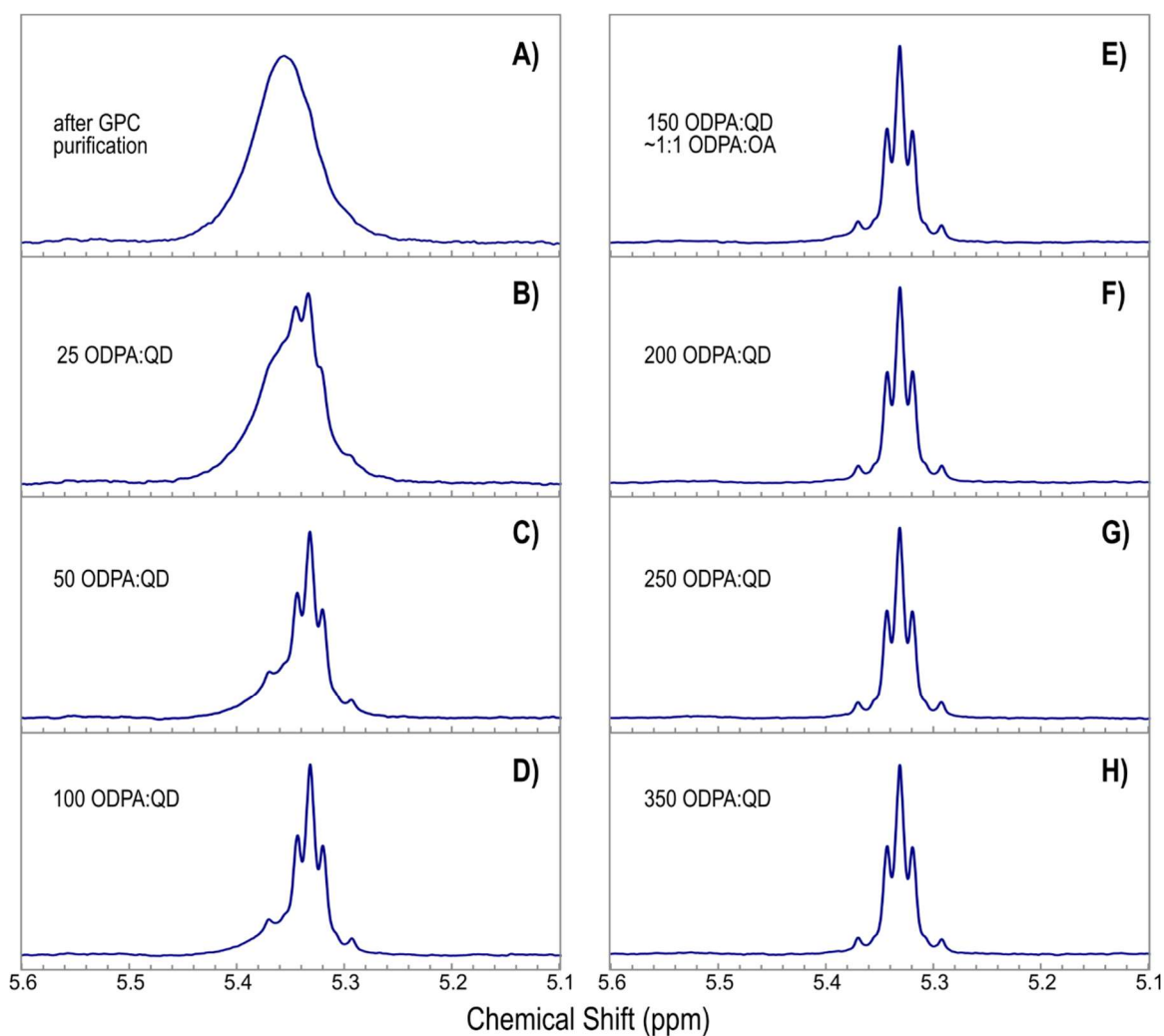


**Figure 4.8** Quantitative <sup>1</sup>H NMR for vinylic proton region of oleate ligands during parallel ODPA–CdSe|OA<sup>−</sup> titration in THF-d<sub>8</sub>. Panel (E) indicates approximately 1:1 molar equivalents of ODPA:OA ligands.



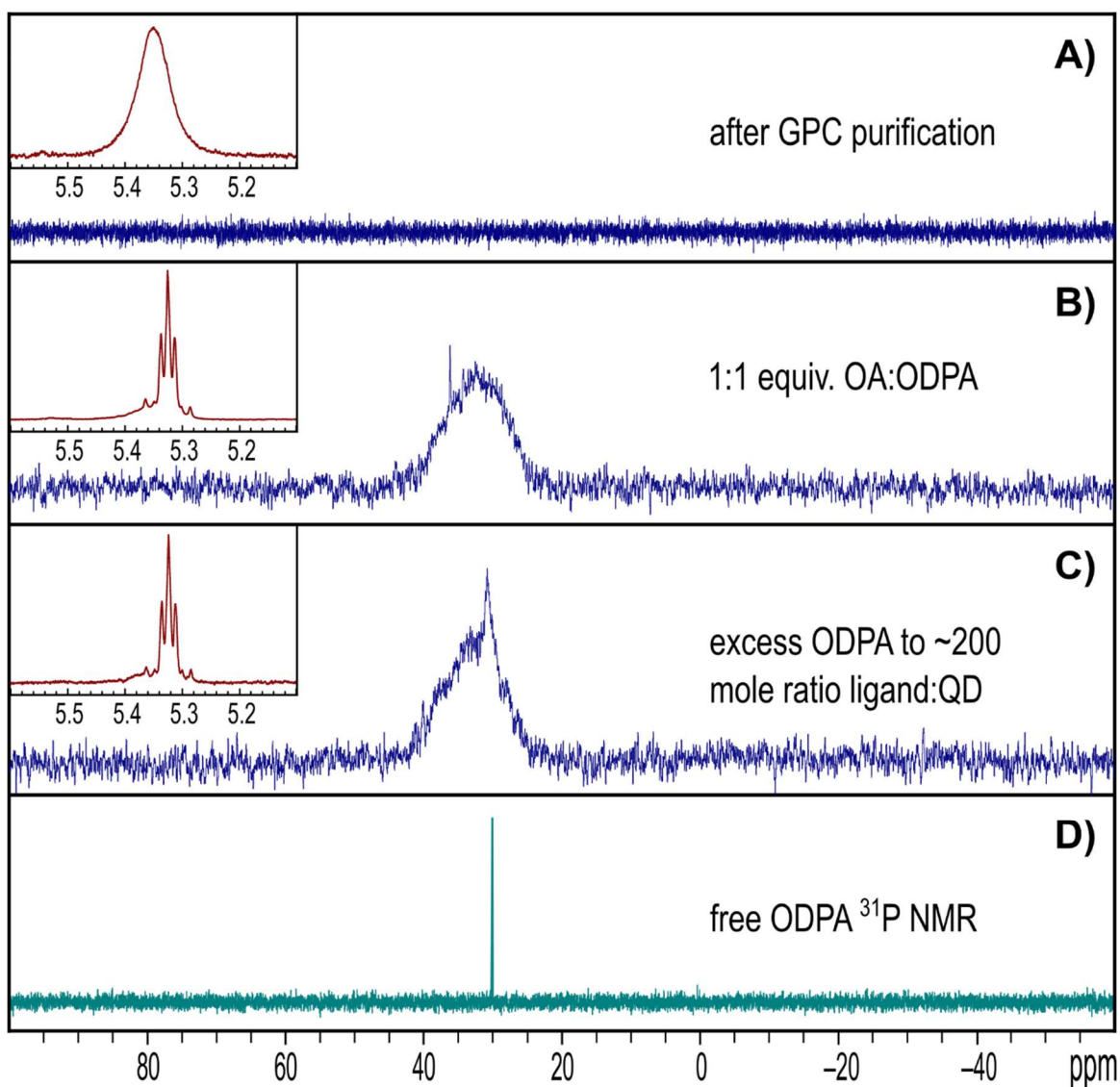


**Figure 4.9** Quantitative  $^{31}\text{P}$   $\{^1\text{H}\}$  NMR in THF-d8 for ODPA-CdSe|OA<sup>-</sup> parallel titration after initial GPC purification (A), at 1:1 mole equivalents ODPA:OA (B) and after THF GPC purification followed by excess addition of ODPA to a total ~200 mole equivalents. Free ODPA in THF-d8 is shown in (D). Insets display zoomed in vinylic OA proton region at corresponding points in the titration.

Figure 4.9 shows another ancillary NMR titration to verify our hypothesis about the termination of endothermic heats in the raw isotherm coinciding with a quantitative ligand exchange. Therein we investigated the concomitant dissociation of OA and adsorption of



ODPA. Whereas the initial  $^1\text{H}$  NMR spectra of purified QDs display broadened resonances of bound  $\text{OA}^-$  species,  $^{31}\text{P}$   $\{^1\text{H}\}$  NMR after GPC purification showed no phosphorus-containing species were present (Figure 4.9A). The next point in this titration corresponds to the 1:1 equiv. X-type ligand exchange (Figure 4.9B). The  $^{31}\text{P}$   $\{^1\text{H}\}$  NMR is dominated by a single broad peak ( $\delta \approx 22\text{-}47$  ppm) indicating a strongly bound titrated phosphonate ligand. Conversely the  $^1\text{H}$  NMR inset at this 1:1 equiv. shows a sharp multiplet for alkenyl protons of dissociated OA, with a small yet perceptible shoulder distorting the symmetry and attributed to a small fraction of persistently adsorbed  $\text{OA}^-$ . This observation is consistent with previous reports that phosphonates immediately exchange with carboxylate ligands as opposed to first adsorbing to vacant sites, and that a slight excess ca 1:1 equiv. is required for complete OA desorption.<sup>63,64,248</sup>

We note that although within the ITC reaction system are native and incoming ligands both covalently bound and weakly adsorbed at the QD surface and free in solution, we sought to unambiguously differentiate between the thermodynamic processes to which our isotherm alluded. The versatility of our GPC purification permitted us to separate ligand-exchanged  $\text{CdSe|ODPA}^-$  from liberated OA and any unassociated ODPA to subsequently probe only what was occurring at the QD surface rather than with the ligand-solvent reservoir. QDs traversed a THF mobile phase GPC (to maintain the solvent environment) and were easily brought back into THF-d8 (Figure 1.4). Excess ODPA was added to  $\sim 200$  total equiv. ODPA:QD, informed by the first apparent analytical endpoint at the greatest *total*  $\Delta H$  in the ITC isotherms. At this point  $^{31}\text{P}$  NMR showed a new and relatively less broadened feature centered about 30.8 ppm ( $\delta \approx 27\text{-}33$  ppm) on top of the original bound phosphonate resonance (Figure 4.9C). We attribute this new signal to neutral

L-type phosphonic acid with a slightly broadened resonance likely due to a fast (on the NMR timescale) dynamic adsorption onto vacant QD sites. Such would comprise a ligand species only datively adsorbing or weakly interacting with the QD and less incumbered by the rotational diffusion of one being tightly bound to the QD surface. This assignment is corroborated by the reference  $^{31}\text{P}$  NMR spectrum of free ODPA ( $\delta = 30.2$  ppm) in Figure 4.9D. The fractional occupation of  $\text{ODPA}^-$  suggested by the NMR titration coincides precisely with the disappearance of the rapid exothermic and endothermic signals, and thus the complete X-type exchange. Subsequently adsorbed excess ODPA following the GPC purification led to an increase in the overall bound P signal and definitively verified the slowest exothermic signal should be attributed to a distinct L-type ODPA dative ligand adsorbing event.

### **4.3 Timetrace analysis toward separated heats isotherm**

#### **4.3.1 Obtaining thermodynamic parameters from timetrace analysis**

Having established the sequential X-type exchange then L-type association reactions underlying the ITC response, we returned to quantitatively analyze the raw heat isotherm to extract thermodynamic parameters. Customarily total areas of isotherm curves within the span of each injection interval are integrated and the appropriate equilibrium model is applied with a nonlinear regression to obtain thermodynamic values.<sup>46,47,50,51,55,60</sup> However, the nature of this exchange reaction along with the variable ITC isotherm response shape we observed herein prompted us to separate contributions from different processes.<sup>56,57</sup> Each ITC injection peak shape is a convolution of the intrinsic instrument response function (IRF) and the binding interaction kinetics.<sup>252</sup> For a single process approaching equilibrium, the isotherm peak width can expand over the course of the titration and this has been used

to retrieve binding parameters.<sup>251</sup> The evolution in time response for this investigation is

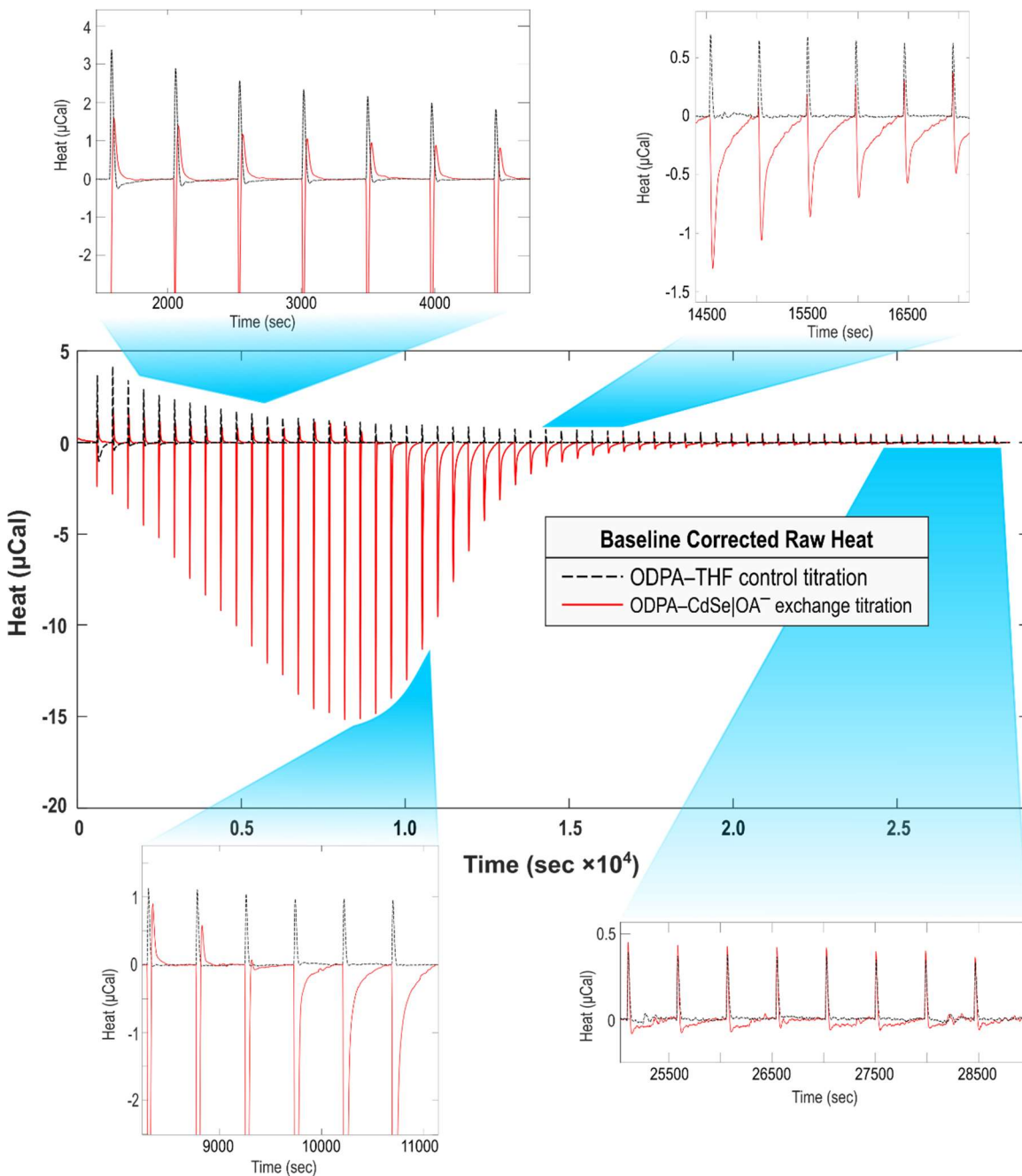


**Figure 4.10** Representative thermogram for ODPA–CdSe|OA<sup>−</sup> (red lines) plotted against ODPA–THF reference titration (black dashes). Zoomed-in region insets highlight the evolution of the kinetic response in the ODPA–CdSe|OA<sup>−</sup> thermogram as an expansion in the exothermic peak widths. Initially the reaction thermograms are characterized by a rapid exotherm, but the rapid exotherm quickly expands as the slower endotherm within the same injection region eventually diminishes. A complete saturation of the QDs with the ODPA ligands is apparent as highlighted by the tail of the ODPA–CdSe|OA<sup>−</sup> thermogram exactly overlaying the reference ODPA–THF thermogram for free ligand introduced into solvent.

clearly differentiated from the IRF, which became more apparent when comparing to reference titration (Figure 4.10). Ultimately the constancy of the [injection] peak onsets and widths in the ODPa–THF control in Figure 4.10 explicitly refutes any presumption that this was merely a feature of the instrument (i.e. distinct from the IRF). Furthermore, the time response is comprised of distinctly non-exponential responses that cannot be explained by the progression of a single exponential kinetic response time.<sup>252</sup> An evolution of slower reaction kinetics, evinced in the increasing isotherm peak widths, moreover suggested different time constants were also associated with the three resolved thermodynamic processes.

Therefore, a more sophisticated approach than merely integrating the raw heat became accessible. We approached our analysis of the isotherms considering these dynamic equilibrium kinetics as if on independent reaction coordinates, as a timetrace analysis of the raw data. The premise of our timetrace analysis was that we could capture the complete titration isotherms as a combination of linearly independent components  $k$  of appropriate basis waveforms intrinsic to the kinetics of each reaction process. To identify these intrinsic waveforms, we considered differences between model waveforms with distinct contributions to the injection peak shapes. Select basis waves for linear combinations of course is not unique; however, by requiring endo- or exothermic signals, waveforms could be identified for an optimized fit to the entire ITC response. Inasmuch if each  $n^{th}$  injection response, considered a given response “decay”  $y_n$  over the reaction time  $t$ , could be adequately described as fractions of fundamental wave components  $w_k(t)$  (Figure 4.11) with assigned physically relevant (endo- vs exothermic) amplitudes  $A$ ; we could contrive such basis waveforms that would resemble the intrinsic heat response of the ligand exchange system.

$$y_n(t) = A_{1,n}w_1(t) + A_{2,n}w_2(t) + A_{3,n}w_3(t) \quad (1)$$

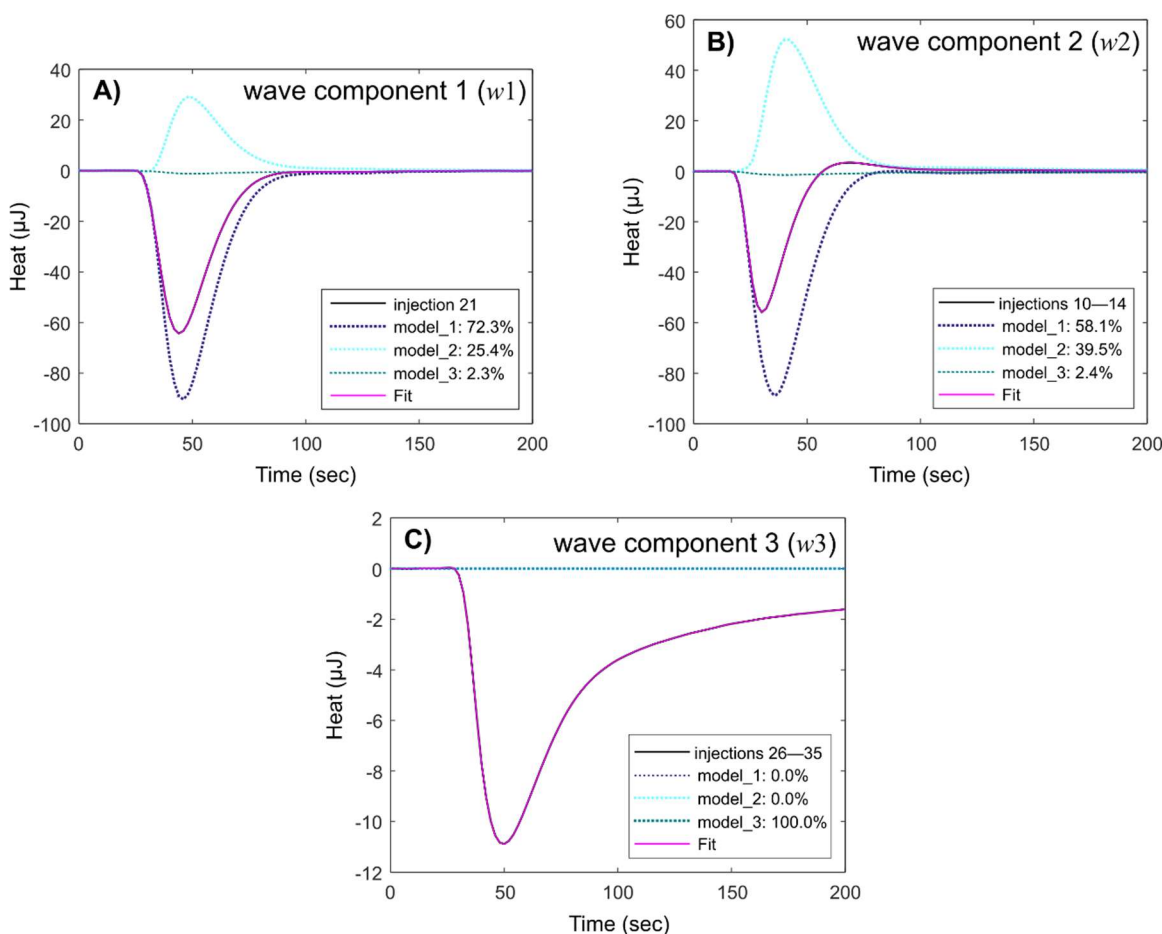


**Figure 4.11** Fundamental wave components  $w_k(t)$  determined as functions of model waveforms selected from baseline corrected and reference subtracted thermograms. Wave component 1 (A) was selected to represent contributions of the expanding exotherm in the exchange regime; wave component 2 (B) was selected to represent contributions from the exotherm and ensuing rapid endotherm of the primarily exothermic exchange regime; waveform component 3 (C) was selected to represent contributions from the slow exotherm characterizing the association regime. A linear combination of the fundamental waveform  $w_k(t)$  components allocated separated heats to 3 physically relevant reaction processes in the isotherms.

Waveform models  $m_k(t)$  were chosen from each titration's raw isotherm as shown in Figure 4.7 E-H, then optimized coefficients  $r_n$  were applied to subtract contributions of those  $m_k(t)$  waveform models on each time response waveform component  $w_k(t)$ . A final fit to the raw data isotherm by the time response decay  $y_n(t)$  over each  $k$  component

consequently populates the total separated heats, which was distributed based on the integrals of those determined waveform components relevant to either endo- or exothermic contributions – again, *rather than* integrating the power signal for each total injection interval. Fundamental wave components  $w_k(t)$  are thus determined

$$w_k(t) = m_k(t) - r_{k,k'}m_{k'}(t) - r_{k,k''}m_{k''}(t) \quad (2)$$

Heat for the extent of reaction in each injection step is obtained based on the amplitude of each waveform component in the observed time responses. The separated heat for the full titration reaction, analogous to the customary integrated heat isotherms but ultimately representing three distinct and physically relevant thermodynamic processes, is depicted in Figure 4.12A. The most immediate advantage to separating the heat signals, as we have demonstrated, is the clear empirical evidence of at least three mathematically resolvable reaction coordinates.

The final isotherms were obtained by integrating the total heat from the separated heats, more appropriately distributed to either the initial quantitative exchange process or the dative association process. A representative integrated isotherm is shown in Figure 4.12B, with the two types of sites represented as either navy or teal  $\diamond$ , the total reaction system heat as  $\square$ . Although we sorted the isotherm heat contributions as three physically relevant reaction coordinates in the system, we (re)combined the rapid exothermic and endothermic signals contributing to the fundamental waveform components  $w_1(t)$  and  $w_2(t)$  (navy and aqua bars respectively) as one *type of* QD surface ligand exchange site, independent of the second ligand association *type of* site (teal bars). Whereas we were able to define two waveforms that combine to adequately describe the heat contributions of the early rapid exothermic and subsequent endothermic processes, their lifetimes are similar and both terminating at an

equivalence point that matches the X-type exchange suggests that an initial equilibrium between these initial processes is somewhat coupled. Additionally, chemical data to categorically distinguish them is presently lacking. Therefore, we combined these initial heat responses to facilitate more accurate consideration of separated equilibrium processes.<sup>57</sup> Contrarily, the slower exothermic heat is extremely well resolved from the latter two processes as treated with our timetrace analysis and its onset is verified by quantitative NMR titrations. Again, complete disappearance of endothermic peaks also validates that the two equilibria are well separated and alluded to independent equilibrium processes as an appropriate interpretation.

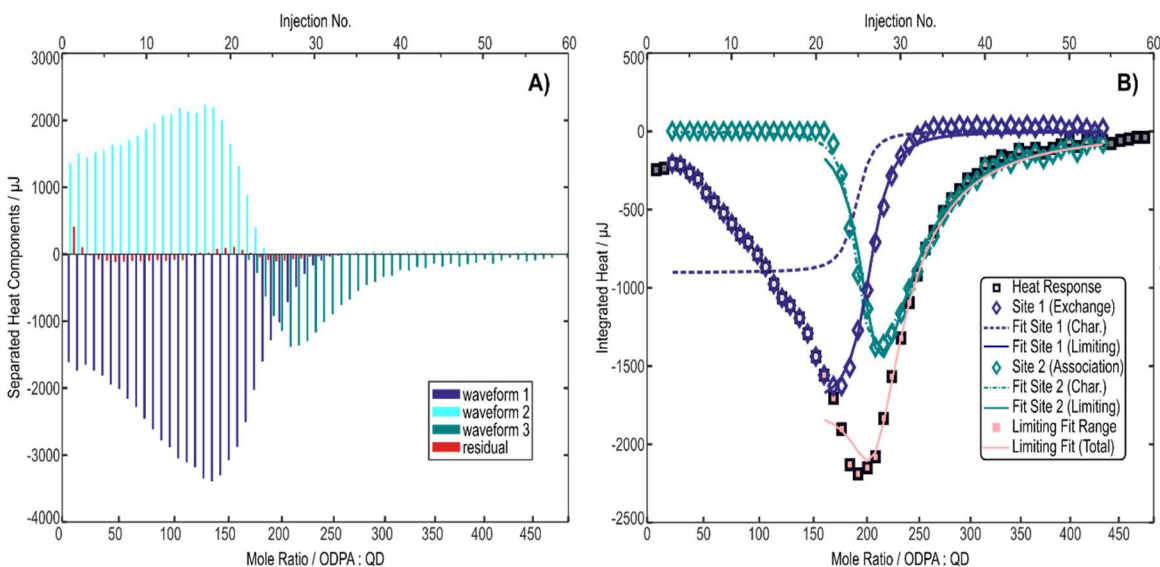


**Figure 4.12** Separated heats (A) and integrated isotherms (B) determined from waveform components specific to each ITC trace for each trial. The navy and teal coloring corresponds to the sequential exchange preceding the association reactions respectively. The integrated isotherms (B) include fits to the two independent types of sites model applied under both *Characteristic* and *Limiting* regimes. The differences in the two regimes by which thermodynamic parameters were obtained are described within the main text, but ultimately distinguishing the different regimes of the two types of independent sites allowed us to best capture the distribution of binding enthalpies  $\Delta H$  evinced in the curvature of the raw heat data thermograms and subsequent isotherms.

#### 4.3.2 Effective two-site binding model for ligand exchange and adsorption

In the case of a QD with two independent types of adsorption sites for the same ligand  $L$ , the fractional occupations of these sites  $\theta_1$  and  $\theta_2$  are described by their association constants  $K_1$  and  $K_2$  at equilibrium the following equations must be solved simultaneously:

$$K_1 = \frac{\theta_1}{1-\theta_1} \times \frac{1}{[L]} \quad (3)$$

$$K_2 = \frac{\theta_2}{1-\theta_2} \times \frac{1}{[L]} \quad (4)$$

However these expressions describe association constants, when in fact we propose the first reaction to proceed as the exchange reaction according to the chemical equation and reaction quotient as follows:



$$K_{\text{exch}} = \frac{[\text{CdSe}|\text{ODPA}^-][\text{OA}]}{[\text{CdSe}|\text{OA}^-][\text{ODPA}]} = \frac{\theta_{\text{exch}}}{1-\theta_{\text{exch}}} \times \frac{[L_1]}{[L_2]} \quad (6)$$

In principle, Eqs. (4) and (6) (with  $L_2$  as  $L$  in Eq. (4)) can be simultaneously solved to describe the conditions at equilibrium. In the present case, given that the exchange reaction proceeds readily and largely precedes binding to vacant sites, and given the initial condition of a negligibly low concentration of free  $L_1$  such that  $[L_1] \approx N_1[\text{QD}]$  at the conclusion of the quantitative ligand exchange; we can make the following approximation:

$$K_{\text{exch}} = \frac{\theta_{\text{exch}}}{1-\theta_{\text{exch}}} \times \frac{[L_1]}{[L_2]} \cong K_{\text{eff}} \times N_1 \times [\text{QD}] \quad (7)$$

The state at equilibrium near the conclusion of the ligand exchange (i.e. at the transition from exchange to association of  $L_2$  to vacant sites) can then be described by simultaneously solving the following two equations:

$$K_{\text{eff}} = \frac{\theta_{\text{exch}}}{1-\theta_{\text{exch}}} \times \frac{1}{[L_2]} \quad (8)$$



$$K_2 = \frac{\theta_2}{1-\theta_2} \times \frac{1}{[L_2]} \quad (9)$$

This approach can in principle be used to obtain best-fit values for  $K_{\text{eff}}$ ,  $N_1$ ,  $\Delta H_1$ ,  $K_2$ ,  $N_2$ , and  $\Delta H_2$  through comparison to experimental results, with  $K_{\text{exch}}$  obtained as  $K_{\text{eff}}/(N_1[\text{QD}])$ . This approximation is valid for  $K_{\text{exch}} \gg 1$  and  $K_2 \ll K_{\text{eff}}$ . We note that although there exists the “Sequential Sites” model that would appropriately assume a fixed sequence of binding to different sites, a specific stoichiometric parameter  $N$  is not solved for each site. Rather each integer value for the total number of distinct sites is fit with parameters  $K$  and  $\Delta H$ . Such a model becomes impractical for a system that accommodates hundreds of ligands and was not determined to provide valuable phenomenological information in the present investigation. Moreover, the condition  $K_I \neq K_{II}$ , met in our system as  $K_{1,\text{eff}} \gg K_2$ , typically renders sequential vs independent sites models equivalent since the system’s thermodynamics dictate binding to the site of highest affinity before that of lower affinity.

#### 4.3.3 Discussion of thermodynamic parameters obtained from effective two sites model

Our application of an effective two types of nonidentical independent sites model to the ITC results is distributed as Site1: X-type exchange and Site2: L-type association. Firstly, note that the total heat reveals the greatest  $\Delta H$  at  $\sim 1:1$  ODPa:OA<sup>−</sup> equivalent, which is not expected for the case of a Langmuir association or even competitive displacement. The observed “build-up” of heat can occur in the case of negative cooperativity or sequential binding to sites having distinct  $\Delta H$ , but it is difficult to adequately constrain uncertainty in the model parameters for each enthalpically equivalent site based on total heat alone. As discussed below, if the heat from the slowest exotherm ( $m_3$ ) is attributed to Site2, the model effectively explains the onset of this exothermic signal, corresponding to filling of Site2 once binding to Site1 has been largely completed. This in turn partially explains the peak in the total heat

seen at  $\sim 1:1$  ODPa: OA<sup>-</sup> equivalency (recall the persistent broadened shoulder in the vinylic region of the <sup>1</sup>H NMR spectra at ca 1:1 equiv.). However, within this model we expect *Langmuiresque* signal for heat corresponding to Site1 with a relatively constant heat per injection until Site1 approaches saturation. Although even after subtracting contributions from  $w_3$ , the remaining heat increases in magnitude over the course of the titrations and does not closely conform to a *Langmuiresque* curve. Nevertheless, in order to facilitate analysis of the well-resolved  $w_3$  signal, herein we represent the ligand exchange as being governed by Eq. (7) with suitable values of  $K_{\text{eff}}$ ,  $N_1$  and  $\Delta H_1$ .

Two approaches to attain these values were considered. First, we could choose a value of  $\Delta H_1$  that accurately describes the total heat evolved throughout the titration reaction. This will be referred to as the “Characteristic” fit (dotted lines in Figure 4.12B) and is constrained on Site2 heats (on  $w_3$ ) to optimize  $K_{\text{eff}}$ ,  $N_1$ ,  $K_2$ ,  $N_2$  and  $\Delta H_2$ . Afterwards  $\Delta H_1$  is solved as a single-parameter fit for the Site1 heat. The Characteristic fit represents the *average* enthalpy of OA<sup>-</sup> to ODPa<sup>-</sup> ligand exchange and is the more macroscopic multisite model<sup>57,250</sup> applied. We also consider a “Limiting” fit (salmon colored solid lines in Figure 4.12B) that attempts to more precisely describe the transition from ligand exchange to ligand association, as the ligand exchange goes to completion. In this case both Site1 and Site2 heat data were used to iteratively solve model parameters, but only over a selected range of injections near the titre point of X-type exchange saturation. Finally, as the system within ITC is at constant temperature and pressure, the fundamental thermodynamic relationships  $\Delta G = -RT\ln K$  and  $\Delta G = \Delta H - T \Delta S$  are used to calculate remaining thermodynamic parameters for both regimes, shown in **Table 4.1**. We note that the data led to Site1 values that were well-constrained parameters and  $K_2$ , but that the fit results for  $N_2$  and  $\Delta H_2$  were

correlated due to a low value of Brandt's  $\epsilon$  parameter,<sup>46,250</sup> thus only their product  $N_2 \times \Delta H_2$  was well-constrained.

**Table 4.1** Thermodynamic equilibrium parameters for oleate exchange with ODPa

EXCHANGE	$K_{\text{eff}}$ $\times 10^5 \text{ M}^{-1}$	$K_{\text{exch}}$ $\times 10^2$	$N_1$ per QD	$\Delta H_1$ $\text{kJ mol}^{-1}$	$\Delta G_1$ $\text{kJ mol}^{-1}$	$\Delta S_1$ $\text{J mol}^{-1} \text{ K}^{-1}$
<i>Characteristic</i>	$12.4 \pm 2.1$	$28.2 \pm 8.0$	$182 \pm 10$	$-6.72 \pm 0.20$	$-19.4 \pm 0.29$	$+43.1 \pm 0.027$
<i>Limiting</i>	$4.04 \pm 0.87$	$9.41 \pm 8.0$	$189 \pm 11$	$-13.8 \pm 0.29$	$-16.7 \pm 0.41$	$+9.66 \pm 0.18$
ASSOCIATION	$K_2$ $\times 10^3 \text{ M}^{-1}$	$*N_2 \times \Delta H_2$ $\times 10^3 \text{ kJ}$	$*N_2$ per QD	$*\Delta H_2$ $\text{kJ mol}^{-1}$	$\Delta G_2$ $\text{kJ mol}^{-1}$	$\Delta S_2$ $\text{J mol}^{-1} \text{ K}^{-1}$
<i>Characteristic</i>	$4.99 \pm 0.19$	$-1.23 \pm 0.23$	$56.7 \pm 5.2$	$-21.9 \pm 2.0$	$-20.9 \pm 0.065$	$-3.29 \pm 3.7$
<i>Limiting</i>	$3.29 \pm 0.34$	$-1.31 \pm 0.76$	$27.8 \pm 7.3$	$-57.6 \pm 20$	$-19.8 \pm 0.19$	$-127 \pm 0.92$

Standard errors of the means on ITC given parameters:  $K$ ,  $N$ ,  $\Delta H$ ; Propagation of errors on calculated parameters:  $K_{\text{exch}}$ ,  $\Delta G$ ,  $\Delta S$ ,  $N_2 \times \Delta H_2$ . \*Reported as product due to low  $\epsilon$  parameter value,<sup>46</sup> signifying  $N_2$  and  $\Delta H_2$  are not independently constrained.

#### 4.3.4 Justification for *X-type exchange* thermodynamic parameters

The thermodynamic parameters  $N_1$  and  $K_{\text{exch}}$  are well-constrained and in general agreement for both fits to the two independent types of sites model. Table 4.2 depicts the statistical strength of applying this model with these well-constrained parameters, even to a titration in which the QD titrand was increased nearly  $2\times$  that of the standard reactions.

**Table 4.2** Q test for ‘Gross Outliers,’ on Site1 for  $\sim 2\times$  initial CdSe|OA<sup>-</sup>

PARAMETER	$K_{\text{exch}}$	$N_{1,\text{exch}}$	$\Delta H_{1,\text{exch}}$	$\Delta G_{1,\text{exch}}$	$\Delta S_{1,\text{exch}}$	Lim $\Delta H_{1,\text{exch}}$
Q - VALUE	0.3271	0.2062	0.5434	0.2397	0.6878	0.2577

A test of outliers compared to  $Q_{\text{crit}}$  of 0.821 for 99% CL on 5 observations; in every instance,  $Q < Q_{\text{crit}}$  and so statistically at the 99% confidence level each thermodynamic parameter could be retained within this sample set. These parameters were also subjected to a  $t$  statistic test with 3 degrees of freedom; with the null hypothesis that the given value was *not significantly different* from the sample's average & standard deviation (not including the tested value) and was ultimately rejected only if  $t > t_{\text{crit}}$ . Only the value of  $\Delta S_{\text{exch}}$  was calculated to be statistically significantly different at a 99%  $t$ -test confidence level, but *not* at the 99.9% confidence level.

We posit that the ligand exchange  $\Delta H_1$  is best conceptualized as a distribution of site-specific energies over a range that does not exceed the value determined by the Limiting

fit. A non-constant  $\Delta H$  for exchange interactions is quite intuitive given the heterogeneous nature of QD surfaces, and even often postulated though not directly accommodated in empirical analyses of experimental results. Recently Drijvers et al. investigated ligand displacement reactions on CdSe nanocrystals and demonstrated adsorption enthalpies that were both binding site specific and dependent. They concluded that each facet of the nanocrystal surface comprises a distribution of binding sites that could in turn be well described by net thermodynamic parameters for ensemble sites attributed to specific surface processes i.e. exchange.<sup>168,197</sup> We note that on a numerical basis,  $K_{\text{exch}}$  and  $\Delta G_{\text{exch}}$  are smaller and less negative than  $K_2$  and  $\Delta G_2$ , respectively, which is counterintuitive since the ligand exchange reaction irrefutably takes precedence. This is understood by noting  $K_{\text{exch}}$  and  $\Delta G_{\text{exch}}$  are defined for a standard concentration of free oleic acid  $[\text{OA}] = 1 \text{ M}$ . Under the actual reaction conditions  $[\text{OA}] \ll 1 \text{ M}$  and ligand exchange becomes more favorable than association of ODPA to vacant sites until the exchange reaction approaches saturation ( $K_{\text{eff}} \gg K_2$ ). Regardless, the ligand exchange reaction is found to proceed in  $\sim 1:1$  equivalency and is both exothermic and entropically favorable, *consistent with* a proton transfer driven X-type desorption-adsorption.

Previously others have reported either endothermic or somewhat ambiguous exothermicity for exchange reactions in similar NC reaction systems.<sup>64,168,171,197,248</sup> Though we conclusively demonstrate overall exothermic character, we also observe that the exchange step of the reaction includes a clearly resolvable endothermic signal. Our timetrace analysis further reveals the significant magnitude of this signal, and that while it broadly accompanies the ligand exchange reaction it is linearly independent of the dominant exothermic contribution to  $\Delta H_1$  and could be identified through differences between representative

injection responses (Figure 4.10). There are several possible explanations for the endothermic heat evolution observed in the X-type exchange reaction. It is reasonable that in the context of “ligand addition energy” ( $\sigma$ ) proposed by Sluydts and coworkers, that the fraction of adsorbed ligand density to expected ligand density on the QD surface would exceed their *expected* oxidation-number sum rule stoichiometric value of  $\sigma = 1$ . When this expected oxidation-number sum rule stoichiometric value exceeds one, their proposed ligand addition energy becomes endothermic for systems within an increasing ligand reservoir;<sup>254</sup> a concept outlining an interaction between OA/ODPA that has been hypothesized previously<sup>171</sup> and is relevant to the excess ligand population that would exist in our reaction system.

Another possible explanation endothermic response could have been the occurrence of crystal reorganization upon phosphonate ligand binding. Our powder XRD patterns confirm that no internal crystal structure reorganization occurs, i.e. zincblende to wurtzite phase transition, as a result of the ligand exchange (Figure 4.13), which is in line with previous investigations that emphatically argued ligand exchange could not induce crystal structure modification even when the QD optical spectra was considerably affected.<sup>40,196</sup> Conversely, *surface* reconstruction is indeed a possibility; to accommodate vacant sites, migrating and rearranging native ligands, and the mixed ligand population. During synthesis the incoming phosphonate ligands would enforce the wurtzite crystal structure, but herein are adsorbing to zincblende QDs.<sup>1,40,196,247,254,255</sup> Additionally, as this initial segment of the thermogram corresponds to a mixed ligand population that has resulted from the immediate exchange of ODPA<sup>-</sup> for OA<sup>-</sup> on purified QD surfaces, protonated OA could remain on the surface temporarily prior to dissociation possibly via migration to initial vacant sites<sup>255</sup> (NMR

confirms that OA does not remain on the surface at equilibrium, but is extruded essentially quantitatively into solution). While different headgroups and conformational space could contribute to differences in molecular footprint and consequent surface rearrangement,<sup>1,40,168,196,247</sup> thoroughly assigning the essential thermodynamic profile of the overall reaction has been the primary focus of this investigation. Although the exact intermediate process that yields the endothermic signal remains unclear, we hypothesize that a rapid proton exchange between ODPA and  $\text{OA}^-$  yielding a slower successive release of OA from its original QD surface site, to either another vacant site or into solution, was resolved by ITC. Regardless of the mechanism yielding the endothermic signal however, both the Characteristic and Limiting  $\Delta H_{\text{exch}}$  are ultimately exothermic. An  $\text{OA}-\text{CdSe}|\text{OA}^-$

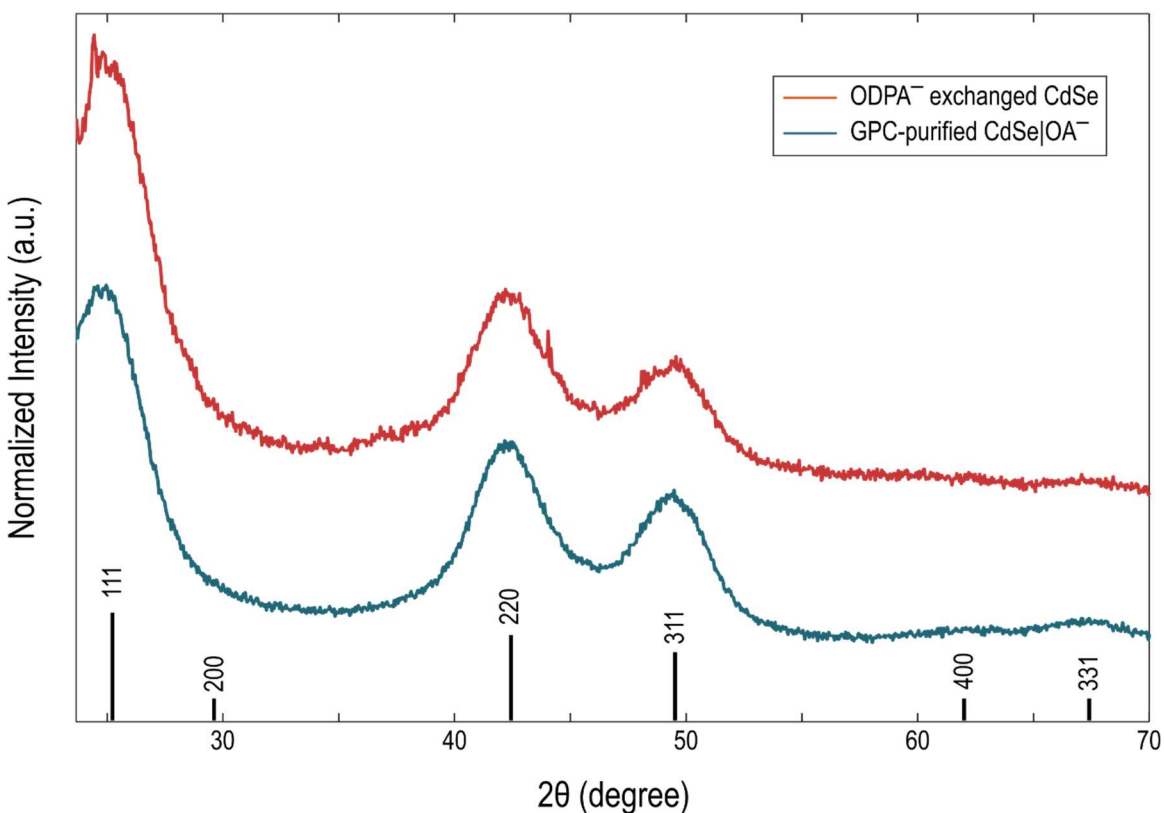


**Figure 4.13** PXRD patterns of the Zinc Blende CdSe QDs: GPC-purified  $\text{CdSe}|\text{OA}^-$  before the ITC titration (A) and  $\text{CdSe}|\text{ODPA}^-$  after the ITC titration (B), with labeled vertical lines to indicate standard Bragg reflection peaks in the respective bulk material.

reference titration was also conducted for which an exclusively *exothermic* thermogram was observed, suggesting that the reverse reaction would be endothermic. Previous reports of endothermic character in exchange reactions were therefore attributed to limitations of indirect measurements<sup>50,64</sup> and interpretations.<sup>34,168,171,197</sup>

#### 4.3.5 Justification for *L-type association* thermodynamic parameters

To address the ODPa L-type association thermodynamic parameters, given in the bottom half of Table 4.1, we first note that  $K_2$  (hence  $\Delta G_2$ ) and the product of  $N_2 \times \Delta H_2$  are well constrained by both fit methods with comparable values. In simple ligand association interactions described by the Langmuir isotherm, Brandt's  $\epsilon$  parameter ( $\epsilon = KN[M]_t$ ) uniquely determines the shape of the integrated heat response and for small values of  $\epsilon$ , the bend in the sigmoidal shape disappears and in fits to data. Consequently,  $N_2$  and  $\Delta H_2$  are correlated and subject to large uncertainties for  $\epsilon < \sim 10$ . Essentially it becomes difficult to distinguish strongly exothermic binding to few sites from weakly exothermic binding to few sites. The fits here are a result of simultaneous equilibrium at two sets of independent sites; but in the limit of  $K_{\text{eff}} \gg K_2$ , once the first set of sites (exchange) are saturated, the binding of ODPa to the second type of QD surface sites resembles a Langmuir isotherm described by  $K_2$ . At this stage of the reaction approximated  $K_2$  describes only the binding of ODPa to a second type of QD surface sites independent of those pertaining to  $K_{1,\text{eff}}$  and  $K_{\text{exch}}$ . The analytical form of this site's model resembles the quadratic polynomial of a Langmuir isotherm.<sup>46,47,50,51,60</sup> Accordingly, we can specify a  $\epsilon$  parameter appropriate to this step as:

$$\epsilon = K_2 \times [\text{QD}]_t \times N_2 \quad (10)$$

The  $\epsilon$  parameters for Site2 revealed by the effective two site model fits are consistently low, indicating that optimized values for  $N_2$  and  $\Delta H_2$  should not be considered

independently despite a well-constrained product  $N_2 \times \Delta H_2$ . Nonetheless, our model calculations for their separate values in both the Characteristic and Limiting regimes are physically realistic, consistent with 1) given an estimate of  $\sim 6$  atoms  $\text{nm}^{-2}$  for the sum of  $N_1$  and  $N_2$ ,<sup>1,34,247</sup> and 2)  $\Delta H_2$  energies exceeding those of  $\Delta H_1$  to meet the criteria for producing an isotherm with the observed curvature in this investigation.<sup>46,47,57</sup> In particular regard to  $N_2$  we further note that a significant reduction of initially adsorbed ligands is consistently attained via GPC purification,<sup>62</sup> and we have previously demonstrated consequent sites available for neutral binding is likewise significant.<sup>60</sup> To this point, the final endpoint and coincident saturation of the QD surface is consistently evident in every raw data thermogram as the final injections can be superimposed with ODPA–THF reference titrations (Figure 4.10). Nevertheless, these values are grayed as decent estimates at best, along with  $\Delta S_2$  (as this is calculated using  $\Delta H_2$ ). Our model's estimate of  $\Delta S_2$  very reasonably suggests unfavorable energetics; considering the reaction system has ODPA ligands titrated to excess with the original OA ligands also in solution. The less favorable energetics yielding a  $(-)\Delta S_2$  could also be deduced from the slower binding kinetics that caused greater injection peak widths for heat signals emerging from adsorption at Site2, as we have previously demonstrated the capacity of ITC to specify reaction kinetics apparent in QD–ligand interfaces, unambiguously corroborated by PL data.<sup>60</sup>

#### 4.4 Variation in synthetic preparation for further investigation

Given the keen precision of ITC to provide equilibrium thermodynamics for this irreversible ligand exchange reaction, we sought to further investigate two common subtleties in QD preparation. Chiefly, the ubiquitous heterogeneity within QD synthetic batches perpetuated by slightly altering the synthetic conditions, can present variation in NC populations even for



different investigators in the same lab. As aforementioned QD thermodynamic parameters were acquired from a single synthetic batch, they will henceforth be referred to as the “Standard (Std)” synthetic preparation. Another batch of QDs was synthesized with the same 1:3:2.2 Cd:Se:OA mole ratio and all the same precursor and solvent materials; with the At the step preceding the rapid precursor injection, this second QD batch was heated 10°C

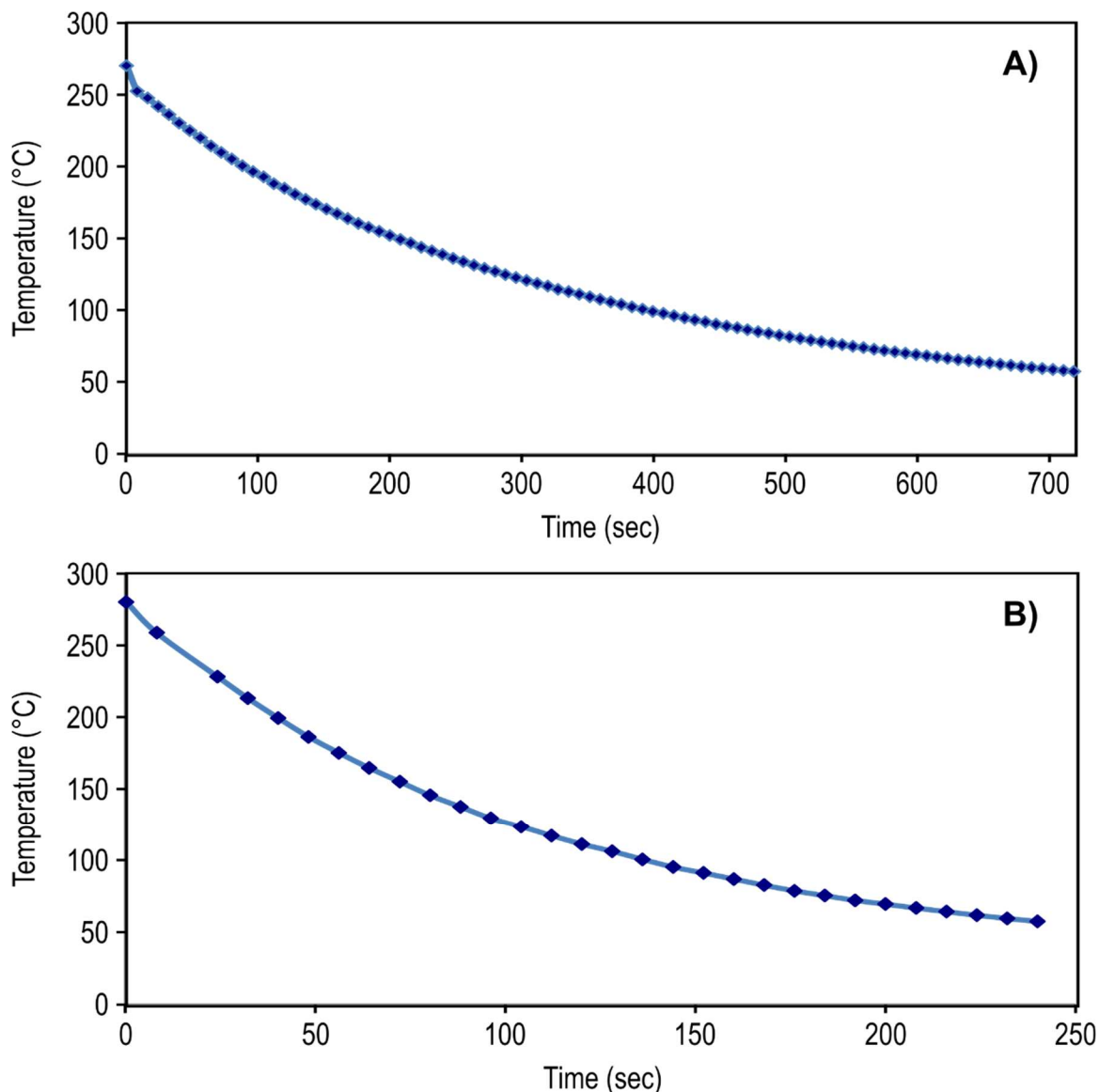


**Figure 4.14** Quenching trajectories for CdSe|OA<sup>-</sup> for the standard (Std) synthetic preparation (A) and the rapid (RQ) synthetic preparation (B) to terminate QD growth immediately after Se precursor injection. Adapted with permission from ref. 62. Copyright 2013 American Chemical Society.

higher, and immediately quenched with a stream of cold air; henceforth referred to as the only difference having been the quenching process used to terminate nucleation and growth. “Rapid Quench (RQ)” synthesis.<sup>62</sup> Whereas the Std QD synthesis was quenched by removing the heat source and allowed to cool The synthetic termination quenching trajectories are shown in Figure 4.14. The resultant RQ QDs had the same lowest energy extinction peak position as the Std QDs as well as indistinguishable TEM images (Figure 4.15). In an investigation to elucidate the primary contributing mechanism for [white light] emissive pathways in small CdSe QDs, Krause et al. demonstrated an vital correlation between PL and QD surface thermodynamics.<sup>35</sup> In one instance they too directly probed the consequences of changing only the synthetic quenching procedure to terminate further NC

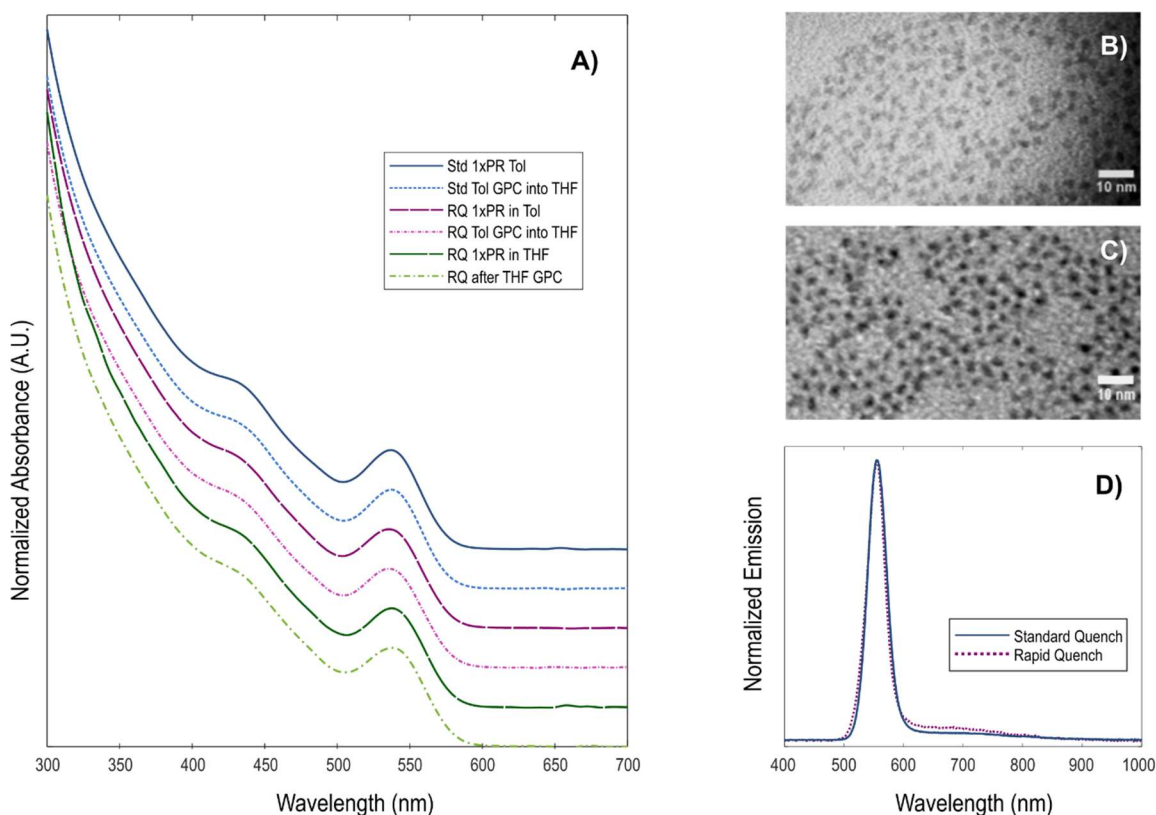


**Figure 4.15** Steady state absorption for standard and rapid quench CdSe |  $\text{OA}^-$  samples prior to and ensuing either toluene or THF mobile phase GPC purification (A); TEM images of the standard (B) and rapid (C) QDs; Steady state PL emission for both synthetic preparations. Both absorption and emission spectra are normalized to their lowest energy extinction peak.

nucleation and growth. Despite their unfortunate characterization of “TOPO-capped” CdSe NCs,<sup>60,198</sup> there are very valid implications of altering the kinetics of this step of NC synthesis that have been shown to cause a significant impact on NC surface ligand densities. It has been posited that more efficient and uniform quenching yields less surface trap emission, though such dynamics are still not entirely understood.<sup>222,228</sup> In the present case the PL emission spectra were comparable and neither displayed significant lower energy broadband surface trap emission. Altering the nucleation temperature and termination of NC growth has primarily been a synthetic knob to achieve different NC sizes and degrees of polydispersity.<sup>17,40,196,249</sup> Interestingly Teunis et al. recently resolved an additional final stage of the LaMer growth model, at which stage ligation was said to occur for the QDs. While the synthetic scheme was specifically tuned to decouple otherwise indistinguishable growth and ligation stages, they explicitly concluded that changes at the ligation stage only affect PL properties and does not alter NC excitonic peak position.<sup>228</sup> Again our observations of the standard vs rapid quench PL and absorption spectra (Figure 4.15A,B) are directly in line with this assertion.

Thermograms for the Std versus RQ reaction titrations, both purified by the toluene GPC, immediately reveal different molar equivalencies for the exchange reactions (Figure 4.16). Moreover, given the robustness of the GPC technique and the propensity to transfer NCs to different solvents between purification and experiments, we also systematically investigated RQ samples either purified by a Toluene GPC and subsequently transferred to THF for the ITC reaction (as was the procedure for the Std trials), or RQ samples purified by a THF GPC and then directly loaded in the ITC for the ligand exchange titration. Solvents can impact NC surface chemistry in several ways due to the local dielectric

environment they impart, their ability to penetrate ligand layers or coordinate to NC surfaces, and relative ligand solubilities directing degree of labile passivation.<sup>1,43,228,247</sup> Immediately pertaining to this study, ODPa is insoluble in toluene. Undeniably dissimilar raw heat thermograms are depicted in Figure 4.16 as well as Figure 4.17, which further

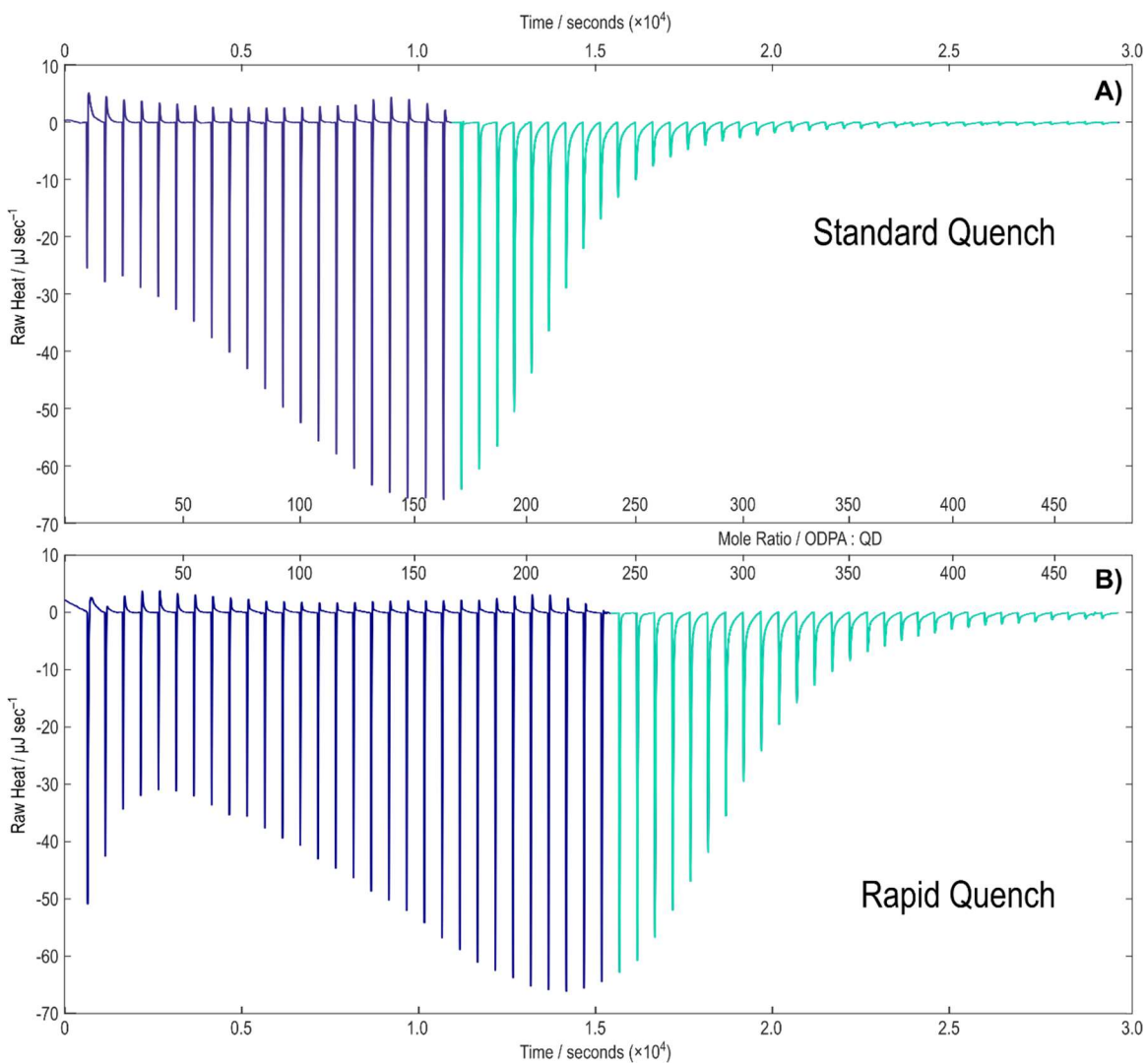


**Figure 4.16** Raw heat thermograms comparing the ODPA–CdSe|OA<sup>−</sup> titrations for initial QDs prepared by either the standard synthetic reaction termination (A) or the rapid synthetic reaction termination; purified via toluene GPC, transferred to anhydrous THF reaction solvent, then loaded into the ITC. The navy and teal coloring correspond to the exchange and association reaction regimes respectively.

analyzed the different mobile phase solvents employed in the GPC purification preparation for ODPA–CdSe|OA<sup>−</sup> titrations, otherwise conducted with *exactly* the same ITC experimental parameters.

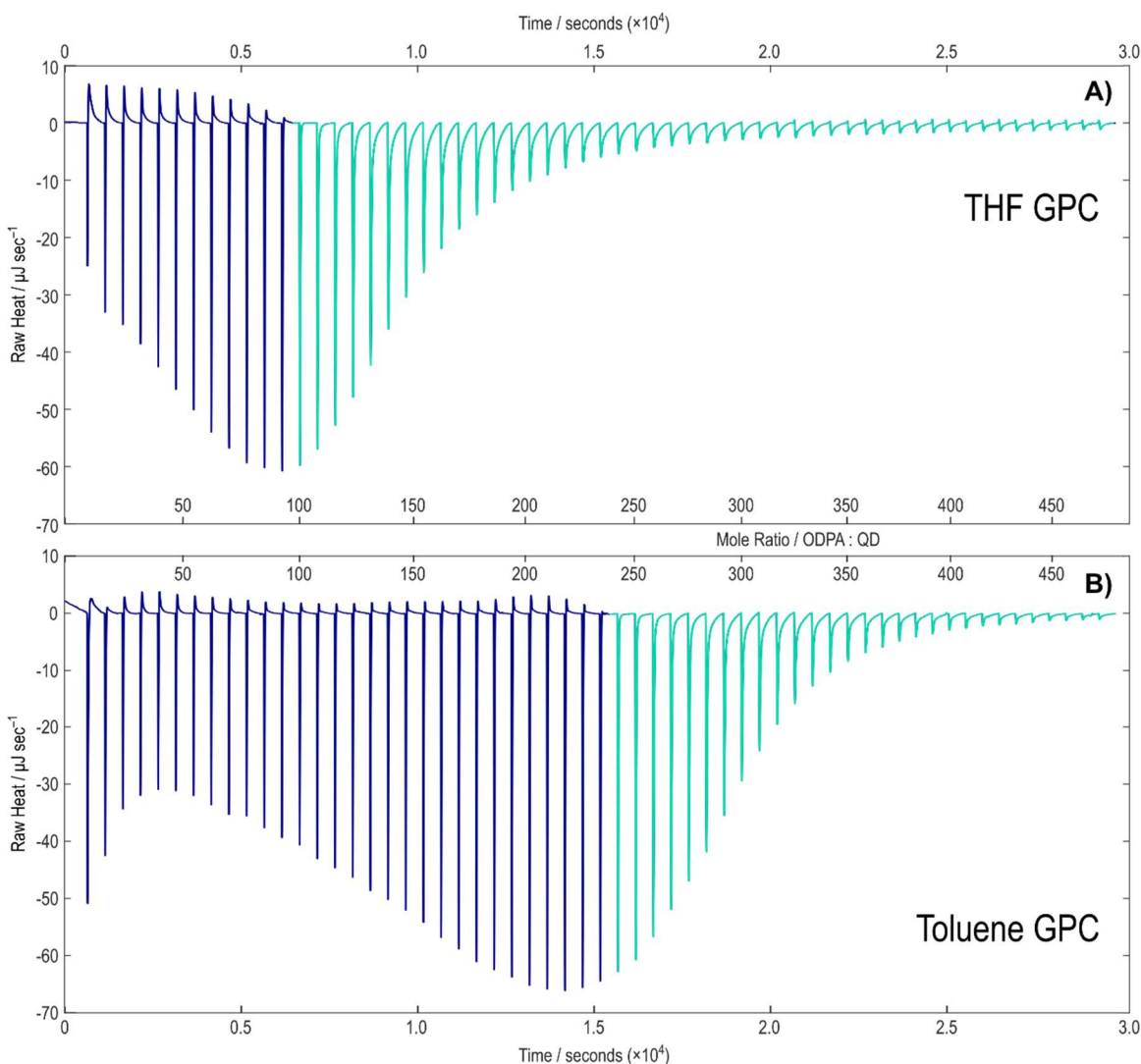


**Figure 4.17** Raw heat thermograms comparing the ODPA–CdSe|OA<sup>−</sup> titrations for initial QDs prepared by the rapid synthetic reaction termination; purified via THF GPC then directly loaded to the ITC (A), or toluene GPC, transferred to anhydrous THF reaction solvent, then loaded into the ITC. The navy and teal coloring correspond to the exchange and association reaction regimes respectively.

The reproducibility of these RQ QD titrations is emphasized in Figure 4.18. Quantitative  $^1\text{H}$  NMR spectra analyzed between different QDs synthetic termination trajectories (Std vs RQ) and between those of the same synthetic procedure but different purification solvents showed from only 4% to 20% difference in initial OA ligand populations, given the compared treatments. Toluene GPC tended to yield higher ligand

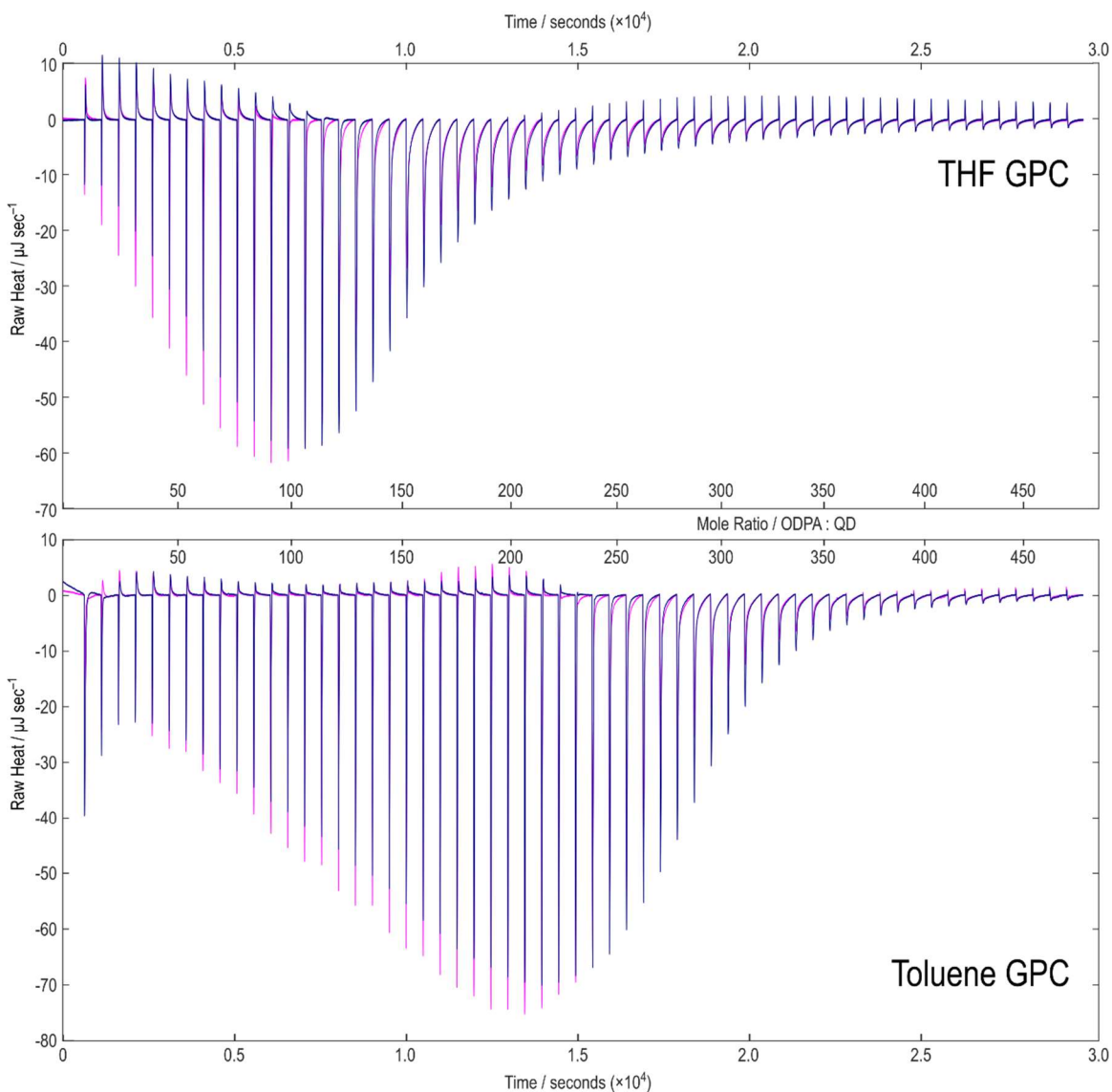


**Figure 4.18** Overlays of repeated raw heat thermograms comparing the ODPA–CdSe|OA<sup>−</sup> titrations for initial QDs prepared by the rapid synthetic reaction termination; purified via THF GPC then directly loaded to the ITC (A), or toluene GPC, transferred to anhydrous THF reaction solvent, then loaded into the ITC.

densities, whether investigating different purification solvents or merely solvent transfer, typically by ~10%. Appropriate relaxation delay and acquisition times were determined relative to each NMR solvent and the ferrocene internal standard as described in Section 4.2.

THF is a moderate Lewis base that has been reported to promote minimal removal of Cd-carboxylate ligands from CdSe surfaces,<sup>34</sup> and so the lower initial ligand populations for QDs purified in with this solvent where expected. Whereas <sup>1</sup>H NMR did reveal slight differences in ligand populations, commonly employed optical spectroscopies failed to indicate significant variances in the different QD surface chemistry. Typically, this would affirm that QD batches are analogous and could be used to continue investigations testing several variables, parameters and hypotheses. However, the extreme differences in the thermograms in Figures 4.16-18, particularly the sequential reaction endpoints should give pause to such assumptions. Table 4.3 contains the values obtained as we were able to apply the same effective two types of independent sites modeling procedure to solve the thermodynamic parameters for the differently purified RQ QDs as was employed for the Std QD batch.

**Table 4.3** Characteristic thermodynamic equilibrium parameters for OA exchange with ODPa on Rapid Quench QDs comparing Toluene GPC vs THF GPC purification solvent

EXCHANGE	$K_{\text{eff}}$ $\times 10^5 \text{ M}^{-1}$	$K_{\text{exch}}$ $\times 10^2$	$N_1$ per QD	$\Delta H_1$ kJ mol <sup>-1</sup>	$\Delta G_1$ kJ mol <sup>-1</sup>	$\Delta S_1$ J mol <sup>-1</sup> K <sup>-1</sup>	LIM $\Delta H_1$ kJ mol <sup>-1</sup>
Tol GPC	9.71	31.0	255	-6.72	-19.7	+44.0	-13.4
THF GPC	8.69	14.0	126	-6.08	-17.6	+38.9	-14.5
ASSOCIATION	$K_2$ $\times 10^3 \text{ M}^{-1}$	$*N_2 \times \Delta H_2$ $\times 10^3 \text{ kJ}$	$N_2$ per QD	$\Delta H_2$ kJ mol <sup>-1</sup>	$\Delta G_2$ kJ mol <sup>-1</sup>	$\Delta S_2$ J mol <sup>-1</sup> K <sup>-1</sup>	—
Tol GPC	3.74	-1.59	69.7	-22.8	-20.2	-8.90	—
THF GPC	2.04	-2.30	113	-20.4	-18.7	-6.00	—

Only *Limiting* regime thermodynamic parameter reported is  $\Delta H_1$ . All values are an average of two raw heat thermograms therefore no variances are included. \*Reported as product ( $N_2 \times \Delta H_2$ ) due to low  $\epsilon$  parameter value,<sup>46</sup> signifying  $N_2$  and  $\Delta H_2$  are not independently constrained.

The same issue of a low  $\epsilon$  parameter for the ODPa association Site2 was encountered, therefore again only the product  $N_2 \times \Delta H_2$  was well-constrained. Table 4.4 lists the Brandt's  $\epsilon$  parameter for each titration's thermodynamic profile, as in each case  $\epsilon < 10$  signifying  $N_2$  and  $\Delta H_2$  are not independently constrained.

**Table 4.4** Brandt's  $\epsilon$ -parameter for Site2 equilibrium thermodynamic parameters describing sequential neutral association of ODPa to exchanged CdSe|ODPa<sup>-</sup>

SAMPLE I.D.	Standard Tol GPC	Standard ~2x initial [QD]	Rapid Quench Tol GPC	Rapid Quench THF GPC
C – PARAMETER	3.512	2.531	3.261	2.723

Thereafter, the statistical significance in the exchange parameters was tested and is shown in Figure 4.19. If these specified parameters were found to be significantly different, then directly addressing consequent differences in related parameters becomes implicit. Two-tailed t-tests (appropriate for smaller sample size comparisons), with a null hypothesis that there was no difference between the tested parameters were employed against the equilibrium thermodynamic parameters solved for the Std QD sample. Values for  $N_{1,exch}$  and  $K_{1,exch}$  immediately appeared different, though only  $N_{1,exch}$  proved to have a statistically significant disparity between all three samples at a 95% confidence level. Previous reports have concluded similar zincblende CdSe QDs of different sizes or having undergone different degrees of purification to maintain comparable ligand densities.<sup>42,165</sup> However, given the minute changes in ligand density that result in drastically different QD photophysical properties and performance,<sup>13,34,81,167,168,197</sup> it remains imperative to carefully probe those QD ligand populations as precisely as possible.



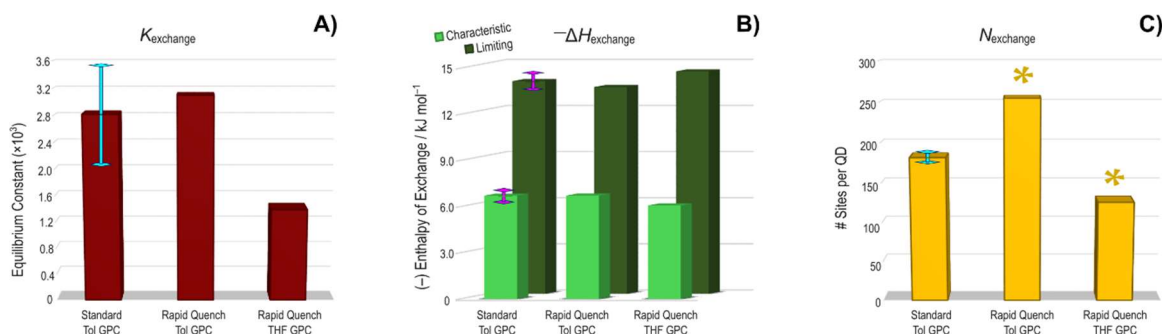


**Figure 4.19** Bar graphs comparing exchange reaction regime equilibrium thermodynamic parameters for standard and rapid quench CdSe|OA<sup>-</sup> samples prior to and ensuing either toluene or THF mobile phase GPC purification. The three thermodynamic parameters: equilibrium constant  $K$ , molar enthalpy  $H$  and number of sites  $N$  in the sequential exchange reaction regime are the primary values retrieved directly from the ITC fits. All other parameters are calculated from or subsequent to these, therefore the 2-tailed t-test statistical analysis applied to these parameters were sufficient to compare reaction systems. Statistically significant differences in parameter magnitudes were determined from the Std Quench toluene GPC titration, as indicated by the error bars. Only the  $N_{\text{exchange}}$  parameter was determined to be significantly different among the samples at a 95% confidence level, as marked with asterisks above those bars.

## 4.5 Conclusion

The capacity of ITC to provide consistent equilibrium thermodynamic parameters for a previously established and continuously investigated quantitative ligand exchange reaction, but for which the reaction quotient had until now proven unattainable, has been categorically demonstrated. The two effective independent [types of] sites: Site1 occupied by chemisorbed X-type exchanged ligands followed by Site2 referring to occupation of associated L-type phosphonic acid ligands, proved an adequate model for this system in both our characteristic and limiting regimes which attend to the distribution of binding enthalpies across inhomogeneous QD facets. While we did not explicitly determine the physical phenomenon contributing to the endothermic signal coupled within the X-type exchange stage of the reaction, we are able to isolate this heat contribution for further analysis. By separating heat contributions according to resolved time responses, we clearly showed the

transition toward the greater exothermic signal is due to the relatively slower process that occurs as the ligand exchange has nearly completed, which enabled us to extract the ligand exchange equilibrium constant. Likewise, the consistency in QD surface chemistry provided by GPC purification also allowed us to employ ITC to unequivocally differentiate between QD samples prepared with only slightly altered synthetic schemes. We hope that the NC community will very carefully consider the impact of various sample preparations and surface treatments on subsequent investigations, notwithstanding the sole parameter  $N$  (surface sites) displaying a statistically significant difference. Whereas our results with a nearly doubled QD concentration that yielded statistically similar thermodynamic parameters can offer some amount of confidence in comparable ligand population dynamics; empirical investigations such as this present study are sorely needed to further inform NC surface chemistry, and consequently comprehensive NC photophysical dynamics. Ultimately, this investigation further mitigates the paucity of consistent thermodynamic information obtained for NC surface dynamics in organic solvents. While equilibrium parameters from native organic surfactant environments have remained unknown or infeasible, the difficulty in obtaining consistent thermodynamic profiles have precluded rational design for NC frameworks as reliable and predictable building blocks for envisioned applications. Eventually we hope that ITC studies will be implemented to such an extent that investigators can have confidence to evaluate reactions that do not require overt spectroscopic signatures. As reactions such as the one presented herein (even with apparently complex reaction coordinates) are evaluated unambiguously, we further hope the ITC technique will quickly be applied to systems beyond the common II–VI and III–V semiconductor families. Inasmuch we expect the incorporation of ITC in NC surface chemistry and related reaction chemistries

to become pervasive in both fundamental studies as well as those with more direct materials and industrial implications.

#### 4.6 Materials & Methods

**Materials.** The following chemicals were used as received. Cadmium oxide (CdO; 99.999%) and Trioctylphosphine (TOP; 97%) were purchased from STREM Chemicals. Oleic Acid (OA; 99%), 1-Octadecene (ODE; 90% technical grade), and Selenium (Se; 99.999%) were purchased from Alfa Aesar. 1-Octadecylphosphonic Acid (ODPA; >99%) was purchased from PCI synthesis. Bio-Beads S-X1 GPC medium was obtained from Bio-Rad Laboratories. Toluene-d<sub>8</sub> (D, 99.5%) and THF-d<sub>8</sub> (D, 99.5%) were obtained from Cambridge Isotope Laboratories. Ferrocene (98%) was purchased from Acros. Toluene (99.5%) and Tetrahydrofuran (THF, 99%) were purchased from Mallinckrodt Chemicals. Acetone (99.9%) was purchased from VWR. Methanol (99.9%) was purchased from Fisher Scientific. Anhydrous THF was dried using the Puresolv system from Innovative Technologies. Synthetic and analytical procedures under inert conditions were carried out using Schlenk line techniques, or in a glovebox under N<sub>2</sub> atmosphere.

**Standard quench CdSe|OA<sup>-</sup> synthesis.** 60 mg CdO and 330 mg OA were introduced into a three-neck flask with 6 mL of ODE as the noncoordinating solvent. The flask was heated to 100°C, and vacuum was applied to remove air and water from the system. The flask was continuously heated to 270°C under N<sub>2</sub> environment to produce a colorless and clear mixture. Afterward, the reaction mixture was cooled to 130°C and vacuum was again applied to remove evolved water. The mixture was reheated to 270°C under N<sub>2</sub>, and 0.64 mL of TOPSe solution (prepared by dissolving Se in TOP in a glovebox,

with concentration 2.2 M) was rapidly injected. The reaction flask was allowed to cool down in ambient air to room temperature. The ratio of Cd:Se:OA was 1:3:2.5

**Rapid quench CdSe | OA<sup>-</sup> synthesis.** CdO and of OA were used to prepare the Cd precursor. CdO was again converted to the Cd(OA)<sub>2</sub> according to the same procedure as described above. The flask was reheated to 280 °C, 2.2 M TOPSe solution was rapidly injected. The reaction flask was immediately cooled down under a stream of air. The ratio of Cd:Se:OA was in this case also 1:3:2.5

**GPC purification of the QDs.** In order to remove most of the synthetic solvent and concentrate the QD sample in either toluene or THF, a single PR cycle with methanol and acetone to flocculate QDs was carried out before the GPC purifications. 1×PR QDs (concentration ranges from 5–150 µM with 0.5–1 mL injection volumes) were then added to the GPC column. After each purification, all QD samples were immediately diluted to the titration reaction concentration and injected into the ITC.

**Toluene GPC.** The GPC column was packed by the previously described method with toluene as the eluent. The as-synthesized QDs were purified by 1× precipitation with methanol and acetone and redispersed in toluene or anhydrous THF. Then the QD solution was added to the column and the sample was collected when the elution volume reached ~1/3 of the total volume of the column (the expected void volume for irregularly spaced spherical beads); this volume corresponds to the fraction at which the purified QDs eluted. The GPC column was rinsed thoroughly (3x the total volume of the column) before subsequent purifications.

**Anhydrous THF GPC.** The GPC column was packed similarly to a previously described method<sup>62</sup> with anhydrous THF as the eluent. A constant flow of N<sub>2(g)</sub> was

maintained over and through the THF GPC to prevent hygroscopic degradation of the column. The Bio-Rad SX-1 Bio-Beads were best swollen if introduced to the anhydrous solvent, applied to the Schlenk line for near complete removal of the solvent, and reswelling of the Bio-Beads without allowing contact to air. Again, the purified QD sample was collected when the elution volume reached  $\sim 1/3$  of the total volume of the column. The GPC column was rinsed thoroughly (4x the total volume of the column) before subsequent purifications.

**NMR analysis of QDs.** Routine NMR samples of the QDs were prepared in toluene- $d_8$ . The QDs' concentration is set at approximately 20  $\mu\text{M}$ ; the exact value in each case was measured by UV-Vis using the calculated molar extinction coefficient. Spectra were recorded on Bruker Avance III 400 MHz or Bruker Avance III HD 400 MHz. The quantitative  $^1\text{H}$  NMR spectra were measured with ferrocene as the internal standard and 30s relaxation delay, allowing the system to reach a reliable equilibrium. The  $^{31}\text{P}$  NMR spectra of QD samples were measured with 512 scans to improve signal-to-noise.

**Advanced NMR techniques.**  $T_1$  was measured by the vendor-supplied inversion recovery pulse sequence experiment.

**$^{31}\text{P}$   $\{^1\text{H}\}$  NMR for quantitative titration.** Spectra were recorded on a Bruker Avance III HD 400 MHz equipped with a nitrogen-based cryogenic probe (Prodigy) with NOE suppression routines applied.

**Isothermal Titration Calorimetry (ITC):** ITC titrations were performed on a VP-ITC calorimeter (Microcal Inc., Northampton, MA). Ligand solutions were titrated from the 300 $\mu\text{L}$  syringe to the sample cell overfilled to its 1.8mL capacity, and the heat response to maintain a constant temperature between the sample cell and reference was monitored. Each experiment was conducted at 22°C and midrange reference power; allowed to equilibrate

prior to an initial 600sec delay; and in order to allow adequate equilibration between each injection, 8-9min intervals were set between each injection for a total 60 injections in 5 $\mu$ L increments. Anhydrous THF was used as the solvent for both the ligands and QDs, as well as the blank solvent in the reference cell. Reference titrations were conducted with the same parameters relevant to the titration reaction to determine any significant heat of dilution between the solvent, ligand solution and QD solutions that may have accounted for signal in the final ligand-QD titrations. Only ligand-solvent titrations were subtracted from ligand-QD titrations, as other reference titrations were determined negligible. The QD solutions were loaded into the sample cell such that the final ligand-to-QD ratio was  $\sim$ 450:1.

## REFERENCES

- (1) Boles, M. A.; Ling, D.; Hyeon, T.; Talapin, D. V. The Surface Science of Nanocrystals. *Nat Mater* **2016**, *15* (2), 141–153. <https://doi.org/10.1038/nmat4526>.
- (2) Owen, J. The Coordination Chemistry of Nanocrystal Surfaces. *Science* **2015**, *347* (6222), 615–616. <https://doi.org/10.1126/science.1259924>.
- (3) Peterson, M. D.; Cass, L. C.; Harris, R. D.; Edme, K.; Sung, K.; Weiss, E. A. The Role of Ligands in Determining the Exciton Relaxation Dynamics in Semiconductor Quantum Dots. *Annual Review of Physical Chemistry* **2014**, *65* (1), 317–339. <https://doi.org/10.1146/annurev-physchem-040513-103649>.
- (4) Wu, X.; Liu, H.; Liu, J.; Haley, K. N.; Treadway, J. A.; Larson, J. P.; Ge, N.; Peale, F.; Bruchez, M. P. Immunofluorescent Labeling of Cancer Marker Her2 and Other Cellular Targets with Semiconductor Quantum Dots. *Nat Biotech* **2003**, *21* (1), 41–46. <https://doi.org/10.1038/nbt764>.
- (5) Morris-Cohen, A. J.; Malicki, M.; Peterson, M. D.; Slavin, J. W. J.; Weiss, E. A. Chemical, Structural, and Quantitative Analysis of the Ligand Shells of Colloidal Quantum Dots. *Chem. Mater.* **2013**, *25* (8), 1155–1165. <https://doi.org/10.1021/cm302108j>.
- (6) Palui, G.; Avellini, T.; Zhan, N.; Pan, F.; Gray, D.; Alabugin, I.; Mattoussi, H. Photoinduced Phase Transfer of Luminescent Quantum Dots to Polar and Aqueous

- Media. *J. Am. Chem. Soc.* **2012**, *134* (39), 16370–16378.  
<https://doi.org/10.1021/ja306621n>.
- (7) Landry, M. L.; Morrell, T. E.; Karagounis, T. K.; Hsia, C.-H.; Wang, C.-Y. Simple Syntheses of CdSe Quantum Dots. *J. Chem. Educ.* **2014**, *91* (2), 274–279.  
<https://doi.org/10.1021/ed300568e>.
- (8) Leatherdale, C. A.; Woo, W.-K.; Mikulec, F. V.; Bawendi, M. G. On the Absorption Cross Section of CdSe Nanocrystal Quantum Dots. *J. Phys. Chem. B* **2002**, *106* (31), 7619–7622. <https://doi.org/10.1021/jp025698c>.
- (9) Hoy, J.; Morrison, P. J.; Steinberg, L. K.; Buhro, W. E.; Loomis, R. A. Excitation Energy Dependence of the Photoluminescence Quantum Yields of Core and Core/Shell Quantum Dots. *J. Phys. Chem. Lett.* **2013**, *4* (12), 2053–2060.  
<https://doi.org/10.1021/jz4004735>.
- (10) Hines, D. A.; Kamat, P. V. Recent Advances in Quantum Dot Surface Chemistry. *ACS Appl. Mater. Interfaces* **2014**, *6* (5), 3041–3057.  
<https://doi.org/10.1021/am405196u>.
- (11) Panfil, Y. E.; Oded, M.; Banin, U. Colloidal Quantum Nanostructures: Emerging Materials for Display Applications. *Angewandte Chemie International Edition* **2018**, *57* (16), 4274–4295. <https://doi.org/10.1002/anie.201708510>.
- (12) Lim, S. J.; Ma, L.; Schleife, A.; Smith, A. M. Quantum Dot Surface Engineering: Toward Inert Fluorophores with Compact Size and Bright, Stable Emission. *Coordination Chemistry Reviews* **2016**, *320–321*, 216–237.  
<https://doi.org/10.1016/j.ccr.2016.03.012>.



- (13) Houtepen, A. J.; Hens, Z.; Owen, J. S.; Infante, I. On the Origin of Surface Traps in Colloidal II–VI Semiconductor Nanocrystals. *Chem. Mater.* **2017**, *29* (2), 752–761. <https://doi.org/10.1021/acs.chemmater.6b04648>.
- (14) Krause, M. M.; Jethi, L.; Mack, T. G.; Kambhampati, P. Ligand Surface Chemistry Dictates Light Emission from Nanocrystals. *J. Phys. Chem. Lett.* **2015**, *6* (21), 4292–4296. <https://doi.org/10.1021/acs.jpcllett.5b02015>.
- (15) Lokteva, I.; Radychev, N.; Witt, F.; Borchert, H.; Parisi, J.; Kolny-Olesiak, J. Surface Treatment of CdSe Nanoparticles for Application in Hybrid Solar Cells: The Effect of Multiple Ligand Exchange with Pyridine. *J. Phys. Chem. C* **2010**, *114* (29), 12784–12791. <https://doi.org/10.1021/jp103300v>.
- (16) Peng, X.; Wickham, J.; Alivisatos, A. P. Kinetics of II-VI and III-V Colloidal Semiconductor Nanocrystal Growth: “Focusing” of Size Distributions. *J. Am. Chem. Soc.* **1998**, *120* (21), 5343–5344. <https://doi.org/10.1021/ja9805425>.
- (17) Chen, O.; Chen, X.; Yang, Y.; Lynch, J.; Wu, H.; Zhuang, J.; Cao, Y. C. Synthesis of Metal–Selenide Nanocrystals Using Selenium Dioxide as the Selenium Precursor. *Angewandte Chemie International Edition* **2008**, *47* (45), 8638–8641. <https://doi.org/10.1002/anie.200804266>.
- (18) Flamee, S.; Cirillo, M.; Abe, S.; De Nolf, K.; Gomes, R.; Aubert, T.; Hens, Z. Fast, High Yield, and High Solid Loading Synthesis of Metal Selenide Nanocrystals. *Chem. Mater.* **2013**, *25* (12), 2476–2483. <https://doi.org/10.1021/cm400799e>.
- (19) Hines, D. A.; Becker, M. A.; Kamat, P. V. Photoinduced Surface Oxidation and Its Effect on the Exciton Dynamics of CdSe Quantum Dots. *J. Phys. Chem. C* **2012**, *116* (24), 13452–13457. <https://doi.org/10.1021/jp303659g>.

- (20) Schapotschnikow, P.; Hommersom, B.; Vlugt, T. J. H. Adsorption and Binding of Ligands to CdSe Nanocrystals. *J. Phys. Chem. C* **2009**, *113* (29), 12690–12698. <https://doi.org/10.1021/jp903291d>.
- (21) Kilina, S.; Ivanov, S.; Tretiak, S. Effect of Surface Ligands on Optical and Electronic Spectra of Semiconductor Nanoclusters. *J. Am. Chem. Soc.* **2009**, *131* (22), 7717–7726. <https://doi.org/10.1021/ja9005749>.
- (22) Liu, H. Tuning the Binding Energy of Surfactant to CdSe Nanocrystal: A Theoretical Study. *J. Phys. Chem. C* **2009**, *113* (8), 3116–3119. <https://doi.org/10.1021/jp808246g>.
- (23) Knowles, K. E.; Peterson, M. D.; McPhail, M. R.; Weiss, E. A. Exciton Dissociation within Quantum Dot–Organic Complexes: Mechanisms, Use as a Probe of Interfacial Structure, and Applications. *J. Phys. Chem. C* **2013**, *117* (20), 10229–10243. <https://doi.org/10.1021/jp400699h>.
- (24) Frederick, M. T.; Weiss, E. A. Relaxation of Exciton Confinement in CdSe Quantum Dots by Modification with a Conjugated Dithiocarbamate Ligand. *ACS Nano* **2010**, *4* (6), 3195–3200. <https://doi.org/10.1021/nn1007435>.
- (25) Buckley, J. J.; Couderc, E.; Greaney, M. J.; Munteanu, J.; Riche, C. T.; Bradforth, S. E.; Brutchey, R. L. Chalcogenol Ligand Toolbox for CdSe Nanocrystals and Their Influence on Exciton Relaxation Pathways. *ACS Nano* **2014**, *8* (3), 2512–2521. <https://doi.org/10.1021/nn406109v>.
- (26) Kuposov, A. Y.; Szymanski, P.; Cardolaccia, T.; Meyer, T. J.; Klimov, V. I.; Sykora, M. Electronic Properties and Structure of Assemblies of CdSe Nanocrystal Quantum Dots and Ru-Polypyridine Complexes Probed by Steady State and Time-

- Resolved Photoluminescence. *Advanced Functional Materials* **2011**, *21* (16), 3159–3168. <https://doi.org/10.1002/adfm.201100415>.
- (27) Fafarman, A. T.; Koh, W.; Diroll, B. T.; Kim, D. K.; Ko, D.-K.; Oh, S. J.; Ye, X.; Doan-Nguyen, V.; Crump, M. R.; Reifsnyder, D. C.; et al. Thiocyanate-Capped Nanocrystal Colloids: Vibrational Reporter of Surface Chemistry and Solution-Based Route to Enhanced Coupling in Nanocrystal Solids. *J. Am. Chem. Soc.* **2011**, *133* (39), 15753–15761. <https://doi.org/10.1021/ja206303g>.
- (28) Nag, A.; Chung, D. S.; Dolzhenkov, D. S.; Dimitrijevic, N. M.; Chattopadhyay, S.; Shibata, T.; Talapin, D. V. Effect of Metal Ions on Photoluminescence, Charge Transport, Magnetic and Catalytic Properties of All-Inorganic Colloidal Nanocrystals and Nanocrystal Solids. *J. Am. Chem. Soc.* **2012**, *134* (33), 13604–13615. <https://doi.org/10.1021/ja301285x>.
- (29) Bernt, C. M.; Burks, P. T.; DeMartino, A. W.; Pierri, A. E.; Levy, E. S.; Zigler, D. F.; Ford, P. C. Photocatalytic Carbon Disulfide Production via Charge Transfer Quenching of Quantum Dots. *J. Am. Chem. Soc.* **2014**, *136* (6), 2192–2195. <https://doi.org/10.1021/ja4083599>.
- (30) Hodes, G. Comparison of Dye- and Semiconductor-Sensitized Porous Nanocrystalline Liquid Junction Solar Cells. *J. Phys. Chem. C* **2008**, *112* (46), 17778–17787. <https://doi.org/10.1021/jp803310s>.
- (31) Liu, W.; Greytak, A. B.; Lee, J.; Wong, C. R.; Park, J.; Marshall, L. F.; Jiang, W.; Curtin, P. N.; Ting, A. Y.; Nocera, D. G.; et al. Compact Biocompatible Quantum Dots via RAFT-Mediated Synthesis of Imidazole-Based Random Copolymer

- Ligand. *J. Am. Chem. Soc.* **2010**, *132* (2), 472–483.  
<https://doi.org/10.1021/ja908137d>.
- (32) Zhao, X.; Shen, Y.; Adogla, E. A.; Viswanath, A.; Tan, R.; Benicewicz, B. C.; Greytak, A. B.; Lin, Y.; Wang, Q. Surface Labeling of Enveloped Virus with Polymeric Imidazole Ligand-Capped Quantum Dots via the Metabolic Incorporation of Phospholipids into Host Cells. *J. Mat. Chem. B* **2016**, *4* (14), 2421–2427. <https://doi.org/10.1039/c6tb00263c>.
- (33) Kuno, M. Band Edge Spectroscopy of CdSe Quantum Dots. PhD Thesis, MIT, 1998.
- (34) Anderson, N. C.; Hendricks, M. P.; Choi, J. J.; Owen, J. S. Ligand Exchange and the Stoichiometry of Metal Chalcogenide Nanocrystals: Spectroscopic Observation of Facile Metal-Carboxylate Displacement and Binding. *J. Am. Chem. Soc.* **2013**, *135* (49), 18536–18548. <https://doi.org/10.1021/ja4086758>.
- (35) Donakowski, M. D.; Godbe, J. M.; Sknepnek, R.; Knowles, K. E.; Olvera de la Cruz, M.; Weiss, E. A. A Quantitative Description of the Binding Equilibria of Para-Substituted Aniline Ligands and CdSe Quantum Dots. *J. Phys. Chem. C* **2010**, *114* (51), 22526–22534. <https://doi.org/10.1021/jp109381r>.
- (36) De Roo, J.; De Keukeleere, K.; Hens, Z.; Van Driessche, I. From Ligands to Binding Motifs and beyond; the Enhanced Versatility of Nanocrystal Surfaces. *Dalton Trans.* **2016**, *45* (34), 13277–13283. <https://doi.org/10.1039/C6DT02410F>.
- (37) Puzder, A.; Williamson, A. J.; Zaitseva, N.; Galli, G.; Manna, L.; Alivisatos, A. P. The Effect of Organic Ligand Binding on the Growth of CdSe Nanoparticles

- Probed by Ab Initio Calculations. *Nano Lett.* **2004**, *4* (12), 2361–2365.  
<https://doi.org/10.1021/nl0485861>.
- (38) Sapra, S.; Poppe, J.; Eychmüller, A. CdSe Nanorod Synthesis: A New Approach. *Small* **2007**, *3* (11), 1886–1888. <https://doi.org/10.1002/sml.200700297>.
- (39) Pu, C.; Peng, X. To Battle Surface Traps on CdSe/CdS Core/Shell Nanocrystals: Shell Isolation versus Surface Treatment. *J. Am. Chem. Soc.* **2016**, *138* (26), 8134–8142. <https://doi.org/10.1021/jacs.6b02909>.
- (40) Gao, Y.; Peng, X. Crystal Structure Control of CdSe Nanocrystals in Growth and Nucleation: Dominating Effects of Surface versus Interior Structure. *J. Am. Chem. Soc.* **2014**, *136* (18), 6724–6732. <https://doi.org/10.1021/ja5020025>.
- (41) Hens, Z.; Martins, J. C. A Solution NMR Toolbox for Characterizing the Surface Chemistry of Colloidal Nanocrystals. *Chem. Mater.* **2013**, *25* (8), 1211–1221. <https://doi.org/10.1021/cm303361s>.
- (42) Nepomnyashchii, A. B.; Harris, R. D.; Weiss, E. A. Composition and Permeability of Oleate Adlayers of CdS Quantum Dots upon Dilution to Photoluminescence-Relevant Concentrations. *Anal. Chem.* **2016**, *88* (6), 3310–3316. <https://doi.org/10.1021/acs.analchem.5b04786>.
- (43) De Roo, J.; Yazdani, N.; Drijvers, E.; Lauria, A.; Maes, J.; Owen, J. S.; Van Driessche, I.; Niederberger, M.; Wood, V.; Martins, J. C.; et al. Probing Solvent–Ligand Interactions in Colloidal Nanocrystals by the NMR Line Broadening. *Chem. Mater.* **2018**, *30* (15), 5485–5492. <https://doi.org/10.1021/acs.chemmater.8b02523>.

- (44) Friebolin, H.; Beconsall, J. K. *Basic One- and Two-Dimensional NMR Spectroscopy: Fourth, Completely Revised and Updated Edition*; WILEY-VCH Verlag GmbH & Co. KGaA, Weinheim.: Heidelberg, Germany, 2005.
- (45) Malicki, M.; Knowles, K. E.; Weiss, E. A. Gating of Hole Transfer from Photoexcited PbS Quantum Dots to Aminoferrocene by the Ligand Shell of the Dots. *Chem. Commun. (Camb.)* **2013**, 49 (39), 4400–4402. <https://doi.org/10.1039/c2cc32895j>.
- (46) Freyer, M. W.; Lewis, E. A. Isothermal Titration Calorimetry: Experimental Design, Data Analysis, and Probing Macromolecule/Ligand Binding and Kinetic Interactions. *Methods Cell Biol.* **2008**, 84, 79–113. [https://doi.org/10.1016/S0091-679X\(07\)84004-0](https://doi.org/10.1016/S0091-679X(07)84004-0).
- (47) Grolier, J.-P. E.; del Río, J. M. Isothermal Titration Calorimetry: A Thermodynamic Interpretation of Measurements. *The Journal of Chemical Thermodynamics* **2012**, 55, 193–202. <https://doi.org/10.1016/j.jct.2012.05.018>.
- (48) Chakraborty, P.; Jin, Y.; Barrows, C. J.; Dunham, S. T.; Gamelin, D. R. Kinetics of Isovalent ( $\text{Cd}^{2+}$ ) and Aliovalent ( $\text{In}^{3+}$ ) Cation Exchange in  $\text{Cd}_1\text{-XMnxSe}$  Nanocrystals. *J. Am. Chem. Soc.* **2016**, 138 (39), 12885–12893. <https://doi.org/10.1021/jacs.6b05949>.
- (49) Xiao, Q.; Huang, S.; Su, W.; Li, P.; Ma, J.; Luo, F.; Chen, J.; Liu, Y. Systematically Investigations of Conformation and Thermodynamics of HSA Adsorbed to Different Sizes of CdTe Quantum Dots. *Colloids and Surfaces B: Biointerfaces* **2013**, 102, 76–82. <https://doi.org/10.1016/j.colsurfb.2012.08.028>.

- (50) Williams, E. S.; Major, K. J.; Tobias, A.; Woodall, D.; Morales, V.; Lippincott, C.; Moyer, P. J.; Jones, M. Characterizing the Influence of TOPO on Exciton Recombination Dynamics in Colloidal CdSe Quantum Dots. *J. Phys. Chem. C* **2013**, *117* (8), 4227–4237. <https://doi.org/10.1021/jp309896e>.
- (51) Jharimune, S.; Sathe, A. A.; Rioux, R. M. Thermochemical Measurements of Cation Exchange in CdSe Nanocrystals Using Isothermal Titration Calorimetry. *Nano Lett.* **2018**, *18* (11), 6795–6803. <https://doi.org/10.1021/acs.nanolett.8b02661>.
- (52) Grossoehme, N.; Spuches, A.; Wilcox, D. Application of Isothermal Titration Calorimetry in Bioinorganic Chemistry. *Journal of Biological Inorganic Chemistry* **2010**, *15* (8), 1183–1191. <https://doi.org/10.1007/s00775-010-0693-3>.
- (53) Mondal, S.; Ghosh, S.; Ghosh, D.; Saha, A. Physico-Chemical Aspects of Quantum Dot–Vasodialator Interaction: Implications in Nanodiagnostics. *J. Phys. Chem. C* **2012**, *116* (17), 9774–9782. <https://doi.org/10.1021/jp210528n>.
- (54) Anderson, N. C.; Owen, J. S. Soluble, Chloride-Terminated CdSe Nanocrystals: Ligand Exchange Monitored by <sup>1</sup>H and <sup>31</sup>P NMR Spectroscopy. *Chem. Mater.* **2013**, *25* (1), 69–76. <https://doi.org/10.1021/cm303219a>.
- (55) Freire, E.; Schön, A.; Velazquez-Campoy, A. Chapter 5 Isothermal Titration Calorimetry: General Formalism Using Binding Polynomials; Enzymology, B.-M. in, Ed.; Biothermodynamics, Part A; Academic Press, 2009; Vol. 455, pp 127–155.
- (56) Pethica, B. A. Misuse of Thermodynamics in the Interpretation of Isothermal Titration Calorimetry Data for Ligand Binding to Proteins. *Anal. Biochem.* **2015**, *472*, 21–29. <https://doi.org/10.1016/j.ab.2014.11.010>.

- (57) Brautigam, C. A. Fitting Two- and Three-Site Binding Models to Isothermal Titration Calorimetric Data. *Methods* **2015**, *76*, 124–136. <https://doi.org/10.1016/j.ymeth.2014.11.018>.
- (58) Frederick, M. T.; Achtyl, J. L.; Knowles, K. E.; Weiss, E. A.; Geiger, F. M. Surface-Amplified Ligand Disorder in CdSe Quantum Dots Determined by Electron and Coherent Vibrational Spectroscopies. *J. Am. Chem. Soc.* **2011**, *133* (19), 7476–7481. <https://doi.org/10.1021/ja200466z>.
- (59) Yang, Y.; Qin, H.; Jiang, M.; Lin, L.; Fu, T.; Dai, X.; Zhang, Z.; Niu, Y.; Cao, H.; Jin, Y.; et al. Entropic Ligands for Nanocrystals: From Unexpected Solution Properties to Outstanding Processability. *Nano Lett.* **2016**, *16* (4), 2133–2138. <https://doi.org/10.1021/acs.nanolett.6b00730>.
- (60) Shen, Y.; Tan, R.; Gee, M. Y.; Greytak, A. B. Quantum Yield Regeneration: Influence of Neutral Ligand Binding on Photophysical Properties in Colloidal Core/Shell Quantum Dots. *ACS Nano* **2015**, *9* (3), 3345–3359. <https://doi.org/10.1021/acsnano.5b00671>.
- (61) Bullen, C.; Mulvaney, P. The Effects of Chemisorption on the Luminescence of CdSe Quantum Dots. *Langmuir* **2006**, *22* (7), 3007–3013. <https://doi.org/10.1021/la051898e>.
- (62) Shen, Y.; Gee, M. Y.; Tan, R.; Pellechia, P. J.; Greytak, A. B. Purification of Quantum Dots by Gel Permeation Chromatography and the Effect of Excess Ligands on Shell Growth and Ligand Exchange. *Chem. Mater.* **2013**, *25* (14), 2838–2848. <https://doi.org/10.1021/cm4012734>.



- (63) Gomes, R.; Hassinen, A.; Szczygiel, A.; Zhao, Q.; Vantomme, A.; Martins, J. C.; Hens, Z. Binding of Phosphonic Acids to CdSe Quantum Dots: A Solution NMR Study. *J. Phys. Chem. Lett.* **2011**, *2* (3), 145–152. <https://doi.org/10.1021/jz1016729>.
- (64) Knauf, R. R.; Lennox, J. C.; Dempsey, J. L. Quantifying Ligand Exchange Reactions at CdSe Nanocrystal Surfaces. *Chem. Mater.* **2016**, *28* (13), 4762–4770. <https://doi.org/10.1021/acs.chemmater.6b01827>.
- (65) Reiss, P.; Carrière, M.; Lincheneau, C.; Vaure, L.; Tamang, S. Synthesis of Semiconductor Nanocrystals, Focusing on Nontoxic and Earth-Abundant Materials. *Chem. Rev.* **2016**, *116* (18), 10731–10819. <https://doi.org/10.1021/acs.chemrev.6b00116>.
- (66) Chan, E. M. Combinatorial Approaches for Developing Upconverting Nanomaterials: High-Throughput Screening, Modeling, and Applications. *Chem. Soc. Rev.* **2015**, *44* (6), 1653–1679. <https://doi.org/10.1039/C4CS00205A>.
- (67) Talapin, D. V.; Lee, J.-S.; Kovalenko, M. V.; Shevchenko, E. V. Prospects of Colloidal Nanocrystals for Electronic and Optoelectronic Applications. *Chemical Reviews* **2010**, *110* (1), 389–458. <https://doi.org/10.1021/cr900137k>.
- (68) Chen, G.; Roy, I.; Yang, C.; Prasad, P. N. Nanochemistry and Nanomedicine for Nanoparticle-Based Diagnostics and Therapy. *Chem. Rev.* **2016**, *116* (5), 2826–2885. <https://doi.org/10.1021/acs.chemrev.5b00148>.
- (69) Wang, W.; Kapur, A.; Ji, X.; Zeng, B.; Mishra, D.; Mattoussi, H. Multifunctional and High Affinity Polymer Ligand That Provides Bio-Orthogonal Coating of

- Quantum Dots. *Bioconjugate Chem.* **2016**, *27* (9), 2024–2036.  
<https://doi.org/10.1021/acs.bioconjchem.6b00309>.
- (70) Weidman, M. C.; Beck, M. E.; Hoffman, R. S.; Prins, F.; Tisdale, W. A. Monodisperse, Air-Stable PbS Nanocrystals via Precursor Stoichiometry Control. *ACS Nano* **2014**, *8* (6), 6363–6371. <https://doi.org/10.1021/nn5018654>.
- (71) Azubel, M.; Kornberg, R. D. Synthesis of Water-Soluble, Thiolate-Protected Gold Nanoparticles, Uniform in Size. *Nano Lett.* **2016**, *16* (5), 3348–3351.  
<https://doi.org/10.1021/acs.nanolett.6b00981>.
- (72) Tan, R.; Shen, Y.; Roberts, S. K.; Gee, M. Y.; Blom, D. A.; Greytak, A. B. Reducing Competition by Coordinating Solvent Promotes Morphological Control in Alternating Layer Growth of CdSe/CdS Core/Shell Quantum Dots. *Chem. Mater.* **2015**, *27* (21), 7468–7480. <https://doi.org/10.1021/acs.chemmater.5b03588>.
- (73) Hassinen, A.; Moreels, I.; de Mello Donegá, C.; Martins, J. C.; Hens, Z. Nuclear Magnetic Resonance Spectroscopy Demonstrating Dynamic Stabilization of CdSe Quantum Dots by Alkylamines. *J. Phys. Chem. Lett.* **2010**, *1* (17), 2577–2581.  
<https://doi.org/10.1021/jz100781h>.
- (74) Shakeri, B.; Meulenberg, R. W. A Closer Look into the Traditional Purification Process of CdSe Semiconductor Quantum Dots. *Langmuir* **2015**, *31* (49), 13433–13440. <https://doi.org/10.1021/acs.langmuir.5b03584>.
- (75) Kowalczyk, B.; Lagzi, I.; Grzybowski, B. A. Nanoseparations: Strategies for Size and/or Shape-Selective Purification of Nanoparticles. *Current Opinion in Colloid & Interface Science* **2011**, *16* (2), 135–148.  
<https://doi.org/10.1016/j.cocis.2011.01.004>.

- (76) Beveridge, J. S.; Buck, M. R.; Bondi, J. F.; Misra, R.; Schiffer, P.; Schaak, R. E.; Williams, M. E. Purification and Magnetic Interrogation of Hybrid Au-Fe<sub>3</sub>O<sub>4</sub> and FePt-Fe<sub>3</sub>O<sub>4</sub> Nanoparticles. *Angew. Chem. Int. Ed.* **2011**, *50* (42), 9875–9879. <https://doi.org/10.1002/anie.201104829>.
- (77) Munro, A. M.; Jen-La Plante, I.; Ng, M. S.; Ginger, D. S. Quantitative Study of the Effects of Surface Ligand Concentration on CdSe Nanocrystal Photoluminescence. *J. Phys. Chem. C* **2007**, *111* (17), 6220–6227. <https://doi.org/10.1021/jp068733e>.
- (78) Kalyuzhny, G.; Murray, R. W. Ligand Effects on Optical Properties of CdSe Nanocrystals. *J. Phys. Chem. B* **2005**, *109* (15), 7012–7021. <https://doi.org/10.1021/jp045352x>.
- (79) Carroll, G. M.; Brozek, C. K.; Hartstein, K. H.; Tsui, E. Y.; Gamelin, D. R. Potentiometric Measurements of Semiconductor Nanocrystal Redox Potentials. *J. Am. Chem. Soc.* **2016**, *138* (13), 4310–4313. <https://doi.org/10.1021/jacs.6b00936>.
- (80) Kern, S. J.; Sahu, K.; Berg, M. A. Heterogeneity of the Electron-Trapping Kinetics in CdSe Nanoparticles. *Nano Lett.* **2011**, *11* (8), 3493–3498. <https://doi.org/10.1021/nl202086b>.
- (81) Li, X.; Nichols, V. M.; Zhou, D.; Lim, C.; Pau, G. S. H.; Bardeen, C. J.; Tang, M. L. Observation of Multiple, Identical Binding Sites in the Exchange of Carboxylic Acid Ligands with CdS Nanocrystals. *Nano Lett.* **2014**, *14* (6), 3382–3387. <https://doi.org/10.1021/nl500885t>.
- (82) Widmer-Cooper, A.; Geissler, P. L. Ligand-Mediated Interactions between Nanoscale Surfaces Depend Sensitively and Nonlinearly on Temperature, Facet

- Dimensions, and Ligand Coverage. *ACS Nano* **2016**, *10* (2), 1877–1887.  
<https://doi.org/10.1021/acsnano.5b05569>.
- (83) Stein, J. L.; Mader, E. A.; Cossairt, B. M. Luminescent InP Quantum Dots with Tunable Emission by Post-Synthetic Modification with Lewis Acids. *J. Phys. Chem. Lett.* **2016**, *7* (7), 1315–1320. <https://doi.org/10.1021/acs.jpcllett.6b00177>.
- (84) Akdas, T.; Distaso, M.; Kuhri, S.; Winter, B.; Birajdar, B.; Spiecker, E.; Guldi, D. M.; Peukert, W. The Effects of Post-Processing on the Surface and the Optical Properties of Copper Indium Sulfide Quantum Dots. *Journal of Colloid and Interface Science* **2015**, *445*, 337–347. <https://doi.org/10.1016/j.jcis.2015.01.014>.
- (85) Akdas, T.; Walter, J.; Segets, D.; Distaso, M.; Winter, B.; Birajdar, B.; Spiecker, E.; Peukert, W. Investigation of the Size–Property Relationship in CuInS<sub>2</sub> Quantum Dots. *Nanoscale* **2015**, *7* (43), 18105–18118.  
<https://doi.org/10.1039/C5NR04291G>.
- (86) Kortan, A. R.; Hull, R.; Opila, R. L.; Bawendi, M. G.; Steigerwald, M. L.; Carroll, P. J.; Brus, L. E. Nucleation and Growth of Cadmium Selenide on Zinc Sulfide Quantum Crystallite Seeds, and Vice Versa, in Inverse Micelle Media. *Journal of the American Chemical Society* **1990**, *112* (4), 1327–1332.  
<https://doi.org/10.1021/ja00160a005>.
- (87) Murray, C. B.; Norris, D. J.; Bawendi, M. G. Synthesis and Characterization of Nearly Monodisperse CdE (E = S, Se, Te) Semiconductor Nanocrystallites. *Journal of the American Chemical Society* **1993**, *115* (19), 8706–8715.
- (88) Vossmeier, T.; Katsikas, L.; Giersig, M.; Popovic, I. G.; Diesner, K.; Chemseddine, A.; Eychmueller, A.; Weller, H. CdS Nanoclusters: Synthesis,

- Characterization, Size Dependent Oscillator Strength, Temperature Shift of the Excitonic Transition Energy, and Reversible Absorbance Shift. *J. Phys. Chem.* **1994**, *98* (31), 7665–7673. <https://doi.org/10.1021/j100082a044>.
- (89) Gaponik, N.; Talapin, D. V.; Rogach, A. L.; Hoppe, K.; Shevchenko, E. V.; Kornowski, A.; Eychmüller, A.; Weller, H. Thiol-Capping of CdTe Nanocrystals: An Alternative to Organometallic Synthetic Routes. *J. Phys. Chem. B* **2002**, *106* (29), 7177–7185. <https://doi.org/10.1021/jp025541k>.
- (90) Yu, P.; Beard, M. C.; Ellingson, R. J.; Ferrere, S.; Curtis, C.; Drexler, J.; Luiszer, F.; Nozik, A. J. Absorption Cross-Section and Related Optical Properties of Colloidal InAs Quantum Dots. *J. Phys. Chem. B* **2005**, *109* (15), 7084–7087. <https://doi.org/10.1021/jp046127i>.
- (91) Virieux, H.; Le Troedec, M.; Cros-Gagneux, A.; Ojo, W.-S.; Delpech, F.; Nayral, C.; Martinez, H.; Chaudret, B. InP/ZnS Nanocrystals: Coupling NMR and XPS for Fine Surface and Interface Description. *J. Am. Chem. Soc.* **2012**, *134* (48), 19701–19708. <https://doi.org/10.1021/ja307124m>.
- (92) Cros-Gagneux, A.; Delpech, F.; Nayral, C.; Cornejo, A.; Coppel, Y.; Chaudret, B. Surface Chemistry of InP Quantum Dots: A Comprehensive Study. *J. Am. Chem. Soc.* **2010**, *132* (51), 18147–18157. <https://doi.org/10.1021/ja104673y>.
- (93) Morris-Cohen, A. J.; Donakowski, M. D.; Knowles, K. E.; Weiss, E. A. The Effect of a Common Purification Procedure on the Chemical Composition of the Surfaces of CdSe Quantum Dots Synthesized with Trioctylphosphine Oxide. *J. Phys. Chem. C* **2010**, *114* (2), 897–906. <https://doi.org/10.1021/jp909492w>.

- (94) Morris-Cohen, A. J.; Frederick, M. T.; Lilly, G. D.; McArthur, E. A.; Weiss, E. A. Organic Surfactant-Controlled Composition of the Surfaces of CdSe Quantum Dots. *J. Phys. Chem. Lett.* **2010**, *1* (7), 1078–1081. <https://doi.org/10.1021/jz100224q>.
- (95) Peng, X.; Wilson, T. E.; Alivisatos, A. P.; Schultz, P. G. Synthesis and Isolation of a Homodimer of Cadmium Selenide Nanocrystals. *Angew. Chem. Int. Ed. Engl.* **1997**, *36* (1–2), 145–147. <https://doi.org/10.1002/anie.199701451>.
- (96) Ding, T. X.; Olshansky, J. H.; Leone, S. R.; Alivisatos, A. P. Efficiency of Hole Transfer from Photoexcited Quantum Dots to Covalently Linked Molecular Species. *J. Am. Chem. Soc.* **2015**, *137* (5), 2021–2029. <https://doi.org/10.1021/ja512278a>.
- (97) Cass, L. C.; Malicki, M.; Weiss, E. A. The Chemical Environments of Oleate Species within Samples of Oleate-Coated PbS Quantum Dots. *Anal. Chem.* **2013**, *85* (14), 6974–6979. <https://doi.org/10.1021/ac401623a>.
- (98) Smith, A. M.; Mohs, A. M.; Nie, S. Tuning the Optical and Electronic Properties of Colloidal Nanocrystals by Lattice Strain. *Nat Nano* **2009**, *4* (1), 56–63. <https://doi.org/10.1038/nnano.2008.360>.
- (99) Yu, W. W.; Qu, L.; Guo, W.; Peng, X. Experimental Determination of the Extinction Coefficient of CdTe, CdSe, and CdS Nanocrystals. *Chem. Mater.* **2003**, *15* (14), 2854–2860. <https://doi.org/10.1021/cm034081k>.
- (100) Yu, W. W.; Peng, X. Formation of High-Quality CdS and Other II–VI Semiconductor Nanocrystals in Noncoordinating Solvents: Tunable Reactivity of Monomers. *Angewandte Chemie International Edition* **2002**, *41* (13), 2368–2371.

[https://doi.org/10.1002/1521-3773\(20020703\)41:13<2368::AID-ANIE2368>3.0.CO;2-G](https://doi.org/10.1002/1521-3773(20020703)41:13<2368::AID-ANIE2368>3.0.CO;2-G).

- (101) Yang, Y.; Li, J.; Lin, L.; Peng, X. An Efficient and Surface-Benign Purification Scheme for Colloidal Nanocrystals Based on Quantitative Assessment. *Nano Res.* **2015**, 8 (10), 3353–3364. <https://doi.org/10.1007/s12274-015-0835-6>.
- (102) Nan, W.; Niu, Y.; Qin, H.; Cui, F.; Yang, Y.; Lai, R.; Lin, W.; Peng, X. Crystal Structure Control of Zinc-Blende CdSe/CdS Core/Shell Nanocrystals: Synthesis and Structure-Dependent Optical Properties. *J. Am. Chem. Soc.* **2012**, 134 (48), 19685–19693. <https://doi.org/10.1021/ja306651x>.
- (103) Li, Z.; Ji, Y.; Xie, R.; Grisham, S. Y.; Peng, X. Correlation of CdS Nanocrystal Formation with Elemental Sulfur Activation and Its Implication in Synthetic Development. *J. Am. Chem. Soc.* **2011**, 133 (43), 17248–17256. <https://doi.org/10.1021/ja204538f>.
- (104) Liu, J.; Liu, R.; Yin, Y.; Jiang, G. Triton X-114 Based Cloud Point Extraction: A Thermoreversible Approach for Separation/Concentration and Dispersion of Nanomaterials in the Aqueous Phase. *Chem. Commun.* **2009**, No. 12, 1514–1516. <https://doi.org/10.1039/B821124H>.
- (105) Ganguly, M.; Pal, A.; Pal, T. Purification of Gold Organosol by Solid Reagent. *J. Phys. Chem. C* **2012**, 116 (16), 9265–9273. <https://doi.org/10.1021/jp2121356>.
- (106) Claridge, S. A.; Goh, S. L.; Fréchet, J. M. J.; Williams, S. C.; Micheel, C. M.; Alivisatos, A. P. Directed Assembly of Discrete Gold Nanoparticle Groupings Using Branched DNA Scaffolds. *Chem. Mater.* **2005**, 17 (7), 1628–1635. <https://doi.org/10.1021/cm0484089>.

- (107) Sperling, R. A.; Pellegrino, T.; Li, J. K.; Chang, W. H.; Parak, W. J. Electrophoretic Separation of Nanoparticles with a Discrete Number of Functional Groups. *Adv. Funct. Mater.* **2006**, *16* (7), 943–948. <https://doi.org/10.1002/adfm.200500589>.
- (108) Arnaud, I.; Abid, J.-P.; Roussel, C.; Girault, H. H. Size-Selective Separation of Gold Nanoparticles Using Isoelectric Focusing Electrophoresis (IEF). *Chem. Commun.* **2005**, No. 6, 787–788. <https://doi.org/10.1039/B413719A>.
- (109) Hanauer, M.; Pierrat, S.; Zins, I.; Lotz, A.; Sönnichsen, C. Separation of Nanoparticles by Gel Electrophoresis According to Size and Shape. *Nano Lett.* **2007**, *7* (9), 2881–2885. <https://doi.org/10.1021/nl071615y>.
- (110) Ho, S.; Critchley, K.; Lilly, G. D.; Shim, B.; Kotov, N. A. Free Flow Electrophoresis for the Separation of CdTe Nanoparticles. *J. Mater. Chem.* **2009**, *19* (10), 1390–1394. <https://doi.org/10.1039/B820703H>.
- (111) Lhuillier, E.; Hease, P.; Ithurria, S.; Dubertret, B. Selective Electrophoretic Deposition of CdSe Nanoplatelets. *Chem. Mater.* **2014**, *26* (15), 4514–4520. <https://doi.org/10.1021/cm501713s>.
- (112) Bass, J. D.; Ai, X.; Bagabas, A.; Rice, P. M.; Topuria, T.; Scott, J. C.; Alharbi, F. H.; Kim, H.-C.; Song, Q.; Miller, R. D. An Efficient and Low-Cost Method for the Purification of Colloidal Nanoparticles. *Angew. Chem. Int. Ed.* **2011**, *50* (29), 6538–6542. <https://doi.org/10.1002/anie.201100112>.
- (113) Kim, D.; Park, H. K.; Choi, H.; Noh, J.; Kim, K.; Jeong, S. Continuous Flow Purification of Nanocrystal Quantum Dots. *Nanoscale* **2014**, *6* (23), 14467–14472. <https://doi.org/10.1039/C4NR04351K>.



- (114) Williams, J. W.; Van Holde, K. E.; Baldwin, R. L.; Fujita, H. The Theory Of Sedimentation Analysis. *Chem. Rev.* **1958**, 58 (4), 715–744. <https://doi.org/10.1021/cr50022a005>.
- (115) Arnold, M. S.; Green, A. A.; Hulvat, J. F.; Stupp, S. I.; Hersam, M. C. Sorting Carbon Nanotubes by Electronic Structure Using Density Differentiation. *Nat Nano* **2006**, 1 (1), 60–65. <https://doi.org/10.1038/nnano.2006.52>.
- (116) Calabretta, M.; Jamison, J. A.; Falkner, J. C.; Liu, Y.; Yuhas, B. D.; Matthews, K. S.; Colvin, V. L. Analytical Ultracentrifugation for Characterizing Nanocrystals and Their Bioconjugates. *Nano Lett.* **2005**, 5 (5), 963–967. <https://doi.org/10.1021/nl047926f>.
- (117) Miller, J. B.; Harris, J. M.; Hobbie, E. K. Purifying Colloidal Nanoparticles through Ultracentrifugation with Implications for Interfaces and Materials. *Langmuir* **2014**, 30 (27), 7936–7946. <https://doi.org/10.1021/la404675v>.
- (118) Jamison, J. A.; Krueger, K. M.; Yavuz, C. T.; Mayo, J. T.; LeCrone, D.; Redden, J. J.; Colvin, V. L. Size-Dependent Sedimentation Properties of Nanocrystals. *ACS Nano* **2008**, 2 (2), 311–319. <https://doi.org/10.1021/nn700144m>.
- (119) Li, P.; Huang, J.; Luo, L.; Kuang, Y.; Sun, X. Universal Parameter Optimization of Density Gradient Ultracentrifugation Using CdSe Nanoparticles as Tracing Agents. *Anal. Chem.* **2016**, 88 (17), 8495–8501. <https://doi.org/10.1021/acs.analchem.6b01092>.
- (120) Smith, A. M.; Duan, H.; Rhyner, M. N.; Ruan, G.; Nie, S. A Systematic Examination of Surface Coatings on the Optical and Chemical Properties of

Semiconductor Quantum Dots. *Phys. Chem. Chem. Phys.* **2006**, 8 (33), 3895–3903.  
<https://doi.org/10.1039/B606572B>.

- (121) Carion, O.; Mahler, B.; Pons, T.; Dubertret, B. Synthesis, Encapsulation, Purification and Coupling of Single Quantum Dots in Phospholipid Micelles for Their Use in Cellular and in Vivo Imaging. *Nat. Protocols* **2007**, 2 (10), 2383–2390. <https://doi.org/10.1038/nprot.2007.351>.
- (122) Prantner, A. M.; Chen, J.; Murray, C. B.; Scholler, N. Coating Evaluation and Purification of Monodisperse, Water-Soluble, Magnetic Nanoparticles Using Sucrose Density Gradient Ultracentrifugation. *Chem. Mater.* **2012**, 24 (21), 4008–4010. <https://doi.org/10.1021/cm302582z>.
- (123) Sapsford, K. E.; Tyner, K. M.; Dair, B. J.; Deschamps, J. R.; Medintz, I. L. Analyzing Nanomaterial Bioconjugates: A Review of Current and Emerging Purification and Characterization Techniques. *Anal. Chem.* **2011**, 83 (12), 4453–4488. <https://doi.org/10.1021/ac200853a>.
- (124) Bai, L.; Ma, X.; Liu, J.; Sun, X.; Zhao, D.; Evans, D. G. Rapid Separation and Purification of Nanoparticles in Organic Density Gradients. *J. Am. Chem. Soc.* **2010**, 132 (7), 2333–2337. <https://doi.org/10.1021/ja908971d>.
- (125) Alkilany, A. M.; Abulateefeh, S. R.; Mills, K. K.; Bani Yaseen, A. I.; Hamaly, M. A.; Alkhatib, H. S.; Aiedeh, K. M.; Stone, J. W. Colloidal Stability of Citrate and Mercaptoacetic Acid Capped Gold Nanoparticles upon Lyophilization: Effect of Capping Ligand Attachment and Type of Cryoprotectants. *Langmuir* **2014**, 30 (46), 13799–13808. <https://doi.org/10.1021/la504000v>.

- (126) Dong, C.; Qian, H.; Fang, N.; Ren, J. Study of Fluorescence Quenching and Dialysis Process of CdTe Quantum Dots, Using Ensemble Techniques and Fluorescence Correlation Spectroscopy. *J. Phys. Chem. B* **2006**, *110* (23), 11069–11075. <https://doi.org/10.1021/jp060279r>.
- (127) Zhang, X.; Shamirian, A.; Jawaid, A. M.; Tyrakowski, C. M.; Page, L. E.; Das, A.; Chen, O.; Iovic, A.; Hassan, A.; Snee, P. T. Monolayer Silane-Coated, Water-Soluble Quantum Dots. *Small* **2015**, *11* (45), 6091–6096. <https://doi.org/10.1002/sml.201501886>.
- (128) Xing, Y.; Chaudry, Q.; Shen, C.; Kong, K. Y.; Zhau, H. E.; Chung, L. W.; Petros, J. A.; O'Regan, R. M.; Yezhelyev, M. V.; Simons, J. W.; et al. Bioconjugated Quantum Dots for Multiplexed and Quantitative Immunohistochemistry. *Nat. Protocols* **2007**, *2* (5), 1152–1165. <https://doi.org/10.1038/nprot.2007.107>.
- (129) Viswanath, A.; Shen, Y.; Green, A. N.; Tan, R.; Greytak, A. B.; Benicewicz, B. C. Copolymerization and Synthesis of Multiply Binding Histamine Ligands for the Robust Functionalization of Quantum Dots. *Macromolecules* **2014**, *47* (23), 8137–8144. <https://doi.org/10.1021/ma501955t>.
- (130) Snee, P. T.; Chan, Y. H.; Nocera, D. G.; Bawendi, M. G. Whispering-Gallery-Mode Lasing from a Semiconductor Nanocrystal/Microsphere Resonator Composite. *Advanced Materials* **2005**, *17* (9), 1131–1136.
- (131) Mekawy, M. M.; Yamaguchi, A.; El-Safty, S. A.; Itoh, T.; Teramae, N. Mesoporous Silica Hybrid Membranes for Precise Size-Exclusive Separation of Silver Nanoparticles. *Journal of Colloid and Interface Science* **2011**, *355* (2), 348–358. <https://doi.org/10.1016/j.jcis.2010.11.056>.

- (132) Gaborski, T. R.; Snyder, J. L.; Striemer, C. C.; Fang, D. Z.; Hoffman, M.; Fauchet, P. M.; McGrath, J. L. High-Performance Separation of Nanoparticles with Ultrathin Porous Nanocrystalline Silicon Membranes. *ACS Nano* **2010**, *4* (11), 6973–6981. <https://doi.org/10.1021/nn102064c>.
- (133) Krieg, E.; Weissman, H.; Shirman, E.; Shimoni, E.; Rybtchinski, B. A Recyclable Supramolecular Membrane for Size-Selective Separation of Nanoparticles. *Nat Nano* **2011**, *6* (3), 141–146. <https://doi.org/10.1038/nnano.2010.274>.
- (134) Alele, N.; Ulbricht, M. Membrane-Based Purification of Proteins from Nanoparticle Dispersions: Influences of Membrane Type and Ultrafiltration Conditions. *Separation and Purification Technology* **2016**, *158*, 171–182. <https://doi.org/10.1016/j.seppur.2015.11.031>.
- (135) Sweeney, S. F.; Woehrle, G. H.; Hutchison, J. E. Rapid Purification and Size Separation of Gold Nanoparticles via Diafiltration. *J. Am. Chem. Soc.* **2006**, *128* (10), 3190–3197. <https://doi.org/10.1021/ja0558241>.
- (136) Pierre, M. C. S.; Haes, A. J. Purification Implications on SERS Activity of Silica Coated Gold Nanospheres. *Anal. Chem.* **2012**, *84* (18), 7906–7911. <https://doi.org/10.1021/ac3016517>.
- (137) Shen, Y.; Roberge, A.; Tan, R.; Gee, M. Y.; Gary, D. C.; Huang, Y.; Blom, D. A.; Benicewicz, B. C.; Cossairt, B. M.; Greytak, A. B. Gel Permeation Chromatography as a Multifunctional Processor for Nanocrystal Purification and On-Column Ligand Exchange Chemistry. *Chemical Science* **2016**, *7* (9), 5671–5679. <https://doi.org/10.1039/C6SC01301E>.

- (138) Al-Somali, A. M.; Krueger, K. M.; Falkner, J. C.; Colvin, V. L. Recycling Size Exclusion Chromatography for the Analysis and Separation of Nanocrystalline Gold. *Anal. Chem.* **2004**, *76* (19), 5903–5910. <https://doi.org/10.1021/ac049355h>.
- (139) Tiede, K.; Boxall, A. B. A.; Tiede, D.; Tear, S. P.; David, H.; Lewis, J. A Robust Size-Characterisation Methodology for Studying Nanoparticle Behaviour in ‘Real’ Environmental Samples, Using Hydrodynamic Chromatography Coupled to ICP-MS. *J. Anal. At. Spectrom.* **2009**, *24* (7), 964–972. <https://doi.org/10.1039/B822409A>.
- (140) Pergantis, S. A.; Jones-Lepp, T. L.; Heithmar, E. M. Hydrodynamic Chromatography Online with Single Particle-Inductively Coupled Plasma Mass Spectrometry for Ultratrace Detection of Metal-Containing Nanoparticles. *Anal. Chem.* **2012**, *84* (15), 6454–6462. <https://doi.org/10.1021/ac300302j>.
- (141) Novak, J. P.; Nickerson, C.; Franzen, S.; Feldheim, D. L. Purification of Molecularly Bridged Metal Nanoparticle Arrays by Centrifugation and Size Exclusion Chromatography. *Anal. Chem.* **2001**, *73* (23), 5758–5761. <https://doi.org/10.1021/ac010812t>.
- (142) López-Serrano, A.; Olivas, R. M.; Landaluze, J. S.; Cámara, C. Nanoparticles: A Global Vision. Characterization, Separation, and Quantification Methods. Potential Environmental and Health Impact. *Anal. Methods* **2013**, *6* (1), 38–56. <https://doi.org/10.1039/C3AY40517F>.
- (143) Wilcoxon, J. P.; Provencio, P. P. Chemical and Optical Properties of CdSe and CdSe/ZnS Nanocrystals Investigated Using High-Performance Liquid

- Chromatography. *J. Phys. Chem. B* **2005**, *109* (28), 13461–13471.  
<https://doi.org/10.1021/jp050062h>.
- (144) Alamo-Nole, L.; Bailon-Ruiz, S.; Perales-Perez, O.; Roman, F. R. Preparative Size-Exclusion Chromatography for Separation and Purification of Water-Stable Cd-Based Quantum Dots. *Anal. Methods* **2012**, *4* (10), 3127–3132.  
<https://doi.org/10.1039/C2AY25629K>.
- (145) Arita, T.; Yoshimura, T.; Adschiri, T. Size Exclusion Chromatography of Quantum Dots by Utilizing Nanoparticle Repelling Surface of Concentrated Polymer Brush. *Nanoscale* **2010**, *2* (8), 1467–1473. <https://doi.org/10.1039/C0NR00157K>.
- (146) Reisch, M. S. HPLC Struggles with Its Version of Moore's Law Technique Confronts Practical Limitations in Pursuit of Greater Speed and Accuracy. *c&en* **2016**, *94* (24), 35–36.
- (147) Pitkänen, L.; Striegel, A. M. Determining the Core, Corona, and Total Size of CdSeS/ZnS Quantum Dots by SEC/QELS and TEM. *Anal Bioanal Chem* **2016**, *408* (15), 4003–4010. <https://doi.org/10.1007/s00216-016-9487-y>.
- (148) Wilcoxon, J. P.; Martin, J. E.; Provencio, P. Size Distributions of Gold Nanoclusters Studied by Liquid Chromatography. *Langmuir* **2000**, *16* (25), 9912–9920. <https://doi.org/10.1021/la000669j>.
- (149) Kanelidis, I.; Vaneski, A.; Lenkeit, D.; Pelz, S.; Elsner, V.; Stewart, R. M.; Rodríguez-Fernández, J.; Lutich, A. A.; Susa, A. S.; Theissmann, R.; et al. Inorganic–Organic Nanocomposites of CdSe Nanocrystals Surface-Modified with Oligo- and Poly(Fluorene) Moieties. *J. Mater. Chem.* **2011**, *21* (8), 2656–2662.  
<https://doi.org/10.1039/C0JM03546G>.

- (150) Tang, C.; Tan, J.; Jin, J.; Xi, S.; Li, H.; Xie, Q.; Peng, X. Observation and Confirmation of Oxidation Reactions Occurring on Ultra-High-Performance Liquid Chromatography Columns. *Rapid Commun. Mass Spectrom.* **2015**, *29* (20), 1863–1873. <https://doi.org/10.1002/rcm.7291>.
- (151) Wang, M.; Bardajee, G. R.; Kumar, S.; Nitz, M.; Scholes, G. D.; Winnik, M. A. Preparative Size-Exclusion Chromatography for Purification and Characterization of Colloidal Quantum Dots Bound by Chromophore-Labeled Polymers and Low-Molecular-Weight Chromophores. *Journal of Chromatography A* **2009**, *1216* (25), 5011–5019. <https://doi.org/10.1016/j.chroma.2009.04.060>.
- (152) Davis, K.; Qi, B.; Witmer, M.; Kitchens, C. L.; Powell, B. A.; Mefford, O. T. Quantitative Measurement of Ligand Exchange on Iron Oxides via Radiolabeled Oleic Acid. *Langmuir* **2014**, *30* (36), 10918–10925. <https://doi.org/10.1021/la502204g>.
- (153) Ye, L.; Pearson, T.; Dolbashian, C.; Pstrak, P.; Mohtasebzadeh, A. R.; Fellows, B.; Mefford, O. T.; Crawford, T. M. Magnetic-Field-Directed Self-Assembly of Programmable Mesoscale Shapes. *Adv. Funct. Mater.* **2016**, *26* (22), 3983–3989. <https://doi.org/10.1002/adfm.201504749>.
- (154) Wang, M.; Dykstra, T. E.; Lou, X.; Salvador, M. R.; Scholes, G. D.; Winnik, M. A. Colloidal CdSe Nanocrystals Passivated by a Dye-Labeled Multidentate Polymer: Quantitative Analysis by Size-Exclusion Chromatography. *Angewandte Chemie International Edition* **2006**, *45* (14), 2221–2224. <https://doi.org/10.1002/anie.200502538>.

- (155) Biesta, W.; van Lagen, B.; Gevaert, V. S.; Marcelis, A. T. M.; Paulusse, J. M. J.; Nielen, M. W. F.; Zuilhof, H. Preparation, Characterization, and Surface Modification of Trifluoroethyl Ester-Terminated Silicon Nanoparticles. *Chem. Mater.* **2012**, *24* (22), 4311–4318. <https://doi.org/10.1021/cm302060f>.
- (156) McLaurin, E. J.; Greytak, A. B.; Bawendi, M. G.; Nocera, D. G. Two-Photon Absorbing Nanocrystal Sensors for Ratiometric Detection of Oxygen. *J. Am. Chem. Soc.* **2009**, *131* (36), 12994–13001. <https://doi.org/10.1021/ja902712b>.
- (157) Wu, J.-K.; Tian, Z.-Q.; Zhang, Z.-L.; Liu, A.-A.; Tang, B.; Zhang, L.-J.; Chen, Z.-L.; Pang, D.-W. Purification of Quantum Dot-Based Bioprobes via High-Performance Size Exclusion Chromatography. *Talanta* **2016**, *159*, 64–73. <https://doi.org/10.1016/j.talanta.2016.05.078>.
- (158) Rheinländer, T.; Kötz, R.; Weitschies, W.; Semmler, W. Different Methods for the Fractionation of Magnetic Fluids. *Colloid Polym Sci* **2000**, *278* (3), 259–263. <https://doi.org/10.1007/s003960050041>.
- (159) Xie, L.; Shen, Y.; Franke, D.; Sebastián, V.; Bawendi, M. G.; Jensen, K. F. Characterization of Indium Phosphide Quantum Dot Growth Intermediates Using MALDI-TOF Mass Spectrometry. *J. Am. Chem. Soc.* **2016**, *138* (41), 13469–13472. <https://doi.org/10.1021/jacs.6b06468>.
- (160) Parobek, D.; Roman, B. J.; Dong, Y.; Jin, H.; Lee, E.; Sheldon, M.; Son, D. H. Exciton-to-Dopant Energy Transfer in Mn-Doped Cesium Lead Halide Perovskite Nanocrystals. *Nano Lett.* **2016**, *16* (12), 7376–7380. <https://doi.org/10.1021/acs.nanolett.6b02772>.



- (161) Kambhampati, P. On the Kinetics and Thermodynamics of Excitons at the Surface of Semiconductor Nanocrystals: Are There Surface Excitons? *Chemical Physics* **2015**, *446*, 92–107. <https://doi.org/10.1016/j.chemphys.2014.11.008>.
- (162) Wang, F.; Tang, R.; Buhro, W. E. The Trouble with TOPO; Identification of Adventitious Impurities Beneficial to the Growth of Cadmium Selenide Quantum Dots, Rods, and Wires. *Nano Lett.* **2008**, *8* (10), 3521–3524. <https://doi.org/10.1021/nl801692g>.
- (163) Owen, J. S.; Park, J.; Trudeau, P.-E.; Alivisatos, A. P. Reaction Chemistry and Ligand Exchange at Cadmium–Selenide Nanocrystal Surfaces. *J. Am. Chem. Soc.* **2008**, *130* (37), 12279–12281. <https://doi.org/10.1021/ja804414f>.
- (164) Cirillo, M.; Strubbe, F.; Neyts, K.; Hens, Z. Thermal Charging of Colloidal Quantum Dots in Apolar Solvents: A Current Transient Analysis. *ACS Nano* **2011**, *5* (2), 1345–1352. <https://doi.org/10.1021/nn103052r>.
- (165) Knittel, F.; Gravel, E.; Cassette, E.; Pons, T.; Pillon, F.; Dubertret, B.; Doris, E. On the Characterization of the Surface Chemistry of Quantum Dots. *Nano Lett.* **2013**, *13* (11), 5075–5078. <https://doi.org/10.1021/nl402192d>.
- (166) Uematsu, T.; Shimomura, E.; Torimoto, T.; Kuwabata, S. Evaluation of Surface Ligands on Semiconductor Nanoparticle Surfaces Using Electron Transfer to Redox Species. *J. Phys. Chem. C* **2016**, *120* (29), 16012–16023. <https://doi.org/10.1021/acs.jpcc.5b12698>.
- (167) Kirkwood, N.; Monchen, J. O. V.; Crisp, R. W.; Grimaldi, G.; Bergstein, H. A. C.; du Fossé, I.; van der Stam, W.; Infante, I.; Houtepen, A. J. Finding and Fixing Traps in II–VI and III–V Colloidal Quantum Dots: The Importance of Z-Type

- Ligand Passivation. *J. Am. Chem. Soc.* **2018**, *140* (46), 15712–15723.  
<https://doi.org/10.1021/jacs.8b07783>.
- (168) Saniepay, M.; Mi, C.; Liu, Z.; Abel, E. P.; Beaulac, R. Insights into the Structural Complexity of Colloidal CdSe Nanocrystal Surfaces: Correlating the Efficiency of Nonradiative Excited-State Processes to Specific Defects. *J. Am. Chem. Soc.* **2018**, *140* (5), 1725–1736. <https://doi.org/10.1021/jacs.7b10649>.
- (169) Dierick, R.; Van den Broeck, F.; De Nolf, K.; Zhao, Q.; Vantomme, A.; Martins, J. C.; Hens, Z. Surface Chemistry of CuInS<sub>2</sub> Colloidal Nanocrystals, Tight Binding of L-Type Ligands. *Chem. Mater.* **2014**, *26* (20), 5950–5957.  
<https://doi.org/10.1021/cm502687p>.
- (170) Turo, M. J.; Shen, X.; Brandon, N. K.; Castillo, S.; Fall, A. M.; Pantelides, S. T.; Macdonald, J. E. Dual-Mode Crystal-Bound and X-Type Passivation of Quantum Dots. *Chem. Commun.* **2016**, *52* (82), 12214–12217.  
<https://doi.org/10.1039/C6CC05951A>.
- (171) De Roo, J.; Justo, Y.; De Keukeleere, K.; Van den Broeck, F.; Martins, J. C.; Van Driessche, I.; Hens, Z. Carboxylic-Acid-Passivated Metal Oxide Nanocrystals: Ligand Exchange Characteristics of a New Binding Motif. *Angew. Chem. Int. Ed.* **2015**, *54* (22), 6488–6491. <https://doi.org/10.1002/anie.201500965>.
- (172) Deng, L.; Wang, X.; Kuang, Y.; Wang, C.; Luo, L.; Wang, F.; Sun, X. Development of Hydrophilicity Gradient Ultracentrifugation Method for Photoluminescence Investigation of Separated Non-Sedimental Carbon Dots. *Nano Res.* **2015**, *8* (9), 2810–2821. <https://doi.org/10.1007/s12274-015-0786-y>.

- (173) Gary, D. C.; Terban, M. W.; Billinge, S. J. L.; Cossairt, B. M. Two-Step Nucleation and Growth of InP Quantum Dots via Magic-Sized Cluster Intermediates. *Chem. Mater.* **2015**, *27* (4), 1432–1441. <https://doi.org/10.1021/acs.chemmater.5b00286>.
- (174) Jadzinsky, P. D.; Calero, G.; Ackerson, C. J.; Bushnell, D. A.; Kornberg, R. D. Structure of a Thiol Monolayer-Protected Gold Nanoparticle at 1.1 Å Resolution. *Science* **2007**, *318* (5849), 430–433. <https://doi.org/10.1126/science.1148624>.
- (175) Zhrebetskyy, D.; Scheele, M.; Zhang, Y.; Bronstein, N.; Thompson, C.; Britt, D.; Salmeron, M.; Alivisatos, P.; Wang, L.-W. Hydroxylation of the Surface of PbS Nanocrystals Passivated with Oleic Acid. *Science* **2014**, *344* (6190), 1380–1384. <https://doi.org/10.1126/science.1252727>.
- (176) White, M. A.; Thompson, M. J.; Miller, G. J.; Vela, J. Got LiZnP? Solution Phase Synthesis of Filled Tetrahedral Semiconductors in the Nanoregime. *Chem. Commun.* **2016**, *52* (17), 3497–3499. <https://doi.org/10.1039/C5CC09635A>.
- (177) Larson, D. R.; Zipfel, W. R.; Williams, R. M.; Clark, S. W.; Bruchez, M. P.; Wise, F. W.; Webb, W. W. Water-Soluble Quantum Dots for Multiphoton Fluorescence Imaging in Vivo. *Science* **2003**, *300* (5624), 1434–1436.
- (178) Erathodiyil, N.; Ying, J. Y. Functionalization of Inorganic Nanoparticles for Bioimaging Applications. *Acc. Chem. Res.* **2011**, *44* (10), 925–935. <https://doi.org/10.1021/ar2000327>.
- (179) Zhang, B.; Hu, R.; Wang, Y.; Yang, C.; Liu, X.; Yong, K.-T. Revisiting the Principles of Preparing Aqueous Quantum Dots for Biological Applications: The

Effects of Surface Ligands on the Physicochemical Properties of Quantum Dots.

*RSC Adv.* **2014**, *4* (27), 13805–13816. <https://doi.org/10.1039/c4ra00288a>.

- (180) Anikeeva, P. O.; Halpert, J. E.; Bawendi, M. G.; Bulović, V. Quantum Dot Light-Emitting Devices with Electroluminescence Tunable over the Entire Visible Spectrum. *Nano Letters* **2009**, *9* (7), 2532–2536.
- (181) Panthani, M. G.; Kurley, J. M.; Crisp, R. W.; Dietz, T. C.; Ezzyat, T.; Luther, J. M.; Talapin, D. V. High Efficiency Solution Processed Sintered CdTe Nanocrystal Solar Cells: The Role of Interfaces. *Nano Lett.* **2014**, *14* (2), 670–675. <https://doi.org/10.1021/nl403912w>.
- (182) Zhitomirsky, D.; Voznyy, O.; Levina, L.; Hoogland, S.; Kemp, K. W.; Ip, A. H.; Thon, S. M.; Sargent, E. H. Engineering Colloidal Quantum Dot Solids within and beyond the Mobility-Invariant Regime. *Nat Commun* **2014**, *5*, 3803. <https://doi.org/10.1038/ncomms4803>.
- (183) Meinardi, F.; Colombo, A.; Velizhanin, K. A.; Simonutti, R.; Lorenzon, M.; Beverina, L.; Viswanatha, R.; Klimov, V. I.; Brovelli, S. Large-Area Luminescent Solar Concentrators Based on /'Stokes-Shift-Engineered/' Nanocrystals in a Mass-Polymerized PMMA Matrix. *Nat Photon* **2014**, *8* (5), 392–399. <https://doi.org/10.1038/nphoton.2014.54>.
- (184) Erickson, C. S.; Bradshaw, L. R.; McDowall, S.; Gilbertson, J. D.; Gamelin, D. R.; Patrick, D. L. Zero-Reabsorption Doped-Nanocrystal Luminescent Solar Concentrators. *ACS Nano* **2014**, *8* (4), 3461–3467. <https://doi.org/10.1021/nn406360w>.

- (185) Geyer, S. M.; Scherer, J. M.; Moloto, N.; Jaworski, F. B.; Bawendi, M. G. Efficient Luminescent Down-Shifting Detectors Based on Colloidal Quantum Dots for Dual-Band Detection Applications. *ACS Nano* **2011**, *5* (7), 5566–5571. <https://doi.org/10.1021/nn2010238>.
- (186) Smith, A. M.; Nie, S. Semiconductor Nanocrystals: Structure, Properties, and Band Gap Engineering. *Acc. Chem. Res.* **2010**, *43* (2), 190–200. <https://doi.org/10.1021/ar9001069>.
- (187) Jasieniak, J.; Smith, L.; Embden, J. van; Mulvaney, P.; Califano, M. Re-Examination of the Size-Dependent Absorption Properties of CdSe Quantum Dots. *The Journal of Physical Chemistry C* **2009**, *113* (45), 19468–19474. <https://doi.org/10.1021/jp906827m>.
- (188) Zhu, H.; Yang, Y.; Lian, T. Multiexciton Annihilation and Dissociation in Quantum Confined Semiconductor Nanocrystals. *Acc. Chem. Res.* **2013**, *46* (6), 1270–1279. <https://doi.org/10.1021/ar300202d>.
- (189) Petruska, M. A.; Malko, A. V.; Voyles, P. M.; Klimov, V. I. High-Performance, Quantum Dot Nanocomposites for Nonlinear Optical and Optical Gain Applications. *Adv. Mater.* **2003**, *15* (7–8), 610–613. <https://doi.org/10.1002/adma.200304450>.
- (190) Leatherdale, C. A.; Bawendi, M. G. Observation of Solvatochromism in CdSe Colloidal Quantum Dots. *Physical Review B* **2001**, *63* (16), 165315.
- (191) Diroll, B. T.; Dadosh, T.; Koschitzky, A.; Goldman, Y. E.; Murray, C. B. Interpreting the Energy-Dependent Anisotropy of Colloidal Nanorods Using

- Ensemble and Single-Particle Spectroscopy. *J. Phys. Chem. C* **2013**, *117* (45), 23928–23937. <https://doi.org/10.1021/jp407151f>.
- (192) Saha, A.; Chellappan, K. V.; Narayan, K. S.; Ghatak, J.; Datta, R.; Viswanatha, R. Near-Unity Quantum Yield in Semiconducting Nanostructures: Structural Understanding Leading to Energy Efficient Applications. *J. Phys. Chem. Lett.* **2013**, *4* (20), 3544–3549. <https://doi.org/10.1021/jz401958u>.
- (193) Minotto, A.; Todescato, F.; Fortunati, I.; Signorini, R.; Jasieniak, J. J.; Bozio, R. Role of Core–Shell Interfaces on Exciton Recombination in CdSe–Cd<sub>x</sub>Zn<sub>1–x</sub>S Quantum Dots. *J. Phys. Chem. C* **2014**, *118* (41), 24117–24126. <https://doi.org/10.1021/jp506778n>.
- (194) Krause, M. M.; Kambhampati, P. Linking Surface Chemistry to Optical Properties of Semiconductor Nanocrystals. *Phys. Chem. Chem. Phys.* **2015**, *17* (29), 18882–18894. <https://doi.org/10.1039/C5CP02173A>.
- (195) Krause, M. M.; Mooney, J.; Kambhampati, P. Chemical and Thermodynamic Control of the Surface of Semiconductor Nanocrystals for Designer White Light Emitters. *ACS Nano* **2013**, *7* (7), 5922–5929. <https://doi.org/10.1021/nn401383t>.
- (196) Chen, O.; Yang, Y.; Wang, T.; Wu, H.; Niu, C.; Yang, J.; Cao, Y. C. Surface-Functionalization-Dependent Optical Properties of II–VI Semiconductor Nanocrystals. *J. Am. Chem. Soc.* **2011**, *133* (43), 17504–17512. <https://doi.org/10.1021/ja208337r>.
- (197) Drijvers, E.; De Roo, J.; Martins, J. C.; Infante, I.; Hens, Z. Ligand Displacement Exposes Binding Site Heterogeneity on CdSe Nanocrystal Surfaces. *Chem. Mater.* **2018**, *30* (3), 1178–1186. <https://doi.org/10.1021/acs.chemmater.7b05362>.

- (198) Kopping, J. T.; Patten, T. E. Identification of Acidic Phosphorus-Containing Ligands Involved in the Surface Chemistry of CdSe Nanoparticles Prepared in Tri-N-Octylphosphine Oxide Solvents. *J. Am. Chem. Soc.* **2008**, *130* (17), 5689–5698. <https://doi.org/10.1021/ja077414d>.
- (199) Chen, P. E.; Anderson, N. C.; Norman, Z. M.; Owen, J. S. Tight Binding of Carboxylate, Phosphonate, and Carbamate Anions to Stoichiometric CdSe Nanocrystals. *J. Am. Chem. Soc.* **2017**. <https://doi.org/10.1021/jacs.6b13234>.
- (200) Anderson, N. C.; Chen, P. E.; Buckley, A. K.; De Roo, J.; Owen, J. S. Stereoelectronic Effects on the Binding of Neutral Lewis Bases to CdSe Nanocrystals. *J. Am. Chem. Soc.* **2018**, *140* (23), 7199–7205. <https://doi.org/10.1021/jacs.8b02927>.
- (201) Gao, Y.; Peng, X. Photogenerated Excitons in Plain Core CdSe Nanocrystals with Unity Radiative Decay in Single Channel: The Effects of Surface and Ligands. *J. Am. Chem. Soc.* **2015**, *137* (12), 4230–4235. <https://doi.org/10.1021/jacs.5b01314>.
- (202) Hartmann, L.; Kumar, A.; Welker, M.; Fiore, A.; Julien-Rabant, C.; Gromova, M.; Bardet, M.; Reiss, P.; Baxter, P. N. W.; Chandezon, F.; et al. Quenching Dynamics in CdSe Nanoparticles: Surface-Induced Defects upon Dilution. *ACS Nano* **2012**, *6* (10), 9033–9041. <https://doi.org/10.1021/nn303150j>.
- (203) Chen, Y.; Vela, J.; Htoon, H.; Casson, J. L.; Werder, D. J.; Bussian, D. A.; Klimov, V. I.; Hollingsworth, J. A. Giant Multishell CdSe Nanocrystal Quantum Dots with Suppressed Blinking. *J. Am. Chem. Soc.* **2008**, *130* (15), 5026–5027.
- (204) Mahler, B.; Spinicelli, P.; Buil, S.; Quelin, X.; Hermier, J.-P.; Dubertret, B. Towards Non-Blinking Colloidal Quantum Dots. *Nat Mater* **2008**, *7* (8), 659–664.

- (205) Orfield, N. J.; McBride, J. R.; Keene, J. D.; Davis, L. M.; Rosenthal, S. J. Correlation of Atomic Structure and Photoluminescence of the Same Quantum Dot: Pinpointing Surface and Internal Defects That Inhibit Photoluminescence. *ACS Nano* **2015**, *9* (1), 831–839. <https://doi.org/10.1021/nn506420w>.
- (206) Chen, O.; Zhao, J.; Chauhan, V. P.; Cui, J.; Wong, C.; Harris, D. K.; Wei, H.; Han, H.-S.; Fukumura, D.; Jain, R. K.; et al. Compact High-Quality CdSe–CdS Core–Shell Nanocrystals with Narrow Emission Linewidths and Suppressed Blinking. *Nat Mater* **2013**, *12* (5), 445–451. <https://doi.org/10.1038/nmat3539>.
- (207) Tan, R.; Blom, D. A.; Ma, S.; Greytak, A. B. Probing Surface Saturation Conditions in Alternating Layer Growth of CdSe/CdS Core/Shell Quantum Dots. *Chem. Mater.* **2013**, *25* (18), 3724–3736. <https://doi.org/10.1021/cm402148s>.
- (208) Kilina, S.; Velizhanin, K. A.; Ivanov, S.; Prezhdo, O. V.; Tretiak, S. Surface Ligands Increase Photoexcitation Relaxation Rates in CdSe Quantum Dots. *ACS Nano* **2012**, *6* (7), 6515–6524. <https://doi.org/10.1021/nn302371q>.
- (209) Landes, C.; Braun, M.; Burda, C.; El-Sayed, M. A. Observation of Large Changes in the Band Gap Absorption Energy of Small CdSe Nanoparticles Induced by the Adsorption of a Strong Hole Acceptor. *Nano Lett.* **2001**, *1* (11), 667–670. <https://doi.org/10.1021/nl015619t>.
- (210) Newton, J. C.; Ramasamy, K.; Mandal, M.; Joshi, G. K.; Kumbhar, A.; Sardar, R. Low-Temperature Synthesis of Magic-Sized CdSe Nanoclusters: Influence of Ligands on Nanocluster Growth and Photophysical Properties. *J. Phys. Chem. C* **2012**, *116* (7), 4380–4389. <https://doi.org/10.1021/jp2086818>.



- (211) Knowles, K. E.; Frederick, M. T.; Tice, D. B.; Morris-Cohen, A. J.; Weiss, E. A. Colloidal Quantum Dots: Think Outside the (Particle-in-a-)Box. *J. Phys. Chem. Lett.* **2012**, *3* (1), 18–26. <https://doi.org/10.1021/jz2013775>.
- (212) Ning, Z.; Molnar, M.; Chen, Y.; Friberg, P.; Gan, L.; Agren, H.; Fu, Y. Role of Surface Ligands in Optical Properties of Colloidal CdSe/CdS Quantum Dots. *Phys. Chem. Chem. Phys.* **2011**, *13* (13), 5848–5854. <https://doi.org/10.1039/c0cp02688c>.
- (213) Spinicelli, P.; Buil, S.; Quelin, X.; Mahler, B.; Dubertret, B.; Hermier, J.-P. Bright and Grey States in CdSe-CdS Nanocrystals Exhibiting Strongly Reduced Blinking. *Physical Review Letters* **2009**, *102* (13), 136801.
- (214) Sillen, A.; Engelborghs, Y. The Correct Use of “Average” Fluorescence Parameters. *Photochemistry and Photobiology* **1998**, *67* (5), 475–486. <https://doi.org/10.1111/j.1751-1097.1998.tb09082.x>.
- (215) Rempel, J. Y.; Trout, B. L.; Bawendi, M. G.; Jensen, K. F. Density Functional Theory Study of Ligand Binding on CdSe (0001), (000 $\bar{1}$ ), and (11 $\bar{2}$ 0) Single Crystal Relaxed and Reconstructed Surfaces: Implications for Nanocrystalline Growth. *J. Phys. Chem. B* **2006**, *110* (36), 18007–18016. <https://doi.org/10.1021/jp064051f>.
- (216) Canzi, G.; Mrse, A. A.; Kubiak, C. P. Diffusion-Ordered NMR Spectroscopy as a Reliable Alternative to TEM for Determining the Size of Gold Nanoparticles in Organic Solutions. *The Journal of Physical Chemistry C* **2011**, *115* (16), 7972–7978. <https://doi.org/10.1021/jp2008557>.

- (217) Ravi, V.; Binz, J. M.; Rioux, R. M. Thermodynamic Profiles at the Solvated Inorganic-Organic Interface: The Case of Gold-Thiolate Monolayers. *Nano Lett.* **2013**, *13* (9), 4442–4448. <https://doi.org/10.1021/nl402315z>.
- (218) Fleischer, C. C.; Payne, C. K. Secondary Structure of Corona Proteins Determines the Cell Surface Receptors Used by Nanoparticles. *J. Phys. Chem. B* **2014**, *118* (49), 14017–14026. <https://doi.org/10.1021/jp502624n>.
- (219) Shanavas, K. V.; Sharma, S. M.; Dasgupta, I.; Nag, A.; Hazarika, A.; Sarma, D. D. First-Principles Study of the Effect of Organic Ligands on the Crystal Structure of CdS Nanoparticles. *J. Phys. Chem. C* **2012**, *116* (11), 6507–6511. <https://doi.org/10.1021/jp2079428>.
- (220) García-Rodríguez, R.; Liu, H. Solution Structure of Cadmium Carboxylate and Its Implications for the Synthesis of Cadmium Chalcogenide Nanocrystals. *Chem. Commun.* **2013**, *49* (71), 7857–7859. <https://doi.org/10.1039/C3CC44103B>.
- (221) Mahler, B.; Lequeux, N.; Dubertret, B. Ligand-Controlled Polytypism of Thick-Shell CdSe/CdS Nanocrystals. *J. Am. Chem. Soc.* **2010**, *132* (3), 953–959. <https://doi.org/10.1021/ja9034973>.
- (222) García-Rodríguez, R.; Liu, H. Mechanistic Insights into the Role of Alkylamine in the Synthesis of CdSe Nanocrystals. *J. Am. Chem. Soc.* **2014**, *136* (5), 1968–1975. <https://doi.org/10.1021/ja4110182>.
- (223) Mourdikoudis, S.; Liz-Marzán, L. M. Oleylamine in Nanoparticle Synthesis. *Chem. Mater.* **2013**, *25* (9), 1465–1476. <https://doi.org/10.1021/cm4000476>.
- (224) Huang, X.; Parashar, V. K.; Gijis, M. A. M. Nucleation and Growth Behavior of CdSe Nanocrystals Synthesized in the Presence of Oleylamine Coordinating

- Ligand. *Langmuir* **2018**, *34* (21), 6070–6076.  
<https://doi.org/10.1021/acs.langmuir.7b01337>.
- (225) Pradhan, N.; Reifsnnyder, D.; Xie, R.; Aldana, J.; Peng, X. Surface Ligand Dynamics in Growth of Nanocrystals. *J. Am. Chem. Soc.* **2007**, *129* (30), 9500–9509. <https://doi.org/10.1021/ja0725089>.
- (226) Nose, K.; Fujita, H.; Omata, T.; Otsuka-Yao-Matsuo, S.; Nakamura, H.; Maeda, H. Chemical Role of Amines in the Colloidal Synthesis of CdSe Quantum Dots and Their Luminescence Properties. *Journal of Luminescence* **2007**, *126* (1), 21–26. <https://doi.org/10.1016/j.jlumin.2006.04.009>.
- (227) LaMer, V. K.; Dinegar, R. H. Theory, Production and Mechanism of Formation of Monodispersed Hydrosols. *J. Am. Chem. Soc.* **1950**, *72* (11), 4847–4854. <https://doi.org/10.1021/ja01167a001>.
- (228) Teunis, M. B.; Liyanage, T.; Dolai, S.; Muhoberac, B. B.; Sardar, R.; Agarwal, M. Unraveling the Mechanism Underlying Surface Ligand Passivation of Colloidal Semiconductor Nanocrystals: A Route for Preparing Advanced Hybrid Nanomaterials. *Chem. Mater.* **2017**, *29* (20), 8838–8849. <https://doi.org/10.1021/acs.chemmater.7b03240>.
- (229) Landes, C.; Burda, C.; Braun, M.; El-Sayed, M. A. Photoluminescence of CdSe Nanoparticles in the Presence of a Hole Acceptor: N-Butylamine. *Journal of Physical Chemistry B* **2001**, *105* (15), 2981–2986.
- (230) Landes, C. F.; Braun, M.; El-Sayed, M. A. On the Nanoparticle to Molecular Size Transition: Fluorescence Quenching Studies. *J. Phys. Chem. B* **2001**, *105* (43), 10554–10558. <https://doi.org/10.1021/jp0118726>.

- (231) Talapin, D. V.; Rogach, A. L.; Kornowski, A.; Haase, M.; Weller, H. Highly Luminescent Monodisperse CdSe and CdSe/ZnS Nanocrystals Synthesized in a Hexadecylamine–Trioctylphosphine Oxide–Trioctylphosphine Mixture. *Nano Lett.* **2001**, *1* (4), 207–211. <https://doi.org/10.1021/nl0155126>.
- (232) Sharma, S. N.; Pillai, Z. S.; Kamat, P. V. Photoinduced Charge Transfer between CdSe Quantum Dots and P-Phenylenediamine. *J. Phys. Chem. B* **2003**, *107* (37), 10088–10093. <https://doi.org/10.1021/jp034109f>.
- (233) Zhong, X.; Feng, Y.; Zhang, Y. Facile and Reproducible Synthesis of Red-Emitting CdSe Nanocrystals in Amine with Long-Term Fixation of Particle Size and Size Distribution. *J. Phys. Chem. C* **2007**, *111* (2), 526–531. <https://doi.org/10.1021/jp064797d>.
- (234) Hines, D. A.; Kamat, P. V. Quantum Dot Surface Chemistry: Ligand Effects and Electron Transfer Reactions. *J. Phys. Chem. C* **2013**, *117* (27), 14418–14426. <https://doi.org/10.1021/jp404031s>.
- (235) Ji, X.; Copenhaver, D.; Sichmeller, C.; Peng, X. Ligand Bonding and Dynamics on Colloidal Nanocrystals at Room Temperature: The Case of Alkylamines on CdSe Nanocrystals. *J. Am. Chem. Soc.* **2008**, *130* (17), 5726–5735. <https://doi.org/10.1021/ja710909f>.
- (236) Fritzinger, B.; Moreels, I.; Lommens, P.; Koole, R.; Hens, Z.; Martins, J. C. In Situ Observation of Rapid Ligand Exchange in Colloidal Nanocrystal Suspensions Using Transfer NOE Nuclear Magnetic Resonance Spectroscopy. *J. Am. Chem. Soc.* **2009**, *131* (8), 3024–3032. <https://doi.org/10.1021/ja809436y>.

- (237) Herrera, I.; Winnik, M. A. Differential Binding Models for Isothermal Titration Calorimetry: Moving beyond the Wiseman Isotherm. *J. Phys. Chem. B* **2013**, *117* (29), 8659–8672. <https://doi.org/10.1021/jp311812a>.
- (238) Harris, R. D.; Amin, V. A.; Lau, B.; Weiss, E. A. Role of Interligand Coupling in Determining the Interfacial Electronic Structure of Colloidal CdS Quantum Dots. *ACS Nano* **2016**, *10* (1), 1395–1403. <https://doi.org/10.1021/acsnano.5b06837>.
- (239) Owen, J. S.; Chan, E. M.; Liu, H.; Alivisatos, A. P. Precursor Conversion Kinetics and the Nucleation of Cadmium Selenide Nanocrystals. *J. Am. Chem. Soc.* **2010**, *132* (51), 18206–18213. <https://doi.org/10.1021/ja106777j>.
- (240) Demarse, N. A.; Quinn, C. F.; Eggett, D. L.; Russell, D. J.; Hansen, L. D. Calibration of Nanowatt Isothermal Titration Calorimeters with Overflow Reaction Vessels. *Analytical Biochemistry* **2011**, *417* (2), 247–255. <https://doi.org/10.1016/j.ab.2011.06.014>.
- (241) García-Rodríguez, R.; Hendricks, M. P.; Cossairt, B. M.; Liu, H.; Owen, J. S. Conversion Reactions of Cadmium Chalcogenide Nanocrystal Precursors. *Chem. Mater.* **2013**, *25* (8), 1233–1249. <https://doi.org/10.1021/cm3035642>.
- (242) Mooney, J.; Krause, M. M.; Saari, J. I.; Kambhampati, P. Challenge to the Deep-Trap Model of the Surface in Semiconductor Nanocrystals. *Phys. Rev. B* **2013**, *87* (8), 081201. <https://doi.org/10.1103/PhysRevB.87.081201>.
- (243) Mooney, J.; Krause, M. M.; Saari, J. I.; Kambhampati, P. A Microscopic Picture of Surface Charge Trapping in Semiconductor Nanocrystals. *The Journal of Chemical Physics* **2013**, *138* (20), 204705. <https://doi.org/10.1063/1.4807054>.


- (244) Baranauskienė, L.; Petrikaitė, V.; Matulienė, J.; Matulis, D. Titration Calorimetry Standards and the Precision of Isothermal Titration Calorimetry Data. *Int J Mol Sci* **2009**, *10* (6), 2752–2762. <https://doi.org/10.3390/ijms10062752>.
- (245) Lindman, S.; Lynch, I.; Thulin, E.; Nilsson, H.; Dawson, K. A.; Linse, S. Systematic Investigation of the Thermodynamics of HSA Adsorption to N-Iso-Propylacrylamide/N-Tert-Butylacrylamide Copolymer Nanoparticles. Effects of Particle Size and Hydrophobicity. *Nano Lett.* **2007**, *7* (4), 914–920. <https://doi.org/10.1021/nl062743+>.
- (246) De Nolf, K.; Cosseddu, S. M.; Jasieniak, J. J.; Drijvers, E.; Martins, J. C.; Infante, I.; Hens, Z. Binding and Packing in Two-Component Colloidal Quantum Dot Ligand Shells: Linear versus Branched Carboxylates. *J. Am. Chem. Soc.* **2017**, *139* (9), 3456–3464. <https://doi.org/10.1021/jacs.6b11328>.
- (247) Antanovich, A. V.; Prudnikau, A. V.; Melnikau, D.; Rakovich, Y. P.; Chuvilin, A.; Woggon, U.; Achtstein, A. W.; Artemyev, M. V. Colloidal Synthesis and Optical Properties of Type-II CdSe-CdTe and Inverted CdTe-CdSe Core-Wing Heteronanostructures. *Nanoscale* **2015**, *7* (17), 8084–8092. <https://doi.org/10.1039/c4nr07134d>.
- (248) Smock, S. R.; Williams, T. J.; Bruchey, R. L. Quantifying the Thermodynamics of Ligand Binding to CsPbBr<sub>3</sub> Quantum Dots. *Angewandte Chemie International Edition* **2018**, *0* (0). <https://doi.org/10.1002/anie.201806916>.
- (249) Hadar, I.; Abir, T.; Halivni, S.; Faust, A.; Banin, U. Size-Dependent Ligand Layer Dynamics in Semiconductor Nanocrystals Probed by Anisotropy Measurements.

*Angewandte Chemie International Edition* **2015**, *54* (42), 12463–12467.  
<https://doi.org/10.1002/anie.201502999>.

- (250) Hansen, L. D.; Fellingham, G. W.; Russell, D. J. Simultaneous Determination of Equilibrium Constants and Enthalpy Changes by Titration Calorimetry: Methods, Instruments, and Uncertainties. *Analytical Biochemistry* **2011**, *409* (2), 220–229.  
<https://doi.org/10.1016/j.ab.2010.11.002>.
- (251) Falconer, R. J. Applications of Isothermal Titration Calorimetry - the Research and Technical Developments from 2011 to 2015. *J. Mol. Recognit.* **2016**, *29* (10), 504–515. <https://doi.org/10.1002/jmr.2550>.
- (252) Burnouf, D.; Ennifar, E.; Guedich, S.; Puffer, B.; Hoffmann, G.; Bec, G.; Disdier, F.; Baltzinger, M.; Dumas, P. KinITC: A New Method for Obtaining Joint Thermodynamic and Kinetic Data by Isothermal Titration Calorimetry. *J. Am. Chem. Soc.* **2012**, *134* (1), 559–565. <https://doi.org/10.1021/ja209057d>.
- (253) Fritzinger, B.; Capek, R. K.; Lambert, K.; Martins, J. C.; Hens, Z. Utilizing Self-Exchange To Address the Binding of Carboxylic Acid Ligands to CdSe Quantum Dots. *J. Am. Chem. Soc.* **2010**, *132* (29), 10195–10201.  
<https://doi.org/10.1021/ja104351q>.
- (254) Sluydts, M.; De Nolf, K.; Van Speybroeck, V.; Cottenier, S.; Hens, Z. Ligand Addition Energies and the Stoichiometry of Colloidal Nanocrystals. *ACS Nano* **2016**, *10* (1), 1462–1474. <https://doi.org/10.1021/acsnano.5b06965>.
- (255) Voznyy, O. Mobile Surface Traps in CdSe Nanocrystals with Carboxylic Acid Ligands. *J. Phys. Chem. C* **2011**, *115* (32), 15927–15932.  
<https://doi.org/10.1021/jp205784g>.

## APPENDIX A

### COPYRIGHT PERMISSIONS



#### Purification technologies for colloidal nanocrystals



Y. Shen, M. Y. Gee and A. B. Greytak, *Chem. Commun.*, 2017, **53**, 827  
DOI: 10.1039/C6CC07998A






If you are not the author of this article and you wish to reproduce material from it in a third party non-RSC publication you must [formally request permission](#) using Copyright Clearance Center. Go to our [Instructions for using Copyright Clearance Center page](#) for details.


Authors contributing to RSC publications (journal articles, books or book chapters) do not need to formally request permission to reproduce material contained in this article provided that the correct acknowledgement is given with the reproduced material.

Permission to reproduce this manuscript as found in language used in Chapter 2 of this Dissertation



 Home
  Help
  Email Support
  Sign in
  Create Account





**Quantum Yield Regeneration: Influence of Neutral Ligand Binding on Photophysical Properties in Colloidal Core/Shell Quantum Dots**  
 Author: Yi Shen, Rui Tan, Megan Y. Gee, et al  
 Publication: ACS Nano  
 Publisher: American Chemical Society  
 Date: Mar 1, 2015  
 Copyright © 2015, American Chemical Society






**PERMISSION/LICENSE IS GRANTED FOR YOUR ORDER AT NO CHARGE**


This type of permission/license, instead of the standard Terms & Conditions, is sent to you because no fee is being charged for your order. Please note the following:

- Permission is granted for your request in both print and electronic formats, and translations.
- If figures and/or tables were requested, they may be adapted or used in part.
- Please print this page for your records and send a copy of it to your publisher/graduate school.
- Appropriate credit for the requested material should be given as follows: "Reprinted (adapted) with permission from (COMPLETE REFERENCE CITATION). Copyright (YEAR) American Chemical Society." Insert appropriate information in place of the capitalized words.
- One-time permission is granted only for the use specified in your request. No additional uses are granted (such as derivative works or other editions). For any other uses, please submit a new request.

Permission to reproduce this manuscript as found in language and figures within Chapter 3 Sections 3.1–3.3 of this Dissertation.

 Home
  Help
  Email Support
  Sign in
  Create Account



**Purification of Quantum Dots by Gel Permeation Chromatography and the Effect of Excess Ligands on Shell Growth and Ligand Exchange**  
 Author: Yi Shen, Megan Y. Gee, Rui Tan, et al  
 Publication: Chemistry of Materials  
 Publisher: American Chemical Society  
 Date: Jul 1, 2013  
 Copyright © 2013, American Chemical Society

**PERMISSION/LICENSE IS GRANTED FOR YOUR ORDER AT NO CHARGE**

This type of permission/license, instead of the standard Terms & Conditions, is sent to you because no fee is being charged for your order. Please note the following:

- Permission is granted for your request in both print and electronic formats, and translations.
- If figures and/or tables were requested, they may be adapted or used in part.
- Please print this page for your records and send a copy of it to your publisher/graduate school.
- Appropriate credit for the requested material should be given as follows: "Reprinted (adapted) with permission from (COMPLETE REFERENCE CITATION). Copyright (YEAR) American Chemical Society." Insert appropriate information in place of the capitalized words.
- One-time permission is granted only for the use specified in your request. No additional uses are granted (such as derivative works or other editions). For any other uses, please submit a new request.

Permission to reproduce figures from this manuscript as found in Chapter 2 and Chapter 4 of this Dissertation: Figure 2.2 and Figure 4.14.